PRECISION MICROWAVE FREQUENCY-OFFSET SEPARATED-OSCILLATORY-FIELDS MEASUREMENT OF THE $\mathbf{2^3P_1}$-TO-$\mathbf{2^3P_2}$ FINE-STRUCTURE INTERVAL IN ATOMIC HELIUM

KOSUKE KATO

A DISSERTATION SUBMITTED TO THE FACULTY OF GRADUATE STUDIES
IN PARTIAL FULFILMENT OF THE REQUIREMENTS
FOR THE DEGREE OF

DOCTOR OF PHILOSOPHY

GRADUATE PROGRAM IN PHYSICS AND ASTRONOMY
YORK UNIVERSITY
TORONTO, ONTARIO
FEBRUARY 2019

Abstract

The 2^3P_1-to-2^3P_2 fine-structure interval in atomic helium is measured using the frequency-offset separated-oscillatory-fields (FOSOF) technique. Two temporally separated microwave fields set up excitation paths that accumulate different quantum-mechanical phases. To detect the atoms that have changed states due to the microwaves, these atoms are excited to a Rydberg state and Stark ionized. The number of resulting ions is counted on a channel electron multiplier. In a typical SOF experiment, the relative phase between the two microwave pulses is toggled between 0° and 180°, and the change in the signal amplitude between the two phases is detected as a function of applied microwave frequency. In the FOSOF technique, two microwave pulses with a slight frequency offset are applied to the atoms. The relative phase seen by the atoms changes continuously due to the frequency offset, leading to a sinusoidally oscillating atomic signal. The phase of the oscillating signal is measured with respect to the phase of a reference generated by combining the frequency-offset microwaves. The phase difference between the

oscillating atomic signal and reference signal crosses zero at resonance and changes linearly as a function of applied microwave frequency.

Major signal-to-noise ratio (SNR) enhancement has been achieved by employing a two-dimensional magneto-optical trap and by using Stark-ionization detection. The excellent SNR allows for a very extensive study of systematic effects. A wide range of experiment parameters has been investigated. The final measured result is 2 291 176 590(25) Hz. This is the most precise measurement of the interval to date and thus the most precise test of the two-electron quantum-electrodynamics theory. When the 2^3P_0-to-2^3P_1 transition is measured at the same level of precision and the combined result of the 2^3P_0-to-2^3P_2 fine-structure interval is compared with a sufficiently precise theory, a sub-part-per-billion determination of the fine-structure constant using a two-electron system will become possible for the first time. Comparison with other fine-structure constant measurements could lead to tests of possible beyond-the-Standard-Model physics.

To My Beloved Family: Kensei, Sara, and Saori

Acknowledgements

I would like to thank Eric Hessels for an opportunity to work on this excellent experiment. Throughout my PhD career, he taught me everything that it takes to become an expert in the field of precision measurements. He gave me encouragement by showing his determination and enthusiasm towards the measurement. His inspirations and ideas (almost) always worked positively. I also appreciate that he patiently explained physical concepts clearly and intuitively. Without his guidance, I would have been lost. I am truly honoured to have worked with him for the last decade of my life (possibly in the future too).

I would like to thank Nikita Bezginov for being an excellent lab mate. You have always been a person who I could talk about anything. Your ideas and suggestions for the experiment were always helpful. I truly enjoyed the little "fresh air" breaks with you. I would also like to thank you for spotting me at the gym. Without your spot, I might not have survived (literally) my PhD.

I would like to thank Taylor Skinner for his great efforts in simulating the

experiment and analyzing the massive amount of data. Without your contribution to the experiment, I could not have completed the measurement.

To Travis Valdez, thank you for being a good friend and giving me tips on Python. Your success outside academia encourages me to think that I can probably survive anywhere after completing this work.

Nikita, Travis, and Taylor, I will never forget the good times that we spent together both inside and outside 309. I cannot predict where we end up in the future, but hopefully we can talk about atoms in fancier places (not Hoops or Shopsys).

I would like to thank Amar Vutha for his intelligent ideas and suggestions. His inputs and guidance were absolutely necessary for completing this work. Without a doubt, he is one of the most brilliant physicists I have ever seen.

I would like to thank Matthew George for his contribution to the measurement especially during the first few years of my PhD. You also taught me many useful tips to become a good experimentalist. I also enjoyed conversations with you outside Petrie about anything.

I would like to thank Cody Storry for letting me use his expensive equipments. Without his support, the experiment would not have been anywhere near this successful. Also, his valuable ideas and suggestions as an true experimentalist always made ways to tackle on problems.

Thank you Kumar for giving me fresh insights on the experimental work during research evaluations. You made me realize important things that I would have missed without your comments.

I would like to thank Wendy Taylor for the use of the digital oscilloscope which became an essential part of the experiment.

I wish to thank Derek and Hana Sandy for being my best friends, more like my family, since I started my undergrad at York. You have always been there for me, supported me and encouraged me during the hard times of my life. I will always remember our friendship as the most important thing in my life.

I would like to thank the York Physics and Astronomy department staff for your help and assistance. I would like to give a special thanks to Marlene Caplan. She had always been very nice, and fun to talk to about anything. She also made my life a lot easier by knowing exactly what to do whenever I had administrative issues.

I wish to thank my sisters Michiko and Hisako. They have always supported and encouraged me to do the best in all matters of my life. You were always worried about whether I could actually finish my experiment or not. Here I am, having finished one of the most brilliant and difficult experiments in the world. I will talk to you about atoms next time we meet.

I cannot show enough appreciation to my mother. She gave me a full support throughout my entire life. Even though she lives half way around the globe, I always felt her close. Her warm welcome for every trip back to Japan always makes me feel

home and comfortable. I thank you for raising me and making me as I am right now.

Lastly, and most importantly, I would like to say a million thanks to my beloved family Kensei, Sara, and Saori. I cannot say enough to show my appreciation to my wife Saori. Without your support, encouragement, and understanding, my dissertation work would not have been possible. I could focus on my research only because you kept the family safe. Thank you most of all for raising and protecting our children (and not giving up on me). I truly admire and respect you as a person, and I will always love you. Kensei, your smile and laughter always made me feel stronger and encouraged. As a two-year-old father, I might not be the greatest, but I will try not to be the worst. Sara, you are too young to have any interaction yet at this point. However, I wish to thank you for being born healthy, and making my life more delightful. Hopefully there will be a time that I talk to you about this brilliant experiment.

Table of Contents

List of Tables

List of Figures

1 Introduction

1.1 Fine-Structure Constant

The fine-structure constant was first introduced by Arnold Sommerfeld in 1916 in his effort of including relativistic effects in Bohr's atomic model. In the early days, it was interpreted as a spectroscopic quantity which defines the finer splitting of energy levels in a single-electron system. During the development of quantum electrodynamics (QED), the fine-structure constant gained its significance as a fundamental constant that represents the coupling strength of the electromagnetic interaction between charged particles.

The fine-structure constant is a dimensionless quantity, written in SI units as

$$\alpha = \frac{1}{4\pi\epsilon_0}\frac{e^2}{\hbar c}, \tag{1.1}$$

where e is the elementary charge, ϵ_0 is the electric permittivity of free space, $\hbar = h/2\pi$ is the reduced Planck constant, and c is the speed of light in vacuum. QED theory does not predict the value of α—it needs to be determined experimentally. The value of α can be determined in a variety of physical systems. Comparison of α obtained from different systems is of importance for two reasons. One reason is that experimentally measurable quantities in dissimilar systems, such as the electron magnetic moment and the helium fine structure, are represented as different forms of QED expansions in α; therefore, different aspects of the QED theory are tested. The second reason is that determinations of α from different systems are not affected by the same systematic effects, and problems associated with a particular experimental technique can be discovered by comparing results. Various systems showing consistent results confirm the level of understanding of physics; however, any unresolved inconsistency may point to beyond-the-Standard-Model physics.

A number of different systems have been used to obtain a precise value of α. The most precise determinations of α come from measurements of the electron magnetic moment (g_e-2) using the single quantum cyclotron [1], and h/m_{Cs} atom-recoil measurements using atom interferometry and Bloch oscillations [2]. Both measurements achieve < 0.25 part-per-billion (ppb) determinations of α. The $g_e - 2$ measurement tests QED at the 0.25 ppb level, tests for possible substructure of the electron [3, 4], tests for the possible presence of dark photons [1, 3, 5], and puts limits on possible dark axial vector bosons [1, 3]. The recoil measurement, along with another α determination, could be used for an absolute mass standard [6].

The helium fine-structure interval also forms an excellent system for a precise determination of α, as well as a precise test of QED. In 1964, Schwartz suggested that a less than 1 part-per-million (ppm) determination of α might be possible by precisely measuring the helium fine structure intervals and improving the theory for these intervals [7]. Over the last five decades, great efforts in experimental and theoretical work have been made to advance the precision of the helium fine structure [8–18]. With the improvements, the helium fine structure measurement is now approaching a precision of 1 ppb. The current precision of 25 Hz for the 2^3P_1-to-2^3P_2 interval [19] combined with a future $<$25-Hz measurement of the 2^3P_0-to-2^3P_1 interval will lead to an approximately $<$1-ppb determination of the 2^3P_0-to-2^3P_2 transition. This will become a 1 ppb test of QED and a $<$0.5 ppb determination of α when compared to a sufficiently precise theory.

1.2 Atomic Structure of Helium

Helium (^{4}He) is the second-simplest atom—with the first being hydrogen. It is composed of two electrons bound to a spinless nucleus containing two protons and two neutrons. The set of quantum numbers describing the energy state of the two electrons of helium are the principal quantum number n_i, the azimuthal quantum number l_i, the spin quantum number s_i, and the projections of the l_i and s_i onto the $\hat{z}$ axis (m_{l_i} and m_{s_i}), with the subscript $i = 1, 2$ denoting the electron number. A helium atom in an arbitrary electronic state is represented as $(n_1 l_1)(n_2 l_2)$ where

l_i denotes s, p, d, etc. for $l_i = 0$, $l_i = 1$, $l_i = 2$, etc. Spectroscopic notation $n^{2S+1}\mathrm{L}$, where $S = s_1 + s_2$, $\mathrm{L} = l_1 + l_2$, is used to label the atomic state. The non-relativistic Hamiltonian for a helium atom consists of two hydrogenic Hamiltonians H_i $(i = 1, 2)$ and an additional term describing the electrostatic repulsion between two electrons. Two electrons in a static Coulomb potential obey a Schrödinger equation of the form,

$$\left[-\frac{\hbar^2}{2\mu}\nabla_1^2 - \frac{\hbar^2}{2\mu}\nabla_2^2 - \frac{\hbar^2}{m_\alpha}\nabla_1 \cdot \nabla_2 + \frac{e^2}{4\pi\epsilon_0}\left(-\frac{Z}{r_1} - \frac{Z}{r_2} + \frac{1}{r_{12}}\right)\right]\psi(\mathbf{r}_1, \mathbf{r}_2) = E\psi(\mathbf{r}_1, \mathbf{r}_2), \tag{1.2}$$

where m_α is the nuclear mass, μ is the reduced mass $\mu = \frac{m_e m_\alpha}{m_e + m_\alpha}$, $Z = 2$ is the atomic number of helium, $\mathbf{r}_1$ and $\mathbf{r}_2$ are the position vectors of two electrons with respect to the nucleus, and $r_{12} = |\mathbf{r}_1 - \mathbf{r}_2|$ is the distance between the two electrons. The electron-electron repulsion term makes the Hamiltonian inseparable and the Schrödinger equation cannot be solved exactly in this case.

1.2.1 Ground State

The ground state of helium is a spin singlet $(S = 0)$ state in which both electrons are in a $1s$ state with antisymmetric (paired) spin configuration. The Pauli exclusion principle does not allow two electrons to have a same set of quantum numbers; therefore the electrons are forced to be in the singlet state. Helium has the highest ground-state binding energy amongst all of the elements due to its closed-shell configuration in the $1s^2$ state. The ground-state energy has been calculated very precisely using the variational method [20].

1.2.2 Excited States

Excited states of helium consist of one electron in the hydrogenic ground state and another in the excited state ($1snl$)—unless it is in a highly unstable doubly excited state. The excited state can be in either the spin singlet ($S = 0$) or triplet ($S = 1$) state depending on the spin orientation of the two electrons (spectroscopic notations of n^1L and n^3L for singlet and triplet states, respectively, as shown in Figure 1.1). The singlet state has a symmetric spatial wavefunction that is associated with the antisymmetric spin function, and the total wavefunction of the triplet state is a product of the antisymmetric spatial wavefunction and symmetric spin function. The singlet state has less binding energy than the triplet counterpart because the electron-electron repulsion is larger in the singlet state than the triplet state. The singlet and triplet states are extremely weakly connected by electric dipole transitions, so that they can be treated as separate systems in most cases. The 2^1S and 2^3S states are metastable states that have very long lifetimes of $19.7 \pm 1.0\,\mathrm{ms}$ [22] and $7870 \pm 510\,\mathrm{s}$ [23], respectively. The 2^3S state is the longest-lived metastable state amongst all of the neutral atoms. The transition between the 2^3S and ground state requires an electron spin flip, making it extremely unlikely to occur in free

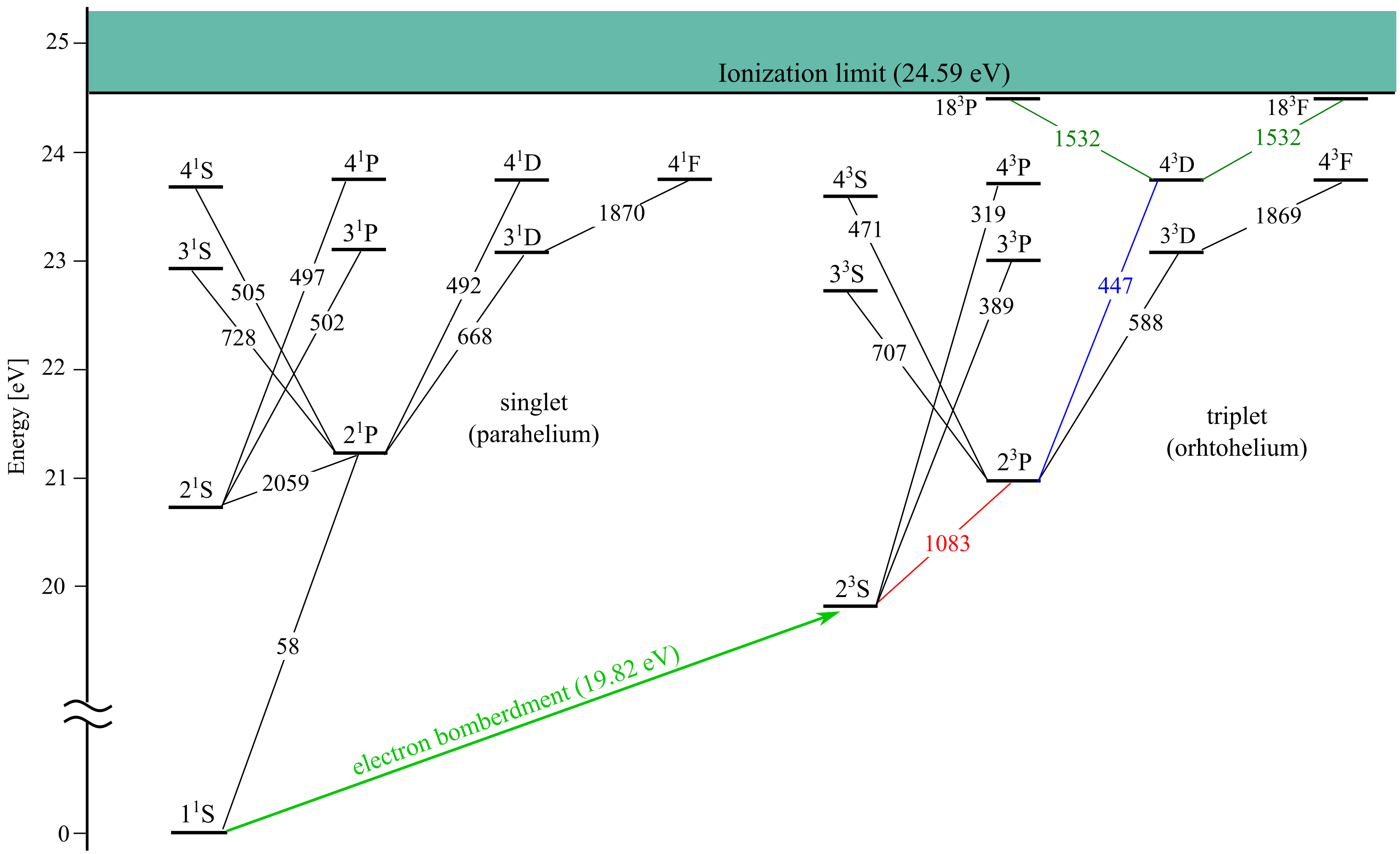

Figure 1.1: Lowest-lying energy states of helium. Electric-dipole transitions with optical wavelengths are indicated as lines connecting two states. Their wavelengths [21] are labelled on the lines in nm. Transitions relevant to the current experiment are shown in colour.

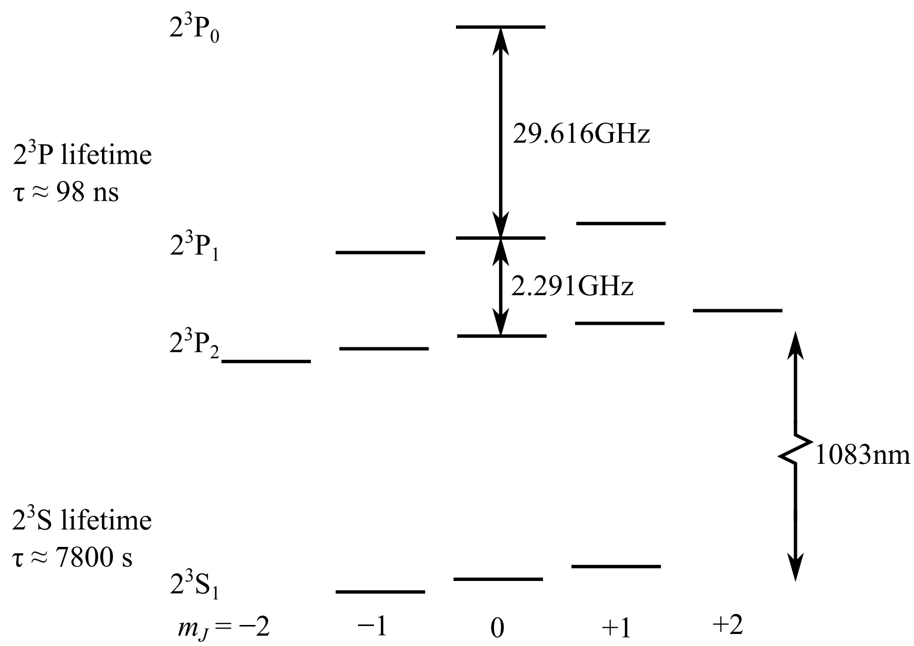

Figure 1.2: The n=2 triple helium energy-level diagram. The degeneracy of the m_J states is lifted by a magnetic field (Not to scale).

space. The forbidden transition makes the 2^3S state effectively the ground state for the triplet system. Transition from the ground state to the 2^1S or 2^3S states can be excited using electron bombardment. Figure 1.1 shows the lowest-lying energy states of helium for both singlet and triplet systems in the spectroscopic notation. Some electric-dipole transitions with their corresponding wavelengths are shown in the figure.

1.3 Helium Fine Structure

1.3.1 Angular Momentum Coupling

Figure 1.2 shows the energy-level diagram of the helium n=2 triplet system. The energy contribution due to the coupling of angular momenta gives rise to the fine-structure splitting. The fine-structure splitting of an atom with two electrons is predominantly described by the spin-orbit and spin-spin interactions. The total angular momentum $\mathbf{J} = \mathbf{L} + \mathbf{S}$ and its projection onto the $\hat{z}$ axis J_z lead to the quantum numbers J and m_J. The spectroscopic notation $n^{2S+1}\mathrm{L}_J$ describes energy states of an atom including the spin-orbit interaction.

The $n^{2S+1}\mathrm{L}_J$ fine structure energy splitting in helium comes primarily from the spin-dependent part of the Breit-Pauli Hamiltonian (the spin-orbit coupling, spin-spin coupling, and spin-other-orbit coupling). The spin-orbit coupling describes the interaction between the electron magnetic moment and its own orbital angular momentum. The spin-orbit coupling increases with the nuclear charge number Z, and it becomes more significant for atoms with higher-Z nuclei. The spin-spin coupling is the interaction between the spin of one electron and the spin of the other electron. The coupling is described as the interaction that originates from the field produced by the magnetic dipole of one electron at the other electron. The spin-other-orbit coupling arises from the field produced at the position of one electron by the orbital motion of the other electron. For a helium atom, contributions from the spin-spin and spin-other-orbit interactions are comparable to that of the spin-orbit interaction. As a result, the peculiar $2^3\mathrm{P}_J$ structure in helium (inverted energy order of J states and the unusually large energy splitting between the $J = 0$ and $J = 1$ states compared to the splitting between the $J = 1$ and $J = 2$ states, as shown in Figure 1.2) arises [24]. The contributions from the leading terms give a reasonable estimate of the energy of the fine-structure state; however, higher-order contributions must be taken into account in order to obtain a precise value of the energy splitting.

1.3.2 QED Description of the Helium Fine Structure

Theoretical calculations for the $2^3\mathrm{P}_J$ states have been performed by G. W. F. Drake (University of Windsor), T. Shi (Chinese Academy of Sciences), and K. Pachucki (Warsaw University). The most current of these results are listed in Table 1.1. In QED, the energies of the fine-structure states are represented as a power series expansion in α and can be written as

$$E_{\mathrm{fs}} = E_{\mathrm{fs}}^{(4)} + E_{\mathrm{fs}}^{(5)} + E_{\mathrm{fs}}^{(6)} + E_{\mathrm{fs}}^{(7)} + \dots . \tag{1.3}$$

The term $E_{\mathrm{fs}}^{(n)}$ represents the energy contribution of the order $mc^2\alpha^n$, where m is the electron mass, and c is the speed of light. The leading term $E_{\mathrm{fs}}^{(4)}$ includes corrections of order up to $mc^2\alpha^4$ described by the Breit-Pauli Hamiltonian. The

Experimental Results			
	ν_{12} (Hz)	ν_{01} (Hz)	ν_{02} (Hz)
This work [19] [2018]	2 291 176 590(25)		
Hessels [27, 28] [2009,2001]	2 291 177 530(350)	29 616 950 900(900)	
Hu [29] [2017]	2 291 177 560(190)		31 908 130 980(130)
Gabrielse [30] [2005]	2 291 175 590(510)	29 616 951 660(700)	31 908 126 780(940)
Shiner [31, 32] [2000,2010]	2 291 175 900(1000)		31 908 131 250(300)
Theoretical Results			
Pachucki [26] [2010]	2 291 178 900(1700)	29 616 952 300(1700)	31 908 131 200(1700)
Shi [25] [2015]	2 291 179 510(1700)	29 616 951 850(1700)	31 908 131 360(1700)

Table 1.1: Summary table of recent $2^3\mathrm{P}_J$ fine-structure experimental and theoretical results. The symbol $\nu_{JJ'}$ denotes the energy difference between the $2^3\mathrm{P}_J$ and $2^3\mathrm{P}_{J'}$ fine-structure states. One standard deviation uncertainties in the last digits are shown in parentheses. Numbers in square brackets are the publication year.

current theoretical work on the $2^3\mathrm{P}_1$-to-$2^3\mathrm{P}_2$ fine-structure interval predicts that $E_{\mathrm{fs}}^{(4)}$ and $E_{\mathrm{fs}}^{(5)}$ together give 2.3-GHz contributions, and $E_{\mathrm{fs}}^{(6)}$ and $E_{\mathrm{fs}}^{(7)}$ give 6.5-MHz and 20-kHz contributions, respectively. The size of the energy contributions from the uncalculated higher-order effects $\mathcal{O}(\alpha^8)$ is estimated to be 1.7 kHz by Shi [25] and Pachucki [26]. The theoretical calculations performed by Pachucki and Shi agree with each other.

1.3.3 Measurements of the Helium Fine Structure

The $n = 2$ triplet system of helium offers a few advantageous features for precision spectroscopy. The narrow natural linewidth of 1.6 MHz allows for a high spectroscopic resolution. The long lifetime (98 ns) of $2^3\mathrm{P}_J$ states makes the experiment more feasible. The splittings (2.291 GHz and 29.616 GHz) are in the frequency range in which microwave components are commercially available. The $2^3\mathrm{S}_1$-to-$2^3\mathrm{P}_J$ transition can be saturated with a small light intensity (0.16 mW/cm^2) and can easily be driven by a 1083-nm diode laser.

A number of groups have measured the fine structure of helium using different methods over the past five decades. Table 1.1 shows the list of recent measurements and calculations of the helium fine structure. Historical measurements of the fine-structure intervals are given in [33]. The research group led by G. Gabrielse (Harvard University) used a saturated absorption spectroscopy setup in a discharge cell to measure the linecentres of all $2^3\mathrm{S}_1$-to-$2^3\mathrm{P}_J$ transitions to infer the energy differences for the $2^3\mathrm{P}_J$-to-$2^3\mathrm{P}_{J'}$ intervals. Groups led by D. Shiner (North Texas University) and S. -M. Hu (University of Science and Technology of China) performed optical spectroscopy on the $2^3\mathrm{S}_1$-to-$2^3\mathrm{P}_J$ transitions on a thermal beam of triplet helium atoms to probe the fine-structure energy differences. E. A. Hessels' group uses microwaves to drive the magnetic-dipole $2^3\mathrm{P}_J$-to-$2^3\mathrm{P}_{J'}$ transitions and directly measure the transition frequencies.

A similar microwave spectroscopy setup is used for the current measurement with an improved experiment scheme and a new spectroscopy method. A variation of separated oscillatory fields (SOF) is used in which the frequency of the separated oscillatory fields are offset slightly. This method was recently developed by Hessels and Vutha [34] and is referred to as FOSOF (frequency-offset SOF). The precision of the measurement is improved significantly compared to the previous microwave measurement.

2 Experimental System

2.1 Experiment Overview

Figure 2.1 shows the experiment setup for the current measurement. Figure 2.2 shows a helium energy-level diagram with the microwave and laser transitions relevant to the current experiment. As shown at the left of Figure 2.1, a thermal beam of metastable helium atoms is produced through electron bombardment in a DC discharge. The discharge puts equal populations in all magnetic sublevels of the metastable 2^3S_1 state. The helium metastable beam exits a small aperture with an angular spread of approximately 50 mrad, and this spread leads to a significant loss in the number of atoms making it to the main experiment region, which is located 86 cm away from the aperture. To significantly reduce this loss, a two-dimensional magneto-optical trap (2DMOT shown in Figure 2.1) is used to focus and collimate the metastable beam. The 2DMOT cooling transitions are shown in Figure 2.2, labelled as 2DMOT.

The main experiment occurs inside a microwave coaxial airline, and this region is

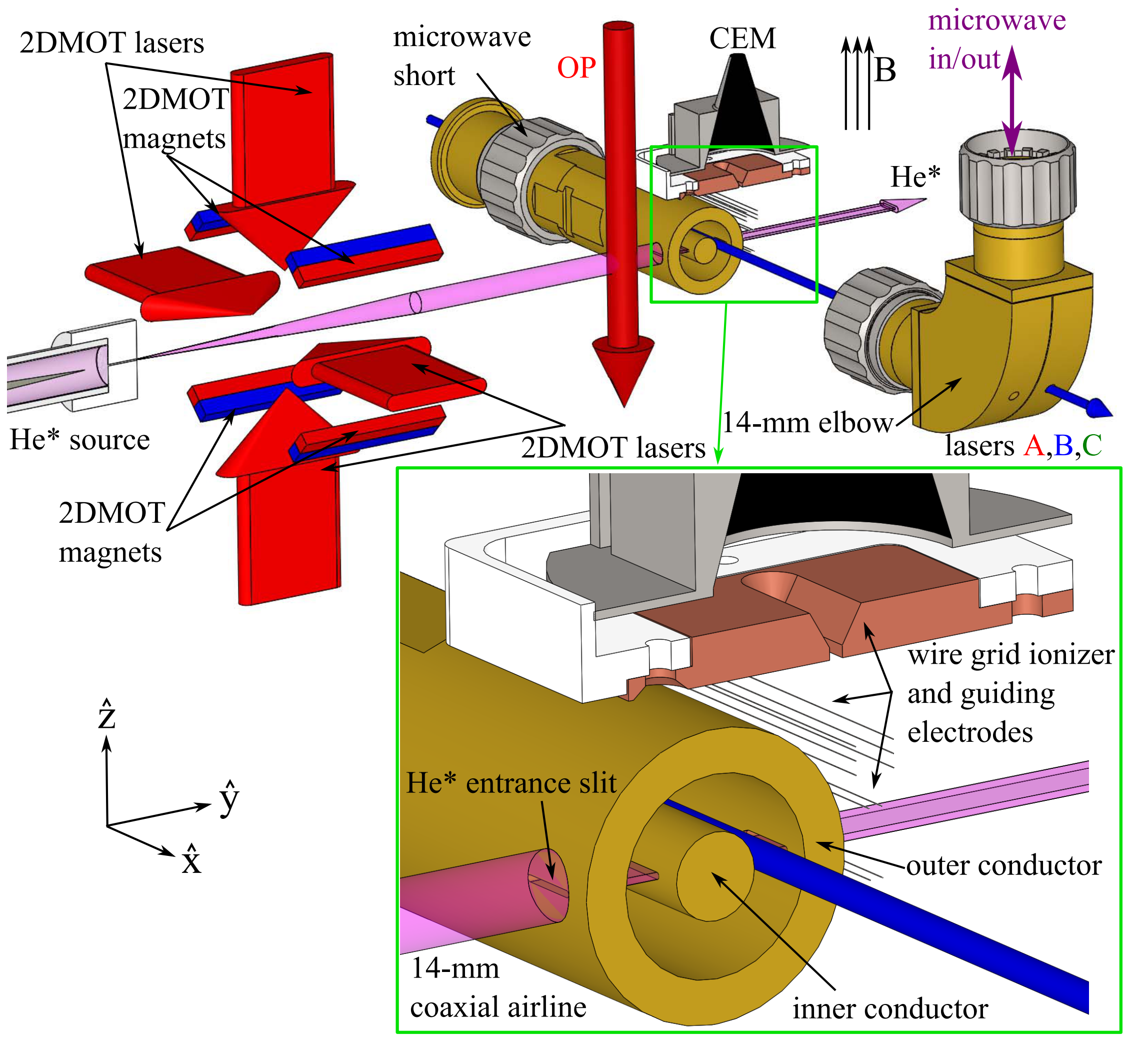

Figure 2.1: Experimental setup (not to scale). A thermal beam of metastable helium atoms emerging from the DC discharge is intensified using a two-dimensional magneto-optical trap (2DMOT). Optical pumping of the metastable 2^3S_1 state (OP) is performed before the atoms enter the microwave region through a 0.5-mm-by-5-mm slit. Only atoms that experience a complete SOF sequence are ionized and detected by channel electron multiplier (CEM).

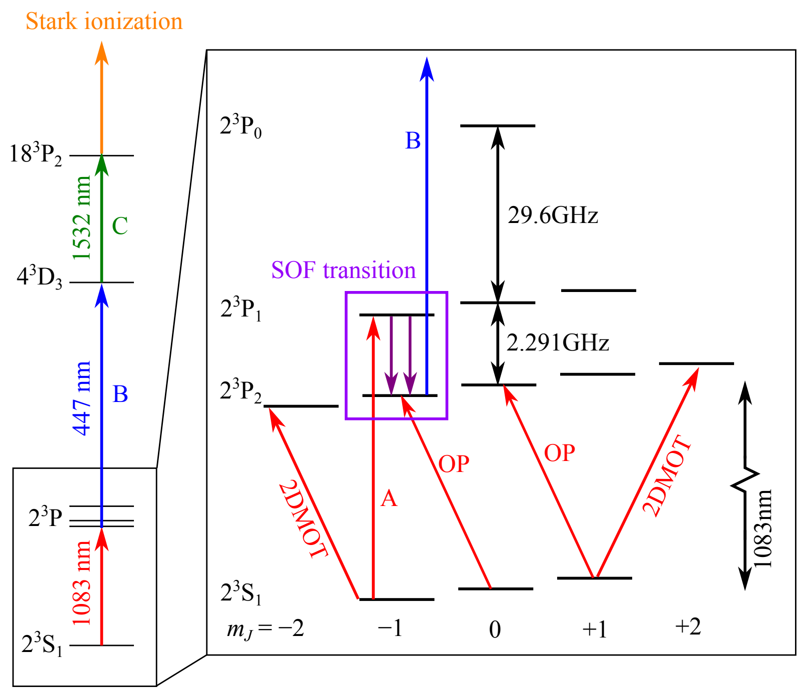

Figure 2.2: Experiment energy-level diagram. Arrows represent laser and microwave excitations. Degeneracy of the magnetic sublevels is lifted by a DC magnetic field

shown on a larger scale in the inset of Figure 2.1. A DC magnetic field in the vertical $\hat{z}$ direction is applied to lift the degeneracy between m_J states. A circularly polarized continuous-wave (CW) 1083-nm laser (OP in Figures 2.1 and 2.2) is directed along the $\hat{z}$-direction, and intersects the atomic beam before the atoms enter the airline. This laser optically pumps atoms into the $2^3S_1(m_J{=}{-1})$ state and empties out the rest of the 2^3S_1 magnetic sublevels. The optically-pumped helium atoms then enter the airline through a small slit (He* entrance slit in Figure 2.1). Once atoms travel past the inner conductor of the airline, the main experimental sequence starts.

Figure 2.3 shows the timing of the experiment sequence and the populations

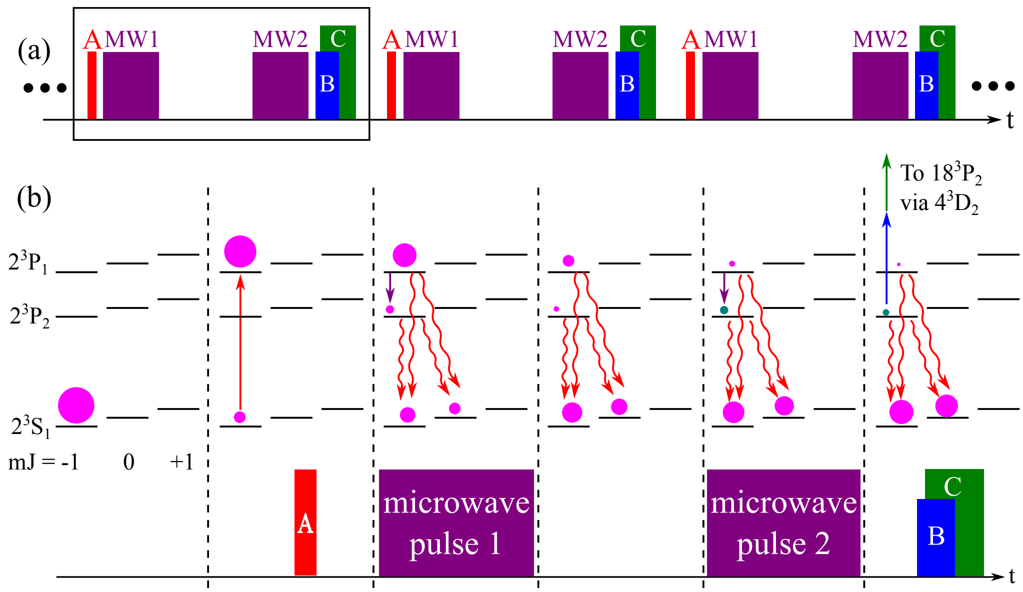

Figure 2.3: Experiment timing diagram. (a) A continuous series of laser and microwave pulses are shown. A (red), B (blue), and C (green) indicate 1083-, 447-, and 1532-nm laser pulses. The purple boxes are the microwave pulses used in the experiment. Panel (b) shows the population transfer during a single experiment sequence (indicated in (a) as a black rectangle). The red wavy arrows represent radiative decay of the 2^3P_J states during the experiment. The green dot represents the atoms that are detected by Stark-ionization of Rydberg atoms. The timing for the pulses varies as discussed in Section 2.11.4

of the atomic states during the experiment sequence. A pulse of linearly polarized 1083-nm laser (A in Figures 2.1, 2.2, and 2.3) tuned to the 2^3S_1-to-2^3P_1 transition is sent through the airline to prepare atoms into the $2^3P_1(m_J{=}-1)$ state. Two temporally separated microwave pulses (purple arrows and boxes in Figures 2.2 and 2.3) drive the $2^3P_1(m_J{=}-1)$-to-$2^3P_2(m_J{=}-1)$ transition. The second microwave pulse is followed by subsequent pulses of 447- and 1532-nm lasers (B and C in Figures 2.1, 2.2, and 2.3). The 447-nm laser drives the transition from the 2^3P_2 state to the

4^3D_3 state, and the 1532-nm laser brings the 4^3D_3 atoms up to the 18^3P_2 Rydberg state. The 18P state lives long enough to exit from the airline before a significant fraction decays down to lower-energy states. At the downstream exit of the airline, an electric field is applied to the Rydberg atoms to induce Stark-ionization, and the number of resulting ions is counted using a channel electron multiplier (CEM) detector.

2.2 Beamline and Vacuum System

Figure 2.4 shows the vacuum system used for the current experiment. The beam of metastable helium atoms produced at the start of the beamline goes through a series of vacuum chambers. The beamline is composed of five sections (as indicated in Table 2.1 and Figure 2.4) and atoms go through the sections in the following order: the metastable helium source, 2DMOT section, main experiment chamber, 1532-nm laser frequency stabilization chamber (laser-locking chamber), and atom-speed measurement chamber. Metastable atoms are produced inside the source chamber and they exit the chamber through a 1-mm-diameter skimmer (as will be discussed in Section 2.3). The atoms then expand into the 2DMOT chamber where the beam of atoms is focused and collimated by the 2DMOT (as will be discussed in Section 2.9). The collimated beam of atoms enters the main experiment chamber where the atoms go through the microwave coaxial airline (shown in Figure 2.1) inside of

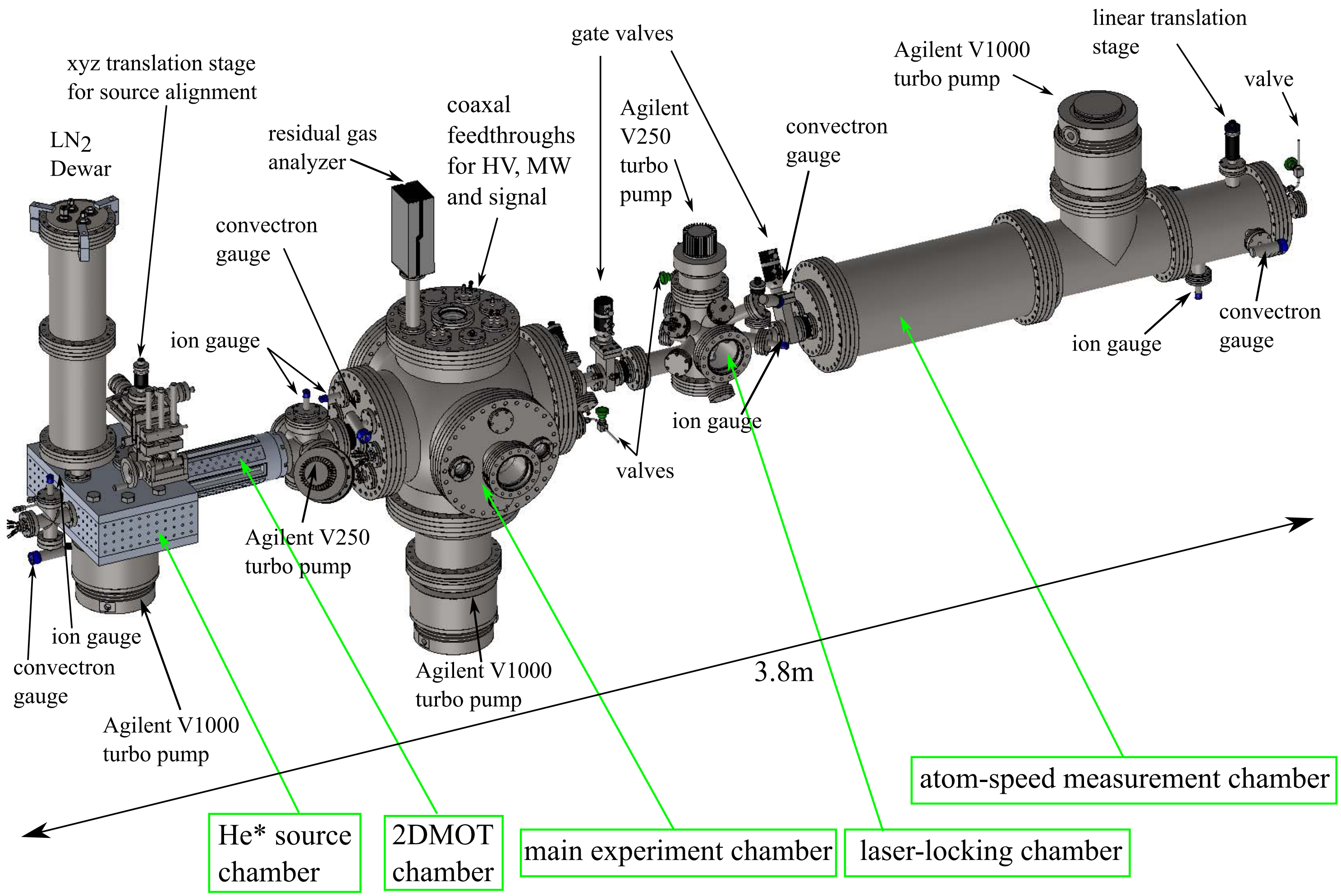

Figure 2.4: Beamline and vacuum system. Main sections of the beamline and vacuum components that constitute the beamline are shown. HV:high voltage, MW:microwave, LN_2:liquid nitrogen.

which the FOSOF experiment happens. The atoms then travel to the laser-locking chamber, in which some of the atoms are excited up to the 18^3P Rydberg state and ionized, and the resulting ion signal is used to stabilize the 1532-nm laser (as will be discussed in Section 2.6.2). The atoms are then sent to the last section of the beamline that hosts an atom-speed measurement system (which will be discussed in Section 2.4). The length of the beamline is 3.8 m in total.

<table>
<tr><th>Section name</th><th>Primary pump</th><th>C_V [L/s]</th><th>Backing pump</th><th>C_V [L/min]</th><th>Base pressure [torr]</th></tr>
<tr><td>Metastable helium source chamber (0–0.3 m)</td><td>Agilent V1001</td><td>1000</td><td>Agilent Triscroll300</td><td>250</td><td>5×10^{-5}</td></tr>
<tr><td>2DMOT chamber (0.3–0.8 m)</td><td>Agilent V250</td><td>250</td><td rowspan="2">Agilent Triscroll300</td><td rowspan="2">250</td><td>5×10^{-7}</td></tr>
<tr><td>Main experimental chamber (0.8–1.5 m)</td><td>Agilent V1001</td><td>1000</td><td>3×10^{-9}</td></tr>
<tr><td>Laser-locking chamber (1.5–2.2 m)</td><td>Agilent V250</td><td>250</td><td rowspan="2">Agilent SH110</td><td rowspan="2">110</td><td>9×10^{-10}</td></tr>
<tr><td>Speed-measurement chamber (2.2–3.8 m)</td><td>Agilent V1001</td><td>1000</td><td>8×10^{-9}</td></tr>
</table>

Table 2.1: List of vacuum pumps used in the experiment. The symbol C_V denotes the pumping speed of the vacuum pumps. Merged rows in the backing pump column indicate that the backing pump is shared by multiple turbo pumps.

It is important to achieve the highest vacuum possible in all sections in order to avoid a loss in number of atoms due to the elastic scattering and collisional ionization with the background gas in the system. The vacuum pressure in each of the sections is maintained by a turbo-molecular pump backed by a dry-scroll pump. Table 2.1 summarizes the vacuum pumps used in the system and the ultimate pressure in each section. A large amount of helium gas is leaked into the source chamber for the metastable helium production. It is critical to maintain the lowest pressure possible especially in the main experiment chamber to ensure the cleanest experiment environment (problems with the increased background pressure will be addressed in Section 2.7). A 1-L/s pumping restriction is installed at the junction between the 2DMOT and main experiment chambers to limit the amount of helium gas leaking into the main experiment chamber. Additionally, a residual gas analyzer (SRS RGA100) is installed on the main experiment chamber to help in understanding the background gas characteristics. Pressures in all chambers and their roughing lines are monitored using ionization (Granville-Phillips 355 Micro-Ion) and Pirani vacuum-pressure gauges (Granville-Phillips 275 Convectron). Roughing-line pressures are typically lower than the lowest measurable pressure of the Pirani gauge, so they are not listed in Table 2.1. Analog outputs from the gauge controllers are used for the interlock system to protect sensitive devices from vacuum failure. In each section of the beamline, a valve is installed to use nitrogen as a back-filling gas instead of ambient air when breaking vacuum. This prevents water molecules in the ambient air to be adsorbed on the vacuum chamber wall, and this makes the successive pump-down process be much faster than the case of air-filling vacuum breaking.

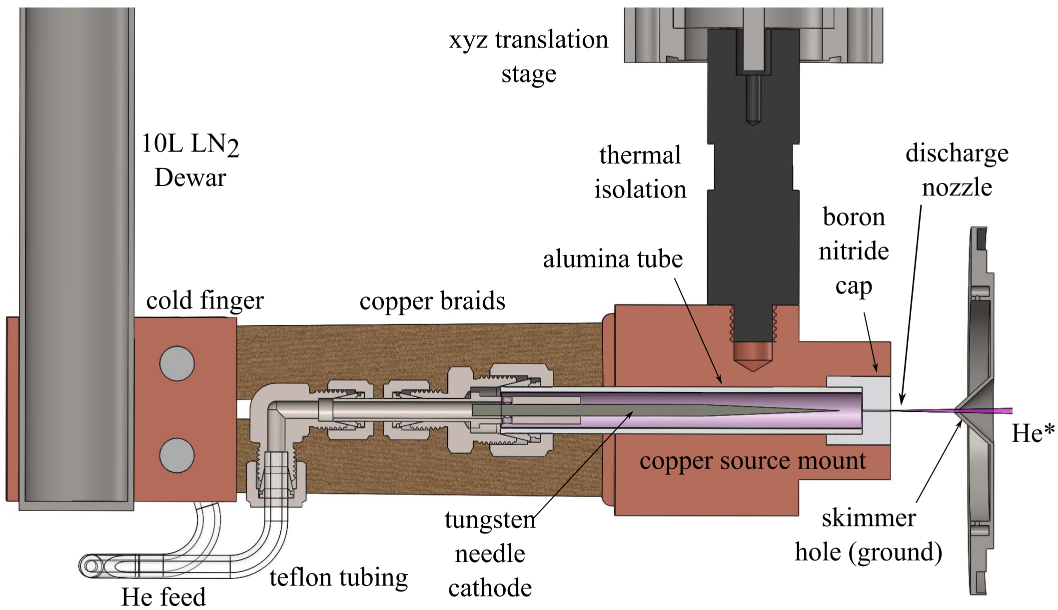

Figure 2.5: Metastable helium source

2.3 Metastable Helium Source

Detailed descriptions on the metastable atom source can be found elsewhere [33, 35–38], so only technical details are presented in this section. A liquid-nitrogen-cooled DC-discharge metastable atom source design is employed in the current experiment. Figure 2.5 shows a schematic of the metastable helium source. It produces metastable atoms by the electron bombardment in the DC discharge via the following process:

$$\mathrm{He} + e^{-}(T) \rightarrow \mathrm{He}^{*} + e^{-}(T - 20\,\mathrm{eV}), \tag{2.1}$$

where the kinetic energy T of an electron is transferred to a helium atom by an inelastic collision. The source produces about 10^{15} $He^*(2^3S_1)$/sterad/s. The main source assembly consists of a needle cathode that is enclosed in an insulating alumina tube capped and sealed with a boron nitride piece with a 0.3-mm-diameter, 1-cm-long nozzle machined at its centre. The source assembly is held by a copper mount that is thermally attached to a liquid-nitrogen-cooled cold finger with copper braids. Sheets of indium are used to make a good thermal contact between the copper braids and the main source assembly. The copper braids are used instead of a solid copper structure to allow for an adjustment of the nozzle position (for signal optimization) using a xyz translation stage. Ultra-pure (99.999 %) helium gas from a cylinder is fed into the source chamber and its flow is regulated using a mass-flow controller (model 1179A51CS1BV-S). PTFE tubing inside the chamber guides the helium gas to the main source assembly. The helium atoms supersonically expand into the low-pressure side of the vacuum chamber through the boron-nitride nozzle [35]. The large pumping restriction of the boron-nitride nozzle ensures a large pressure gradient between the high- and low-pressure regions of the vacuum chamber. The pressure inside the alumina tube is measured using a capacitance gauge (Edwards 600AB 100TR) and is at 50 torr in a typical source operation. The DC discharge essential in producing the metastable atoms is maintained between the needle cathode and stainless-steel grounded skimmer hole through the boron-nitride nozzle. Ignition of the arc is achieved by applying 5 kV (supplied by the Glassman high-voltage power supply (model PS/FR06R50.0GA1)) between the needle cathode and skimmer hole. A 100-kΩ resistor chain ensures the current-limited operation of the power supply. Once the arc is ignited, the voltage output from the power supply drops down to 3.1 kV and draws a typical set current of 25 mA. The voltage drop across the needle cathode to the skimmer hole is approximately 600 V.

The source operation without liquid-nitrogen cooling is avoided due to the low melting point of indium, as molten indium falling into the turbo pump damages the pump. An interlock is installed to shut down the source in case the temperature of the source reaches a set threshold value, which ensures a safe operation of the source in the case of liquid-nitrogen exhaustion. To avoid exhaustion of the liquid nitrogen and to allow for a round-the-clock operation of the experiment, an automatic liquid-nitrogen filling system has been implemented. Two cryogenic solenoid valves (ASCO 8222G002LT) are installed in series in the liquid-nitrogen transfer line. When a low level of liquid nitrogen is detected by the cryogen-level sensor (J.C. CONTROLS SN2-7), the sensor outputs AC power to the solenoid valves, enabling the transfer line. The AC power line is controlled by a computer-controlled power strip.

Stable operation of the source is essential in performing precision measurements. The design of this source is very robust, and requires no regular maintenance. The typical failure mode of similar DC-discharge sources is wearing of the boron-nitride nozzle due to the constant exposure to an intense plasma. Another typical issue is the formation of an insulating layer on the needle cathode, making it more difficult to ignite an arc over time. These failure modes do not appear to be issues with the source design used here. This source has been fully operational without performing any maintenance for over three years.

2.4 Atom-Speed Measurement

Figure 2.6 shows the atom-speed measurement setup. The speed of atoms emerging from the metastable helium source is monitored in the last section of the beamline. The chamber (shown in Figure 2.4) hosts an optical chopper (Stanford Research Systems SR540), a Stern-Gerlach (SG) magnet, and a CEM detector on a translation stage. The beam produced by the DC-discharge source consists of singlet- and triplet-metastable helium atoms, as well as UV photons. When the beam is chopped (with a 98 % off, 2 % on chopper), it becomes a series of pulses that contain all three components of the beam. The pulse then travels through a 1.1-m drift section. During the travel, the UV photons and atoms separate spatially due to their speed difference. From the difference in arrival time and the length of travel, the speed of atoms can be determined (using what we refer to as the time-of-flight (TOF) method). Figure 2.7 shows the typical TOF signal. The data gives information about the beam's most probable speed and its speed distribution. The peak on the

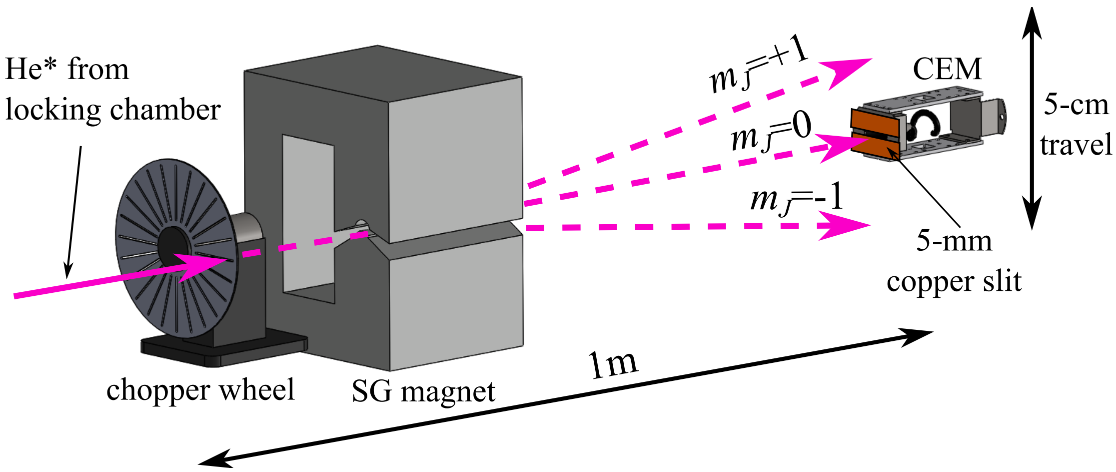

Figure 2.6: Time-of-Flight (TOF) measurement setup. A chopped beam of metastable atoms separates from UV photons in the 1.1-m drift section. The Stern-Gerlach (SG) magnet separates different magnetic sublevels. The time-resolved signal from the CEM is monitored.

left is the chopped UV signal, and the one on the right is the mixture of triplet and singlet atoms. The TOF signal is constantly monitored on an oscilloscope for diagnostics of the 2DMOT and source operation.

The location of the CEM is occasionally changed to check the distribution of atoms in the magnetic sublevels of 2^3S_1 states. The SG magnet deflects m_J=±1 states in the vertical direction and by changing the position of the CEM, the distribution of atoms in different m_J states is probed. No significant difference in the TOF signal is found for different m_J states—indicating that the singlet and triplet atoms have the same speed distribution.

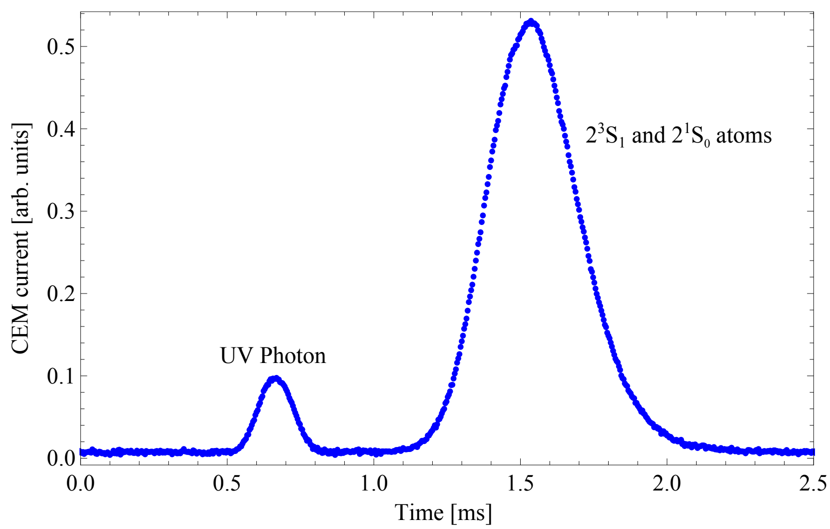

Figure 2.7: A typical Time-of-Flight (TOF) signal. The speed of atoms is determined from the time difference and flight distance. From the data, the speed is estimated to be around 1100 m/s.

2.5 1083-nm Laser Systems

Two 1083-nm lasers are used in the current experiment. One of the lasers is locked to the 2^3S_1-to-2^3P_2 transition and it is used for multiple applications: the 2DMOT (2DMOT in Figure 2.2), optical pumping (OP in Figure 2.2), and frequency stabilization of detection lasers (lasers B and C in Figures 2.1, 2.2, and 2.3). The other laser is used to excite the 2^3S_1-to-2^3P_1 transition (laser A in Figures 2.1, 2.2, and 2.3) to prepare atoms in the 2^3P_1 state for the experiment. Details of the optics setup of each laser are presented in this section.

Application	Locking	1532-nm pump	Optical pumping	447-nm pump	2DMOT
Frequency [MHz]	f_0	f_0	$f_0 - 20 \pm f_{\mathrm{EOM}}$	$f_0 - 20 + 185$	$f_0 - 20$

Table 2.2: Summary of the 2^3S_1-to-2^3P_2 laser frequencies. The frequency of the 2^3S_1-to-2^3P_2 laser is adjusted for each application. f_0 is the resonance frequency of the 2^3S_1-to-2^3P_2 transition. Two AOMs are used to generate frequencies given in the table. The AOM frequencies are set to $f_{\mathrm{AOM1}} = 185\,\mathrm{MHz}$ and $f_{\mathrm{AOM2}} = 175\,\mathrm{MHz}$. f_{EOM} denotes the driving RF frequency of the fiber-EOM.

2.5.1 2^3S_1-to-2^3P_2 Laser System

Figure 2.8 shows the schematic diagram of the 1083-nm 2^3S_1-to-2^3P_2 laser system. This laser is used for the 2DMOT, optical pumping of the 2^3S_1 state, and stabilization of the detection lasers (447- and 1532-nm lasers). Table 2.2 summarizes the applications and corresponding frequencies of the 2^3S_1-to-2^3P_2 laser.

The 1083-nm laser light is emitted from a distributed Bragg reflector (DBR) laser diode (Photodigm PH1083DBR) (DL in Figure 2.8). The laser diode outputs 40 mW of optical power. The diode is driven by a Melles Griot diode laser driver (06DLD203A). The laser light from the diode goes through two 30-dB (OFR IO-5-1083-HP and Conoptics 715) optical isolators (30dB in Figure 2.8) before coupling into the 15-W Nufern fiber amplifier (NuAmp NUA-1064-PB-0015-C2). The fiber coupler (FC in Figure 2.8) is mounted on a x-y translation stage to optimize the coupling. A 30-dB isolator is installed on the output of the fiber amplifier to suppress

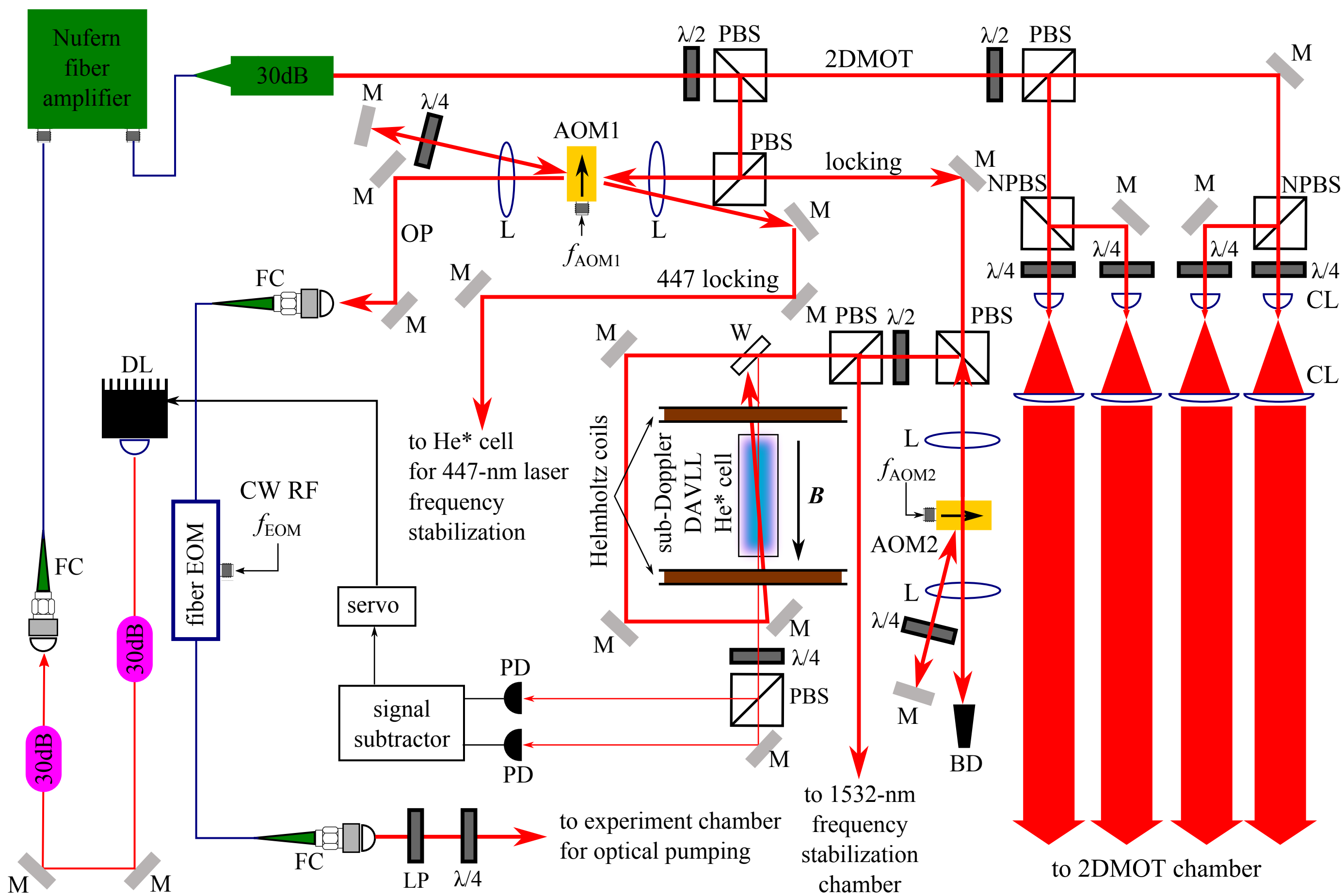

Figure 2.8: 1083-nm 2^3S_1-to-2^3P_2 laser system. DL:diode laser, M:mirror, 30dB:30-dB optical isolator, FC:fiber coupler, $\lambda/2$:half-wave plate, PBS:polarizing beam splitter, NPBS:non-polarizing beam splitter, AOM:acousto-optic modulator, L:lens, CL:cylindrical lens, $\lambda/4$:quarter-wave plate, BD:beam dump, EOM:electro-optic modulator, LP:linear polarizer, W:glass wedge, PD:photodiode.

any back-reflection.

The amplified output is first split into two paths using a half-wave plate and a polarizing beam splitter cube ($\lambda/2$ and PBS in Figure 2.8) (this combination will be referred to as $\lambda/2$-PBS). One of the paths is used for the 2DMOT. The 2DMOT laser path (labelled as 2DMOT in Figure 2.8) is split into four paths using a $\lambda/2$-PBS and two 50-50 non-polarizing beam splitter cubes (NPBS in Figure 2.8). A circular polarization required for the 2DMOT operation is produced by having each of the four paths to go through a quarter-wave plate ($\lambda/4$ in Figure 2.8). These beams then go through pairs of cylindrical lenses (1- and 10-cm focal lengths, CL in Figure 2.8) for beam expansion. The expanded laser beams are sent to the 2DMOT chamber (details of the 2DMOT setup are given in Section 2.9).

The other path is used for multiple applications: optical pumping and frequency stabilization of the detection lasers (447- and 1532-nm lasers). The laser frequency is adjusted by using two acousto-optic modulators (AOMs) for each application. This path first goes through a PBS and an AOM (AOM1 in Figure 2.8) in the dual-pass configuration [33, 39]. The AOM is driven by a continuous wave (CW) RF signal with the frequency $f_{\mathrm{AOM1}} = 185\,\mathrm{MHz}$. This AOM produces three laser paths with different frequencies. The frequency-unshifted laser path (OP in Figure 2.8) is used for the optical pumping of the $2^3\mathrm{S}_1$ state. This path is coupled into a fiber-based electro-optic modulator (fiber-EOM in Figure 2.8) (the use of the

EOM is explained in Section 2.8). The output of the fiber-EOM goes through a linear polarizer and a quarter-wave plate (LP and $\lambda/4$ in Figure 2.8) to produce an appropriate polarization for the optical pumping. It is then sent to the main experiment chamber. The first-order diffracted path is retro-reflected back into the AOM. The dual-pass produces two paths with frequency shifts of $+f_{\mathrm{AOM1}}$ and $+2f_{\mathrm{AOM1}}$. The path with the frequency shift of $+f_{\mathrm{AOM1}}$ (labelled as 447 locking in Figure 2.8) is used as a pump laser for the 447-nm laser frequency stabilization (the 447-nm laser system is described in Section 2.6.1). The path with the $+2f_{\mathrm{AOM1}}$ frequency shift (labelled as locking in Figure 2.8) is sent to the second AOM (AOM2 in Figure 2.8). This AOM is also in the dual-pass configuration driven by a CW RF signal with the frequency $f_{\mathrm{AOM2}} = 175\,\mathrm{MHz}$. AOM2 is configured such that the dual-pass output path acquires a frequency shift of $-2f_{\mathrm{AOM2}}$. The dual-pass output of AOM2 acquires a net frequency shift of $2f_{\mathrm{AOM1}} - 2f_{\mathrm{AMO2}} = +20\,\mathrm{MHz}$ with respect to the initial laser frequency (laser diode output frequency). This path is split by a $\lambda/2$-PBS and sent to the frequency stabilization setups for this laser itself (which locks it to the 2^3S_1-to-2^3P_2 transition) and for the 1532-nm laser (the 1532-nm laser system is described in Section 2.6.2).

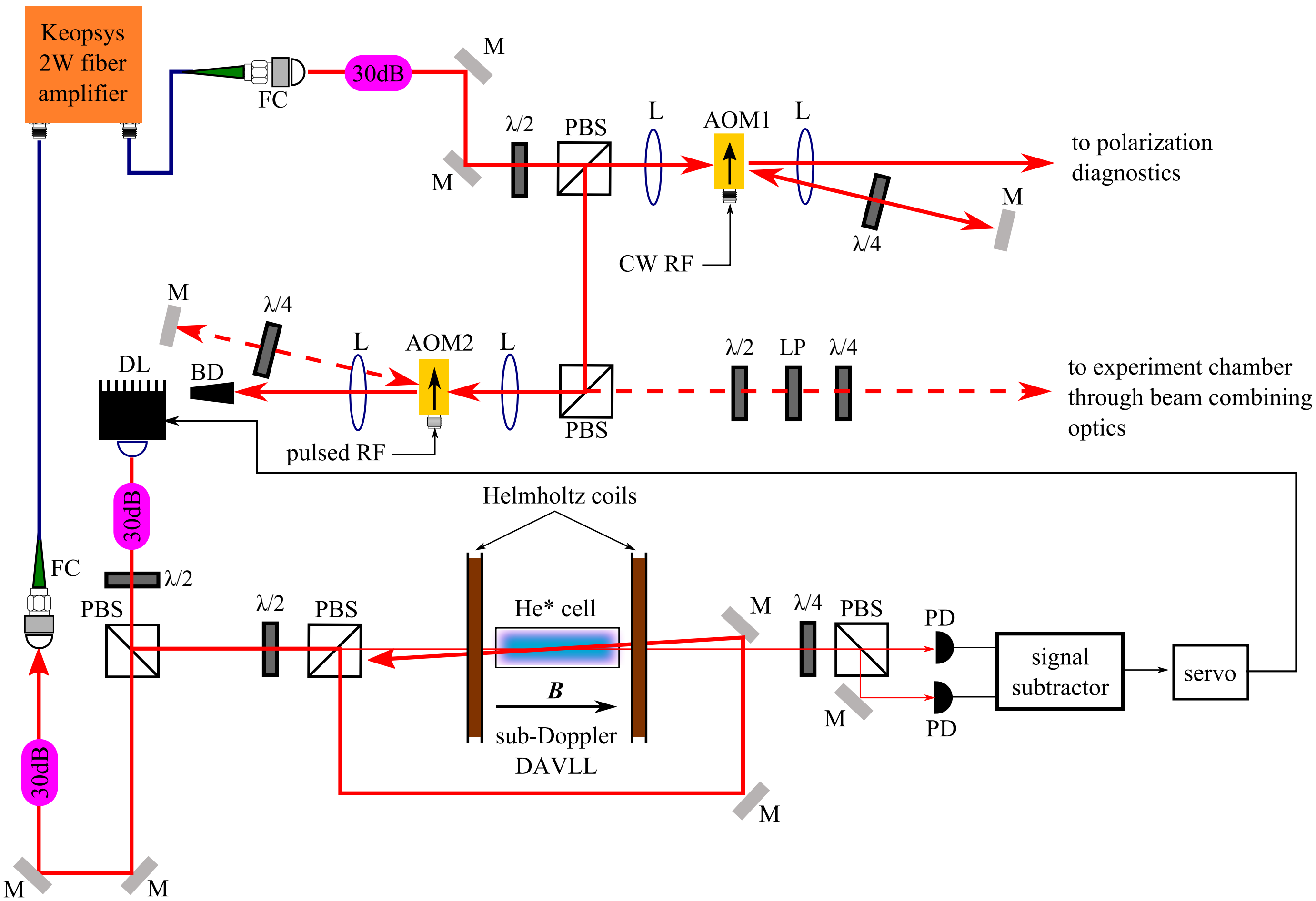

Figure 2.9: 1083-nm 2^3S_1-to-2^3P_1 laser system. DL:diode laser, M:mirror, 30dB:30-dB optical isolator, FC:fiber coupler, $\lambda/2$:half-wave plate, PBS:polarizing beam splitter, AOM:acousto-optic modulator, L:lens, $\lambda/4$:quarter-wave plate, BD:beam dump, LP:linear polarizer, PD:photodiode. Dashed lines indicate the pulsed laser paths.

2.5.2 2^3S_1-to-2^3P_1 Laser System

Figure 2.9 shows the schematic diagram of the 2^3S_1-to-2^3P_1 laser system. This laser excites the 2^3S_1-to-2^3P_1 transition to prepare atoms in the 2^3P_1 state. A same model of DBR laser as in the 2^3S_1-to-2^3P_2 laser system is used (DL in Figure 2.9). The laser light from the diode first goes through a 30-dB optical isolator to reduce the back-reflection into the laser diode. It is then split into two paths. One is used for the frequency stabilization (sub-Doppler DAVLL in Figure 2.9, which will be discussed in Section 2.5.3), and another path is sent to the Keopsys 2-W fiber amplifier. The output of the amplifier goes through a 30-dB isolator to minimize the back-reflection into the amplifier. The amplified output goes through two AOMs in the dual-pass configuration. The first AOM (AOM1 in Figure 2.9) is driven by a CW 200-MHz RF signal. The dual-pass output of this AOM acquires a net downward frequency shift of 400 MHz. The second AOM (AOM2 in Figure 2.9), driven by a pulsed RF signal, produces laser pulses used for the main experiment (laser pulsing is detailed in Section 2.11.3). AOM2 shifts up the laser frequency so that the net frequency shift from the two AOMs is close to zero. The laser pulses are sent to the main experiment chamber after being combined with the detection lasers (Sections 2.6.1 and 2.6.2). The polarization of the pulsed laser is adjusted by using the combination of a half-wave plate, a linear polarizer, and a quarter-wave plate ($\lambda/2$, LP, and $\lambda/4$ in Figure 2.9, respectively). The linear polarizer sets the polarization orientation for the experiment, and the $\lambda/4$-plate compensates for the birefringence associated with optics that this laser beam goes through before interacting with atoms. The half-wave plate controls the optical power used for the experiment by rotating the polarization before the linear polarizer. The unshifted output from the AOM1 is used for diagnostics of the polarization of this laser when interacting with atoms.

2.5.3 Stability of the 1083-nm Lasers

The sub-Doppler dichroic-absorption-vapor-laser lock (DAVLL) technique [40–42] is employed for the frequency stabilization of both 1083-nm lasers. The sub-Doppler DAVLL setup is shown in both Figures 2.8 and 2.9. A typical saturated absorption spectroscopy setup with a pair of Helmholtz coils around the RF-discharge cell constitutes the sub-Doppler DAVLL setup. The Helmholtz coils set up a DC magnetic field aligned with the laser propagation axis. Linearly polarized counter-propagating pump and probe beams are overlapped within the cell. The applied magnetic field lifts the degeneracy of the magnetic sublevels and sets the quantization axis of the atoms. The linearly polarized light that propagates along the atom's quantization axis can be represented as light whose polarization is a linear combination of σ^+ and σ^- polarizations. This implies that both $\Delta m = +1$ and $\Delta m = -1$ transitions are driven simultaneously within the cell. The $\Delta m = +1$ and $\Delta m = -1$ transitions are Zeeman shifted by $\pm g\mu_B B/h$, where g is the Lande g-factor, μ_B is the Bohr Magneton, B is the applied magnetic field, and h is the Planck constant. The σ^+ and σ^- polarization components are split by a quarter-wave plate and a polarizing beam splitter. The two signals, $\Delta m = +1$ and $\Delta m = -1$ absorption signals, are then subtracted to obtain the error signal necessary for the frequency stabilization. The error signal is fed to a 100-kHz analog PID controller (SRS SIM960). The correction signal is applied to the current modulation input of the diode laser controller. To enhance the long-term stability of the laser frequency, a secondary feedback is applied to the temperature fine-adjust input of the laser controller.

Unlike the original DAVLL technique [43] where a Doppler broadened transition is used to obtain the error signal, the sub-Doppler DAVLL technique uses a narrow Doppler-free absorption signal for the error signal generation. The sub-Doppler DAVLL technique provides a higher frequency-noise sensitivity and a smaller magnetic field requirement for the error signal generation.

A beat-note detection [44] is set up using the two lasers to evaluate the frequency stability of each laser. The two lasers are both tuned to the 2^3S_1-to-2^3P_1 transition for this test and have slightly different lockpoints ($\sim 20\,\mathrm{MHz}$). The two laser beams are overlapped and sent to a fast photodiode for the beat-note detection. The frequency of the beat-note is monitored and tallied into a histogram. The histogram

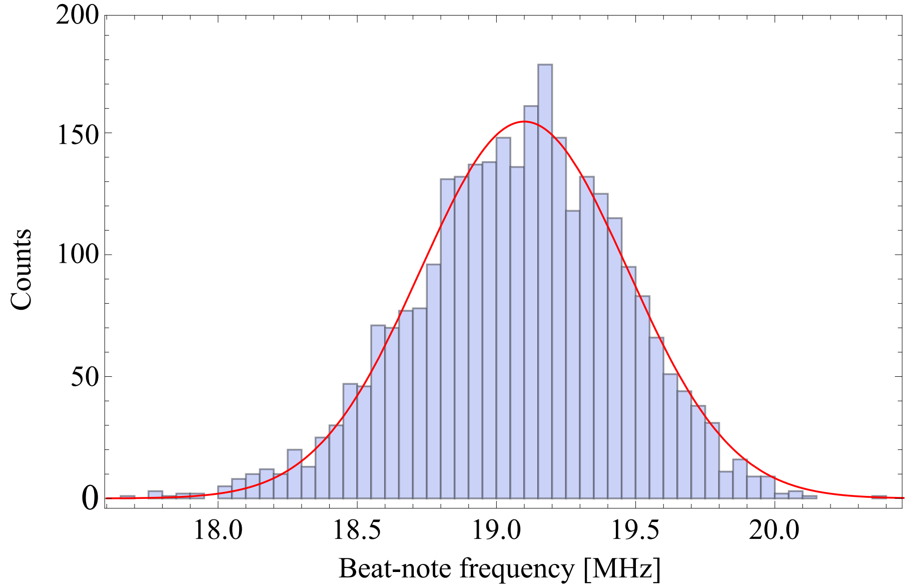

Figure 2.10: A histogram showing the 1083-nm laser frequency stability. The beat-note frequency is monitored and beat-note centre is tallied to estimate the frequency jitter.

of the beat-note frequencies is shown in Figure 2.10. The histogram is fit to a Gaussian function to extract the width of the distribution. Fit results show that each 1083-nm laser is locked to about ± 500 kHz.

2.6 Detection Laser Systems

Shortly after the microwave drives the 2^3P_1-to-2^3P_2 transition, subsequent 447- and 1532-nm lasers (laser B and C in Figures 2.2, 2.1, and 2.3) excite 2^3P_2 atoms up to the 18^3P Rydberg state for the Stark-ionization detection. This section describes the setup of the 447- and 1532-nm laser systems.

2.6.1 447-nm 2^3P_2-to-4^3D_3 Laser System

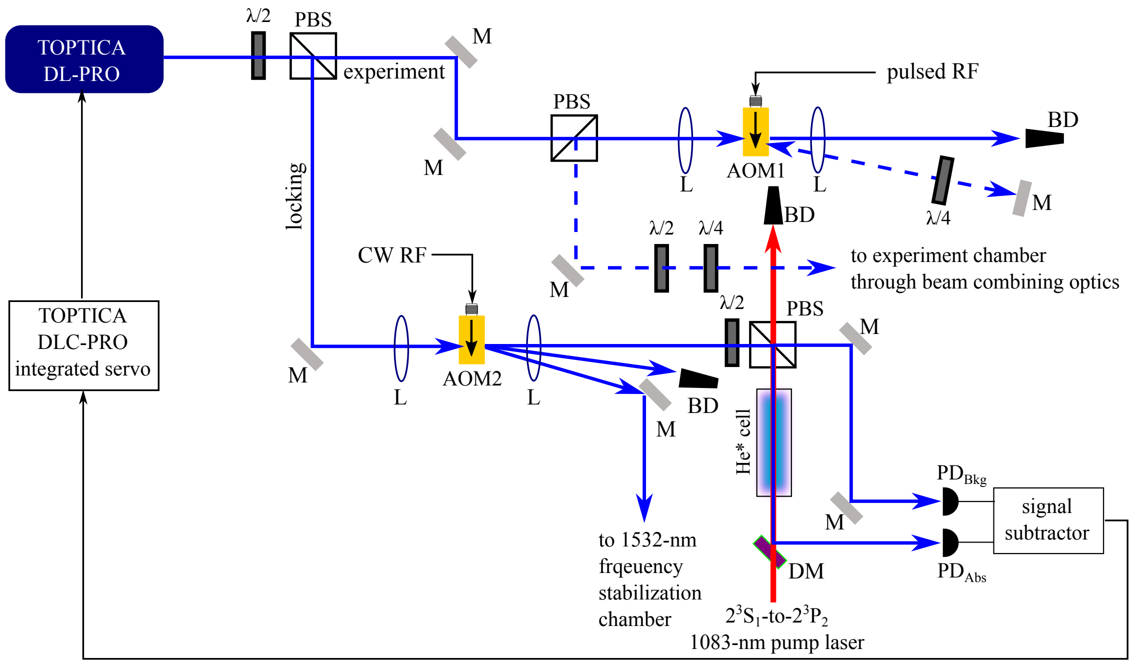

Figure 2.11: 447-nm 2^3P_2-to-4^3D_3 laser system. M:mirror, $\lambda/2$:half-wave plate, PBS:polarizing beam splitter, AOM:acousto-optic modulator, L:lens, $\lambda/4$:quarter-wave plate, BD:beam dump, DM:dichroic mirror, PD:photodiode. Dashed lines indicate the pulsed laser paths.

Figure 2.11 shows the schematic diagram of the 447-nm laser system. The 447-nm laser is used to drive the 2^3P_2-to-4^3D_3 transition and is also used for the frequency stabilization of the 1532-nm laser. 40-mW of 447-nm laser light is produced by the external-cavity diode-laser system (Toptica DL-PRO HP). The laser beam is first split into two paths. One of the paths is used for the frequency stabilization of this laser and of the 1532-nm laser, and the other path is used for the main experiment (labelled as experiment in Figure 2.11). The path for the main experiment goes through an AOM (AOM1 in Figure 2.11) in the dual-pass configuration. This AOM is driven by a pulsed RF signal to generate the laser pulses for the experiment (laser pulsing is detailed in Section 2.11.3). The frequency of the laser pulses is shifted by $2f_{\mathrm{RF}}$ relative to the other path. f_{RF} is typically set around 200 MHz because the AOM diffraction efficiency peaks at that frequency. The driving frequency of AOM1 is changed slightly for different experiment settings. The laser path for the frequency stabilization goes through another AOM (AOM2 in Figure 2.11). The unshifted path is sent to the laser-locking setup, and the second-order diffracted path is sent to the 1532-nm laser-locking chamber. The second-order diffraction path acquires a same frequency shift ($2f_{\mathrm{RF}}$) as the pulsed laser. The laser frequency needs be locked $2f_{\mathrm{RF}}$ away from the resonance to have the pulsed laser path and 1532-nm laser-locking path to be on the atomic resonance.

The laser-locking setup consists of two paths. One of the paths is sent to the helium discharge cell (He* cell in Figure 2.11) and is overlapped with a counter-propagating 1083-nm pump laser inside the cell. The two laser beams are overlapped using a dichroic mirror (DM in Figure 2.11). The 447-nm laser absorption signal is monitored on a photodiode ($\mathrm{PD_{Abs}}$ in Figure 2.11). The 1083-nm pump laser continuously excites the $2^3\mathrm{S}_1$-to-$2^3\mathrm{P}_2$ transition to maintain a constant population in the $2^3\mathrm{P}_2$ state and the 447-nm laser drives the $2^3\mathrm{P}_2$-to-$4^3\mathrm{D}_3$ transition. The other path goes straight to a photodiode ($\mathrm{PD_{Bkg}}$ in Figure 2.11) for background subtraction of the absorption signal.

The compensation for the frequency shift caused by the AOM1 is achieved by using a Doppler-shifted resonance of the 447-nm 2^3P_2-to-4^3D_3 transition induced by the detuning of the 1083-nm pump laser. The velocity distribution of atoms inside the cell is described by the Maxwell-Boltzmann distribution. The Doppler-broadening of the transition due to the velocity distribution allows atoms to be on resonance with a wide range of the 1083-nm laser detuning. The Doppler width of a transition is

$$\Delta\nu_{\text{Doppler}} = \frac{2\nu_0}{c}\sqrt{\frac{2\ln(2)k_B T}{m_{\text{He}}}}, \tag{2.2}$$

where ν_0 is the transition frequency, c is the speed of light in vacuum, k_B is the Boltzmann constant, T is the temperature in kelvin, and m_{He} is the helium mass. At room temperature ($T \sim 300\,\text{K}$), the Doppler width of the 1083-nm 2^3S_1-to-2^3P_2 transition is 1.7 GHz. The detuned pump laser excites atoms in a particular velocity group, and the 447-nm laser interacts with these moving 2^3P_2 atoms, giving rise to a Doppler-shifted resonance of the 447-nm 2^3P_2-to-4^3D_3 transition. Locking the laser frequency onto the Doppler-shifted absorption signal of the 447-nm 2^3P_2-to-4^3D_3 transition compensates for the AOM frequency shift if the detuning of the 1083-nm laser is appropriately chosen. Since the atoms see a 2.4 times (f_{447}/f_{1083}) larger Doppler shift for the 447-nm 2^3P_2-to-4^3D_3 transition than for the 1083-nm 2^3S_1-to-2^3P_2 transition, the relationship between the detuning of the 1083-nm pump laser and 447-nm laser is

$$\Delta f_{\mathrm{lock}}(447) = -2.4 \times \Delta f_{\mathrm{pump}}(1083), \tag{2.3}$$

where the negative sign results from the fact that the two lasers are counter-propagating. Using Equation 2.3, the 1083-nm pump laser detuning required to compensate for the typical 400 MHz shift on the 447-nm laser is 165 MHz.

A conventional frequency-modulated error signal generation method is used for stabilizing the 447-nm laser frequency [45]. The frequency-modulated 447-nm absorption signal is sent to the integrated servo circuit of the laser diode controller (TOPTICA DLC-PRO) to obtain the error signal. The correction signal is applied to the piezo-controlled grating mount and the driving current of the diode.

2.6.2 1532-nm 4^3D_3-to-18^3P_2 Laser System

Figure 2.12 shows the schematic diagram for the 1532-nm 4^3D_3-to-18^3P_2 laser system. The 1532-nm laser drives the final transition that brings atoms in the 4^3D_3 state up to the 18^3P_2 state for Stark ionization. The laser light is produced by a DBR laser diode in a butterfly package (Alcatel A1905LMI, DL in Figure 2.12), which outputs an optical power of 20 mW. The laser output is coupled into a 200-mW erbium-doped fiber amplifier (Thorlabs EDFA100P). The output from the amplifier is pulsed using an AOM in a single-pass configuration (laser pulsing is detailed in Section 2.11.3). The laser pulses are sent to the main experiment chamber after

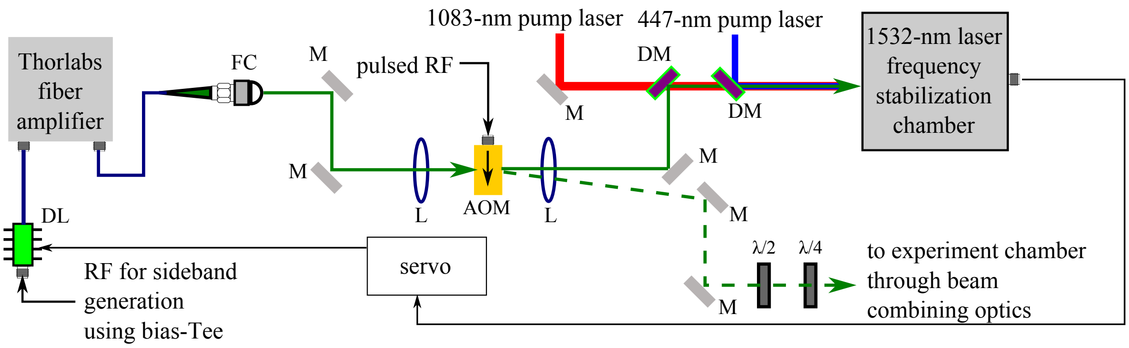

Figure 2.12: 1532-nm 4^3D_3-to-18^3P_2 laser system. DL:diode laser, M:mirror, FC:fiber coupler, $\lambda/2$:half-wave plate, AOM:acousto-optic modulator, L:lens, $\lambda/4$:quarter-wave plate, LP:linear polarizer, DM:dichroic mirror. Dashed line indicates the pulsed laser path.

being combined with the 1083- and 447-nm laser pulses (described in Sections 2.5.1 and 2.6.1). The unshifted laser beam is used for the frequency stabilization. This laser is overlapped with the 1083- and 447-nm pump lasers using two dichroic mirrors. The overlapped lasers are sent to the frequency stabilization chamber in which some fraction of metastable helium atoms in the beamline are excited to the Rydberg state and ionized. The laser frequency is stabilized to the resonance of the ion signal. This lock-to-beam method is necessary since the RF electric field in the discharge cell perturbs the Rydberg states and the 1532-nm laser cannot excite the 4^3D_3-to-18^3P_2 transition inside the cell. Figure 2.13 shows a cross-sectional view of the Stark ionizer for the frequency stabilization. The overlapped lasers interact with the beam of metastable atoms and produce 18^3P Rydberg atoms. The Rydberg atoms are then ionized by a DC electric field set up between a copper

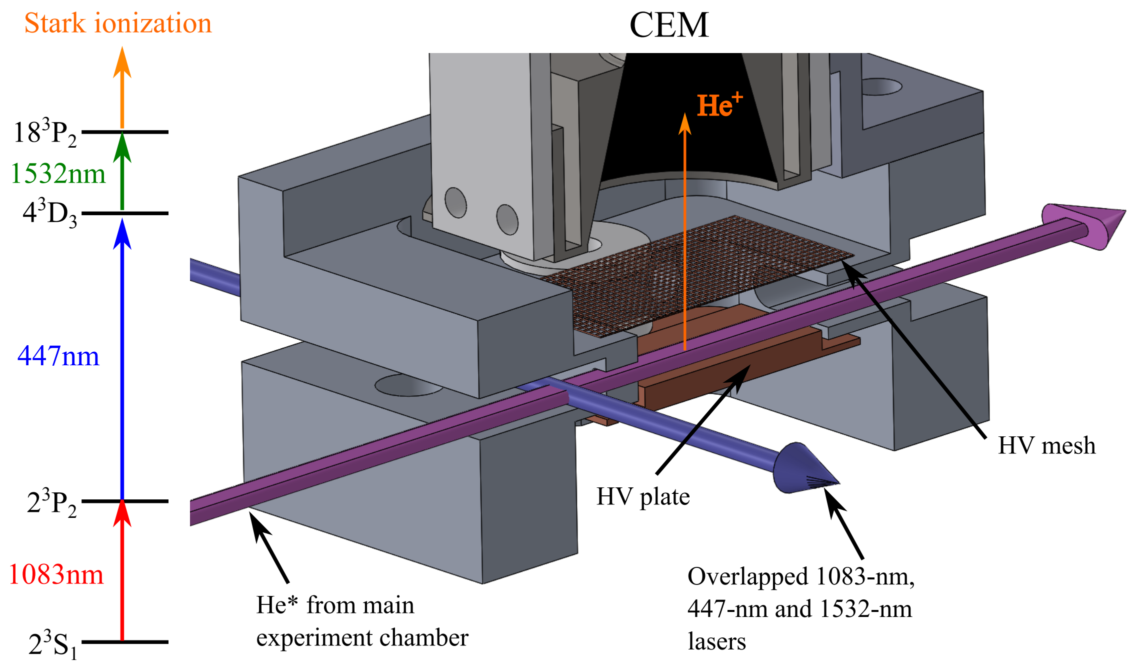

Figure 2.13: Cross-sectional view of the Stark ionizer for 1532-nm laser frequency stabilization. The energy level diagram for the ionization scheme is shown at the left. The overlapped lasers and metastable helium beam intersect at the field-free region and 18^3P atoms are created. The 18^3P atoms then proceed to the region with the ionizing electric field. Resulting ions are accelerated towards the CEM and counted.

plate and a copper mesh with 90 % transparency (HV plate and HV mesh in Figure 2.13). The two electrodes are separated by 5 mm. The laser excitation is isolated from the ionizing electric field by a 1-mm-by-5-mm slit with a wall thickness of 5 mm, because any residual electric field at the interaction location would cause a lineshape distortion due to the DC Stark effect on the 18^3P state. The helium ions are accelerated towards the CEM located above the copper mesh and the number of ions is counted. The frequency of the laser is modulated to obtain an error signal [45]. The correction signal is applied to the current modulation input of the laser diode controller. A secondary correction is applied to the temperature fine-adjust input of the controller. The frequency shift due to the AOM pulsing is compensated by utilizing the sideband-locking method. The laser diode package contains an integrated bias-Tee for current modulation. Small sidebands are added to the primary laser frequency by applying an RF signal to the bias-Tee. By locking the laser frequency onto the sideband resonance, the laser frequency is properly adjusted for the experiment. The lockpoint of this laser is manipulated by changing the driving frequency of the bias-Tee.

2.7 Stark-Ionization Detector for the Main Experiment

The Stark-ionization detector is shown in Figure 2.14. The energy-level diagram of the detection scheme is also shown. The simulation and design of the detector is done by Daniel Fitzakerly. Pulsed 1083-, 447- and 1532-nm lasers (Sections 2.5.2, 2.6.1, and 2.6.2) are combined and sent through the 14-mm microwave coaxial airline. Atoms that have undergone the microwave transition are excited up to the $18^3\mathrm{P}_2$ state inside the 14-mm microwave coaxial airline. The $18^3\mathrm{P}_2$ Rydberg state lives long enough ($\sim 6\,\mu$s) to allow the atoms to exit the coaxial airline before a significant fraction decays down to lower-energy states. A high-voltage wire grid composed of five pairs of 50-μm-diameter wires is positioned at the exit of the airline.

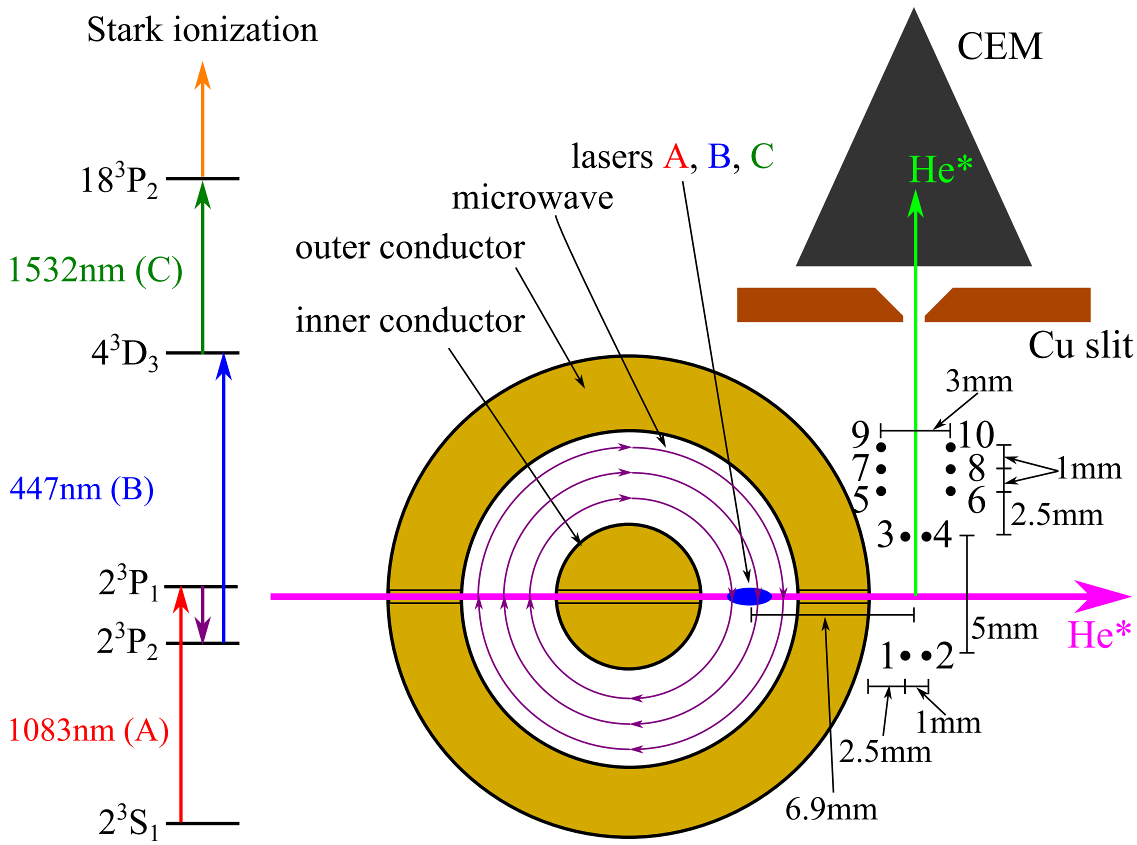

Figure 2.14: Stark-ionization detector. A number is assigned to each wire for convenience. Atoms excited up to 18P states are ionized in the area within wires 1 to 4. They are then guided by wires 5 to 10 into the copper slit. The number of ions passing through the copper slit is counted by the CEM detector.

An electric field applied by four wires (wires 1 to 4 in Figure 2.14) ionizes the 18^3P_2 atoms and accelerates the resulting ions towards the CEM. Six wires (wires 5 to 10 in Figure 2.14), positioned above the main ionizing wire grid, guide the ions into a 1-mm-wide slit machined into a copper plate. Table 2.3 shows the typical operation voltage setting of the wire grid. The high voltages are applied using two multichannel high-voltage power supplies (CAEN R1471ETD 8-channel and

HV part	1	2	3	4	5	6	7	8	9	10	Cu_{slit}	CEM
PS channel	ETD0	ETD1	ETD2	ETD3	ET0	ET1	ETD4	ETD5	ET2	ET3	ETD4	ETD5
voltage setting [V]	+1850	+1970	-2260	-1900	-750	-50	+280	+200	-100	-200	-1750	-1000

Table 2.3: Ionizer wire-grid voltage setting. HV part describes the part of the ionizer in Figure 2.14, PS channel are the power supply channels (ETD for R1741ETD and ET for R1740ET). The number after ETD and ET indicates the channel number of the power supply.

R1470ET 4-channel power supplies) The number of ions that passes through the copper slit is measured using a CEM detector. The CEM detector is particularly well suited for the ion detection because of its almost-unity ion detection efficiency and a gain factor which allows the detected signal to rise above the inherent noise floor for current detection. In this detection scheme, the main source of the background signal is collisionally ionized helium atoms and background gas molecules [46]. The background ion counts increase linearly as a function of the chamber pressure, so it is important to maintain the lowest pressure possible. The ionizer is designed such that the Ryderg atoms are ionized very locally, and ions created outside of the main ionization region are deflected away from the copper slit. This design greatly reduces the chance of background ions being detected by the CEM. The low background level and the high detection efficiency enabled us to achieve shot-noise limited detection.

Figure 2.15 shows a Fourier-transformed CEM signal. The nearly-frequency-

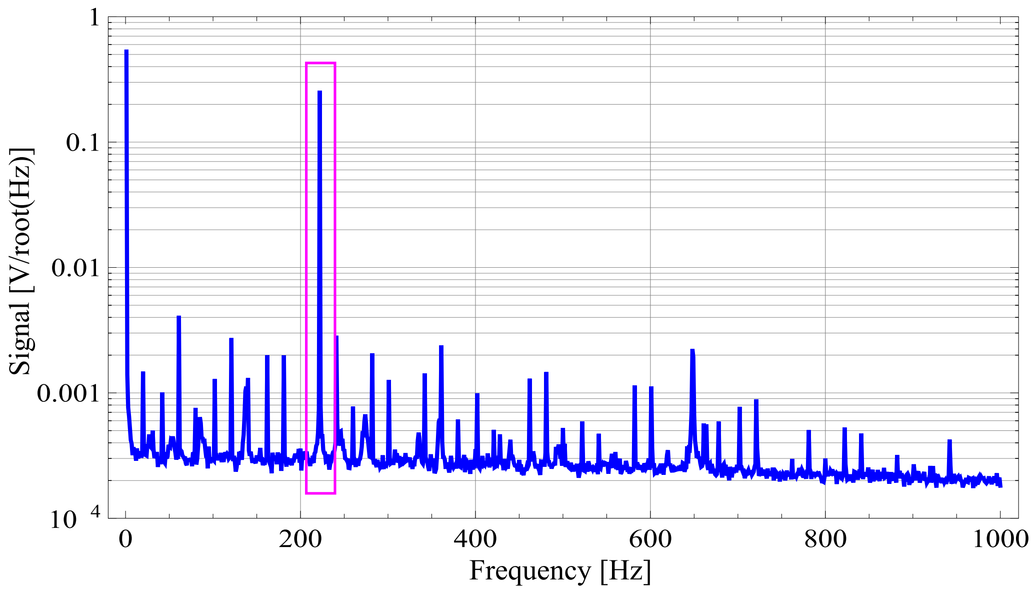

Figure 2.15: Fourier transformed CEM signal (see Section 2.11.1.2). The pink rectangle indicates the detected signal. The flat broadband noise spectrum indicates shot-noise limited detection if the FOSOF frequency is tuned away from the noise peaks in the spectrum.

independent noise floor shown is due to shot noise, and the peak shown in pink is the detected signal (see Section 2.11.1.2). The noise is dominated by the shot-noise of the signal itself. The other peaks in the Fourier-transformed signal are due to specific noise sources, such as harmonics of 60 Hz.

2.8 Optical Pumping of 2^3S_1 state

Figure 2.16 illustrates the optical pumping process of the 2^3S_1 states. The atoms in 2^3S_1 state are optically pumped into either m_J=+1 or m_J=−1 state using the

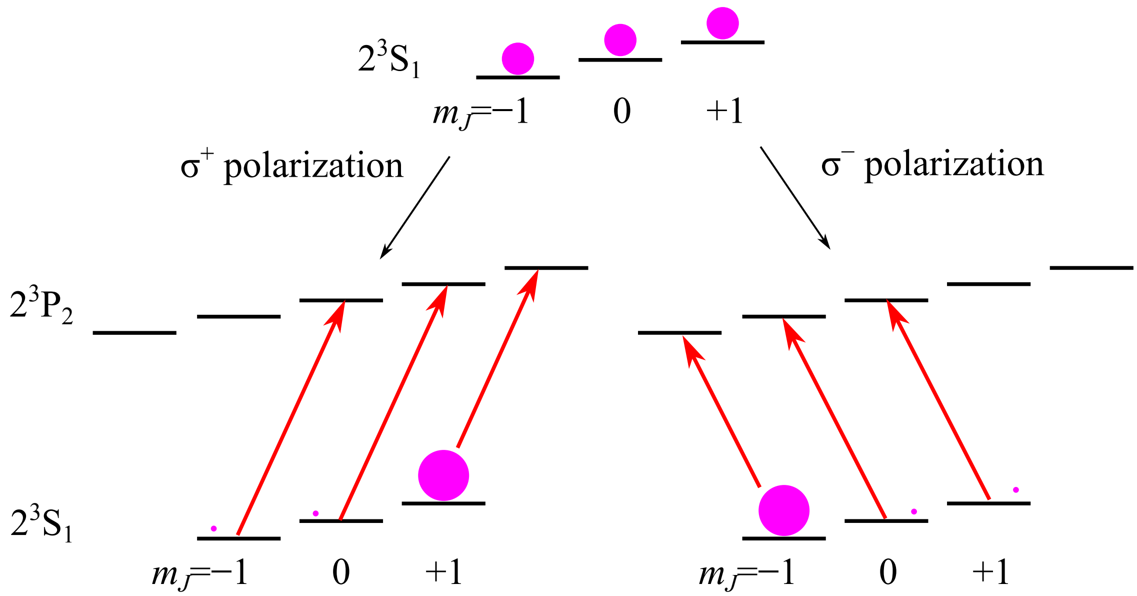

Figure 2.16: Optical pumping of 2^3S_1 states. Magnetic sublevels of 2^3S_1 states are equally populated before optical pumping. The pumping direction is determined by the circular polarization of the pumping laser. Small dots in the figure indicate left-over population after optical pumping.

1083-nm laser tuned to the 2^3S_1-to-2^3P_2 transition (OP in Figures 2.2 and 2.5.1) before they enter the main experiment region. The optical pumping ensures a clean experimental environment where only intended transitions are driven by the 1083-nm laser pulse (A in Figure 2.2). Optical pumping also increases the number of atoms that can be used for the experiment by a factor of 3 because the three magnetic sublevels of the 2^3S_1 state are initially equally populated. The handedness of the circular polarization (σ^+ or σ^- polarizations) that determines the direction of the optical pumping is changed by turning a quarter-wave plate by 90 degrees ($\lambda/4$ after the fiber-EOM in Figure 2.8). Almost all of the population in the 2^3S_1

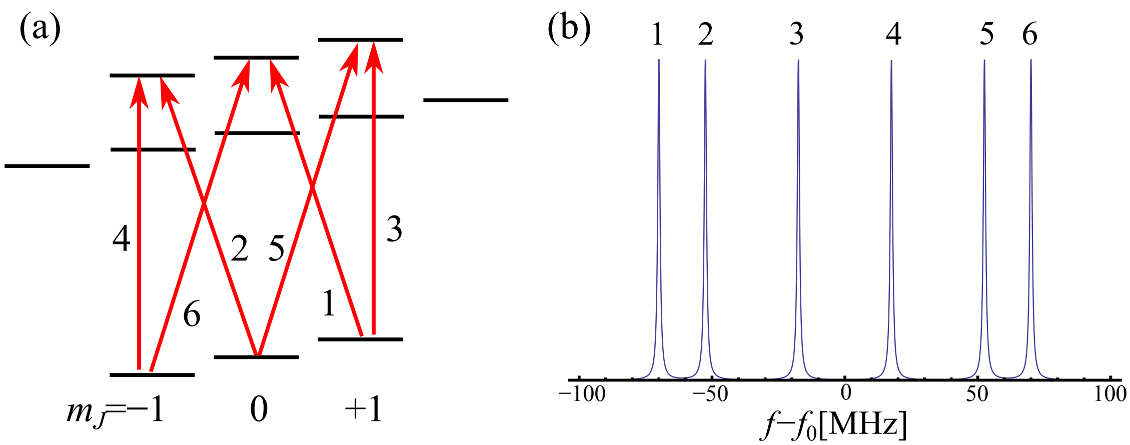

Figure 2.17: Expected lines of 2^3S_1-to-2^3P_1 Transition. Panel (a) shows the energy level diagram with possible transitions. Note that the 2^3S_1 ($m_J = 0$)-to-2^3P_1 ($m_J = 0$) is a forbidden transition. In a 25-G field, the transitions are expected to shift as shown in (b).

states is transferred into either the m_J=−1 or m_J=+1 state depending on the laser polarization. Half of the experimental data is taken with the optical pumping configured for the m_J=−1 state and the other half is for the m_J=+1 state, to test for any detection-state-dependent systematic effects. An EOM is used to ensure that the optical pumping works efficiently for a wide range of magnetic fields. The EOM driving RF frequency is changed for different magnetic field settings of the experiment (Section 2.10.3).

The efficiency of the optical pumping process is tested by sweeping the 2^3S_1-to-2^3P_1 laser frequency (laser A in Figure 2.14) while observing the Stark-ionization detection and observing the signal strength of possible transitions, as shown in Figure 2.17(b). The signal size of each of the possible transitions indicates the

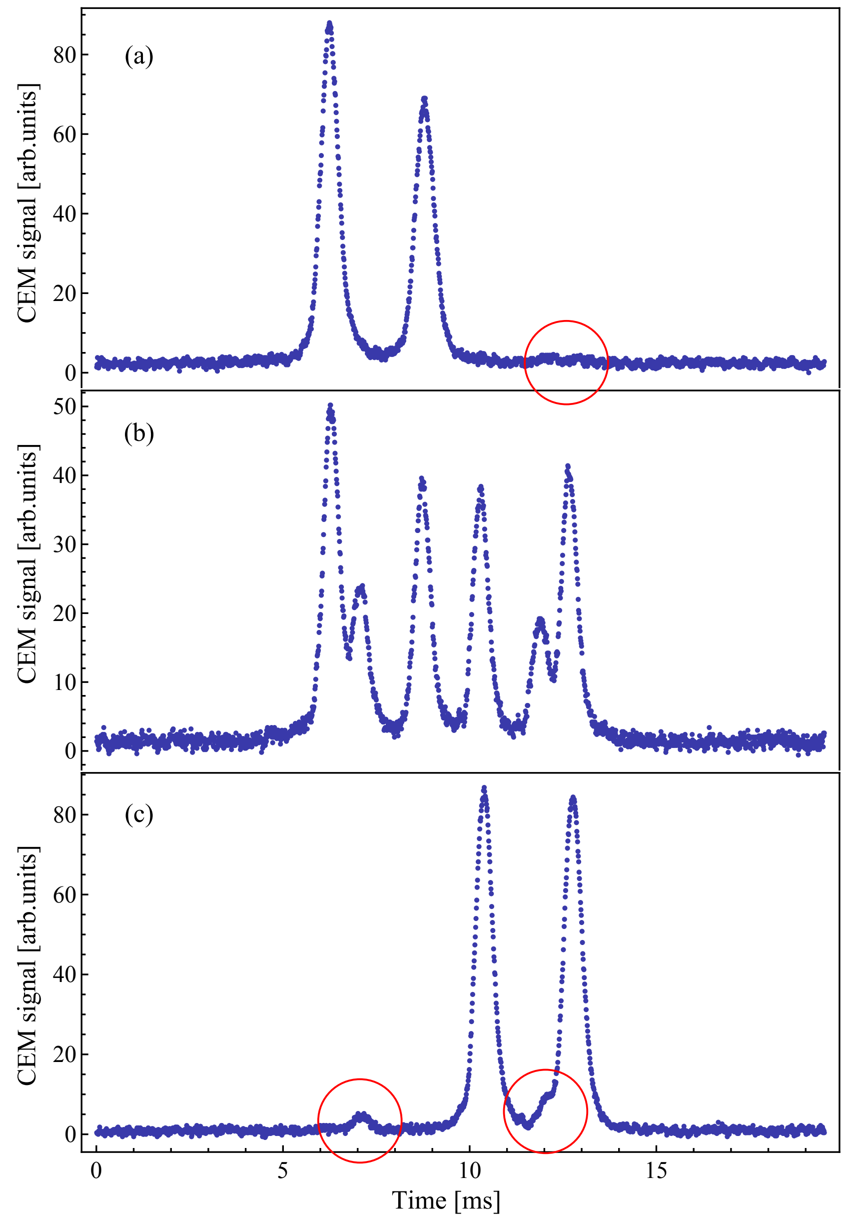

Figure 2.18: Experimental observation of optical pumping. The figure shows frequency scans of the 2^3S_1-to-2^3P_1 laser. The laser frequency increases from left to right in the figure. Panels (a) and (c) show how the population is transferred with optical pumping into the $2^3S_1(m_J{=}-1)$ and $2^3S_1(m_J{=}+1)$ states, respectively. Panel (b) shows the distribution of population without optical pumping. The red circles indicate the population left behind due to the imperfect laser polarization.

population in each magnetic sublevel of the 2^3S_1 state. For this test, the 2^3S_1-to-2^3P_1 laser is intentionally set to elliptical polarization to drive every possible transition in the system, and a large magnetic field ($\sim$ 25 G) is applied to the experiment region to Zeeman shift the transitions by a large amount, so that each transition is well resolved. The energy-level diagram of the possible transitions and expected lines as a function of the laser frequency (for a 25-G field) are shown in Figure 2.17. When all of the population is transferred into the $2^3S_1(m_J{=}{+}1)$ state, only lines 1 and 3 are detectable. Only lines 4 and 6 are detectable when atoms are pumped into the $2^3S_1(m_J{=}{-}1)$ state. Figure 2.18 shows the experimental verification for optical pumping. Frequency scans of the 2^3S_1-to-2^3P_1 laser are shown. Figure 2.18(b) shows the transitions without optical pumping. All magnetic sublevels of 2^3S_1 are occupied; therefore, all of the six transitions are visible. Figures 2.18(c) and 2.18(a) indicate the population with optical pumping. Two dominant peaks are visible in these two plots, as expected. The much smaller peaks inside of the red circles indicate left-over populations after the optical pumping due to an imperfect laser polarization. Note that these data were taken at the early stage of the experiment, and further improvements on the optical pumping quality were made later in the experiment. With the improved optical pumping system, $\sim$99 % pumping efficiency was achieved.

2.9 Two-Dimensional Magneto-Optical Trap (2DMOT)

The divergence of the metastable helium beam leads to a significant loss in the number of atoms that participate in the main experiment. In the current experiment, a two-dimensional magneto-optical trap (2DMOT) is used to intensify the metastable helium beam. A significant improvement in the signal-to-noise ratio (SNR) is realized. The theoretical framework of the method is well described in the literature [47–49], so only technical details are presented in this section.

2.9.1 2DMOT Setup

Figure 2.19 shows the 2DMOT setup. The inset in Figure 2.19 shows the cross section of the 2DMOT setup with magnetic field lines and laser polarizations. The setup consists of two 10-cm-long cooling sections that are separated by 5 cm (cooling lasers in Figure 2.19). The first section is positioned right after the skimmer hole, where atoms enter the 2DMOT chamber from the source. The role of the first cooling section is to trap as many atoms as possible before the beam expansion exceeds the spatial capture range of the 2DMOT. The second section, which is located 5 cm downstream from the first section, further focuses and concentrates the metastable atomic beam that are trapped in the first section, and it also allows for a small deflection of the beam. Four expanded 1083-nm laser beams that are

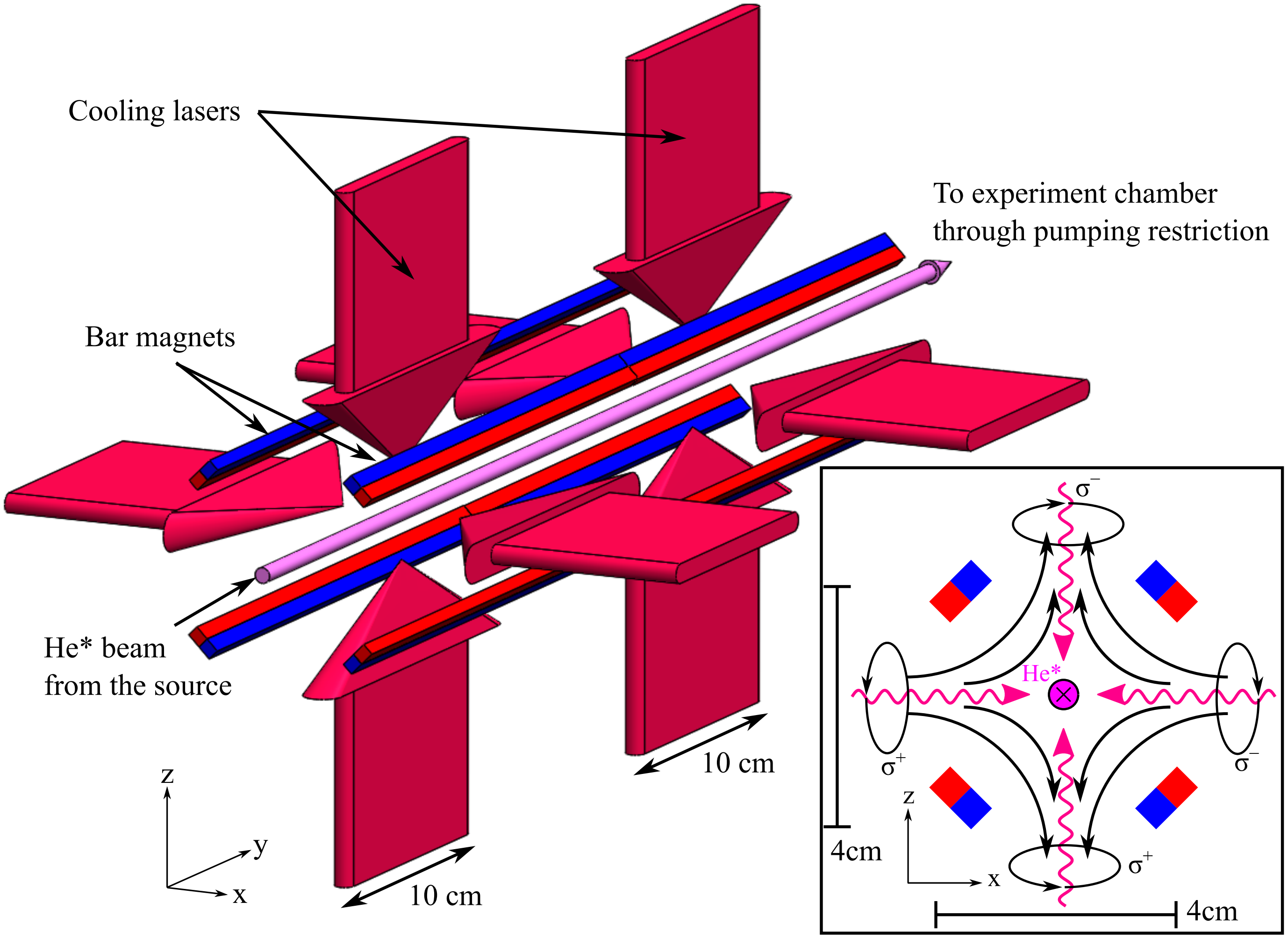

Figure 2.19: 2DMOT setup. A two-section 2DMOT is implemented. The inset shows the cross section of the 2DMOT with magnetic field lines and laser polarizations.

detuned by $-20\,\mathrm{MHz}$ from the 2^3S_1-to-2^3P_2 transition are used (Section 2.5.1). The polarization of each laser beam (σ^+ or σ^-, as shown in Figure 2.19) is chosen appropriately for the 2DMOT operation.

The two-dimensional quadrupole magnetic field required for the 2DMOT operation is produced by four 30-cm-long permanent bar-magnets [49] that are magnetized along their widths. The field within the cooling region is measured and mapped using a 3-axis Gaussmeter (Lakeshore 460 with probe MMZ-2508-UH). The vector plot in Figure 2.20(a) is constructed using the measured field. Figures 2.20(b) and 2.20(c) show the magnitudes of the magnetic fields along the x and z axes (the coordinate system is shown in Figure 2.19). Over the probed area of $\pm 3\,\mathrm{mm}$ from the beam axis, the magnetic field varies linearly along both axes. The data are fit to a linear model and the field gradients were found to be 13.8 ± 0.1 and 13.74 ± 0.04 Gauss/mm along the x and z axes, respectively.

The number of atoms that successfully pass through the entrance slit at the microwave region is occasionally checked with a Faraday cup on a translation stage that is installed between the main experiment chamber and the laser-locking chamber. The ion signal from the locking chamber and the TOF signal from the atom speed measurement chamber act as constant monitors of the 2DMOT operation.

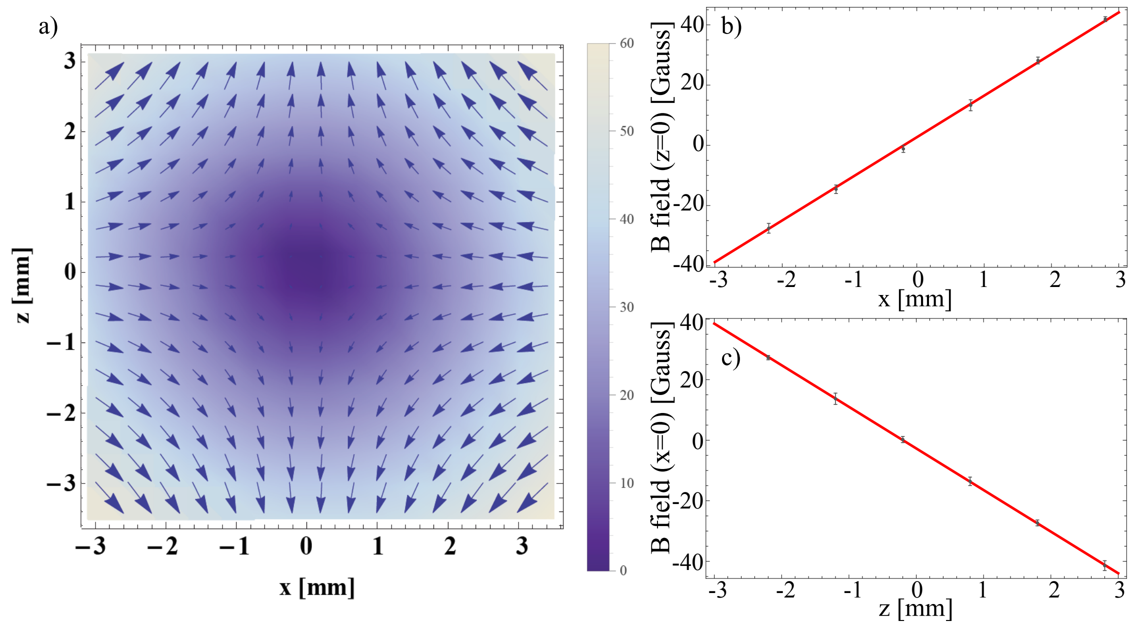

Figure 2.20: Magnetic field generated by the bar-magnets of Figure 2.19. Panel (a) shows the vector plot constructed from the measured fields. Panels (b) and (c) show the measured fields along the centre axes. The data is fit to a linear function to determine the field gradient, and it was found to be ≈13.8 Gauss/mm in both directions

2.9.2 Simulations of Atomic Trajectories

Using the geometry and fields described in the previous section, simple simulations were performed to estimate the operating parameters of the 2DMOT and to predict the atomic trajectories. The helium atoms emerging from the source have an initial diameter of 1 mm, and a uniform distribution of atoms within that area is assumed. The speed distribution of the atoms is estimated by the time-of-flight data described in Section 2.4. The initial speed of an individual atom is chosen using the probability distribution function described in [35]. An initial beam divergence of 50 mrad is assumed. The cooling laser is assumed to have an elongated Gaussian intensity profile. Figure 2.21 shows the simulated atomic trajectories with and without application of the 2DMOT to the beam. Trajectories indicated in green are without application of the 2DMOT. The blue lines are the simulated trajectories within the cooling section. The pink lines are the simulated trajectories after the atoms exit the 2DMOT section. Figures 2.21(a) and 2.21(b) show a significant compression of atoms within the 2DMOT region. Figures 2.21(c) and 2.21(d) indicate that the atomic transverse velocity components V_x and V_z are suppressed further by including the second cooling section. Figure 2.22 shows the simulated spatial distribution of atoms at the 0.5-mm-by-5-mm entrance slit to the airline. The green rectangle represents the slit, and the figure shows that the simulation predicts that most of the atoms enter this slit with the 2DMOT included in the system.

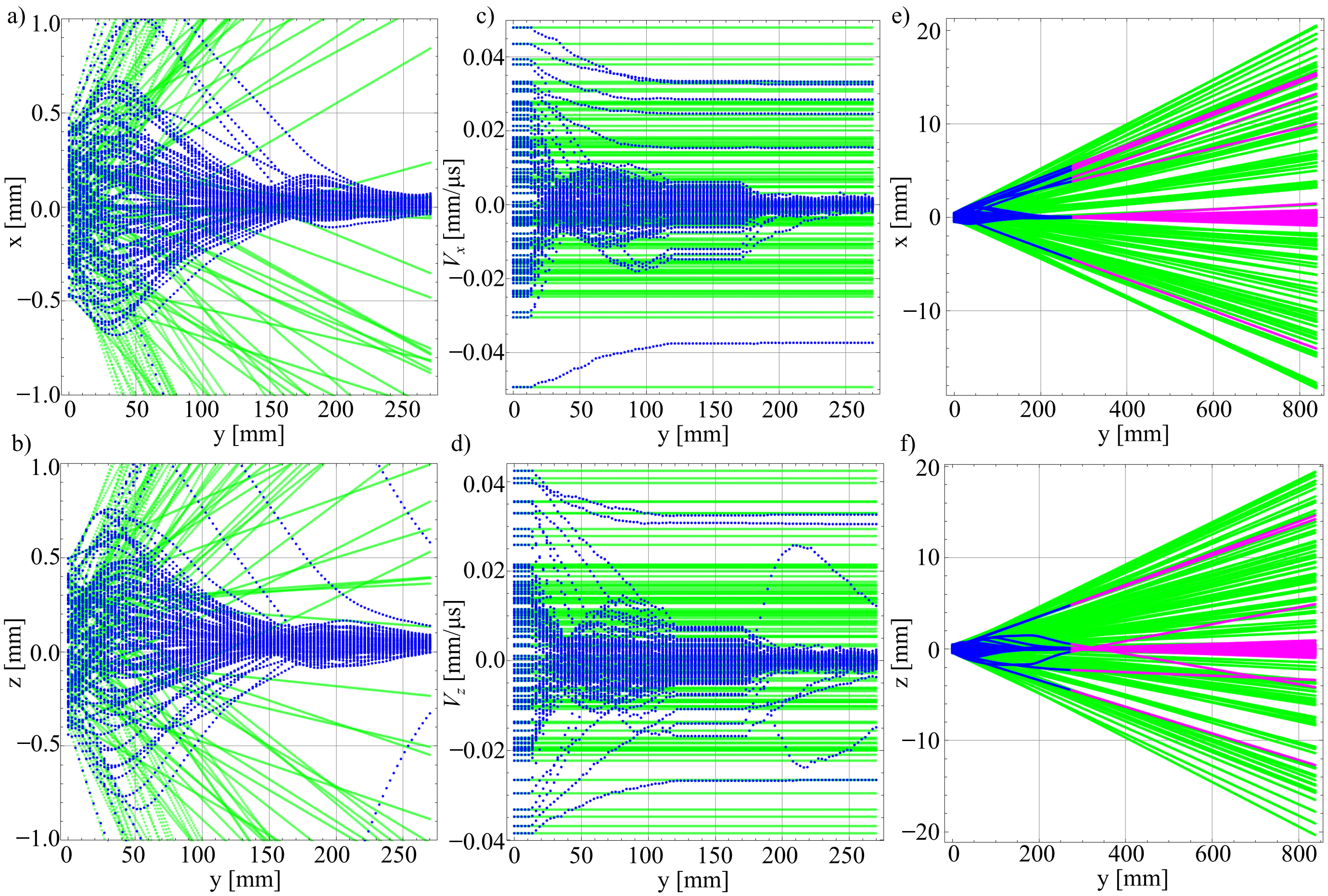

Figure 2.21: Simulation results of atomic trajectories. a) and b) show the atomic trajectory within the cooling region in the x and z directions. c) and d) show trajectory in the velocity space V_x and V_z. Panels e) and f) are the simulated trajectories after the cooling region. The blue trajectories indicate atoms that experience the cooling process. The green trajectories are without the 2DMOT applied. Pink points are the trajectories after the 2DMOT section.

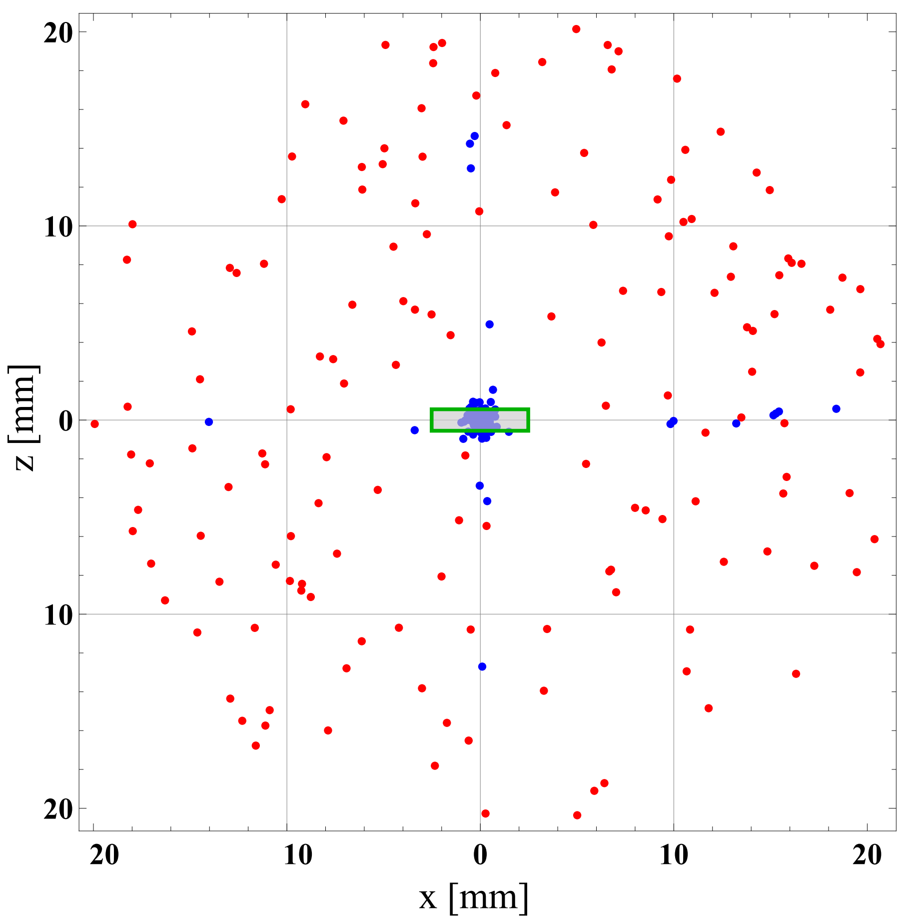

Figure 2.22: The simulated distribution of atoms at the microwave region. The red points indicate the distribution without application of the 2DMOT, and the blue points indicate the distribution with the 2DMOT. The green rectangle at the centre of the plot indicates the size of the entrance slit.

2.9.3 Improvements to the Experiment

The 2DMOT significantly increases the number of atoms that go through the entrance slit located at the main experiment region. The 2DMOT increased the metastable atom flux to 7×10^{12} He*/cm^2/s. Figure 2.23 shows the TOF signal (obtained using the chopper in Figure 2.6) recorded at the end of the beamline to illustrate the signal gain with the 2DMOT included in the system. In this plot, the signal height increased by about a factor of 25 and the speed distribution is shifted towards lower speeds. The number of atoms detected by the CEM is proportional to the area under the curve. The actual gain in the FOSOF signal of atoms is significantly more than the estimated factor of 25, at least in part due to the fact that slower atoms lead to larger signals. For the actual FOSOF experiment signal (Stark ionization signal described in Section 2.7), a signal gain of about a factor of 60 was observed. The large signal gain allows for a extensive study of systematic effects in a reasonable time frame.

The larger atomic flux along the beamline ensures a better SNR for the ion signal in the 1532-nm laser-locking chamber. As a result, the power of all lasers used in the production of the Rydberg atoms in the locking chamber can be reduced and a larger fraction of the laser power can be allocated for the main experiment.

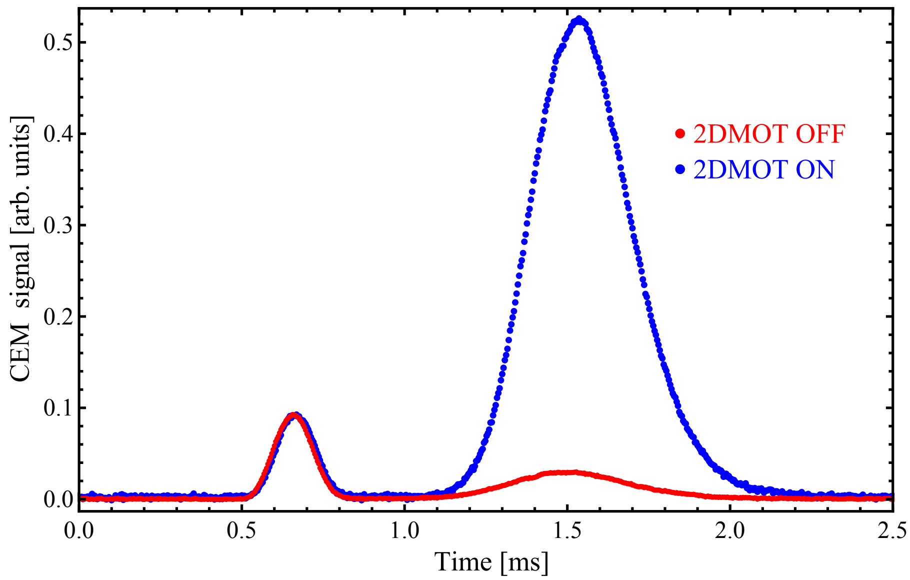

Figure 2.23: The TOF signal with and without the 2DMOT applied to the helium beam. A significant increase in signal size is observed. A shift in the arrival time is also seen in the plot. This shift is because the 2DMOT works better for the atoms moving slowly and it therefore favours these slower atoms.

2.10 Magnetic Field System

The magnetic field system for the current experiment is shown in Figure 2.24. Four pairs of nested coils are used to control the magnetic field around the experiment region. Their geometries and current-to-field conversion factors (k) are summarized in Table 2.4. Each pair of coils is characterized by measuring the field as a function of applied current using a three-axis gaussmeter at the approximate location of the experiment (the laser interaction region in Figure 2.14). The current applied to each pair of coils is monitored with a precision shunt resistor (IET Labs, DCCS/0.01).

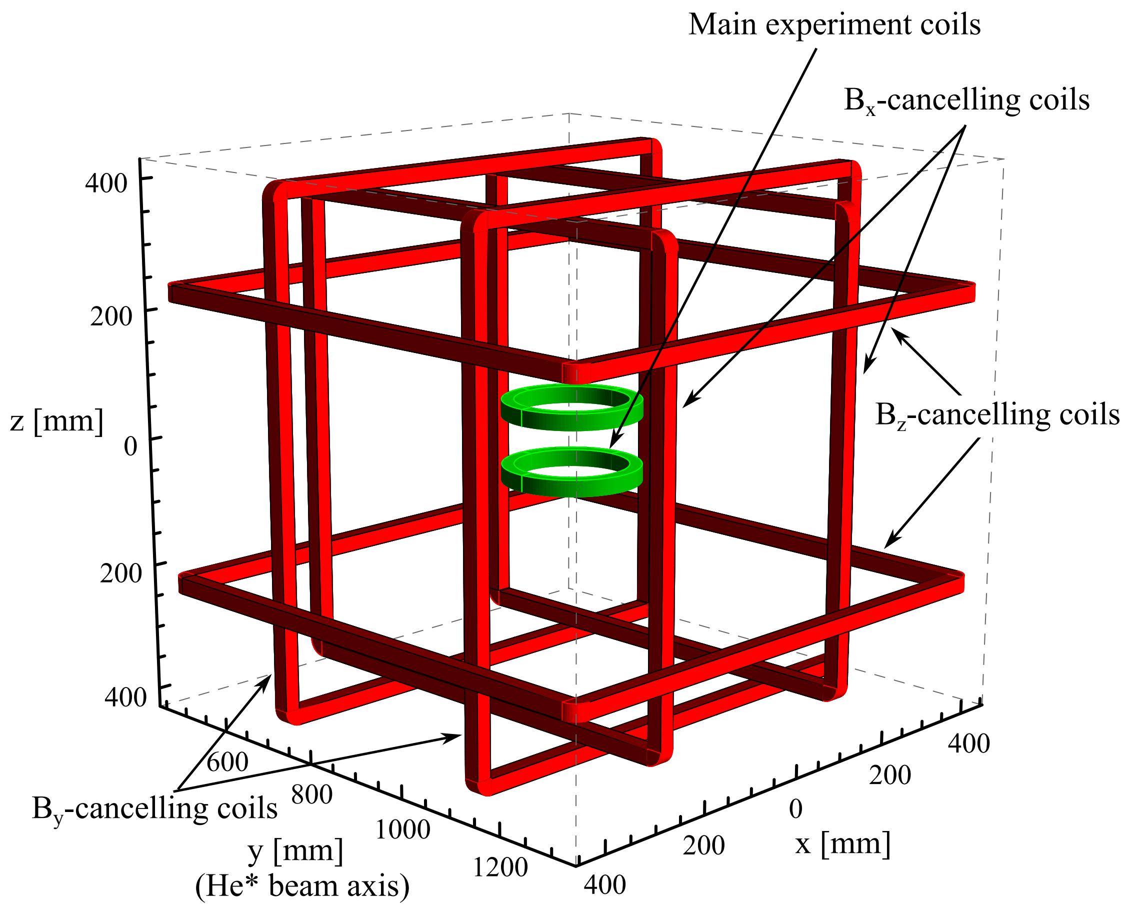

Figure 2.24: Coils used in the experiment. Coils in red are the residual field cancelling coils, and coils in green are the main field coils. These coils are centred on the intersection of the atomic beam axis and the airline axis of Figure 2.1.

2.10.1 Residual Field Cancelling Coils

The three pairs of coils (the red square coils in Figure 2.24) oriented along the x-, y-, and z-axis, designed based on [50], are used to cancel the three components of the background magnetic field around the experiment. These coils surround the main experiment chamber. The current to each pair of coils is supplied by

	Main Helmholtz coils	B_x-coils	B_y-coils	B_z-coils
Shape	Circular	Square	Square	Square
Dimensions	20 cm $\times$10 cm	73 cm$\times$73 cm$\times$39 cm	78 cm$\times$78 cm$\times$43 cm	83 cm$\times$83 cm$\times$45 cm
k [Gauss/A]	10.866$\pm$0.010	3.470$\pm$0.010	3.241$\pm$0.010	3.074$\pm$0.010

Table 2.4: Summary of magnetic field coil parameters. The current-to-field conversion factor k is determined by measuring the field as a function of applied current. Dimensions are given in (coil radius)$\times$(coil separation) for the main experiment coils, and (side length)$\times$(side length)$\times$(coil separation) for the background field cancelling coils.

a triple-output DC power supply (Keithley 2231A-30-3). Each component of the background magnetic field is cancelled to approximately 10 mG. The uncertainty of 10 mG is assigned to each residual field component due to the fluctuation of the gaussmeter reading and the uncertainty associated with the position of the probe.

2.10.2 Main Helmholtz Coils

The pair of green coils in Figure 2.24 applies a magnetic field to lift the degeneracy of the magnetic sublevels of the $2^3\mathrm{P}_1$ state, as well as to test for magnetic field related systematic effects. Each coil is made of 123 turns of 2.6-mm enamel-coated copper wire and has a radius of 20 cm. This pair of coils is wound around an aluminium mount that is designed to host the microwave airline at the centre of the coils, where the magnetic field is most uniform. Since the coils are installed inside the vacuum

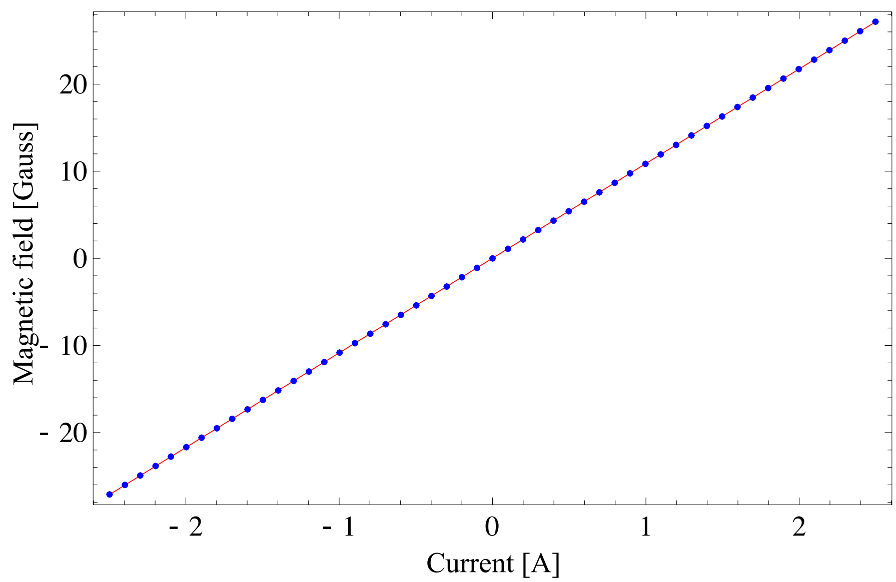

Figure 2.25: Magnetic field as a function of applied current. The data is fit to a linear model to extract the value of $k = B/I$. Uncertainties are smaller than the plotted points.

chamber, where the heat generated by the coils cannot be dissipated by convection, chilled water is fed into the vacuum chamber through a VCR feedthrough to cool the entire coil mount. The current to the coils is supplied by a precision current supply (Agilent E3648A). The magnetic field produced by the coils is proportional to the applied current I: $B = kI$, and a precise determination of the k-value is necessary to apply appropriate corrections to the experimental data. The value of 10.866 G/A listed in the Table 2.4 is determined to a precision of 0.001 G/A from the linear fit shown in Figure 2.25; however, the uncertainty associated with the probe positioning seems to dominates over the fit uncertainty (the position of the

	Optical pumping	1083-nm laser pulse	447-nm laser pulse	1532-nm laser pulse
Transition	2^3S_1-to-2^3P_2	2^3S_1-to-2^3P_1	2^3P_2-to-4^3D_3	4^3D_3-to-18^3P_2
Frequency shifting element	EOM	AOM	AOM	bias-Tee
RF source	Rigol 4162	SynthUSBII	SynthUSBII	Marconi2022

Table 2.5: Instruments for shifting laser frequencies to compensate for Zeeman shifts. The table summarizes the devices used to compensate for the first-order Zeeman shift for different laser applications. The transition used in each application is also shown. The frequency of the RF is varied for different magnetic field settings. Each entry in the RF source row is the name of the RF generator model.

experiment location cannot be known exactly, and the positioning of the probe is only approximate). An uncertainty of 10 mG/A is assigned to the k value of this pair of coils. The accuracy of k is re-evaluated using the experimental data in Section 4.1.2.

2.10.3 Laser Frequency Settings for Various Magnetic Fields

Laser frequencies need to be adjusted for different magnetic field settings to compensate for the first-order Zeeman shifts. Table 2.5 shows the laser applications and devices used to shift the laser frequencies. RF signals from the instruments shown in the table are fed into the frequency shifting elements. Table 2.6 shows the RF setting of each frequency shifting element for different magnetic field settings. Values in Table 2.6(a) are used when the optical pumping is configured to pump the 2^3S_1 population into the $m_J = +1$ state and Table 2.6(b) for the $m_J = -1$ state.

B [G]	I [A]	OP1 EOM [MHz]	OP2 EOM [MHz]	1083-nm AOM [MHz]	447-nm AOM [MHz]	1532-nm bias-Tee [MHz]
5	0.461	30	25	196.5	196.0	178.9
10	0.922	40	40	193.0	194.0	178.7
15	1.384	50	55	189.5	192.1	178.5
20	1.845	60	70	186.0	212.5	198.4
25	2.306	70	85	182.5	212.5	195.3
30	2.767	80	100	179.0	212.5	192.1
35	3.228	90	115	175.5	212.5	189.0

(a) RF generator settings when optical pumping is configured for the $m_J = +1$ state.

B [G]	I [A]	OP1 EOM [MHz]	OP2 EOM [MHz]	1083-nm AOM [MHz]	447-nm AOM [MHz]	1532-nm bias-Tee [MHz]
5	0.461	12.5	0	203.5	196.0	178.9
10	0.922	25.0	10	207.0	194.0	178.7
15	1.384	37.5	20	210.5	192.1	178.5
20	1.845	50.0	30	214.0	212.5	198.4
25	2.306	62.5	40	217.5	212.5	195.3
30	2.767	75.0	50	221.0	212.5	192.1
35	3.228	87.5	60	224.5	212.5	189.0

(b) RF generator settings when optical pumping is configured for the $m_J = -1$. state

Table 2.6: RF generator settings for different magnetic field settings. (a) shows the RF settings when optical pumping is configured for the $m_J = +1$ state. (b) is for the $m_J = -1$ state. OP1 and OP2 indicate the channel 1 and channel 2 outputs of the 2-channel Rigol 4162 arbitrary waveform generator, respectively.

The RF settings are found experimentally by optimizing the ionizer signal (Section 2.7) for each magnetic field setting.

2.11 Microwave and Laser Pulsing Systems for the Separated-Oscillatory-Fields Experiment

2.11.1 Separated-Oscillatory-Fields Technique

The present experiment exploits the newly developed frequency-offset separated-oscillatory-fields (FOSOF) technique [34], and is the first demonstration of the technique. The FOSOF technique is a variation of the Ramsey separated-oscillatory-fields (SOF) technique. The objective of this section is to provide an intuitive understanding of the SOF and FOSOF techniques. A brief mathematical description of the SOF and FOSOF lineshapes is given in Section 3.1.

2.11.1.1 Separated Oscillatory Fields on 2^3P_1-to-2^3P_2 Transition

Ever since Norman Ramsey's invention of separated-oscillatory-fields technique [51], it has been one of the most widely used methods in the field of precision measurements. The method uses an interference phenomenon to effectively narrow the transition linewidth to acquire higher resolution in measuring a transition linecentre in a quantum system. The natural linewidth, a resolution limit on a typical spectroscopy setup, can be overcome using this SOF interference, and the resulting sub-natural linewidth is used to achieve greater spectroscopic precision.

The two states involved in our measurement are the 2^3P_1 and 2^3P_2 states. Figure

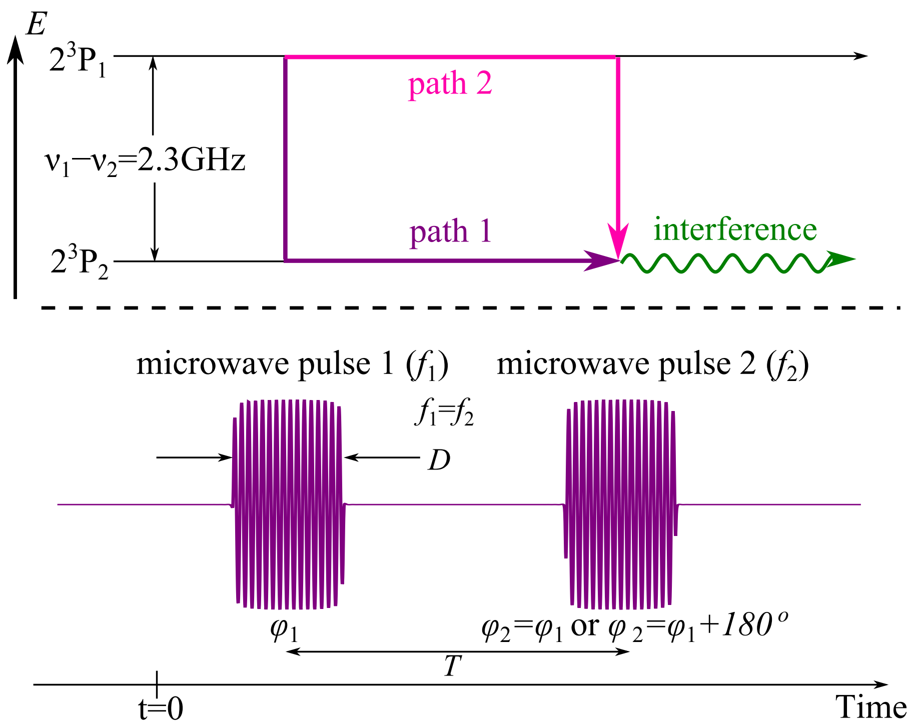

Figure 2.26: SOF overview. Before atoms interact with the first microwave pulse, all of the population is in the 2^3P_1 state. Two excitation paths (path 1 and path 2) accumulate different quantum-mechanical phases and the amplitudes of the two paths interfere.

2.26 shows a SOF scheme for the 2^3P_1-to-2^3P_2 transition. At time $t = 0$, all atoms in the two-level system are in the 2^3P_1 state. In an SOF experiment, two temporally separated microwave pulses with a pulse duration D are applied. The first microwave pulse puts the system into a superposition of the 2^3P_1 and 2^3P_2 states. Some time T after the first pulse, a second microwave pulse is applied. During the time T, atoms in the 2^3P_1 and 2^3P_2 states accumulate different quantum-mechanical phases. The probability amplitudes with different evolution phase factors interfere when recombined by the second pulse. Atoms in the 2^3P_2 state are detected after the end of the second microwave pulse.

The probability of finding atoms in the 2^3P_2 state after the second microwave pulse can be derived (for microwave powers well below saturation) from time-dependent perturbation theory, and it can be written as

$$P(\Delta\omega) = \left|\frac{VD}{2}\right|^2 \cos^2\left(\frac{\Delta\omega T}{2} + \phi\right) \mathrm{sinc}^2\left(\frac{\Delta\omega D}{2}\right), \tag{2.4}$$

where $\Delta\omega = \omega - \omega_0 = 2\pi(f - f_0)$, V is the matrix element of the transition, and $\phi = \phi_2 - \phi_1$ is the relative phase between the two microwave pulses.

In a typical SOF experiment, the relative phase between two pulses is toggled between $\phi_2 - \phi_1 = 0$ and $\phi_2 - \phi_1 = 180°$, and the resulting signals are subtracted to obtain an interference signal that is fit to an analytical solution to the SOF model for linecentre determination. Figure 2.27(a) shows the fraction of population expected by Equation 2.4 with $T = 300\,\mathrm{ns}$ and $D = 100\,\mathrm{ns}$. An exponential decay factor of $e^{-(T+D)\gamma}$, where $\gamma = 1/\tau$ with $\tau = 98\,\mathrm{ns}$, is included to calculate the population fraction that does not radiatively decay before the end of the second pulse. Both $\phi = 0°$ and $\phi = 180°$ interference patterns are shown. In the experiments performed by J. S. Borbely et. al. [27] in 2009, the relative phase between the microwave pulses was toggled between 0° and 180° using a microwave delay line, and the signal at the toggle frequency was recorded to obtain the signal shown in Figure 2.27(b). The width of the central interference fringe is given by $1/(2T)$.

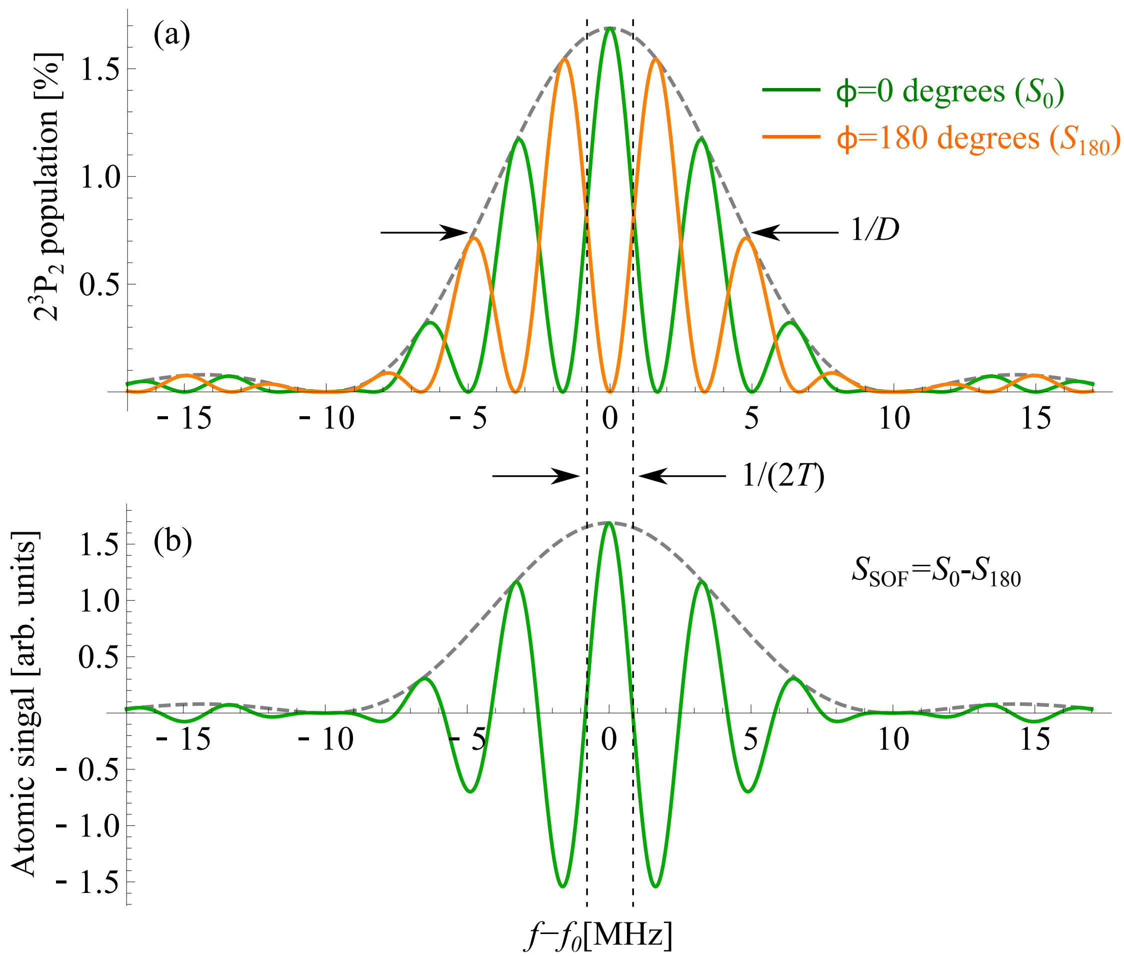

Figure 2.27: SOF interference signals for T=300 ns and D=100 ns. Signals S_0 and S_{180} are subtracted to obtain the interference shown in (b).

2.11.1.2 FOSOF Technique

The FOSOF technique used in the current experiment is a modified SOF technique in which the frequencies of the two microwave pulses are slightly offset from each other [34]. For the FOSOF technique, two microwave generators are used to prepare the frequency-offset microwave pulses (at frequencies $f_1 = f + \delta f$ and $f_2 = f - \delta f$). The microwave frequency f is offset by $\pm\delta f$. The frequency offset causes the relative phase between the two microwave pulses to vary continuously in time. As a result, the SOF interference continuously cycles between constructive and destructive interference at the frequency $2\delta f$. Figure 2.28(a) shows snapshots of the SOF interference for different times. In the figure, time steps of $0.25/(2\delta f)$ are used (the relative phase changes by $\pi/2$ in this time step). At time $t = 0$ in the figure, the two pulses are in phase. As the time progress, the shape of the interference pattern changes continuously, and the 2^3P_2 population at a particular applied microwave frequency changes sinusoidally. Figure 2.28(b) shows this oscillation of 2^3P_2 population as a function of time. The oscillations at three different frequencies are shown. In all three cases, the population oscillates at the frequency $2\delta f$, but have different phases depending on the applied microwave frequency. The FOSOF technique measures this phase as a function of applied microwave frequency to determine the resonance linecentre. Since phase is a relative quantity, a stable

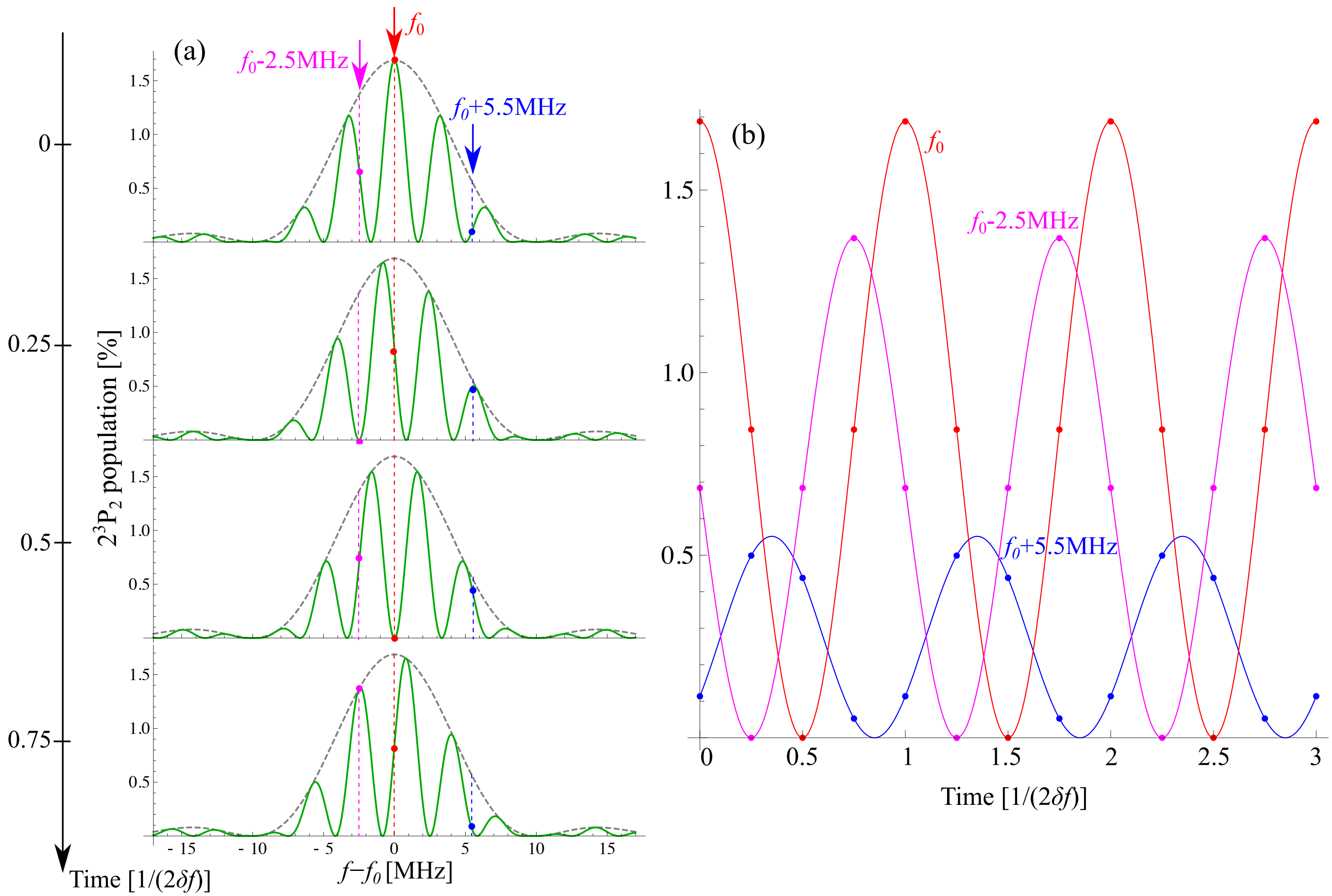

Figure 2.28: FOSOF signal progression in time. At time t=0, the two microwave pulses are in phase. As time progresses, the signal oscillates sinusoidally. The oscillations at three different frequencies are shown in (b). The oscillations have the same frequency $2\delta f$, but different phases.

reference with a constant phase needs to be supplied for all measurements to obtain phase differences. The reference sine wave is generated by combining the two microwave generator outputs. The power combination process produces a beat note between the two microwaves that oscillates at the frequency difference of $|f_1 - f_2| = 2\delta f$. The phase difference between the atomic and beat oscillations as a function of microwave frequency (Figure 2.30) gives the information necessary to determine the linecentre.

One of the major concerns about the FOSOF technique is a phase shift due to the frequency response of the microwave components or due to the detector used in the system. Each microwave component has a reflection coefficient, and the reflection causes interference between forward-going and reflected waves. The interference induces a frequency-dependent distortion in the phase and amplitude of the microwaves. The time constant of the detection system also contributes to a phase offset. To eliminate these effects, two experiments, denoted as experiment I and II, are performed. Figure 2.29 shows the timing diagrams for experiment I and II. In these experiments, the order of the microwave pulses seen by atoms is reversed, i.e., atoms interact with the pulse with frequency $f + \delta f$ first in experiment I and $f - \delta f$ first in experiment II. The sign of the FOSOF phase difference is opposite for experiment I and II. Subtraction of observed phase differences from experiments I and II cancels out the phase shifts due to the detector and microwave reflections.

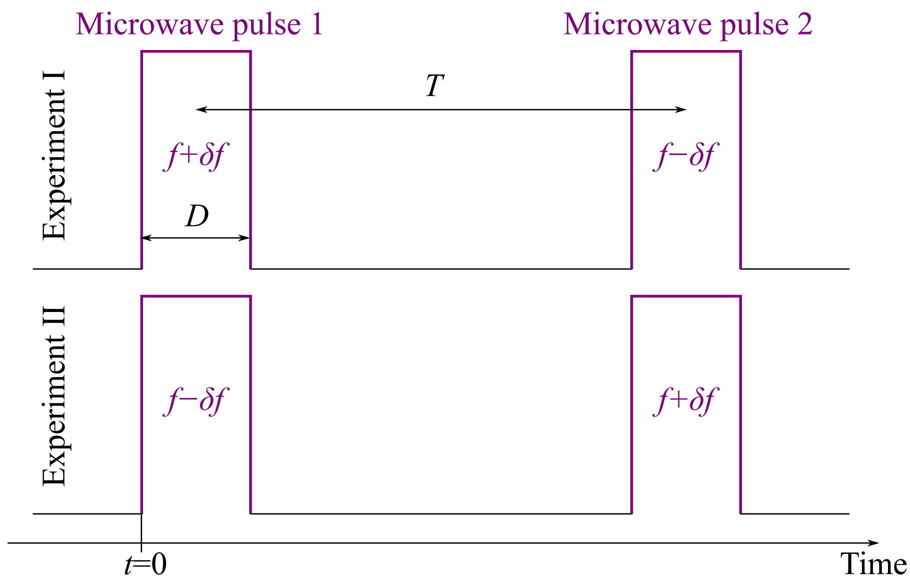

Figure 2.29: FOSOF timing diagrams for experiment I and II. The order of microwave pulses are reversed between experiment I and II. The expected difference in FOSOF phase between experiment I and II is illustrated in Figure 2.30.

Figures 2.30(a), 2.30(b) and 2.30(c) show the FOSOF interference phases at three different microwave frequencies. Phase differences $\Delta\theta_{\mathrm{I}}$ and $\Delta\theta_{\mathrm{II}}$ are extracted in each frequency. Figure 2.30(d) shows the expected phase variation as a function of applied microwave frequency in experiment I and II. The two lines in the figure are subtracted to obtain a true lineshape. Time-dependent perturbation theory (TDPT) predicts a linear phase lineshape $\Delta\theta = \Delta\omega T$ (where $\Delta\omega = 2\pi(f - f_0)$) that crosses zero phase at the center of the resonance. However, a slight, but important, deviation from this prediction becomes apparent in solving the time-dependent Schrödinger equation for the FOSOF experiment. A brief theoretical framework of SOF and FOSOF using the time-dependent Schrödinger equation and its deviation from the simple TDPT prediction are described in Section 3.2.

There are a few notable advantages in using the FOSOF technique. First, in the TDPT regime, where the amplitude of the microwave field is small, the lineshape is linear and can be fit to a simple straight line to extract the linecentre. Second, cancellation of phase imperfections is possible by using two experiment configurations (I and II), whereas SOF requires four configurations (see [33] for details on the four configurations). Third, the offset frequency δf can be set to a frequency with the minimum noise in the Fourier spectrum of the signal to achieve the best signal-to-noise ratio (refer to Figure 2.15 for the Fourier-transformed FOSOF signal and noise spectrum). Finally, the FOSOF linecentre determination depends solely on the phase extraction from the oscillating signal. Amplitude noise in the signal (the laser frequency noise, acoustic noise, source stability, and so on) does not directly affect this phase measurement.

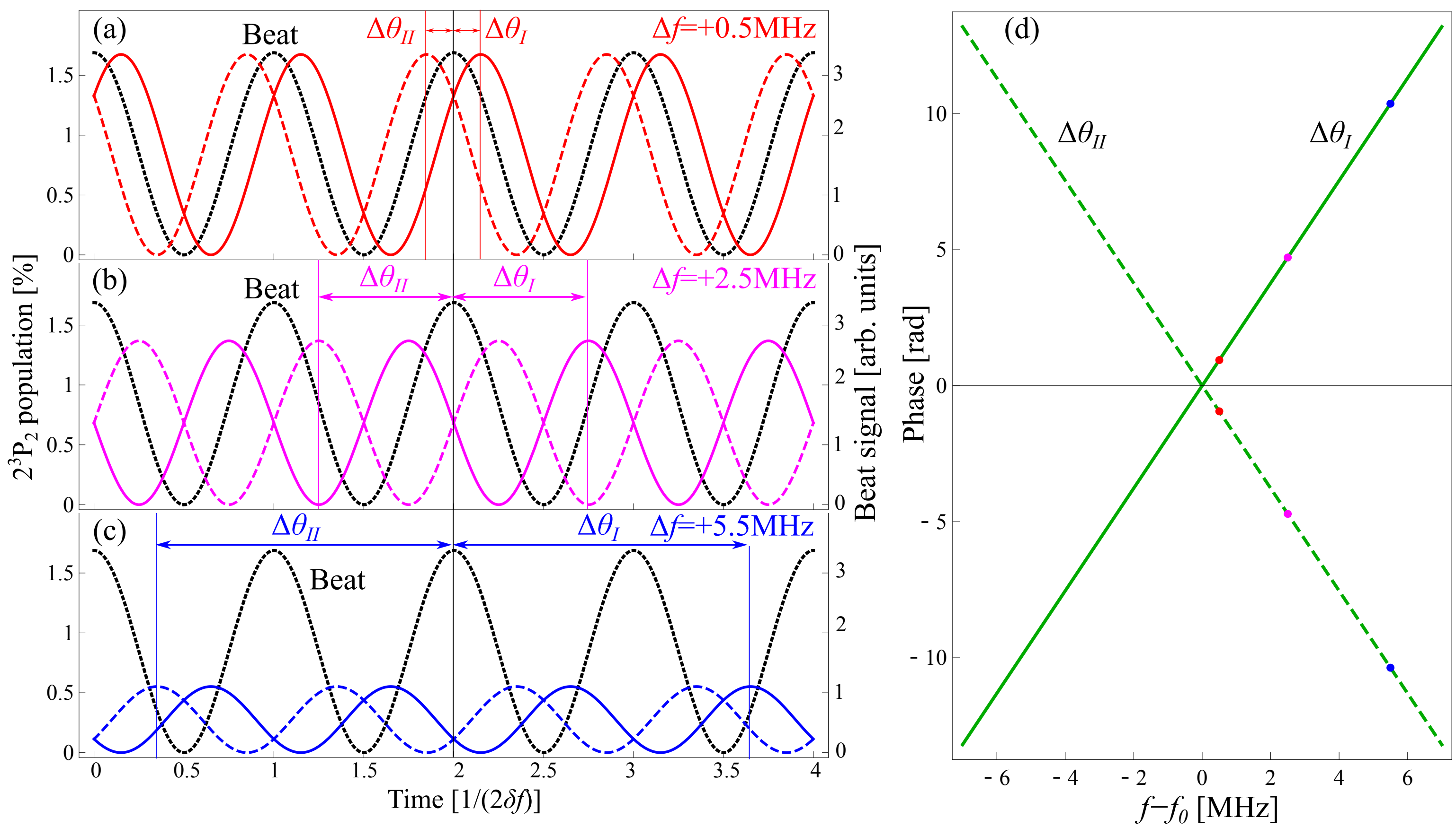

Figure 2.30: FOSOF phase determination scheme. $\Delta\theta_{\mathrm{I}}$ and $\Delta\theta_{\mathrm{II}}$ are extracted by taking the phase difference between the atomic FOSOF and beat signals. The phase extraction is illustrated in three different frequencies in (a), (b) and (c). The coloured solid and dashed lines indicate the atomic signals for experiment I and II, respectively, and the black dashed line is the beat reference signal. In (d) the TDPT lineshape in experiment I and II are drawn. Points on the lines illustrate the phases determined in (a). Here only 3 microwave frequencies are shown for illustration purposes, whereas the actual FOSOF measurements use a much larger number frequencies.

2.11.2 Microwave System

2.11.2.1 Microwave System Overview

Figure 2.31 illustrates the schematic of the microwave system. As described in Section 2.11.1.2, the FOSOF technique requires two microwave pulses whose frequencies are slightly offset from each other. Wiltron and HP microwave generators (Wiltron68169B and HP83640A) output CW microwaves with a small offset frequency $f_1 = f + \delta f$ and $f_2 = f - \delta f$. The outputs from the two generators are sent to a temperature-stabilized enclosure in which various microwave components are mounted. The system in the enclosure generates the microwave pulses and the reference (beat note) sine wave required for the FOSOF experiment. The details on the enclosure will be described in Section 2.11.2.2. The microwave pulses generated in the temperature-stabilized enclosure are sent to the Alga 100W microwave amplifier. The amplified microwave pulses go through a circulator (JQL 6058545 in Figure 2.31) and the output of the circulator is coupled into the main experiment chamber through a type-N vacuum feedthrough. Inside the vacuum chamber (main experiment chamber of Figure 2.4), this feedthrough is connected to the 14-mm microwave coaxial airline, where atoms interact with the microwave fields (14-mm microwave airline in Figure 2.1). An 18-cm-long, 0.7-cm-diameter type-N coaxial cable is used to connect the vacuum side of the feedthrough and the microwave

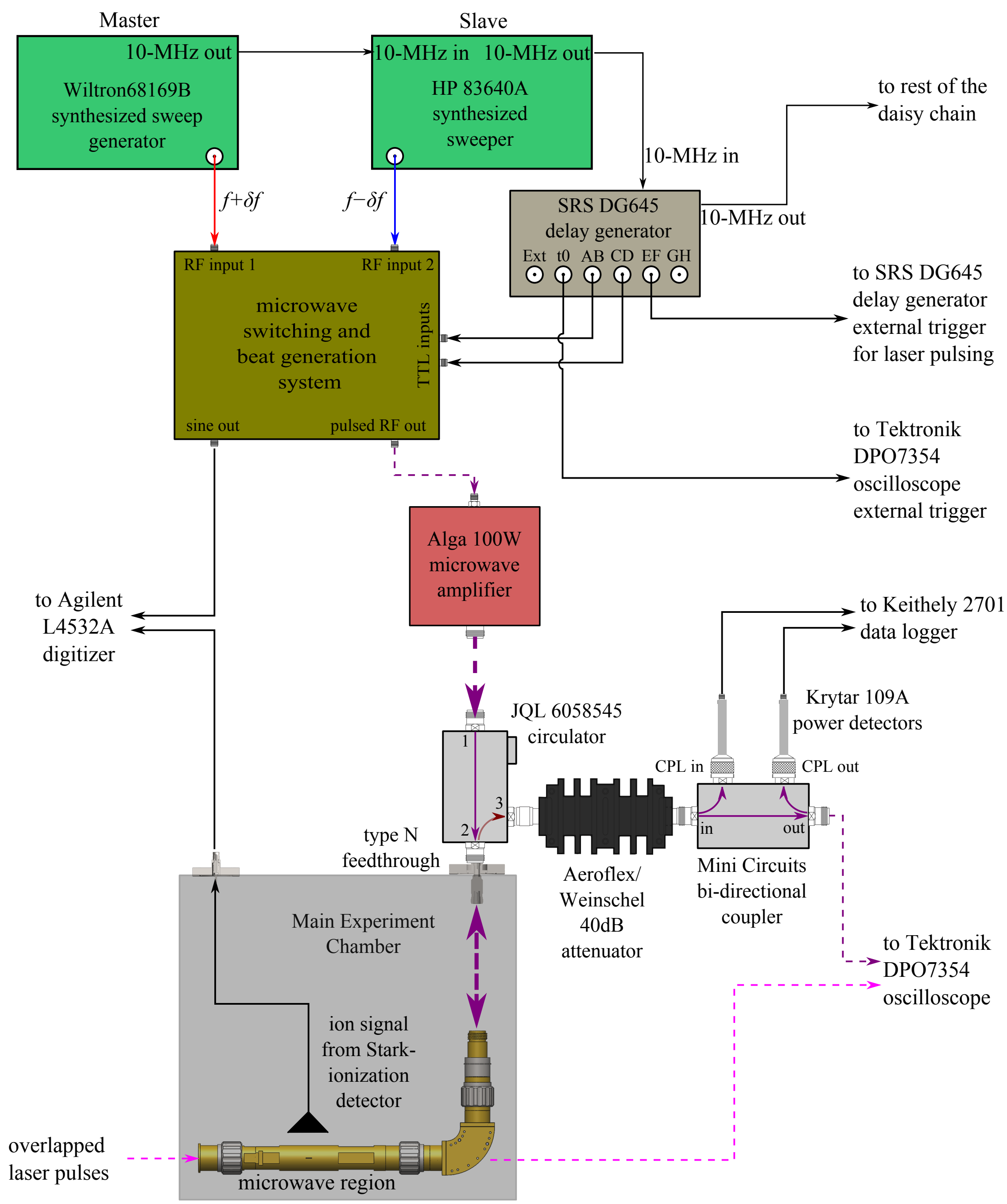

Figure 2.31: Microwave system overview

region. One end of the airline is shorted to retro-reflect the microwave power. The reflected microwave power goes back to the circulator and the circulator redirects the reverse power into its third port, and thus protects the amplifier from the reverse power reflected from the short. The redirected reverse microwave power is attenuated by a 40-dB attenuator (Weinschel model 57-40-43). The attenuated microwave pulses go through a 10-dB bi-directional coupler. The power of the coupled outputs are measured using power detectors (Krytor 109A). The microwave pulses from the output port of the coupler is monitored on a digital oscilloscope (Tektronix DPO7354). The oscilloscope traces of the microwave pulses are used for monitoring the microwave pulse timing and simulations that model the atomic signal for the experiment. The power detector readings are used as an independent check of the microwave power, and are compared to the power measured using the oscilloscope.

2.11.2.2 Details of the Microwave Switching and FOSOF Beat Reference Generation

Figure 2.32(a) shows a schematic of the microwave system inside the temperature-stabilized enclosure in which microwave components are firmly attached to a temperature-stabilized aluminum breadboard. A 50-Ω power-resistor chain is used as a heater for temperature stabilization. The system consists of two microwave paths dedicated to switching and to reference-beat-signal generation.

The CW microwave outputs from the two generators are coupled into the enclosure. The power of each CW microwave input is first split by a power splitter (PS in Figure 2.32(a)). One of the outputs from each power splitter goes through a series of 25-dB isolators (ISO in Figure 2.32(a)) and is coupled into a power combiner (PC in Figure 2.32(a)). The power combiner combines the two inputs with the small frequency offset and it outputs a beat signal. A power detector (Kryter109A, PD in Figure 2.32(a)) is used to measure the beat signal. The power detector has a nonlinearity that becomes more significant for a lower power input. The nonlinearity distorts the reference sine wave around the nodes of the beat signal, causing higher harmonics to appear in its Fourier spectrum. A 30-dB attenuator (30dB in Figure 2.32(a)) is used at one of the inputs of the power combiner to offset the beat signal. The offset ensures a nearly linear operation of the power detector.

The other microwave paths from the first pair of power splitters go through high-isolation microwave switches (Mini-Circuits ZASWA-2-50DR) for pulsing (SW1 and SW2 in Figure 2.32(a)). A delay generator (SRS DG645) is used to control the switches. TTL signals from AB and CD outputs of the delay generator are sent to the TTL inputs of SW1 and SW2, respectively, in Figure 2.32(a). These TTL pulses determine the time-separation and duration of the microwave pulses used in the experiment. The pulses produced by SW1 and SW2 are then combined using a

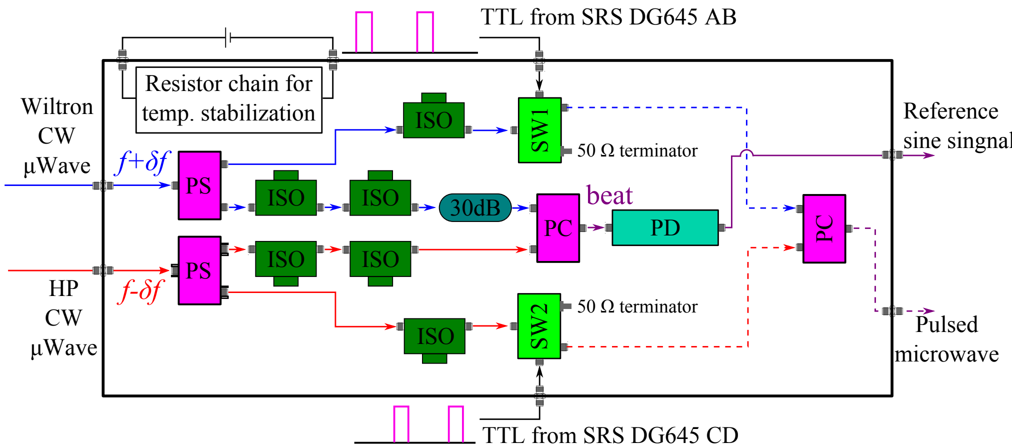

(a) Temperature-stabilized FOSOF microwave switching system. Dashed and solid lines indicate the pulsed and CW microwave paths, respectively. PS:power splitter, PC:power combiner, ISO:25-dB isolator, SW:switch, 30dB:30-dB attenuator, PD:power detector.

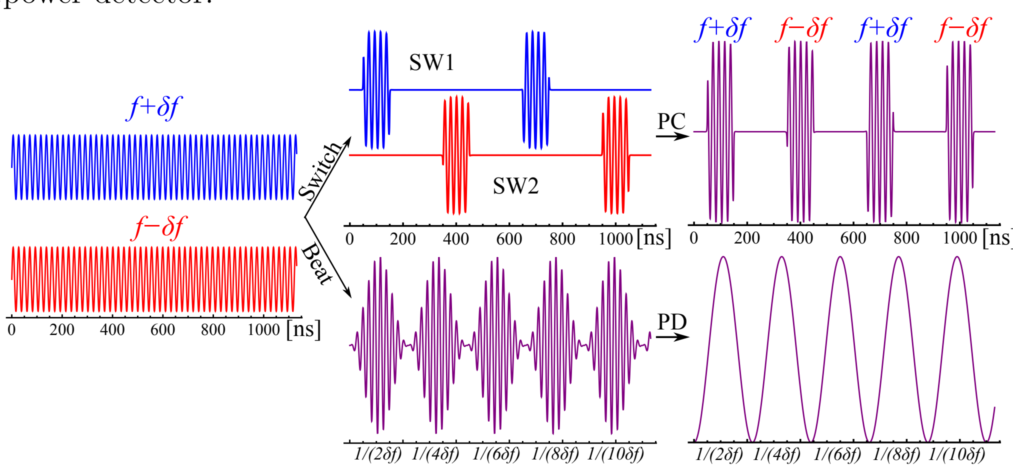

(b) Schematic illustration of the microwave switching and FOSOF beat signal generation. The switching path generates a continuous series of microwave pulses whose frequency alternates between $f + \delta f$ and $f - \delta f$. The figure shows the pulse sequence with the pulse separation and duration of 300 ns and 100 ns, respectively. The beat-note envelope oscillation is obtained by using a power detector.

.

Figure 2.32: Details of the temperature-stabilized switching and FOSOF reference signal generation.

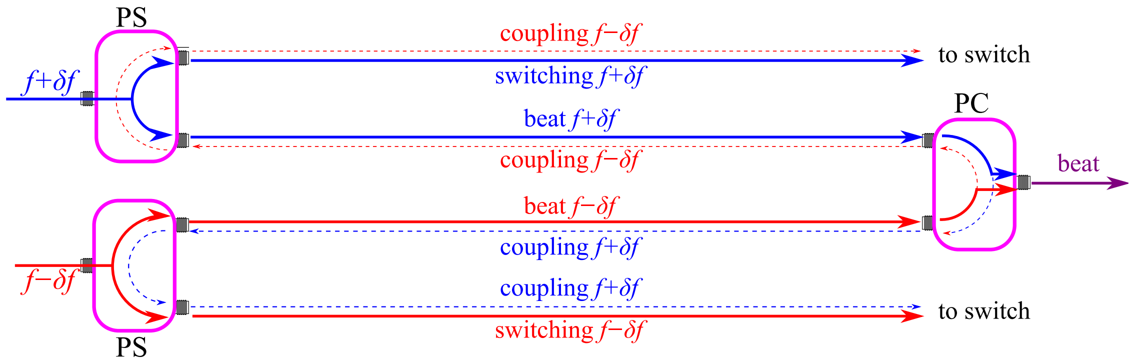

Figure 2.33: Microwave coupling between the switching and beat generation systems. A small fraction of the microwave power used to generate the beat signal couples into the other input port of the power combiner. The microwave power eventually couples into the switching path, giving rise to an oscillation in the pulse amplitude. Dashed lines indicate the undesired coupling of microwaves. PS:power splitter and PC:power combiner.

power combiner. The output of the combiner is a continuous sequence of identical shaped pulses whose frequency alternates between $f + \delta f$ and $f - \delta f$ (see Figure 2.32(b)).

A high isolation is required between the switching and beat signal generation paths to avoid microwave coupling between the paths. The microwave coupling scheme is shown in Figure 2.33. Each power combiner/splitter in the system has a typical input/output isolation of 20 dB. A small CW microwave power in the $f - \delta f$ beat signal generation path can couple into the the $f + \delta f$ switching path (labelled switching $f + \delta f$ in Figure 2.33) and vice versa. The coupling induces an interference between the CW $f \pm \delta f$ and the pulsed $f \mp \delta f$ microwaves and causes the pulse amplitude to oscillate at the same frequency as the beat signal oscillation.

The pulse amplitude oscillation adds a constant phasor onto the FOSOF atomic phasor and causes a frequency-dependent oscillation in the FOSOF phase. The oscillation distorts the FOSOF lineshape and thus introduces a systematic effect. The isolators and attenuator installed in the beat signal generation paths provide 80-dB isolation between the two paths. Including the isolations from the two power combiners that the microwaves have to go through to couple into the switching path, the total isolation between the two systems becomes 120 dB. The 120-dB suppression of microwave coupling makes the lineshape distortion negligibly small, and therefore it can be ignored for the experimental data analysis.

2.11.2.3 Details of the Microwave Region

Figure 2.34 shows the microwave-coaxial airline. The rest of the microwave system is shown in Figure 2.31. 14-mm (General Radio GR900 series) microwave components are used for the construction to ensure a good mechanical stability and a low voltage standing-wave ratio (VSWR). Typical VSWR specifications on these components range from 1.0005 to 1.005. Microwave pulses are fed into a type-N-to-14-mm adaptor (GR900-QNJ type-N-to-14-mm adaptor in Figure 2.34). The pulses are then coupled into a 14-mm elbow (GR900-EL elbow in Figure 2.34). The output-end of the elbow is attached to a 15-cm precision airline (GR900-LZ15 15-cm airline in Figure 2.34) with a 0.5-mm-by-5-mm slit where atoms enter the microwave region

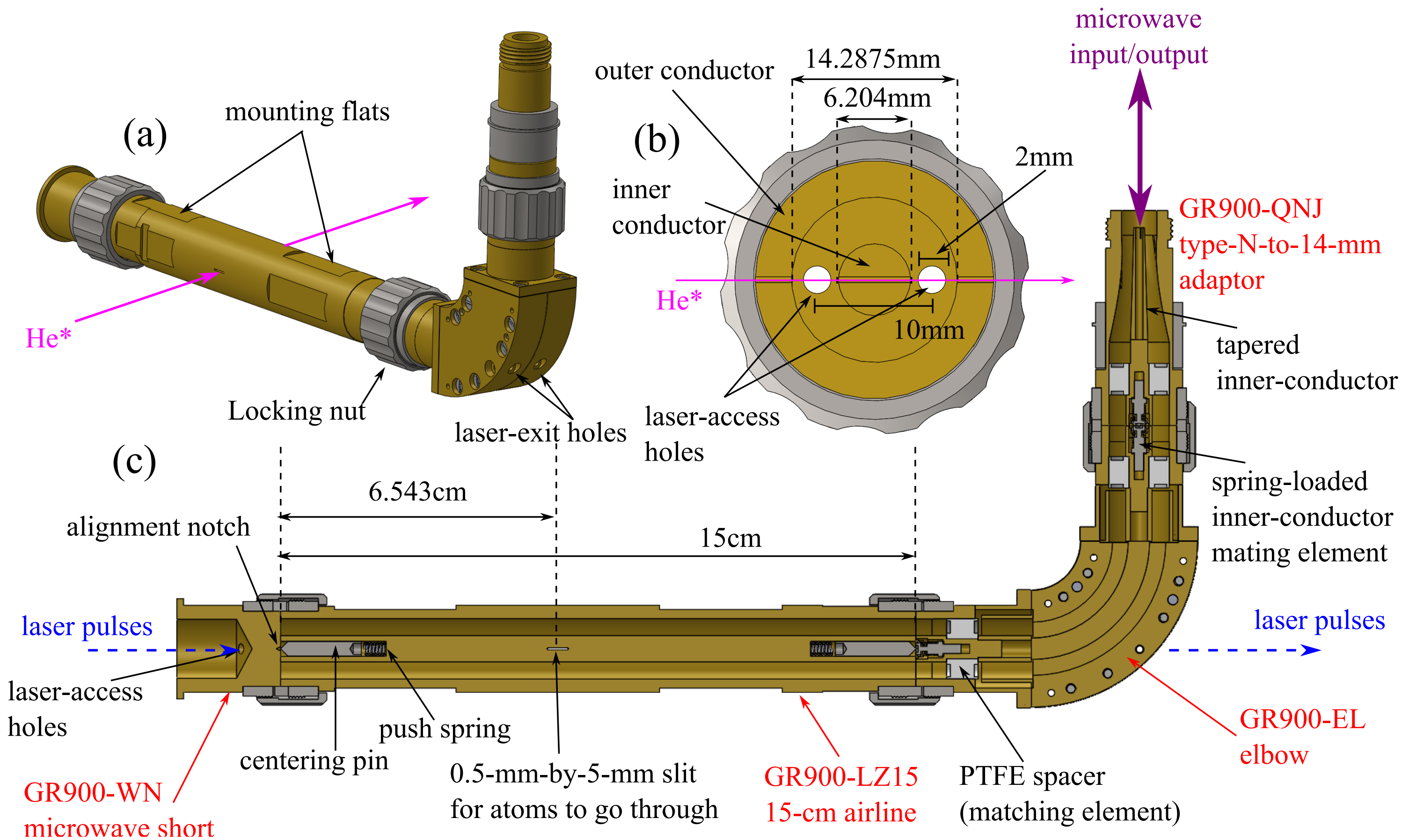

Figure 2.34: Details of the microwave region. (a) shows the overview of the microwave region. The helium beam is illustrated with the pink arrow. (b) is the cross-sectional view of the coaxial airline. (c) is the cross-sectional view showing the internal structure of the airline. The main components of the microwave regions are labelled in red.

and interact with the microwave pulses. The other end of the airline is shorted (GR900-WN microwave short in Figure 2.34) at a half-wavelength (6.543 cm) away from the atom-microwave interaction location. The microwaves are reflected from the short, and the interference between the incoming and reflected microwaves creates a standing wave which introduces a magnetic field anti-node at the interaction location (the transition of interest is a magnetic-dipole transition). This reflection effectively quadruples the microwave intensity seen by the atoms. The reflected microwave pulses follow the path of the incoming microwaves and exit from the microwave region. 2-mm holes are machined at the short and elbow for laser pulses to enter and exit the microwave region (Figure 2.34). The laser pulses enter from the short and exit at the elbow. Two laser-access holes machined at the downstream and upstream side of the inner conductor allow for experiments at two different locations in the microwave region to test for possible position-dependent systematic effects (Section 4.4.1).

2.11.3 Laser Switching System

As described in Sections 2.5.2, 2.6.1, and 2.6.2, laser pulses are generated by sending pulsed RF signals to acousto-optic modulators (AOMs). Figure 2.35 illustrates the RF system for the laser pulsing. A delay generator (SRS DG645) generates three TTL control signals for switching. The delay generator is externally triggered by a

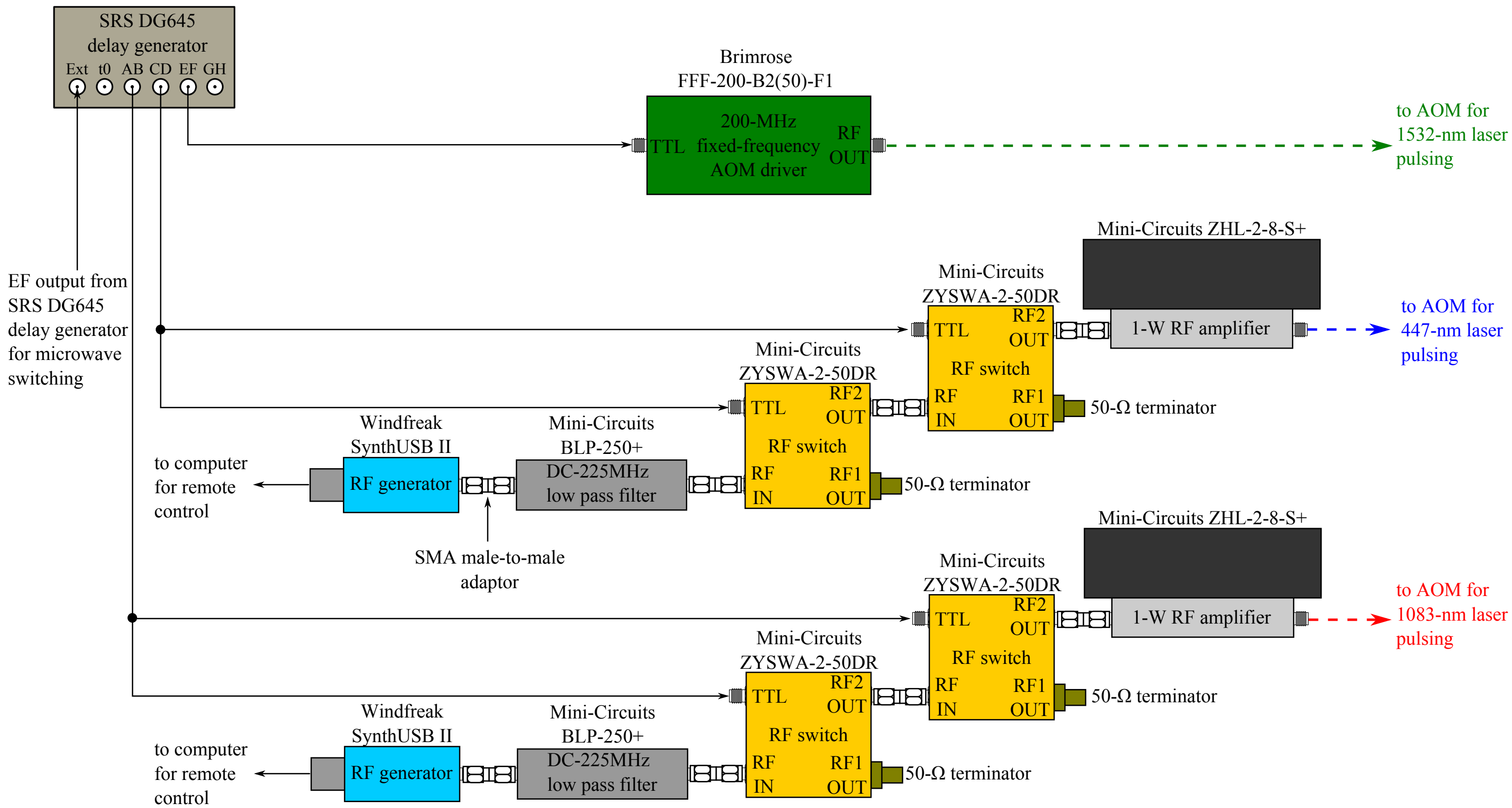

Figure 2.35: RF system for the AOM laser pulsing. CW RF signals are pulsed using switches and an AOM driver. TTL control signals for the RF switches and AOM driver are generated by the SRS DG645 delay generator which is externally triggered by the delay generator for the microwave switching. The pulsed RF signals are sent to the AOMs for laser pulsing (Sections 2.5.2, 2.6.1, and 2.6.2).

TTL signal from the EF output of the other delay generator used for microwave switching. A fixed-frequency AOM driver (Brimrose FFF-200-B2(50)-F1), which includes a switch and an amplifier, takes the EF output from the delay generator and outputs 1-W RF pulses. The output of the driver is used to pulse the 1532-nm laser (Section 2.6.2). RF pulses for the 1083- and 447-nm lasers are generated by two identical systems (shown in the lower part of Figure 2.35). A USB-controlled RF synthesizer (Windfreak SynthUSBII) outputs a 0-dBm RF signal whose frequency is tuned based on the magnetic field setting of the experiment (Section 2.10.3). The RF signal goes through a low-pass filter for higher harmonics suppression. The filtered signal then goes through two RF switches (Mini-Circuits ZYSW A-2-50DR) connected in series. Both the switches take the same TTL signal from the delay generator (AB and CD outputs for 1083- and 447-nm lasers, respectively). Two switches are used to ensure a high extinction ratio of the pulsed RF signal. The pulsed RF signal is amplified by a 1-W RF amplifier (Mini-Circuits ZHL-2-8-S+) and then is sent to the AOM.

2.11.4 Microwave- and Laser-Pulse Timings

Figure 2.36 shows the setup for adjusting and monitoring the experiment timing. Figure 2.37 is the timing diagram of the delay generator outputs for a particular experiment setting. The microwave and laser pulses generated by using two delay

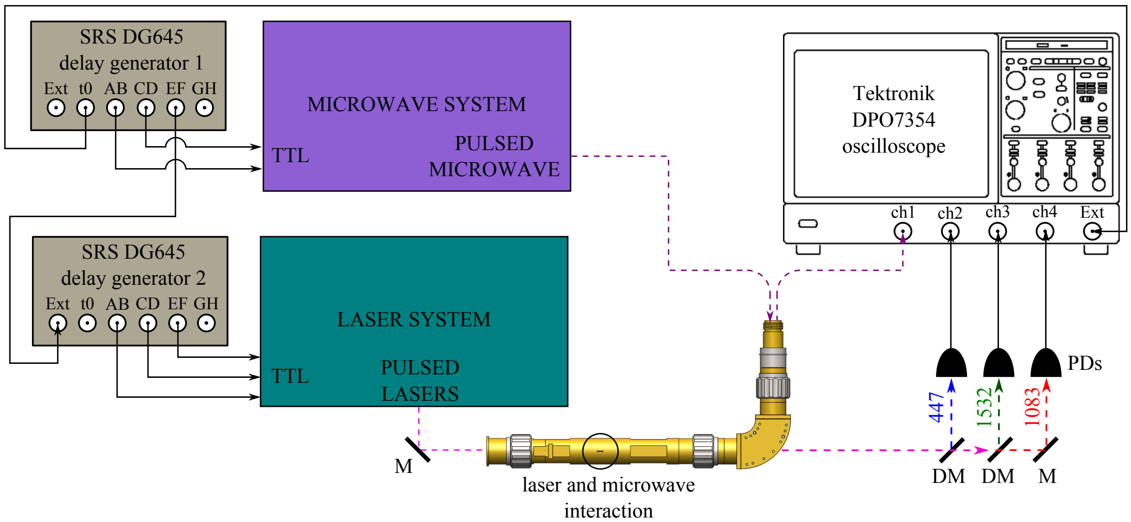

Figure 2.36: Experiment timing monitoring. The microwave pulses generated in the microwave system are sent to the microwave region and the reflected microwave pulses are sent to the channel 1 of the oscilloscope. The overlapped laser pulses are split using dichronic mirrors (DM) after passing through the microwave region and monitored on channel 2 to channel 4 of the oscilloscope. M:mirror, PDs:photodiodes.

generators (SRS DG645 delay generator 1 and 2 in Figure 2.36) are monitored on a digital oscilloscope. The reflected microwave pulses are sent to channel 1 of the oscilloscope. Laser pulses are split using dichroic mirrors (DM in Figure 2.36) after passing through the microwave region. The pulse shape and timing of each laser are monitored on a photodiode. Channels 2 to 4 are dedicated for the laser pulse monitoring. The microwave and laser pulses travel from the interaction location to the measurement location, and the travel time leads to a time delay of the oscilloscope trace. The cable length of each monitoring system is adjusted such that the oscilloscope trace approximately represents the true experiment timing that

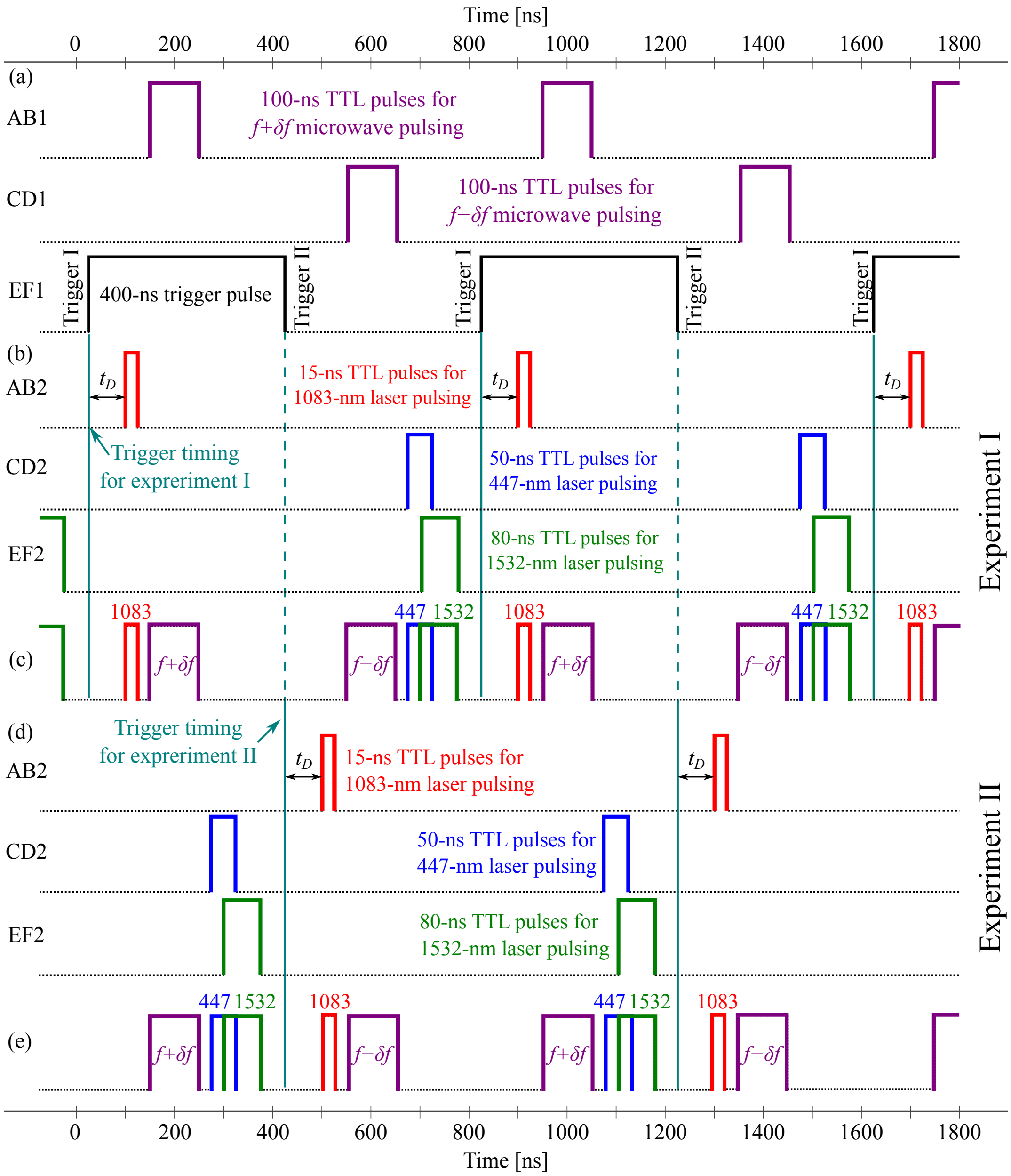

Figure 2.37: Microwave and laser pulse timing diagram for $T = 400\,\mathrm{ns}$ and $D = 100\,\mathrm{ns}$ experiment. The delay generator 1 outputs the TTL pulses shown in (a). The EF output of this delay generator is used to trigger the delay generator used for pulsing lasers. TTL pulses from delay generator 2 are shown in (b) and (d). The trigger pulse (EF1) in (a) is used to shift the experiment timing from (b) to (d) and vice versa. (c) and (e) show the combined experiment sequence for the experiment I and II, respectively. t_D indicates the insertion delay.

atoms experience.

The delay generator 1 outputs the TTL pulses shown in Figure 2.37(a). This generator is internally triggered. The combination of AB and CD outputs (AB1 and CD1 in Figure 2.37(a)) produces a continuous series of microwave pulses whose frequency alternates between $f+\delta f$ and $f-\delta f$. The EF output (EF1 in Figure 2.37(a)) of the delay generator 1 generates a pulse whose duration corresponds to the pulse separation T (400 ns in the case of Figure 2.37). This pulse is sent to the external trigger input of the delay generator 2. Once the delay generator 2 acquires the trigger signal, it starts the delay cycle after an insertion delay (t_D in Figure 2.37(b) and 2.37(d)). The AB, CD, and EF outputs are used to produce the laser pulses for the experiment. Since each of the AOMs used for the laser pulsing has a propagation delay (A time delay caused by the propagation of RF pulses inside the AOM crystal), the delay settings were determined for each experiment timing by adjusting the laser pulses based on the oscilloscope trace of the microwave pulses. The experiment reversal (described in Section 2.11.1.2 and illustrated as a change in pulse timing between Figures 2.37(b) and 2.37(d)) that changes the order of the microwave pulses seen by the atoms (atoms see the $f+\delta f$ pulse first in experiment I and the $f-\delta f$ pulse first in experiment II) is performed by toggling the trigger edge setting of the delay generator 2. A rising edge trigger setting is used in experiment I and a falling edge trigger setting is used in experiment II. This

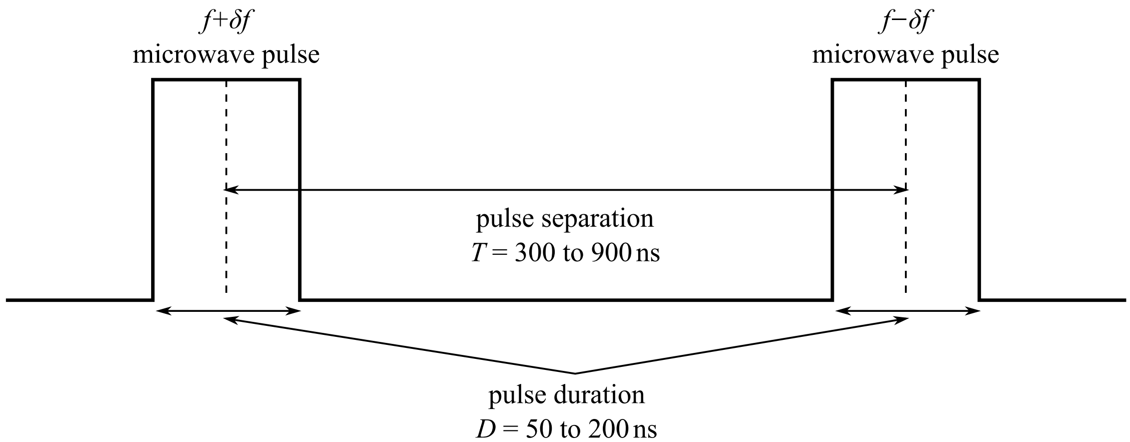

Figure 2.38: FOSOF experiment timing parameters. T changes the width of the interference fringe, D changes the spectral width of the microwave pulse. T and D range from 300 to 900 ns and from 50 to 200 ns, respectively. Total of 18 different combinations of T and D are used in the experiment.

experiment reversal method does not involve any change in the microwave system (only of the timing of the laser pulses); therefore, it ensures a stable operation of the microwave components throughout the experiment (the microwave components perform the same tasks at the same rate throughout the experiment).

2.11.5 Experiment Timing Parameters

Figure 2.38 shows the experiment timing parameters that are varied in the current experiment. The experiment timing parameters T and D are denoted as (T,D). Table 2.7 shows all the (T,D) combinations and corresponding delay settings of the delay generators. The major advantage in using the SOF (or FOSOF) technique is the ability to vary the transition lineshape by changing the pulse separation

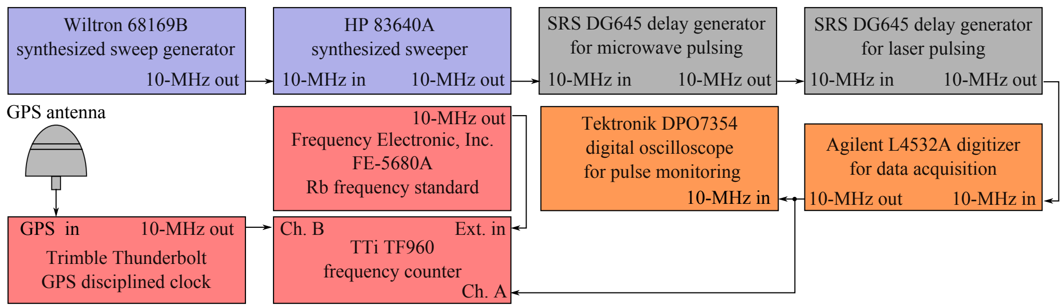

Figure 2.39: Synchronization of the 10-MHz timebases of instruments.

T and duration D. The (T,D) dependence of the SOF lineshape is described (in the low-power limit) by Equation 2.4. The width of the SOF interference fringe is proportional to $1/(2T)$, and the width of the sinc envelope of the transition is $1/D$. Consistent results in different lineshapes confirm the level of understanding of the measurements. Various (T,D) combinations are investigated in the current experiment.

2.11.6 Synchronization of Instruments

Figure 2.39 shows the timebase synchronization of the instruments used in the experiment. The 10-MHz internal timebase of the Wiltron microwave generator is used as a timebase for the experimental system. The 10-MHz output of the Wiltron generator is daisy-chained with the instruments shown in the figure. Since the oscilloscope only has a 10-MHz input, the output of the digitizer is split into two arms, and one of them is fed into the oscilloscope. The other arm of the digitizer

Timing Parameters		DG645 delay generator 1							DG645 delay generator 2					
T	D	Trigger Rate [Hz]	A	B	C	D	E	F	A	B	C	D	E	F
300	50	1666666.66667	50	52	350	53	100	300	150	15	0	50	80	80
300	100	1666666.66667	50	103	350	103	100	300	150	15	50	50	130	80
300	150	1666666.66667	25	152	325	153	100	300	125	15	75	50	155	80
375	120	1333333.33333	50	122	425	123	175	375	225	15	220	50	150	80
400	50	1250000.00000	50	52	450	53	200	400	250	15	200	50	80	80
400	100	1250000.00000	50	103	450	103	200	400	250	15	250	50	130	80
400	200	1250000.00000	50	203	450	203	200	400	250	15	350	50	230	80
450	150	1111111.11111	50	152	500	153	250	450	300	15	400	50	180	80
500	50	1000000.00000	50	52	550	53	300	500	350	15	400	50	80	80
500	100	1000000.00000	50	103	550	103	300	500	350	15	450	50	130	80
500	125	1000000.00000	50	127	550	128	300	500	350	15	475	50	155	80
600	50	833333.33333	50	52	650	53	400	600	450	15	600	50	80	80
600	100	833333.33333	50	103	650	103	400	600	450	15	650	50	130	80
600	150	833333.33333	50	152	650	153	400	600	450	15	700	50	180	80
600	200	833333.33333	50	203	650	203	500	600	450	15	750	50	230	80
700	100	714285.71429	50	103	750	103	500	700	550	15	850	50	130	80
800	100	625000.00000	50	103	850	103	600	800	650	15	1050	50	130	80
900	100	555555.55556	50	103	950	103	700	900	750	15	1250	50	130	80

Table 2.7: (T,D) combinations and corresponding timing settings of the two delay generators used in the experiment. T, D, and the delay settings (A to F) are measured in ns. The internal trigger rate of the delay generator 1 is set to $1/(2T)$. Delay settings A, C, and E are the time measured with respect to the start of the delay cycle. Settings B, D, and F define the TTL pulse duration. Settings shown in the table produce the pulses described in Figure 2.37.

10-MHz output is sent to channel A of a frequency counter (TTi TF960) to monitor the timebase of the Wiltron generator. A rubidium clock (Frequency Electronics, Inc. FE-5680A) is used as an external reference for the frequency counter. A 10-MHz output of a GPS-disciplined clock (Trimble Thunderbolt E) is monitored on channel B of the frequency counter to verify the Rb clock frequency.

2.12 Data Acquisition

Figure 2.40 shows the schematic overview of the data acquisition system. The data acquisition system of the experiment can be divided into three groups: the FOSOF atomic and reference beat signals acquisition, the microwave and laser pulse monitoring, and the experimental parameter logging. This section describes each component of the data acquisition system.

2.12.1 FOSOF Atomic and Reference Beat Signals

A 2-channel 16-bit digitizer (Agilent L4532A) is used for the main experimental data acquisition. The FOSOF atomic signal and the reference beat signal from the microwave switching box (Section 2.11.2.2) are fed into the channel 1 and 2 of the digitizer, respectively. The digitizer sample rate is fixed at 10000 samples/s (Sa/s), a sufficiently high sample rate to resolve the signal oscillating at the offset frequency (the typical offset frequency used in the experiment is 280 Hz). Two channels of

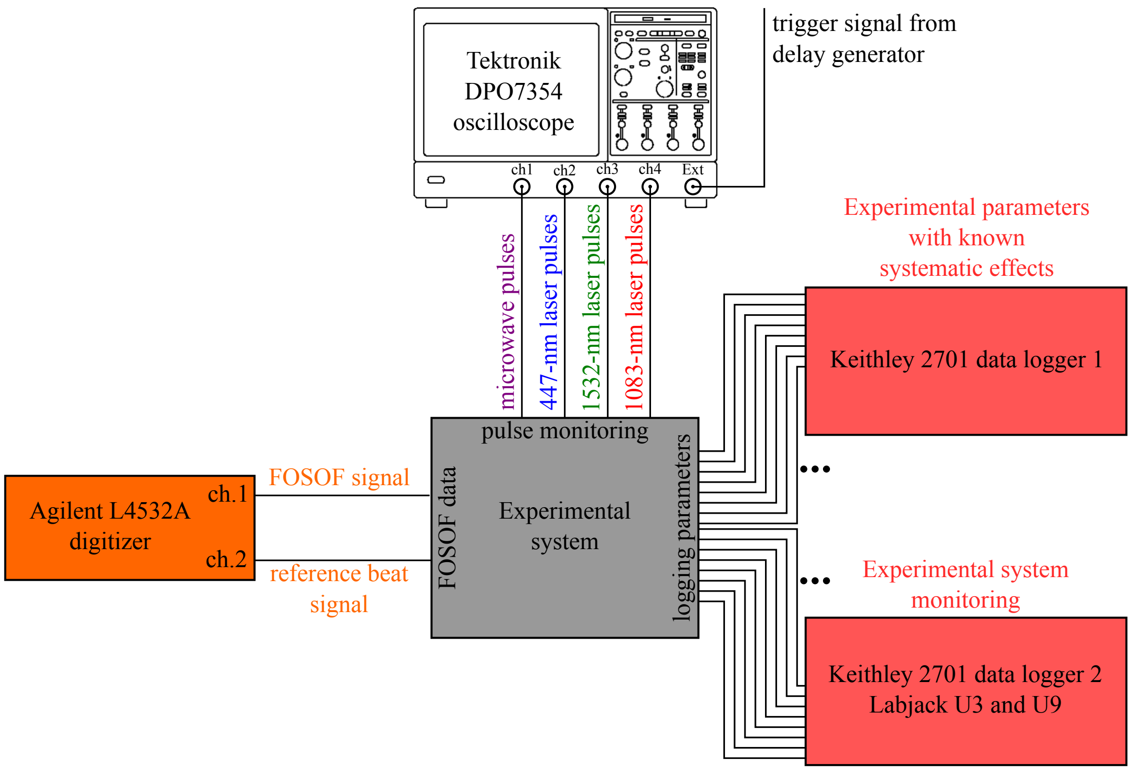

Figure 2.40: Data acquisition system. A 2-channel digitizer is used to acquire FOSOF signals. Microwave and laser pulses are monitored on a digital oscilloscope. Other experimental parameters are monitored on two data loggers and a few labjacks. The three dots between the loggers indicate that there are more parameters being logged than the number lines shown in the figure.

the digitizer are synchronized for a simultaneous data acquisition, which ensures no systematic phase delay between channels. To avoid any changes in digitizer performance which may depend on the voltage scale, the scale setting is fixed at ± 4V for both channels.

2.12.2 Microwave and Laser Pulses

A digital oscilloscope (Tektronix DPO7354) is used to monitor the microwave and laser pulses. Channel 1 is allocated for the microwave pulses, and channels 2, 3, and 4 are used to monitor 447-nm, 1083-nm, and 1532-nm laser pulses, respectively. When acquiring data for the microwave pulses, only channel 1 is enabled to achieve the maximum sample rate of 40 GSa/s that is required for resolving the 2.3-GHz microwave pulses. 10-GSa/s setting is used for the laser pulse monitoring. The microwave and laser pulse data are transferred to and saved on the computer for every frequency setting used in every data set taken in the experiment. The acquired microwave pulses are used for a microwave power monitoring and the simulation of the experiment.

2.12.3 Experimental Parameter Logging

Two data loggers (Keithley model 2701) and two Labjacks (U3 and U9) are used to log experimental parameters. One of the loggers monitors experimental parameters that are directly related to known systematic effects: the power of the microwave pulses, and the current and voltage used to apply magnetic field. The data logging of these parameters is synchronized with the main data acquisition protocol to ensure that the obtained linecentre is not affected by any outliers associated with a variation in these experimental parameters. The other logger and labjacks constantly logs many parameters (the ambient temperature, current for the metastable helium source, humidity in the lab, pressure in each section of the beamline, etc.). Obtained linecentres are plotted as a function of each parameter to test for possible systematic effects.

2.13 Data Processing Prior to the Lineshape Fitting Routine

Figure 2.41 shows a small fraction of the digitizer trace for the FOSOF experiment I and II (the trace length ranges from 5 s to 40 s depending on the experimental parameters). To fit the data with the expected FOSOF lineshape, the phase difference between the FOSOF atomic and reference beat signals needs to be found (indicated as $\Delta\theta_{\mathrm{I}}$ and $\Delta\theta_{\mathrm{II}}$, where I and II denote experiment I and II). Extraction of the phase and amplitude information of each signal is obtained by taking the sine and cosine inner products (at the offset frequency). For the inner product, each data point of the digitizer trace is multiplied by the sine and cosine functions whose oscillation frequencies correspond to the FOSOF oscillation frequency $2\delta f$, and these are summed. The result of the inner product can be represented as $Re^{i\theta}$ where R and θ are the amplitude and phase of the signal, and are found using

$$R = \sqrt{X^2 + Y^2} \tag{2.5}$$

$$\theta = \arctan(\frac{Y}{X}), \tag{2.6}$$

where $X = R\cos(\theta)$ and $Y = R\sin(\theta)$ are the real and imaginary parts of $Re^{i\theta}$. The method is the same as that used for a lock-in amplifier [52]. The saved digitizer traces can be accessed any time and re-analyzed if necessary; whereas, in a typical lock-in amplifier operation, the information about the raw input signal is lost, and

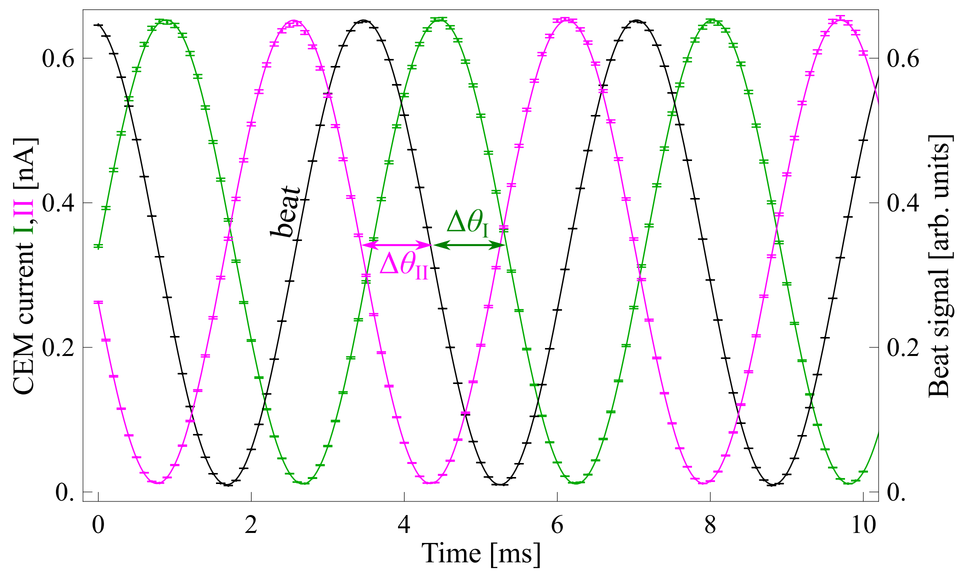

Figure 2.41: Digitizer trace of the FOSOF signal. A small fraction of the digitizer trace is shown. This figure represents an average of four similar traces. $\Delta\theta_{\mathrm{I}}$ and $\Delta\theta_{\mathrm{II}}$ are used for linecentre determination.

the raw signal becomes inaccessible after the time of data acquisition.

For our analysis, the digitizer trace is typically broken up into fifty segments and the phase of each segment is determined using the inner-product method. The fifty phases are then averaged to obtain the best-estimate value. The standard deviation of the average phase is used to assign an uncertainty to the phase value. Once the phase and its uncertainty are obtained, the phase differences, $\Delta\theta_{\mathrm{I}} = \theta_{\mathrm{beat}} - \theta_{\mathrm{I}}$ and $\Delta\theta_{\mathrm{II}} = \theta_{\mathrm{beat}} - \theta_{\mathrm{II}}$, are calculated. The final FOSOF phase (which eliminates phase lags as described in Section 2.11.1.2) $\overline{\Delta\theta} = (\Delta\theta_{\mathrm{I}} - \Delta\theta_{\mathrm{II}})/2$ is then calculated.

As described in Section 2.11.1.2, the FOSOF phase changes linearly with frequency (to first order). Since the described method of phase determination cannot

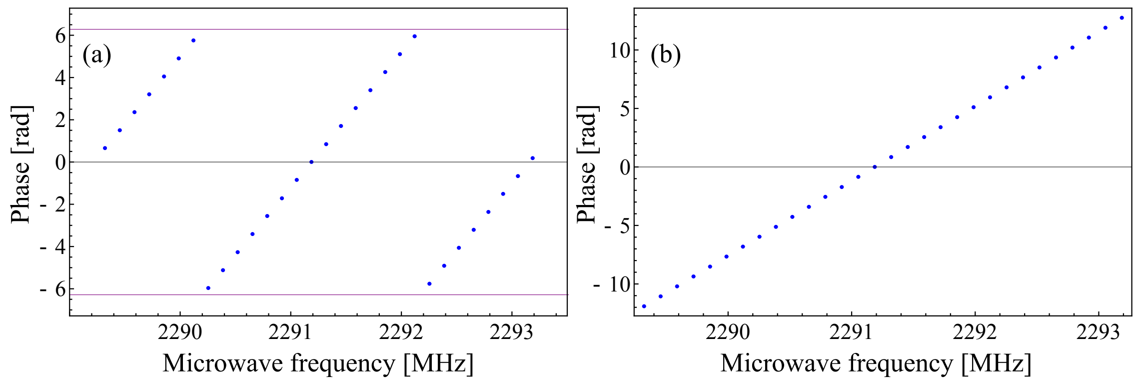

Figure 2.42: Phase-stitching of the FOSOF phase. (a) and (b) are the FOSOF data without and with the phase-stitching process, respectively. The FOSOF phase cycles between phases -2π and 2π radians (a). The data in (b) is used to determine the linecentre.

distinguish between θ and $\theta + 2N\pi$, the data phase plots (Figure 2.42) show discontinuities. The FOSOF phase is stitched based on the assumption that it grows linearly. Figure 2.42 shows the stitching process. The discontinuities shown in Figure 2.42(a) are removed, and this data is fit to the expected lineshape for linecentre determination.

3 Atomic Lineshape and Linecentre Determination

This chapter discusses the analytic lineshape of the FOSOF technique obtained by solving the Schrödinger equation. The analytic lineshape is used to fit the FOSOF data for the linecentre determination. Reconstruction of an SOF signal from the FOSOF data is also performed, and the results are fit to the SOF lineshape to test the consistencies between SOF and FOSOF.

3.1 Analytic Solution to the FOSOF Lineshape

It is possible to derive an analytic FOSOF lineshape by assuming a continuously varying relative phase between the two microwave pulses. The derivation assumes instant turn-on and turn-off of the microwave pulses and perfect amplitude and phase profiles. Fabjan and Pipkin [53] derive a general SOF lineshape using the time-dependent Schrödinger equation for a two-level system, and their intermediate result is used to derive the FOSOF lineshape. Lombardi and Borbely [33,54] also give a detailed derivation of the SOF lineshape specifically for the helium $2^3\mathrm{P}_J$-to-$2^3\mathrm{P}_{J'}$ transitions, so only a brief derivation is given in this section. The derivation closely follows Fabjan and Pipkin [53], but different notation is used to be consistent with the content of this thesis.

The two states involved in the SOF transition are $2^3\mathrm{P}_1$ and $2^3\mathrm{P}_2$, and these are represented as $|1\rangle$ and $|2\rangle$, respectively. The Hamiltonian describing the atom-field interaction is

$$H = H_0 + H_\mathrm{D} - \boldsymbol{\mu} \cdot \mathbf{B}_0 \cos(\omega t + \delta), \tag{3.1}$$

where H_0 gives the energy levels of the two states:

$$H_0 |1\rangle = \hbar\omega_1 |1\rangle, \quad H_0 |2\rangle = \hbar\omega_2 |2\rangle, \tag{3.2}$$

and H_D accounts for the decay rate associated with each of the two states:

$$H_\mathrm{D} |1\rangle = -\frac{1}{2} i\hbar\gamma_1 |1\rangle, \quad H_\mathrm{D} |2\rangle = -\frac{1}{2} i\hbar\gamma_2 |2\rangle, \tag{3.3}$$

where $\gamma = 1/\tau$ is the radiative decay rate of the state. $\gamma_1 = \gamma_2 = 1/\tau$ in this particular case since the $2^3\mathrm{P}_1$ and $2^3\mathrm{P}_2$ states have the same lifetime of $\tau = 98\,\mathrm{ns}$. $\boldsymbol{\mu}$ is the magnetic-dipole-moment operator which is defined to as,

$$\boldsymbol{\mu} = \frac{\mu_\mathrm{B}}{\hbar}(g_\mathrm{s}\mathbf{S} + g_\mathrm{l}\mathbf{L}), \tag{3.4}$$

where μ_B is the Bohr magneton, g_s and g_l are the spin and angular-momentum g-factors, respectively, and $\mathbf{S}$ and $\mathbf{L}$ are the spin and orbital angular momentum operators. $\mathbf{B}_0 \cos(\omega t + \delta)$ represents the microwave magnetic field defined by the oscillating frequency ω, the amplitude $\mathbf{B}_0$, and the phase δ. The polarization of the microwave is oriented in the $\hat{z}$ direction, so $\mathbf{B}_0 = \mathrm{B}_0 \hat{z}$. The two-level system is described by a 2-component wavefunction that is a superposition of two states:

$$|\Psi\rangle = c_1(t)\,|1\rangle + c_2(t)\,|2\rangle\,. \tag{3.5}$$

The components of the $|\Psi\rangle$ give the amplitude of being in state $|1\rangle$ and $|2\rangle$. The time evolution of the system is described by the time-dependent Schrödinger equation:

$$i\hbar \frac{\partial}{\partial t}\,|\Psi\rangle = H\,|\Psi\rangle\,. \tag{3.6}$$

Substituting Equation 3.5 into Equation 3.6 with the Hamiltonian of Equation 3.1 yields two coupled equations:

$$i\dot{c_1}(t) = \omega_1 c_1(t) - i\tfrac{1}{2}\gamma c_1(t) + 2V c_2(t)\cos(\omega t + \delta) \tag{3.7}$$

$$i\dot{c_2}(t) = \omega_2 c_2(t) - i\tfrac{1}{2}\gamma c_2(t) + 2V c_1(t)\cos(\omega t + \delta)\,, \tag{3.8}$$

where

$$\begin{aligned} V &= -\,\langle 1|\,\boldsymbol{\mu}\cdot\mathbf{B}_0\,|2\rangle \\ &= -\,\frac{\mu_B}{2\hbar^2}\,\langle 1|\,(g_{\mathrm{s}}\mathbf{S} + g_{\mathrm{l}}\mathbf{L})\cdot\mathbf{B}_0\,|2\rangle \end{aligned} \tag{3.9}$$

is the magnetic-dipole matrix element. The magnetic-dipole matrix elements of the $2^3\mathrm{P}_J$-to-$2^3\mathrm{P}_{J'}$ transitions are evaluated and tabulated in [33, 54].

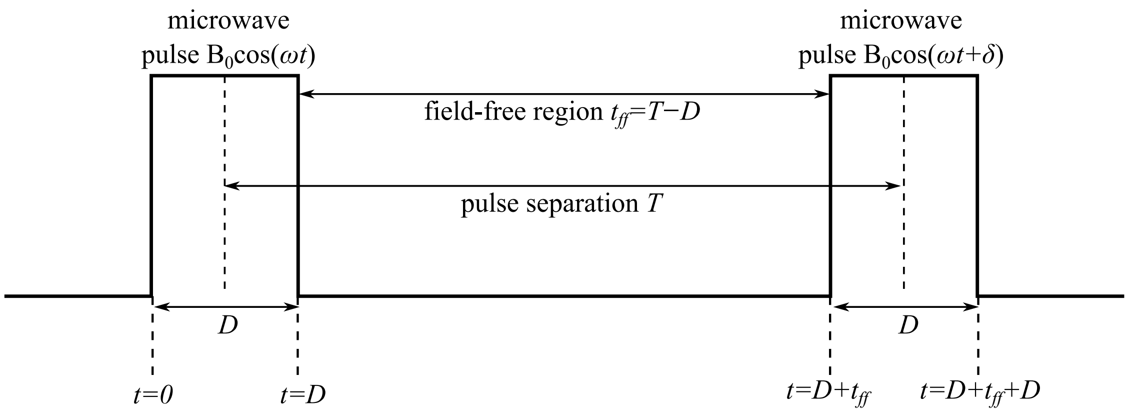

Figure 3.1: Interaction Timing for the lineshape fitting function

Figure 3.1 shows the timing of the SOF experiment. At time $t = 0$, all atoms are in state $|1\rangle$, and they enter the microwave field $\mathbf{B}_0 \cos(\omega t)$, where the phase of this microwave field is assumed to be zero. The atoms then leave the microwave field at time $t = D$ and spend a time t_{ff} ($t_{ff} = T - D$) in a field-free region. After the field-free region, the atoms are again exposed to a microwave field $\mathbf{B}_0 \cos(\omega t + \delta)$ for a duration of D. Equations 3.7 and 3.8 need to be integrated with initial conditions for the timing provided by the Figure 3.1 to obtain amplitude of the wavefunction for the SOF experiment. Fabjan and Pipkin give the SOF amplitudes $c_1(T + D + T)$ and $c_2(T + D + T)$ at the exit of the second microwave pulse (Equations 19(a) and 19(b) of [53]):

$$c_1(D+T+D) = \exp[-\gamma(D+T) - i(\omega+\omega_1+\omega_2)D - i\omega_1 T]$$
$$\times\{\left(\cos\left(\tfrac{1}{2}aD\right) + i\tfrac{\Delta\omega}{a}\sin\left(\tfrac{1}{2}aD\right)\right)^2 - \exp[-i(\delta+\Delta\omega(T-D))]\left(\tfrac{2V}{a}\right)^2\sin^2\left(\tfrac{1}{2}aD\right)\}, \tag{3.10}$$

$$\begin{aligned} c_2(D+T+D) = {} & \exp[-\gamma(D+T) + i(\omega-\omega_1-\omega_2)D - i\omega_2 T] \\ & \times\left(-i\tfrac{2V}{a}\sin\left(\tfrac{1}{2}aD\right)\right)\{\left(\cos\left(\tfrac{1}{2}aD\right) - i\tfrac{\Delta\omega}{a}\sin\left(\tfrac{1}{2}aD\right)\right) \\ & + \exp[i(\delta+\Delta\omega(T-D))]\left(\cos\left(\tfrac{1}{2}aD\right) + i\tfrac{\Delta\omega}{a}\sin\left(\tfrac{1}{2}aD\right)\right)\}, \end{aligned} \tag{3.11}$$

where $\Delta\omega = \omega - \omega_0$ is the microwave detuning from the atomic resonance ($\omega_0 = \omega_1 - \omega_2$), and $a = \sqrt{4V^2 + \Delta\omega^2}$. In the current experiment, only atoms that make a microwave transition to $|2\rangle$ are detected and the probability $\left|c_2(D+T+D)\right|^2$ at $\delta = 0°$ and $\delta = 180°$ needs to be evaluated and subtracted to obtain the SOF lineshape. It can be shown that the analytic solution to the SOF lineshape can be written as,

$$\begin{aligned} P_{\mathrm{SOF}}(T,D,V,\Delta\omega) = {} & \left|c_2(D+T+D)\right|^2_{\delta=0°} - \left|c_2(D+T+D)\right|^2_{\delta=180°} \\ = {} & \frac{16e^{-\gamma(T+D)}}{(4V^2+\Delta\omega^2)^2}V^2\sin^2\left(\frac{1}{2}D\sqrt{4V^2+\Delta\omega^2}\right) \\ & \times\{\cos(\Delta\omega(T-D))(4V^2+\Delta\omega^2)\cos\left(D\sqrt{4V^2+\Delta\omega^2}\right) \\ & - \Delta\omega\sqrt{4V^2+\Delta\omega^2}\sin\left(\Delta\omega(T-D)\right)\sin\left(D\sqrt{4V^2+\Delta\omega^2}\right)\}. \end{aligned} \tag{3.12}$$

Equation 3.12 describes the SOF interference pattern inside the envelope function whose width is determined by the width of the applied microwave pulses.

The FOSOF lineshape can be derived from Equation 3.11 by assuming a continuously changing $\delta = 2\pi(2\,\delta f\, t)$. The phase of the resulting sinusoidal variation of signal obtained from Equation 3.11 needs to be determined. Equation 3.11 involves complex numbers, and the phase associated with the real and imaginary components of the equation can be found by adding the arguments of the complex factors: $\cos\left(\frac{1}{2}aD\right) + i\frac{\Delta\omega}{a}\sin\left(\frac{1}{2}aD\right)$, and $\cos\left(\frac{1}{2}aD\right) - i\frac{\Delta\omega}{a}\sin\left(\frac{1}{2}aD\right)$. The factor $-i\frac{2V}{a}\sin\left(\frac{1}{2}aD\right)$ can be ignored since it adds the same phase factor to the two terms. The second term in the argument of the exponential $e^{\Delta\omega(T-D)}$ is an additional phase factor that needs to be added to the phase. The total phase of Equation 3.11 is found by adding all three phase factors and can be written as

$$\Delta\theta(T,D,V,\Delta\omega) = \Delta\omega(T-D) + 2\tan^{-1}\left[\frac{\Delta\omega\tan\left(\sqrt{4V^2+\Delta\omega^2}D/2\right)}{\sqrt{4V^2+\Delta\omega^2}}\right]. \quad (3.13)$$

Equation 3.13 predicts the variation in phase of the interference cosine of the SOF lineshape. This lineshape slightly deviates from the linear lineshape ($\Delta\omega T$ in Equation 2.4) predicted by the time-dependent perturbation theory (TDPT) in the limit of $V \to 0$. A detailed description of this deviation is discussed in Section 3.2.

The amplitude of the FOSOF signal as a function of microwave frequency can also be derived by taking the absolute value of the product of the complex terms used to derive Equation 3.13 with $-i\frac{2V}{a}\sin\left(\frac{1}{2}aD\right)$ term included. The amplitude of the FOSOF signal with the exponential decay factor can be written as,

$$\begin{aligned} A(T,D,V,\Delta\omega) &= \frac{4V^2 e^{-(T+D)\gamma}}{4V^2+\Delta\omega^2}\sin^2\left(\frac{1}{2}D\sqrt{4V^2+\Delta\omega^2}\right) \\ &\times\left(\cos^2\left(\frac{1}{2}D\sqrt{4V^2+\Delta\omega^2}\right)+\frac{\Delta\omega^2}{4V^2+\Delta\omega^2}\sin^2\left(\frac{1}{2}D\sqrt{4V^2+\Delta\omega^2}\right)\right). \end{aligned} \tag{3.14}$$

The second part of Equation 3.13 is only well defined between the phase values between -π to +π radians. Discontinuities occur at the phases -π and +π radians, and the function value cycles between these two phases. In order to obtain a smooth function, a phase-stitching needs to be performed (similar to the process described in Section 2.13). Figure 3.2 illustrates the function discontinuity and the phase-stitching. In Figure 3.2(a), the second part of Equation 3.13 is plotted. The discontinuity shown in the figure also shows up in the total function plotted in 3.2(b). The stitched phase is shown in Figure 3.2(c). The function used to plot Figure 3.2(c) has the form,

$$\begin{aligned} \overline{\Delta\theta}(T,D,V,\Delta\omega) &= \Delta\omega T \\ &+\mathrm{mod}_{2\pi}\left[\pi+2\tan^{-1}\left[\frac{\Delta\omega\tan\left(\sqrt{4V^2+\Delta\omega^2}D/2\right)}{\sqrt{4V^2+\Delta\omega^2}}\right]-\Delta\omega D\right]-\pi, \end{aligned} \tag{3.15}$$

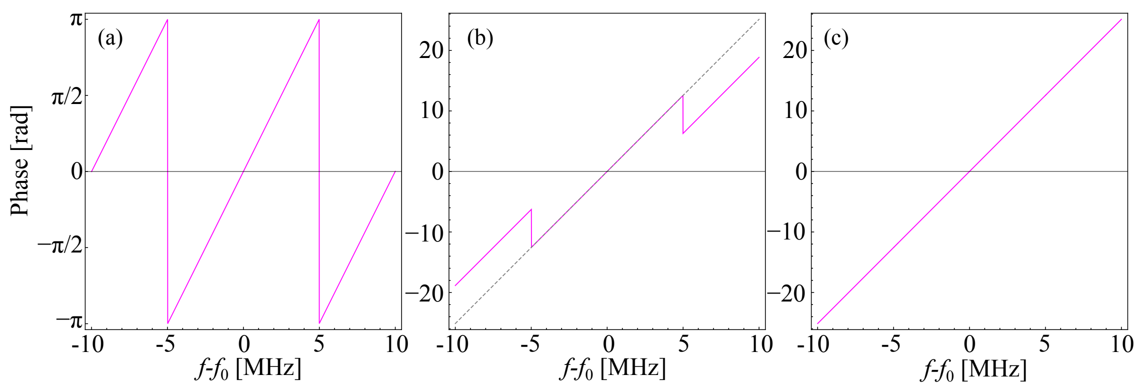

Figure 3.2: Phase-stitching of FOSOF lineshape. (a) shows the discontinuity associated with the second part of Equation 3.13. (b) and (c) are the plots of FOSOF lineshape of Equation 3.13 without and with the phase-stitching, respectively. The gray line in (b) indicates where the stitched phases end up. The lineshape shown in (c) is used to fit the experimental data to determine the linecentres.

where $\mathrm{mod}_{2\pi}$ indicates the modulus of 2π is taken for the second part of the equation. Equation 3.15 is used for plotting a theoretical lineshape, and fitting of the FOSOF data.

3.2 Theoretical Lineshapes

The advantage of using the SOF technique is not only the narrowing of the transition linewidth, but also the ability to change the lineshape by adjusting T and D and V, which allows for a study of systematic effects. Various lineshapes associated with different T, D, and V are investigated in the current experiment. Figures 3.3 and 3.4 shows three lineshapes with different T for a fixed D and V. In Figure 3.3, the effect of changing T on the FOSOF lineshape of Equation 3.15 is shown on a single plot.

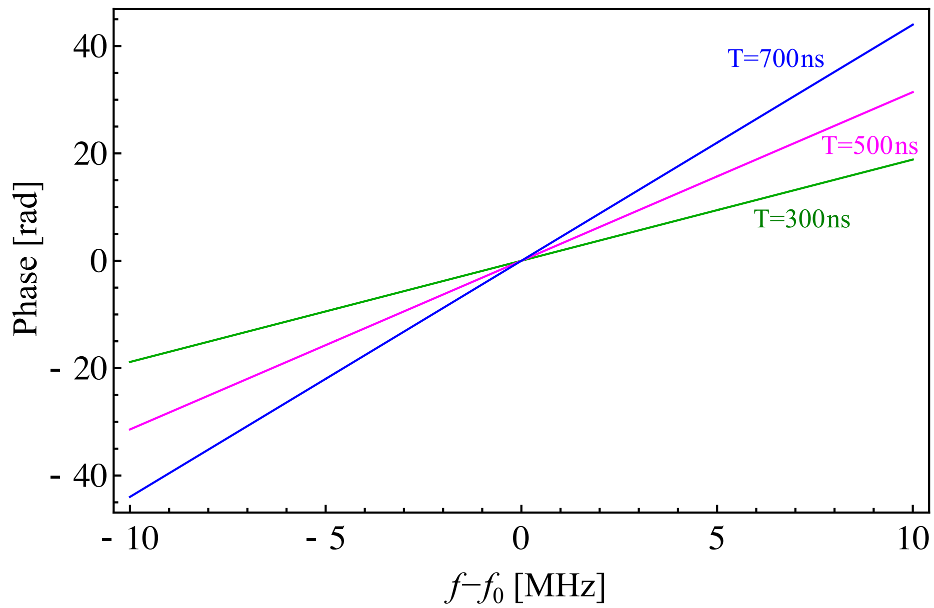

Figure 3.3: Effect of T on FOSOF theoretical lineshapes. Equation 3.15 with D=100 ns and V=1 rad/s is plotted for three different values of T.

Figure 3.4 summarizes the change in SOF and FOSOF lineshapes. As illustrated at the left of the figure (SOF in Figure 3.4, plotted using Equation 3.12), the width of the interference changes for different T values used. The interference width is given by $1/2T$. The FOSOF lineshape, shown in the middle (FOSOF phase in Figure 3.4), is a mostly linear function whose slope is given by $2\pi T$. These lineshapes are the same as the ones shown in Figure 3.3. The FOSOF phase deviation from the TDPT prediction (shown at the right of Figure 3.4, labelled as FOSOF-TDPT) remains constant over the range of T. This is because the deviation only depends on the effective field amplitude that the atoms experience.

Figure 3.5 shows the effect of V on the FOSOF lineshape. Figure 3.5 shows that

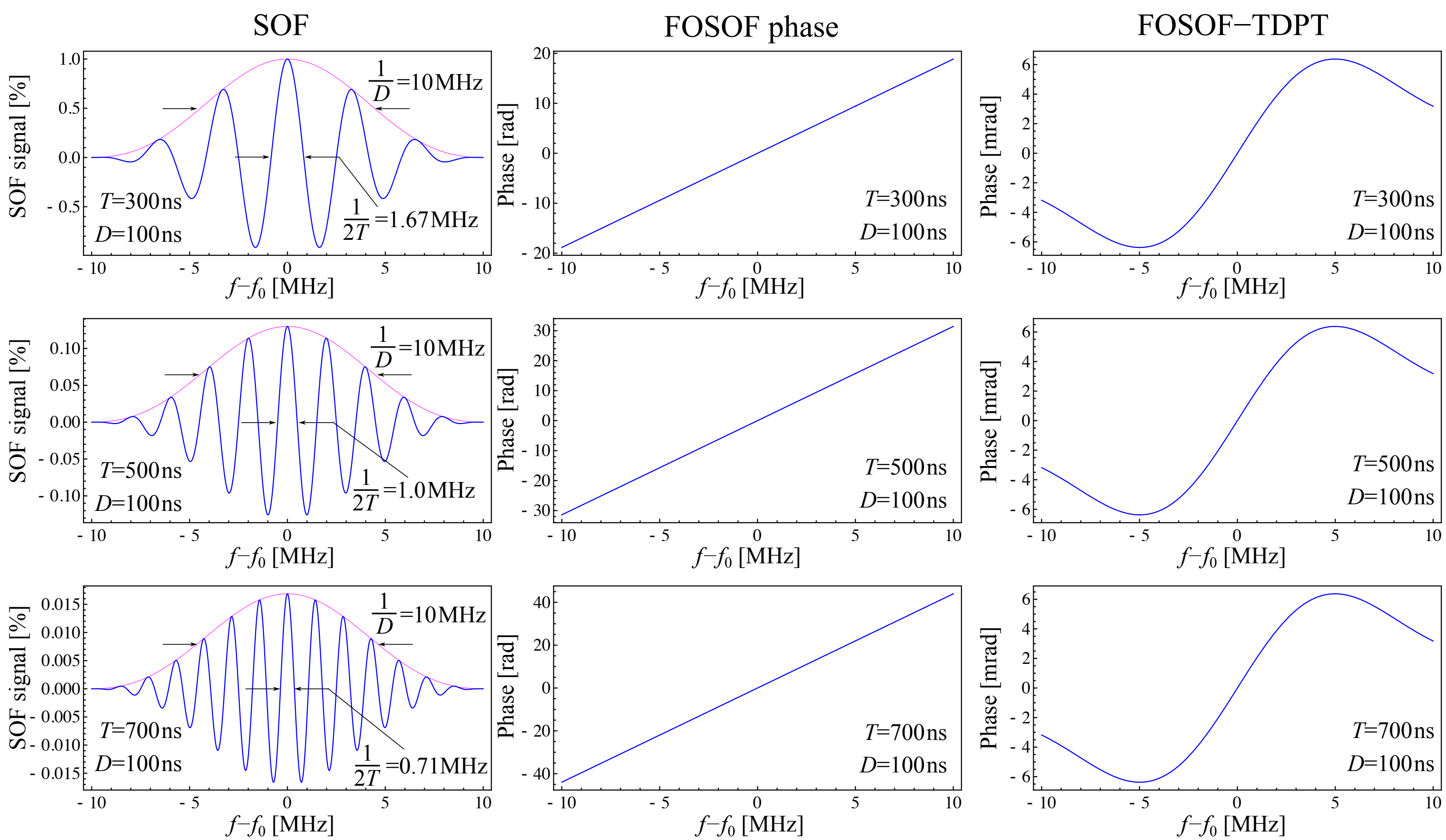

Figure 3.4: Theoretical SOF and FOSOF lineshapes for different T. In the figure, parameters D=100 ns and V=1 rad/s are used. Variations in the width of the SOF interference and the FOSOF phase slope are observed. FOSOF-TDPT (i.e., the second term of Equation 3.15) remains the same for different T values.

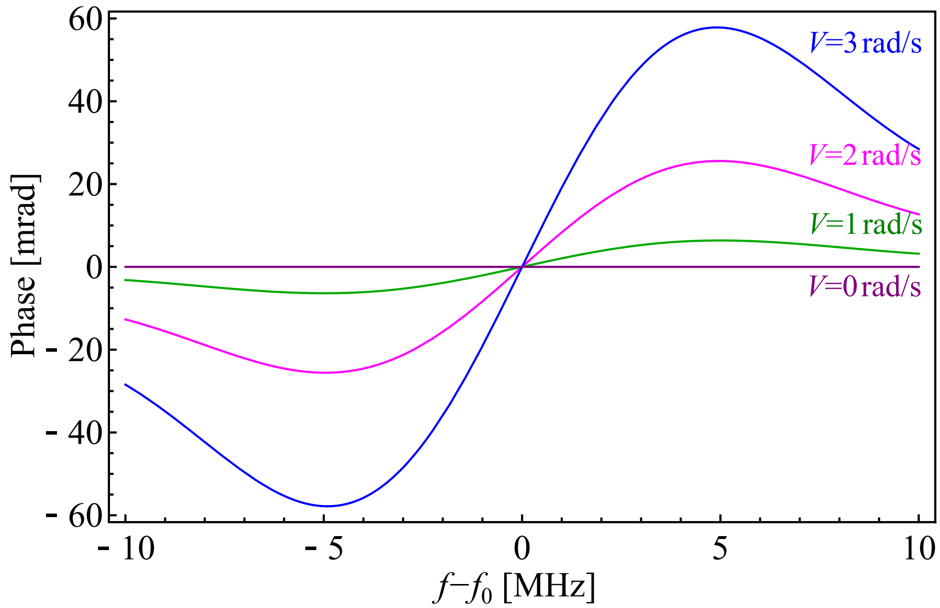

Figure 3.5: Effect of V on the FOSOF theoretical lineshape (shown here for T=400 ns and D=100 ns). FOSOF-TDPT lineshape (the second term of Equation 3.15) grows as V increases. For V=0 rad/s the TDPT prediction of a linear lineshape is exact.

as V approaches to zero, the TDPT linear lineshape is restored, and the FOSOF-TDPT lineshape is zero. Figure 3.6 illustrates three lineshapes with different D for a fixed T and V. D governs the spectral width of the microwave pulse (the width of the envelope of the SOF interference goes as $1/D$). Three SOF lineshapes shown at the left of the figure have different widths for different D values. The width of the SOF interference and FOSOF phase slope does not change because T remains constant. The FOSOF-TDPT lineshapes show that the size of the deviation grows as D increases. The figure also shows that the FOSOF-TDPT difference is maximized around the half width point of the transition.

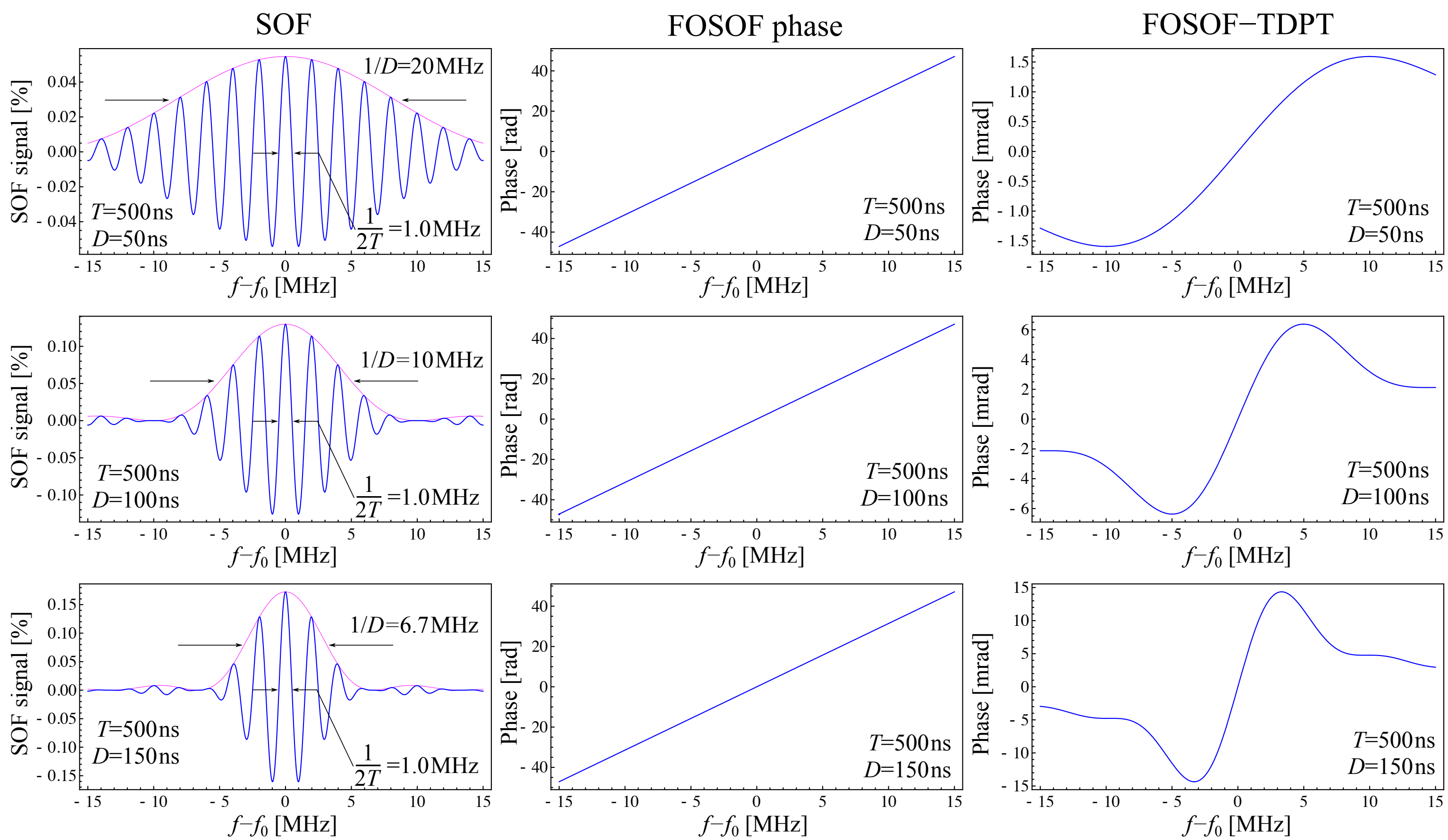

Figure 3.6: Theoretical SOF and FOSOF lineshapes for different D. The width of the transition (pink solid line in the SOF column) changes for different D. The SOF interference and FOSOF phase slope remains constant for all three cases. The FOSOF-TDPT difference is maximum around the half-width of the transition.

definition	fit parameter	comments
Pulse separation	T	floated with the nominal experiment value as an initial guess. Sensitive to phase slope.
Pulse duration	D	fixed with the nominal experiment value
Microwave field amplitude	V	fixed with the best guess of the fractional microwave power
resonant frequency	f_0	floated, a quantity to be determined from the fit
microwave frequency	f	function variable

Table 3.1: Summary of fit parameters.

3.3 FOSOF Experimental Lineshapes

Figures 3.7 through 3.12 show the experimental FOSOF lineshapes for the 18 timings used in the experiment. Experimental lineshapes for multiple microwave power settings are shown. The plots at the top show the averaged data points (averaged over the full data set considered in this thesis) along with a fit using Equation 3.15. The error bar associated with each data point is too small to be seen on this scale. The middle plot shows the same data points and fit with the TDPT linear prediction $(2\pi T(f - f_0))$ subtracted. The subtraction scales up the plots at the top by about a factor of 100, and the error bars start to become visible in some of the plots. The fit residuals are shown at the bottom of the figure. Residuals for different power settings are shown separately. Typically, three different microwave power settings are shown. The reduced chi-square of the fits is typically less than 1 (with 30 degrees of freedom).

Table 3.1 shows a summary of fit parameters. The lineshape used is Equation

3.15, with $2\pi(f - f_0)$ substituted in place of $\Delta\omega$. Typically, the pulse separation T and the resonant frequency f_0 are floated. Other parameters (the pulse duration D and the microwave power V) are fixed with the nominal experimental settings. Different sets of floating parameters are used to check the consistency in fit linecentres. Very small ($\sim$1 Hz) variations in fit linecentres are observed when different sets of parameters are floated; therefore, the measured linecentres are independent of the floating parameters if the fixed values are chosen properly.

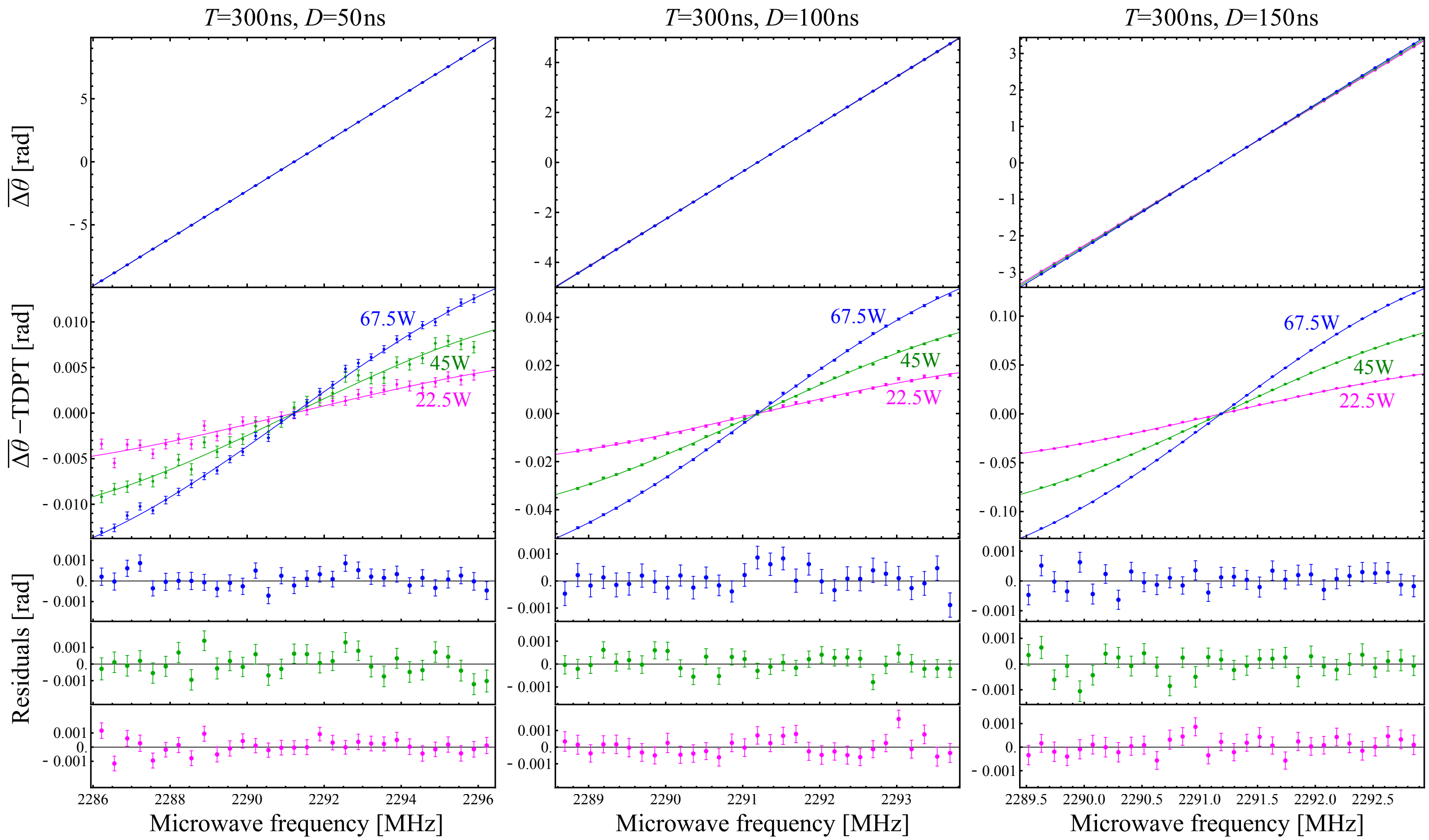

Figure 3.7: FOSOF experimental lineshapes and fits: (T,D)=(300,50) ns, (300,100) ns,(300,150) ns.

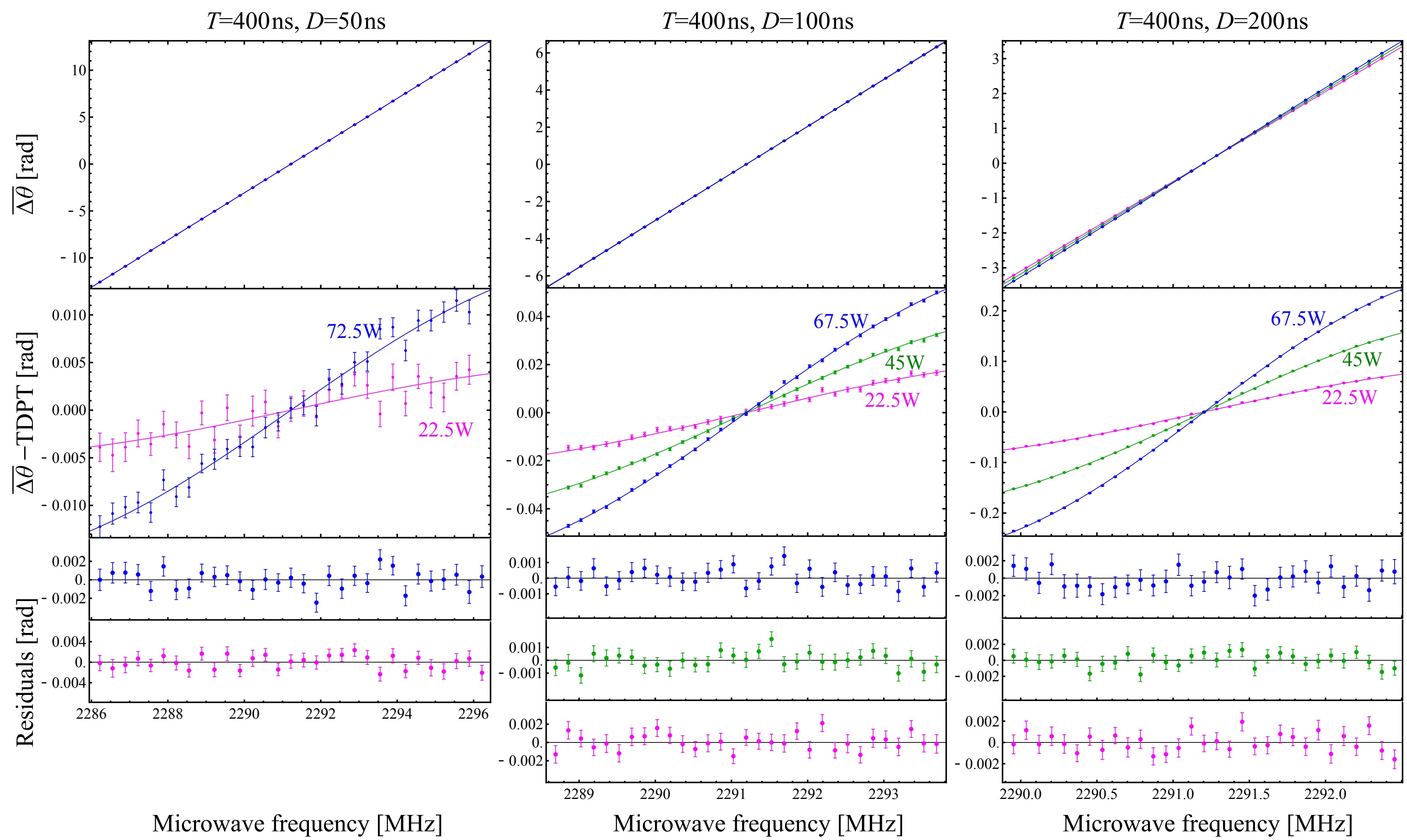

Figure 3.8: FOSOF experimental lineshapes and fits: (T,D)=(400,50) ns, (400,100) ns, (400,200) ns.

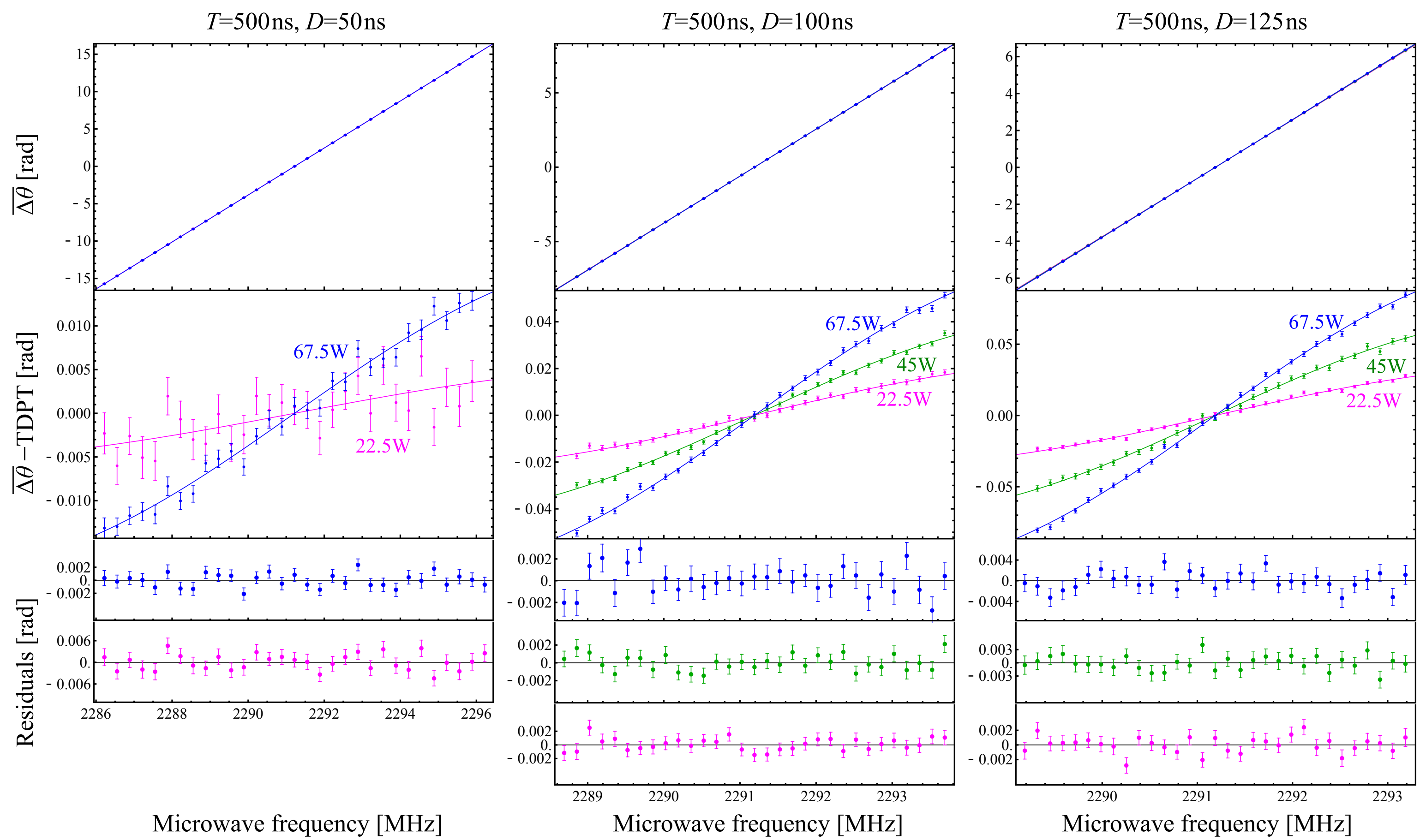

Figure 3.9: FOSOF experimental lineshapes and fits: (T,D)=(500,50) ns, (500,100) ns, (500,125) ns.

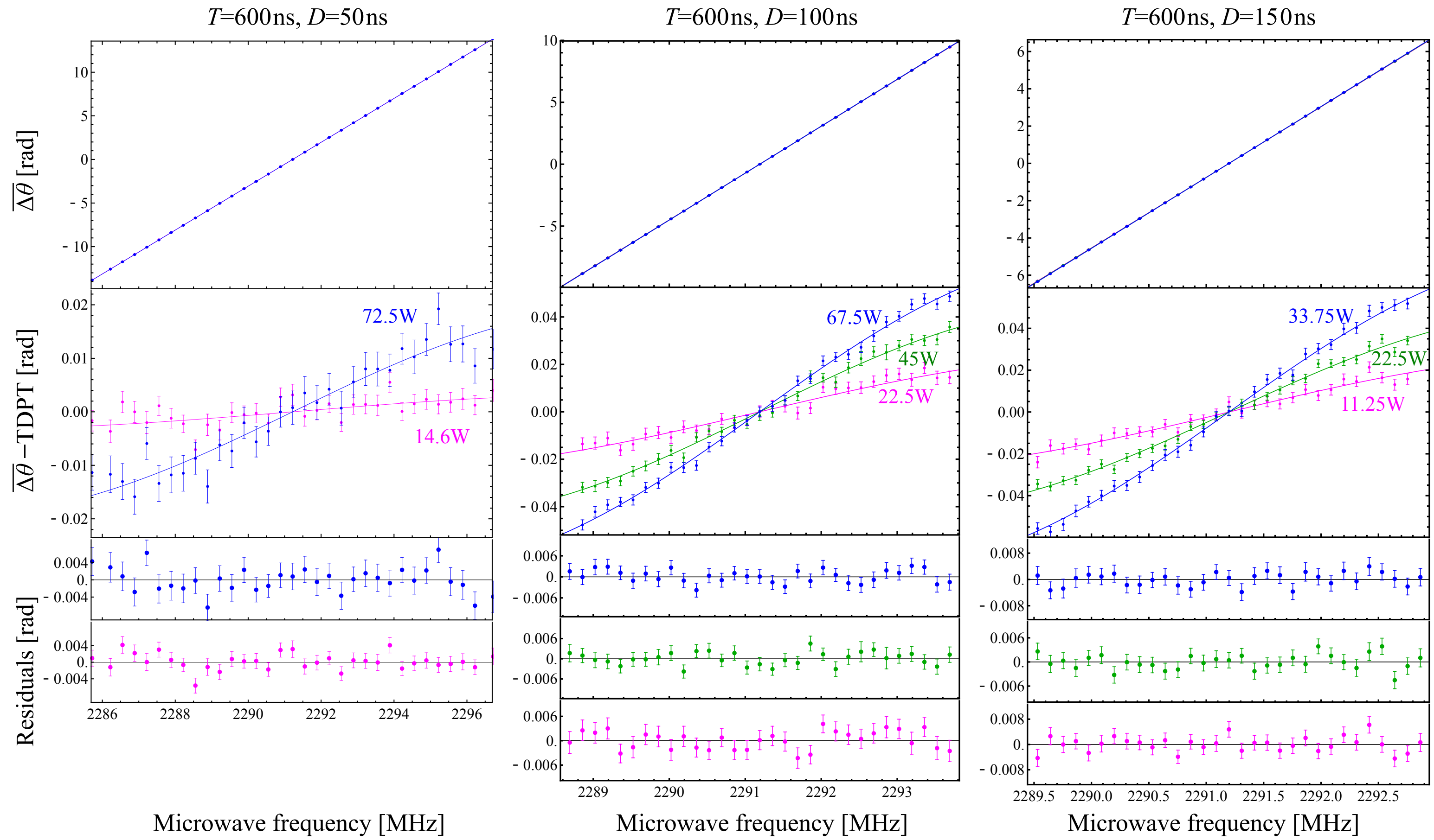

Figure 3.10: FOSOF experimental lineshapes and fits: (T,D)=(600,50) ns, (600,100) ns, (600,150) ns.

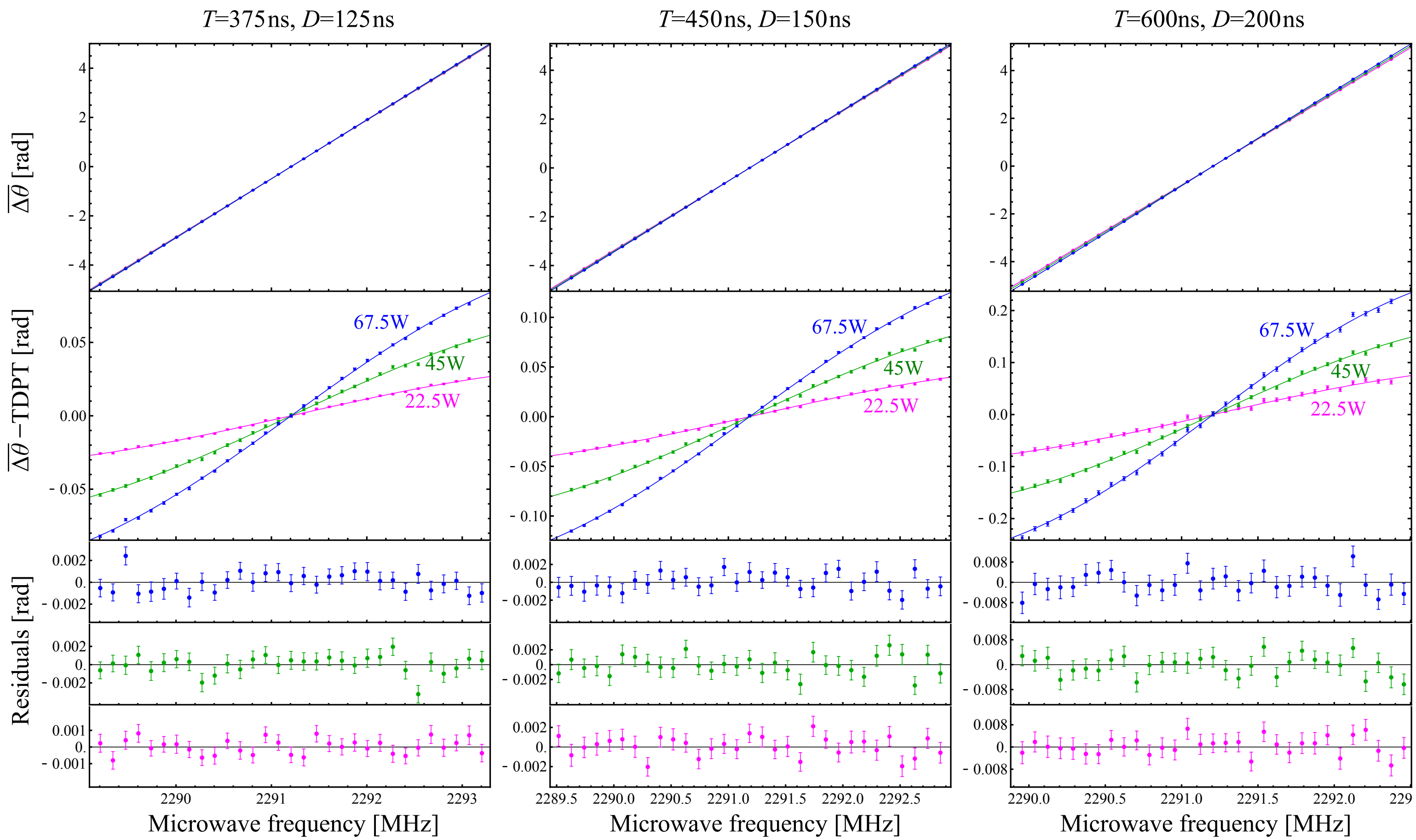

Figure 3.11: FOSOF experimental lineshapes and fits: (T,D)=(375,125) ns, (450,150) ns, (600,200) ns.

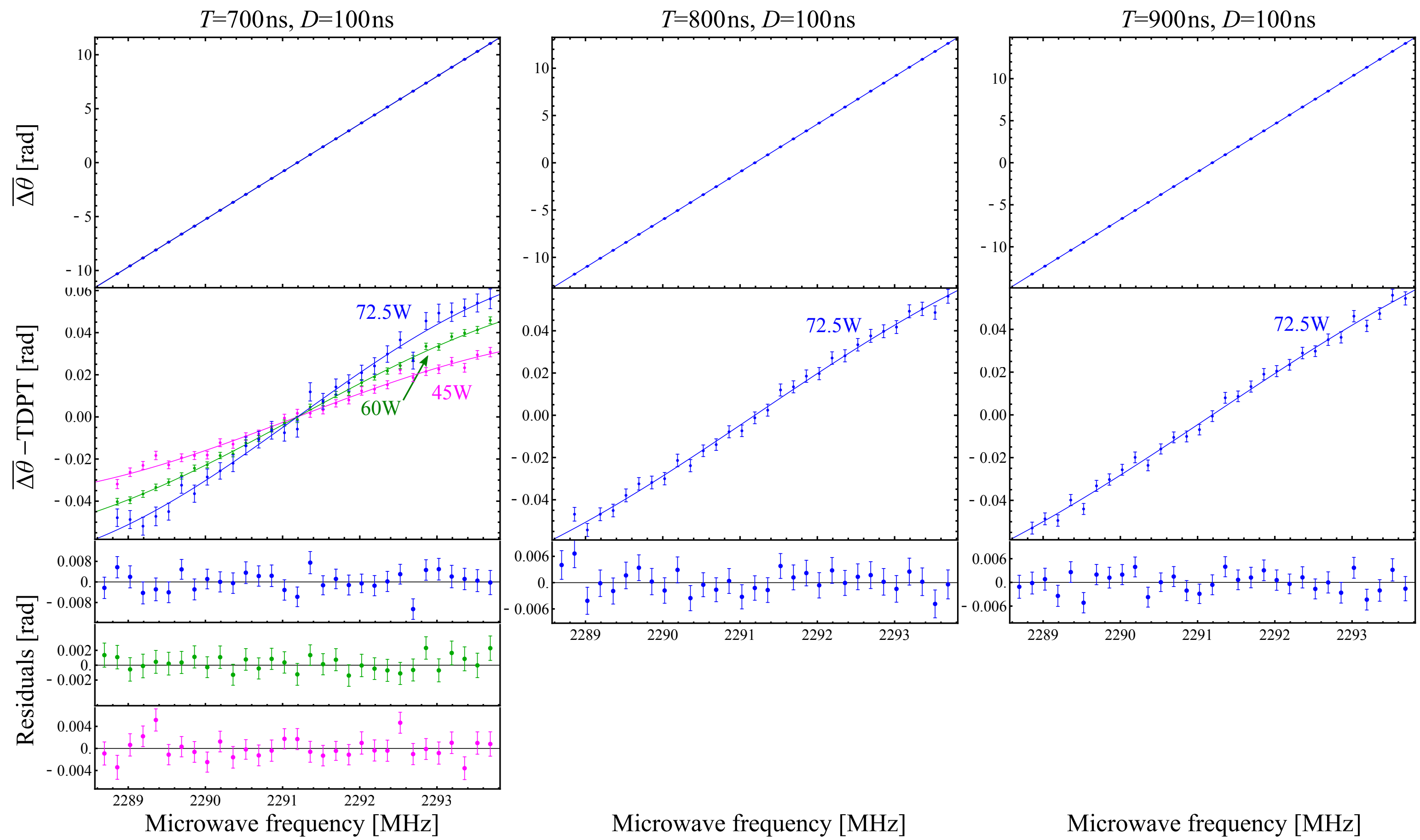

Figure 3.12: FOSOF experimental lineshapes and fits: (T,D)=(700,100) ns, (800,100) ns, (900,100) ns.

3.4 Measured Linecentres

Table A.2 in Appendix-A gives a summary of the linecentres obtained from fits of the experimental data and also gives the applied systematic corrections and their uncertainties (as discussed in Chapter 4). A significant amount of data is collected to test for systematic effects. A detailed description of the systematic corrections and their associated uncertainties is given in Chapter 4. A total of 3608 experiments were performed between April 24 to June 14, 2018. Column one is the run number assigned to each row of the table. Columns two through four show the microwave parameters, the pulse separation T, the pulse duration D, and the microwave power P, used in the experiment. Column five is the magnetic field setting B of the experiment. The sign indicates that the magnetic field direction is reversed from $+\hat{z}$ to $-\hat{z}$ direction. Column six is the polarization angle of a quarter-wave plate for optical pumping direction. The combination of the sign of B and polarizer angle determines the m_J state (m_J=+1 or -1) used in the experiment. Columns seven and eight are the linecentres obtained from fits and the associated fit uncertainties. Columns nine through twelve are the systematic corrections applied to the measured linecentres and their uncertainties. Column thirteen shows linecentres after the systematic corrections are applied. Column fourteen is the total uncertainty obtained by adding all uncertainties in quadrature.

Column fifteen gives the normalized weights used to take the weighted average of the data runs. Identifiers are assigned to data runs used for the study of systematic effects, and are shown at column sixteen. Table A.1 shows the definition of each identifier. Numbers in columns seven and thirteen are with respect to the final measured result of 2 291 176 590 Hz.

4 Systematic Effects

The excellent signal-to-noise ratio obtained in the current experiment allowed for an extensive study of systematic effects. In this chapter, details on systematic effects and corresponding corrections and uncertainties are discussed. It should be noted that the order of data acquisition is randomized whenever possible to eliminate the possible effects of time-dependent linecentre shifts. However, there was no evidence for such time-dependent shifts in the data set.

4.1 DC Zeeman Shifts

The largest systematic correction applied to the measured linecentres comes from the quadratic DC Zeeman shift. The DC magnetic field perturbs the atomic system and shifts the energy levels. To first-order, the $2^3\mathrm{P}_1(\mathrm{m}_J=\text{-}1)$-to-$2^3\mathrm{P}_2(\mathrm{m}_J=\text{-}1)$ transition does not have a DC Zeeman shift since the two states shift at the same rate. However, these states shift differently when higher-order effects are taken into account. In second-order, the $2^3\mathrm{P}_1(m_J=-1)$ and $2^3\mathrm{P}_2(m_J=-1)$ states repel each other at a quadratic rate of $0.4295\,\mathrm{kHz/G^2}$ [54]. Since the scale of the shift is large, it it necessary to have a precise knowledge of the applied field to apply accurate corrections to the measured linecentres. The magnetic field system is described in Section 2.10. The magnetic field B is the combination of applied and residual fields at the location of the experiment. Therefore, B can be written as

$$B = \sqrt{(kI + B_0^{\parallel})^2 + (B_0^{\perp})^2}, \tag{4.1}$$

where I is the current applied to the Helmholtz coils, and k is the current-to-field conversion factor (in Gauss per Ampere) for the main Helmholtz coils, and $B_0^{\parallel}$ and $B_0^{\perp}$ are the residual-field components that are parallel and perpendicular to the Helmholtz axis. As described in Section 2.10, the magnetic field at the location of the experiment was measured using a 3-axis gaussmeter. The residual fields $B_0^{\parallel}$ and $B_0^{\perp}$ are cancelled to $\pm 10\,\mathrm{mG}$. k for the main Helmholtz coils was found to be $k_{\mathrm{gaussmeter}}$=$10.866 \pm 0.010\,\mathrm{G/A}$. However, the difficulty in positioning the probe exactly at the location of the experiment poses questions about the accuracy of this measurement.

4.1.1 Uncertainty in the Residual Magnetic Field

In the presence of $B_0^{\parallel}$, the quadratic Zeeman shift has the form,

$$\Delta\nu_{\mathrm{DC\ Zeeman}}(I) = \beta\left((kI)^2 + 2kIB_0^{\parallel} + B_0^2\right), \tag{4.2}$$

where $\beta = 0.4295\,\mathrm{kHz/G^2}$ is the quadratic Zeeman shift rate. The $B_0^2 = (B_0^{\perp})^2 + (B_0^{\|})^2$ term is negligible since $|B_0|$ is less than 10 mG, leading to a contribution of < 0.04 Hz. In order to cancel the contribution from the linear term in Equation 4.2, half of the data is taken with positive current and half with negative current. The linear term gets cancelled when linecentres from the two types of data are averaged together.

4.1.2 Uncertainty in the Applied Magnetic Field

Precise values of k and I are required to apply appropriate corrections for the quadratic Zeeman shift. The current I is measured to an accuracy of better than 0.002 % by measuring the voltage across a precision shunt resistor (IET Labs, Inc. model DCCS-0.01). Linecentres are determined as a function of applied magnetic field to test the k value obtained with the gaussmeter ($k_{\mathrm{gaussmeter}}$=10.866±0.010 G/A). Figure 4.1 shows an example of linecentres obtained versus current in the Helmholtz coils. The data are fit to Equation 4.2 (ignoring the small B_0^2 term), floating parameters k and $B_0^{\|}$. The residual field parameter $B_0^{\|}$ is found to be 0.002±0.005 G, which is consistent with zero. The value of k, however, is determined to be slightly different from the value obtained with the gaussmeter method. The parameter k from the fit is k_{fit}=10.846±0.001 G/A, and this value is 0.2 % smaller than $k_{\mathrm{gaussmeter}}$. The atomic data are taken with the experimental setup for the actual experiment

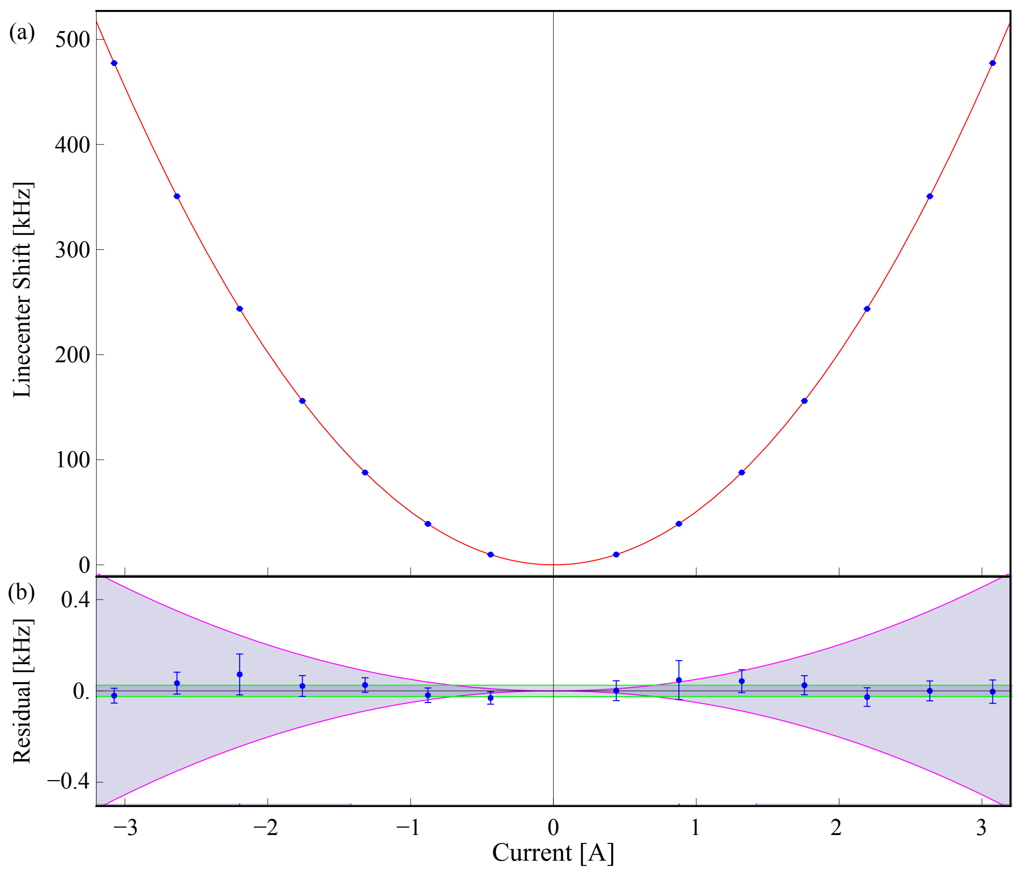

Figure 4.1: Magnetic field calibration curve. Panel (a) shows the data fit to Equation 4.2. Panel (b) show the residuals of the fit. The band bounded by the pink lines indicates the result of an additional 0.1 % uncertainty in the DC Zeeman correction (column 10 in Table A.2), and the band bounded by the green lines is the final quoted uncertainty of 25 Hz.

and therefore measures the magnetic field at the correct position; therefore it is more reliable. However, if there is a position-dependent variation in k around the experiment region which causes the two values to disagree, then an additional uncertainty needs to be assigned because the position of the excitation inside the microwave region may change slightly depending on the laser alignment.

Table 4.1 shows measured (using averages of the full data set of Table A.2) and predicted Zeeman shifts (based on determinations of k and I) for different currents applied to the Helmholtz coils. The first and second columns show the nominal field setting and corresponding applied current to the Helmholtz coils. Column 3 shows the average measured linecentres at currents given in column 2, and column 4 shows the difference between the linecentre obtained at the smallest current shown in the table (I_0) and the other currents I. This column indicates the experimentally observed DC Zeeman shifts with respect to I_0. Linecentres listed in this column are obtained by averaging NR and LB data types in Table A.2 without applying a DC Zeeman correction and without applying the DC Zeeman uncertainty (i.e., subtracting the DC Zeeman correction and uncertainty in columns 9 and 10 from the corrected linecentres in column 13 of Table A.2). Column 5 of Table 4.1 is the predicted DC Zeeman shift based on fields obtained by $B(I) = k_{\text{fit}} I$. Percentage difference between the measured and predicted Zeeman shifts (column 6) shows an average difference of 0.086 %. The data in column 4 is re-fit to Equation 4.2 for a further

Nominal B [Gauss]	I [A]	$\nu_{\mathrm{avg}}(I)$ [Hz]	$\nu_{\mathrm{avg}}(I) - \nu_{\mathrm{avg}}(I_0)$ [Hz]	$\beta((k_{\mathrm{fit}}I)^2 - (k_{\mathrm{fit}}I_0)^2)$ [Hz]	Difference between col. 4 and col. 5 [%]	$\beta((k_{\mathrm{data}}I)^2 - (k_{\mathrm{data}}I_0)^2)$ [Hz]	Difference between col. 4 and col. 7 [%]
3.175	I_0=0.293806(10)	2 291 180 950(9)					
4.762	0.439791(5)	2 291 186 356(6)	5 406(11)	5 411(2)	0.092	5 407(2)	0.002
9.524	0.878683(8)	2 291 215 558(11)	34 608(14)	34 648(7)	0.115	34 620(7)	0.035
19.048	1.757554(19)	2 291 332 546(18)	151 596(20)	151 709(29)	0.075	151 588(29)	0.005
28.572	2.635487(40)	2 291 527 294(22)	346 344(24)	346 572(64)	0.066	346 297(64)	0.014
33.334	3.075265(49)	2 291 654 035(29)	473 085(30)	473 462(87)	0.080	473 087(87)	0.0003

Table 4.1: Comparison between the measured and predicted DC Zeeman shifts. The first column is the field setting. The second column is the current applied to the Helmholtz coils. $\nu_{\mathrm{avg}}(I)$ is the measured linecentres with the applied current. Linecentres shown here are obtained by taking NR and LB data types (refer to Table A.1 for identifiers) in Table A.2 and averaging the linecentres (column 13 in Table A.2) without DC Zeeman correction and uncertainty (columns 9 and 10 in Table A.2) at fields shown in the first column. The values in columns 1 and 2 are also averaged (with the same weights as used for ν_{avg}) for data taken at almost identical field settings. One standard deviation uncertainties are shown in parentheses. $\nu_{\mathrm{avg}}(I) - \nu_{\mathrm{avg}}(I_0)$ is the difference between the linecentre obtained with the smallest applied current and linecentre with other applied currents, where I_0 indicates the smallest applied current shown in the first row. $\beta((k_{\mathrm{fit}}I)^2 - (k_{\mathrm{fit}}I_0)^2)$ and $\beta((k_{\mathrm{data}}I)^2 - (k_{\mathrm{data}}I_0)^2)$ are the predicted DC Zeeman shifts based on fields calculated using k_{fit} and k_{data} with respect to field at I_0. Columns 6 and 8 show the percentage difference between the measured and predicted DC Zeeman shifts using k_{fit} and k_{data}.

Parameters	Linecentre ν_{exp} [Hz]	$\Delta\nu$ [Hz]
Negative field polarity	2 291 176 593(12)	+3
Positive field polarity	2 291 176 592(13)	+2
|B| in range 0 to 5 G	2 291 176 584(11)	−6
|B| in range 5 to 10 G	2 291 176 592(16)	+2
|B| in range > 10 G	2 291 176 567(62)	−23

Table 4.2: Summary of measured linecentres with different magnetic field settings. The consistency of results demonstrated in this table eliminates the possibility of having effects larger than the level of precision of the current experiment. The table also shows the results of opposite magnetic field directions. $\Delta\nu = \nu_{\text{exp}} - \nu_{12}$ is the difference between the measured linecentre $\Delta\nu_{\text{exp}}$ and the final measured result of $\nu_{12} = 2\,291\,176\,590\,\text{Hz}$.

adjustment on the value of k. This fit (which is based on the full data set used for the current measurement) suggests k_{data}=10.842±0.001 G/A, which agrees to better than 0.1 % with k_{fit}. Column 7 and 8 shows predicted linecentres based on $\beta(k_{\text{data}}I)^2$ and difference between the measured and predicted linecentres, respectively. Shifts predicted by $\beta(k_{\text{data}}I)^2$ are used to correct all measured linecentres. The observed discrepancy between the k_{fit} and k_{data} sets a limit on the knowledge of the applied field, and a conservative 0.1 % uncertainty (slightly larger than the average difference of 0.086 % from the prediction of $\beta(k_{\text{fit}}I)^2$) is assigned to the DC Zeeman correciton for all of the experimental runs to account for the position-dependent variation of k. Most of our data are taken at fields smaller than 5 G, where 0.1 % correction uncertainty yields < 10 Hz contribution to the total uncertainty. Agreement between the data taken at low and high fields verifies the 0.1 % understanding of the applied fields, as illustrated in Figure 5.1 and Tables 4.1 and 4.2.

4.2 Microwave Power Shifts

Linecentre shifts related to the power of the microwave pulses are discussed in this section. Numerical integration of the time-dependent Schrödinger equation was carried out by Taylor Skinner to model the experiment based on the oscilloscope traces of the microwave pulses used in the experiment, or based on models of possible imperfections in the microwave fields. In particular, systematic effects due to frequency-dependent microwave power variation (Section 4.2.3) and distorted phase and amplitude profiles for the microwave pulses (Section 4.2.4), are extensively modelled. All shifts described in this section follows a linear trend versus microwave power, and vanish at zero microwave power.

4.2.1 AC Zeeman Shifts

The oscillating microwave magnetic field introduces AC Zeeman shifts to the 2^3P_1-to-2^3P_2 linecentre. A detailed description of AC Zeeman shifts is given in [54], so only a brief explanation is given here. Figure 4.2 illustrates the microwave magnetic and electric fields inside the coaxial airline. Within the coaxial airline, the microwave magnetic field is, to a good approximation, pointing in the $\hat{z}$ direction. For our coaxial geometry, the relationship between microwave field and power that atoms

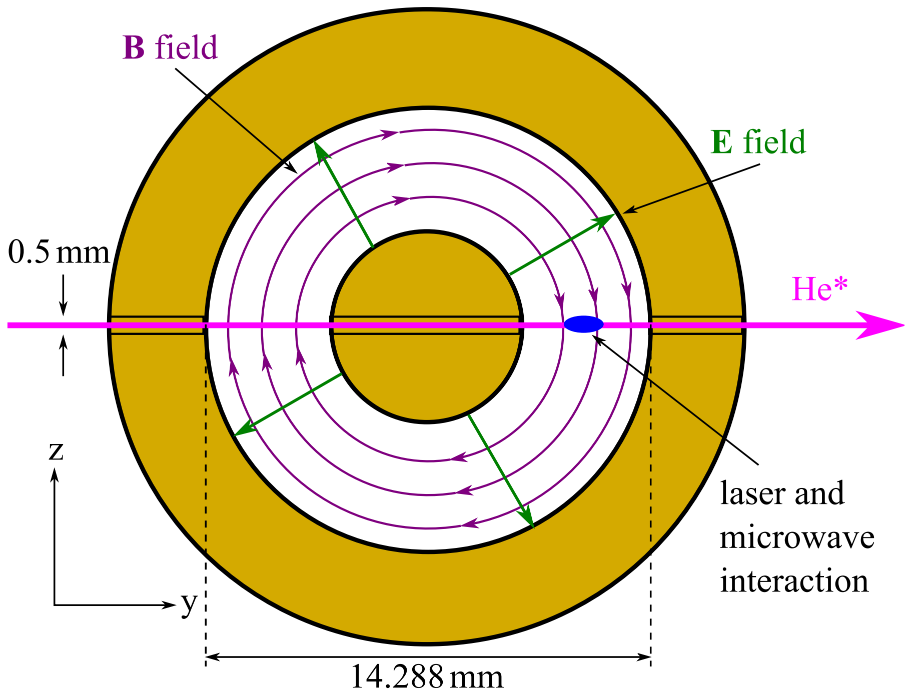

Figure 4.2: Microwave magnetic and electric field lines inside the coaxial airline.

see is given by [55]

$$B_{mw}(r) = 2\mu_0 \left(\frac{a}{r}\right) \left[\left(\frac{1}{\pi a^2}\right)\sqrt{\frac{\epsilon_0}{\mu_0}}\left(\ln\left(\frac{b}{a}\right)\right)^{-1} P_{mw}\right]^{1/2}, \tag{4.3}$$

where a is the radius of the inner conductor, b is the radius of the inner wall of the outer conductor, r is the location of the interaction measured from the central axis of the inner conductor, ϵ_0 is the electric permittivity of vacuum, μ_0 is the magnetic permeability of vacuum, and P_{mw} is the microwave power in the coaxial transmission line. The a/r factor is the field reduction factor necessary to account for the decreasing field as a function of distance from the surface of inner conductor. In the current experiment, the microwave is reflected from the short at the end of the microwave region. This gives the factor of 2 in Equation 4.3. The 14-mm coaxial airline geometry (dimensions of the microwave region are given in Section 2.11.2.3) has a=3.102 mm and b=7.144 mm. The interaction of the atoms with the first microwave pulse happens at approximately r=5.123 mm, the average of a and b. The pulse separation T used in the experiment ranges from 300 to 900 ns. With the most probable atomic speed of v_{mode}=1100 m/s, atoms travel a distance of approximately $v_{mode}T$ during the time T. The average interaction location r is therefore half way between $(a+b)/2$ and $(a+b)/2+v_{mode}T$. Plugging a, b and r values into Equation 4.3 gives B_{mw}. For the $2^3\mathrm{P}_1(m_J{=}\pm1)$-to-$2^3\mathrm{P}_2(m_J{=}\pm1)$ transitions, the AC Zeeman shift rate is given by [54]

$$\Delta\nu_{\text{AC Zeeman}} = (+54\,\text{Hz})\,\frac{B_z^2}{\mathrm{G}^2}. \tag{4.4}$$

The AC Zeeman effect for the case of SOF experiment is suppressed by approximately a factor D/T [33] because the microwaves are on for a fraction of the time defined by the experimental timing parameters T and D. Table 4.3 summarizes the expected AC Zeeman shifts for different experimental timing parameters for the maximum available microwave power of 75 W. The AC Zeeman shifts are $\lesssim$100 Hz, and are even smaller at the typical powers used for the measurements.

Pulse separation T [ns]	Pulse duration D [ns]	Interaction location r [mm]	SOF suppression D/T	Microwave field B_{mw} [Gauss]	AC Zeeman shifts $\Delta\nu_{\text{AC Zeeman}}$ [Hz]
300	50	5.486	0.167	1.986	35
300	100	5.486	0.333	1.986	71
300	150	5.486	0.500	1.986	106
375	125	5.577	0.333	1.953	69
400	50	5.607	0.125	1.943	25
400	100	5.607	0.250	1.943	51
400	200	5.607	0.500	1.943	102
450	150	5.668	0.333	1.922	67
500	50	5.728	0.100	1.902	20
500	100	5.728	0.200	1.902	39
500	125	5.728	0.250	1.902	49
600	50	5.849	0.083	1.863	16
600	100	5.849	0.167	1.863	31
600	150	5.849	0.250	1.863	47
600	200	5.849	0.333	1.863	62
700	100	5.970	0.143	1.825	26
800	100	6.091	0.125	1.789	22
900	100	6.212	0.111	1.754	18

Table 4.3: Expected AC Zeeman shifts for different experimental timing parameters for the maximum microwave power of 75 W.

4.2.2 AC Stark Shifts

The oscillating electric field of the microwave pulses cause linecentre shifts due to the AC Stark effect. The AC Stark shift rate of the 2^3P_1-to-2^3P_2 transition is estimated in [54]. A microwave electric field in the $\hat{z}$ direction causes a shift of

$$\Delta\nu_{\text{AC Stark}} = (-7.78 \pm 0.57)\,\text{kHz}\,\frac{E_z^2}{(\text{kV/cm})^2}, \tag{4.5}$$

and the electric field in the $\hat{y}$ direction causes a shift of

$$\Delta\nu_{\text{AC Stark}} = (-0.6 \pm 1.2)\,\text{kHz}\,\frac{E_y^2}{(\text{kV/cm})^2}. \tag{4.6}$$

As in the case of the AC Zeeman shift, the shift for SOF experiment is suppressed by a factor D/T. As it can be seen from Figure 4.2, the microwave field component E_z is significantly smaller than E_y due to the geometry. The geometry restricts the size of E_z to be $< 5\,\%$ of E_y; therefore the shift rate associated with the z-component of the electric field is negligible. The size of the E_y^2 would be significant for the microwave power used in the current experiment. However, the reflection of the microwave pulse from the short located a half wavelength away from the interaction region cancels out the electric field at the location of interaction. That is, there is an electric field node at this position. With the slit width of 5 mm, the maximum electric field (at a position of ± 2.5 mm from the centre of the slit —i.e., from the position of the node) is suppressed by a factor of < 0.0035. With this suppression, the shift is estimated to be $< 1\,\mathrm{Hz}$. There are, however, short periods of time near the beginning and the end of the pulses when the electric field does not get cancelled by the reflection. It takes $0.22\,\mathrm{ns}$ for the microwave to return to the interaction location after a reflection off of the short in Figure 2.34. Using a reduction factor of $2(0.22\,\mathrm{ns})/T$ (the factor of 2 is because of the two 0.22-ns periods during which the electric field is not cancelled), the net AC Stark shifts are negligibly small ($< 1\,\mathrm{Hz}$).

4.2.3 Shifts Due to Frequency-Dependent Microwave-Power Variation

The microwave power seen by the atoms is not perfectly independent of frequency over the frequency range used in the experiment due to the frequency responses of various RF components in the system. The changing microwave power over the frequency range of the experiment causes a lineshape distortion and shifts the linecentre. Simulation of this effect predicts that the linecentre shifts due to the frequency-dependent microwave power is proportional to the applied microwave power. No shifts are seen in the low-power TDPT regime (i.e., the shift extrapolates to zero as $P_{mw} \to 0$).

In order to achieve the best power flatness versus frequency, the output power level of both the HP and Wiltron microwave generators are adjusted for every frequency used in the experiment. The power of the microwave pulses used in the experiment is monitored using a power detector and an oscilloscope. The power flatness calibration was performed at every power setting used in the experiment. This calibration was performed twice before the start of the data acquisition. The level of power flatness was $< 0.05\,\%/\mathrm{MHz}$, assuming that the oscilloscope and diode give an accurate measurements of the microwave power. Simulation results with $0.05\,\%/\mathrm{MHz}$ flatness level shows a shift of 150 Hz (at full power) assuming experimental timing parameters T=300 ns and D=100 ns, with the shift extrapolating to zero at zero power.

Recent (February 2019) investigation of the power flatness using atoms [56] reveals that the power detector reading and oscilloscope traces do not represent the actual power seen by the atoms. Reflections in the microwave system and imperfect isolation in the circulator cause the detector reading to oscillate as a function of applied microwave frequency, even when the atoms experience perfect power flatness. As a result, the quoted 0.05% power-flatness level is underestimated. The effect of imperfect power flatness is eliminated by the extrapolations to zero power, as discussed in Section 4.2.5.

4.2.4 Shifts Due to Imperfect Microwave Phase and Amplitude

The most subtle systematic effect arises from distortions of the phase and amplitude of the microwave pulses. The phase distortion is most prominently observed at the beginning and end of the microwave pulses. Sudden switching of microwaves causes the phase during the rise and fall times of the pulses to become shifted compared to the time at which microwaves are fully on. Figure 4.3(a) shows an example of an oscilloscope trace of the microwave pulses for T=400 ns and D=100 ns. Figure 4.3(b) shows an expanded view of one of the pulses in Figure 4.3(a). The plot shows a small increase of the pulse amplitude over the duration of the pulse. Figure 4.4 shows three segments of the microwave pulse of Figure 4.3(b). Figures 4.4(a) and 4.4(c) show the beginning and end of the pulse, respectively. Figure 4.4(b) shows a central fraction of the microwave pulse. The sine wave in pink is a fit to the central part of the microwave pulse shown in Figure 4.4(b). At the beginning and end of the pulse, data points are out of phase with the pink line, showing an indication of phase distortion at these times.

Integration of the Schrödinger equation based on oscilloscope traces of microwave pulses (an example is shown in Figure 4.3) show that the linecentre shift is approximately proportional to the inverse of the pulse separation ($1/T$), the pulse duration D, and the microwave power P. That is,

$$\Delta\nu \propto D\frac{P}{T}, \tag{4.7}$$

where $\Delta\nu$ denotes the linecentre shift. Experiments with various T, D, P combinations were performed to understand this effect. Since the effect of the microwave phase and amplitude imperfections is expected to vanish at zero microwave power, all measured linecentres are extrapolated to zero power. The data collected with different T, D, and P parameters approximately follow the trend predicted by

Equation 4.7 (shown in Figures 4.5 through 4.7). The method and results of the power extrapolation are discussed in Section 4.2.5.

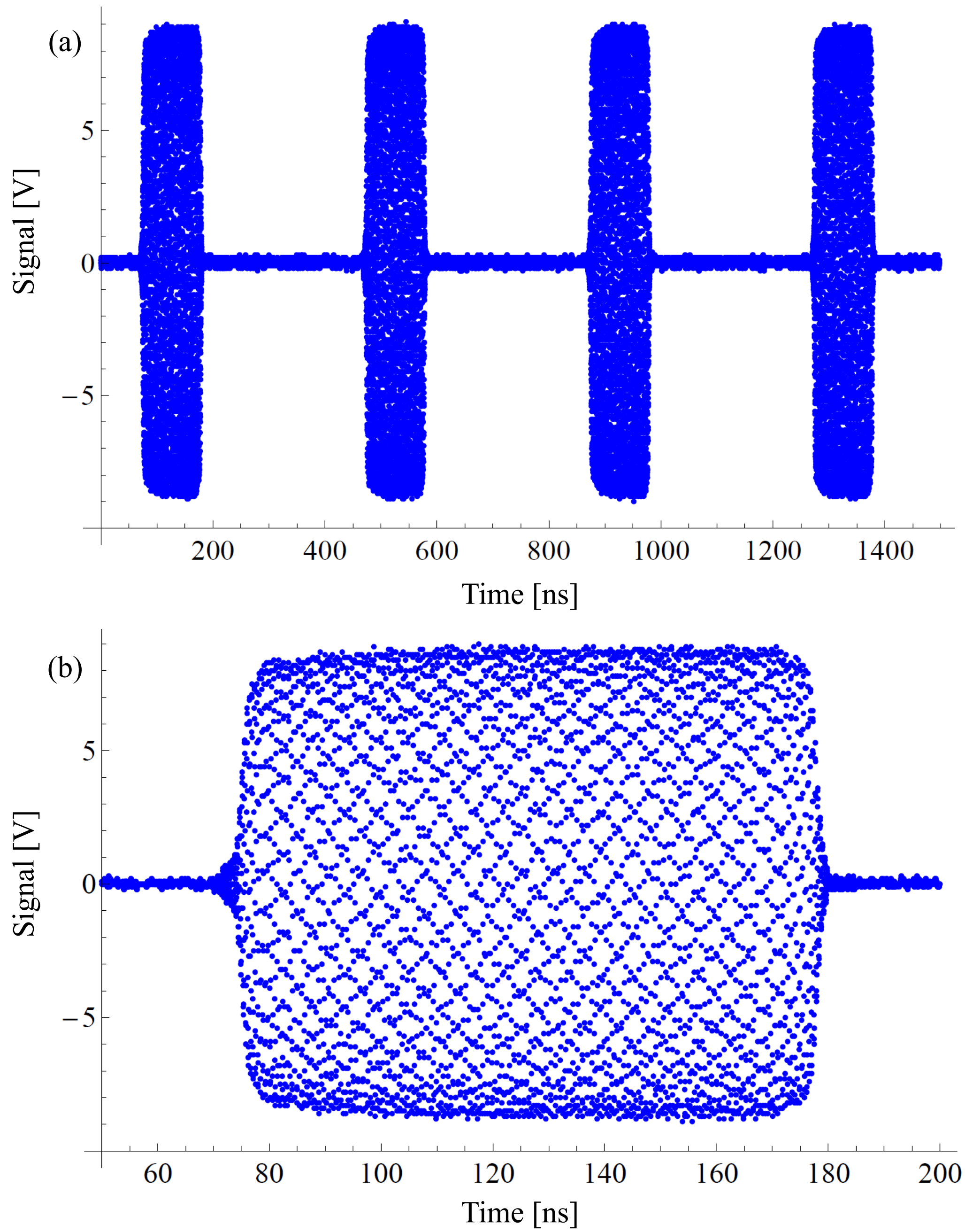

Figure 4.3: Shape of the microwave pulses. (a) shows an oscilloscope trace of T=400 ns and D=100 ns microwave pulses, and (b) shows a pulse in (a) in a blown-up scale. A small amplitude variation is observed.

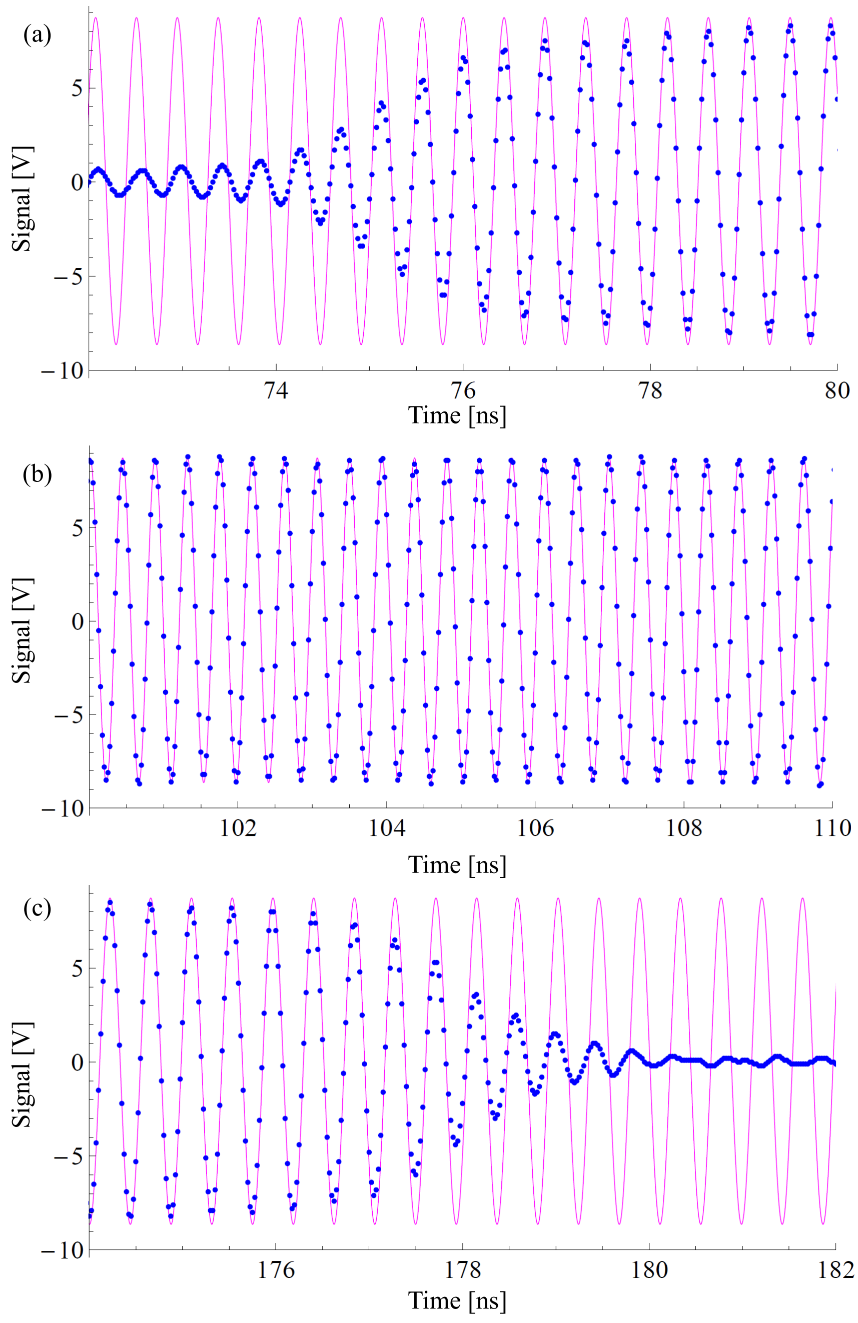

Figure 4.4: Phase distortion of the microwave pulse. The pink sine wave represents a fit to data shown in (b), and the same fit is shown in both (a) and (c) as a reference. The data in (a) and (c) do not follow the fit during turn-on and -off of the microwave pulse, showing an indication of phase imperfection.

4.2.5 Extrapolation of Linecentres to Zero Microwave Power

All systematic effects discussed in earlier sections (AC Zeeman effect, AC Stark effect, frequency-dependent power variation, and microwave phase and amplitude distortions) depend linearly on applied microwave power. Experiments with various T, D, and P combinations are performed, and all measured linecentres are extrapolated to zero microwave power (linecentres are first corrected by the DC Zeeman shifts before the power extrapolation).

For a particular value of D, linecentres are expected to shift linearly with P/T (Equation 4.7). The value of P used is based on an average of power detector readings (described in Sections 2.11.2.1 and 2.12.3). Linecentres with associated P/T are fit to a linear model, floating the slope and y-intercept. Figures 4.5 through 4.7 show such linear fits, and Table 4.4 shows the extrapolation results for different values of D. The extrapolation slopes shown in Table 4.4 follow approximately the trend predicted by Equation 4.7. The values in the final column of Table 4.4 are based on integration of Schrödinger equation using the oscilloscope trace as an input. The measured and simulated P/T slopes do not agree with each other, and this disagreement indicates that the oscilloscope trace is not a true representation of the microwave fields seen by the atoms. Nonetheless, since all of the shifts extrapolate to zero, the extrapolations shown in Figures 4.5 through 4.7 should give

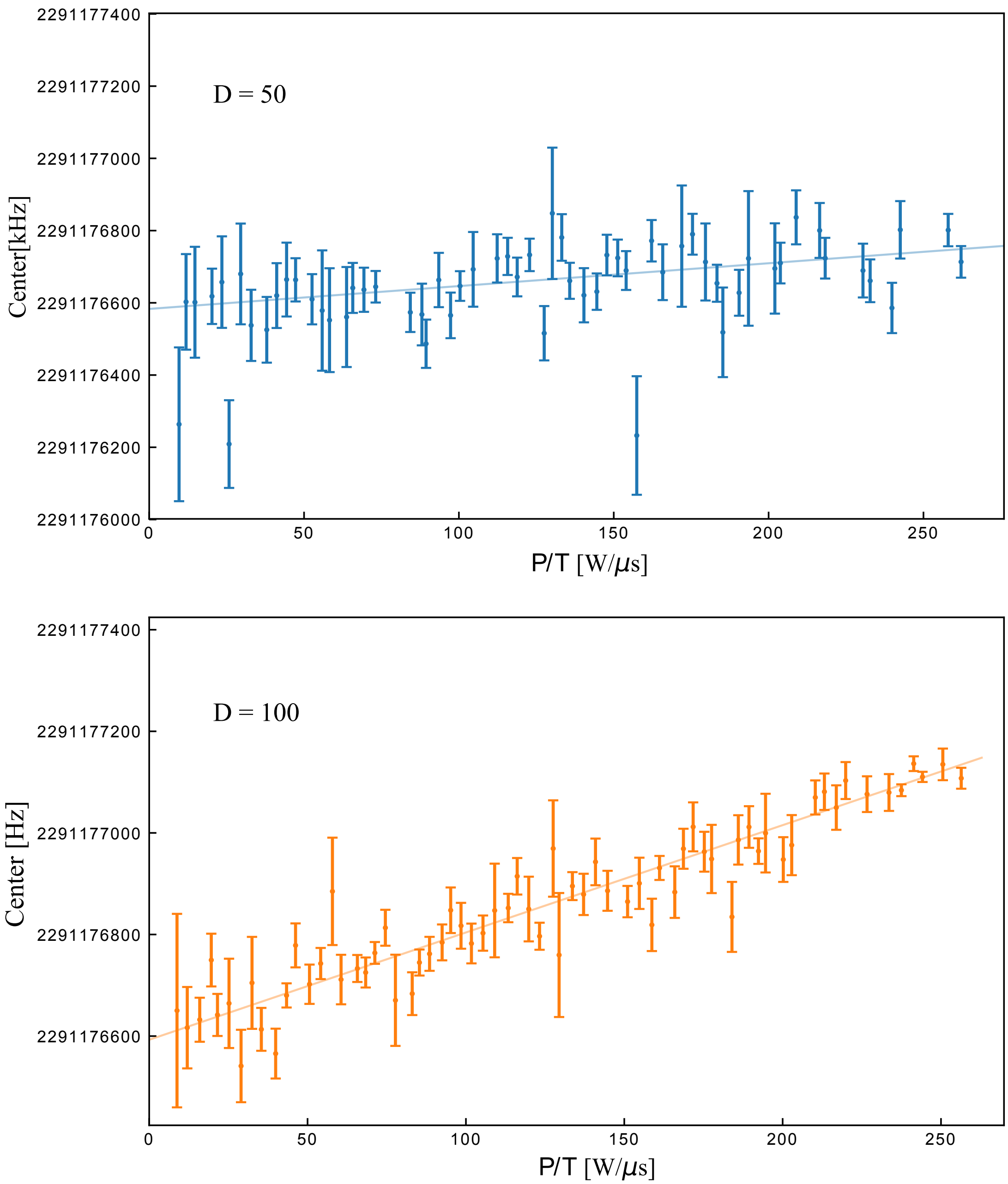

Figure 4.5: Extrapolation of D=50 and D=100 data.

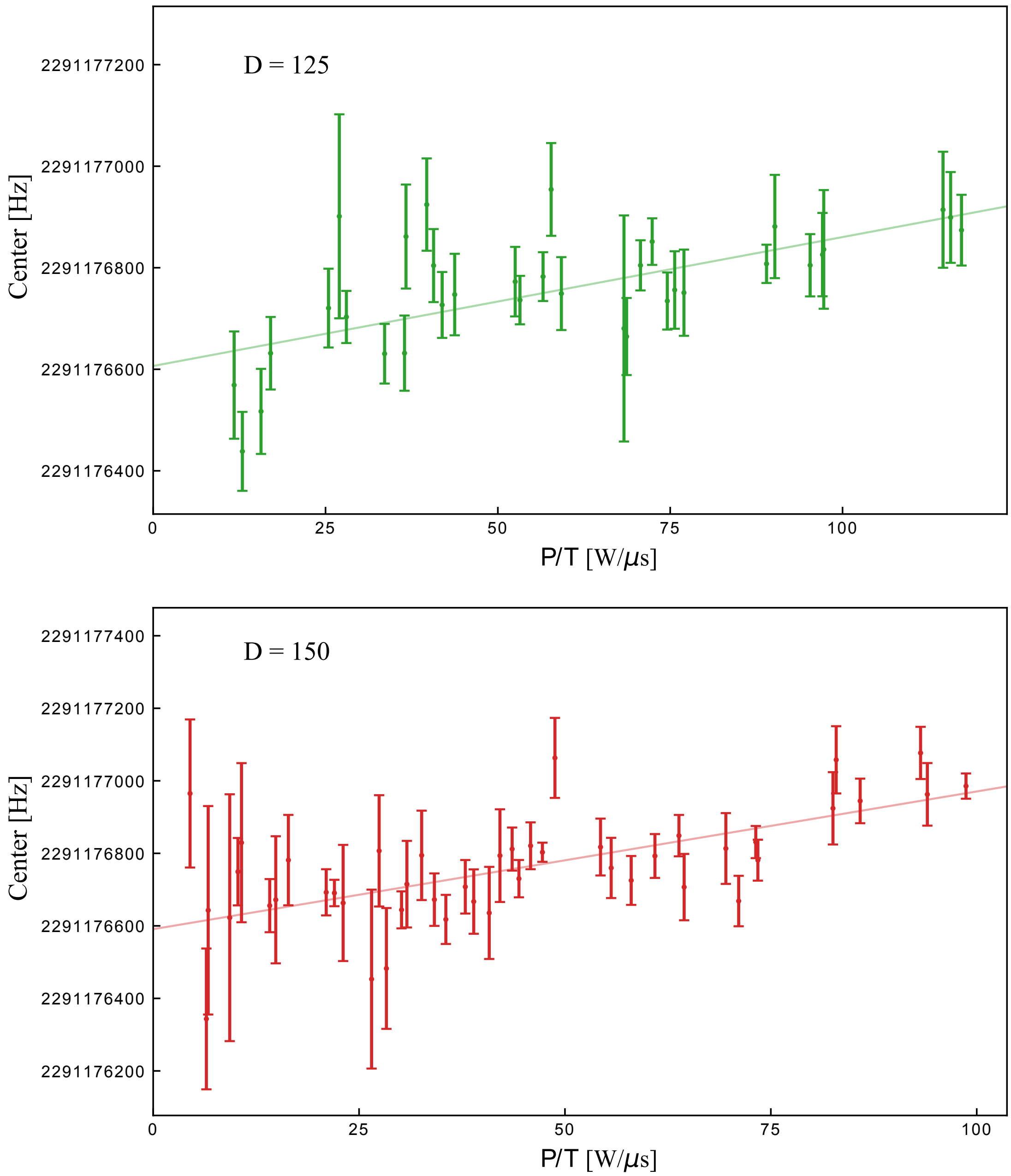

Figure 4.6: Extrapolation of D=125 and D=150 data.

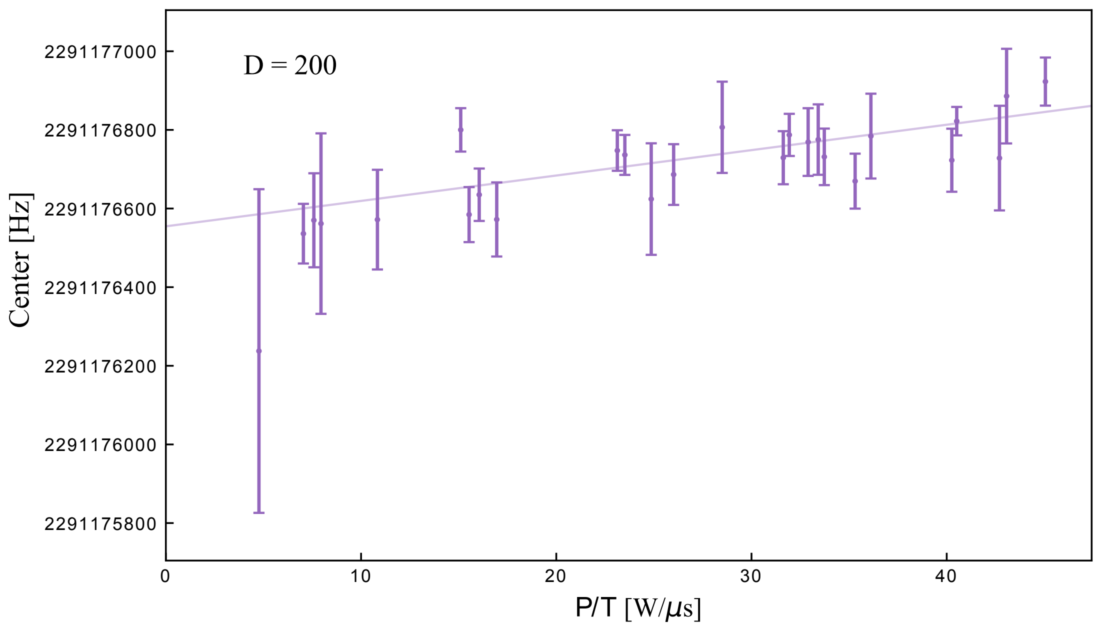

Figure 4.7: Extrapolation of D=200.

the unshifted centres. A validity of this extrapolation demonstrated by the fact that the extrapolated values in column 4 of Table 4.4 agree with each other (to within their uncertainties) despite having very different extrapolation slopes.

All linecentres are corrected to the zero-power value using the slopes shown in Figures 4.5 through 4.7 and in Table 4.4. The uncertainty of the fit slope is included in the correction. The slope correction and its uncertainty (columns 11 and 12 in Table A.2) account for all of the microwave-power-dependent systematic effects described in this chapter. Table 4.5 shows the average of extrapolation results for all 18 timings used in the experiment. Consistency in extrapolated linecentres with

Pulse duration D [ns]	Measured P/T slope [Hz/(W/μs)]	Measured P/T slope uncertainty [Hz/(W/μs)]	Extrapolation frequency [Hz]	Extrapolation uncertainty [Hz]	Simulated P/T slope [Hz/(W/μs)]
50	0.63	0.13	2 291 176 583	20	-1.64
100	2.11	0.05	2 291 176 593	9	-2.45
125	2.54	0.44	2 291 176 607	29	-1.93
150	3.80	0.43	2 291 176 591	25	-3.78
200	6.5	1.4	2 291 176 555	40	-5.35

Table 4.4: Result of microwave power extrapolation

different (T, D) combinations verifies the validity of the power extrapolation.

One concern is that the size of the extrapolation depends on the level of the microwave phase and amplitude distortions. More severe distortions are intentionally introduced to the microwave system to test the variation in the extrapolation. This resulted in an extrapolation with a significantly larger slope for graphs similar to Figure 4.5, but still gave the same value for the linecentre when extrapolated to $P_{mw} = 0$, verifying that any effect due to the microwave pulse imperfection (independent of the size of the distortion) is cancelled when the data is extrapolated to zero microwave power.

T [ns]	D [ns]	Linecentre ν_{exp} [Hz]	$\Delta\nu$ [Hz]
300	50	2 291 176 598(44)	+8
300	100	2 291 176 602(13)	+12
300	150	2 291 176 612(24)	+22
375	125	2 291 176 593(35)	+13
400	50	2 291 176 584(40)	−6
400	100	2 291 176 593(15)	+3
400	200	2 291 176 564(35)	−26
450	150	2 291 176 575(27)	−15
500	50	2 291 176 565(46)	−25
500	100	2 291 176 580(19)	−10
500	125	2 291 176 616(27)	+26
600	50	2 291 176 525(61)	−65
600	100	2 291 176 602(30)	+12
600	150	2 291 176 574(39)	−16
600	200	2 291 176 576(68)	−14
700	100	2 291 176 529(22)	−61
800	100	2 291 176 612(50)	+22
900	100	2 291 176 609(83)	+19

Table 4.5: Summary of extrapolation results for various T and D. Extrapolated linecentres are averaged separately for different (T,D) combinations. $\Delta\nu = \nu_{\text{exp}} - \nu_{12}$ is the difference from the final measured result of $\nu_{12} = 2\,291\,176\,590\,\text{Hz}$. One standard deviation uncertainties are shown in parentheses.

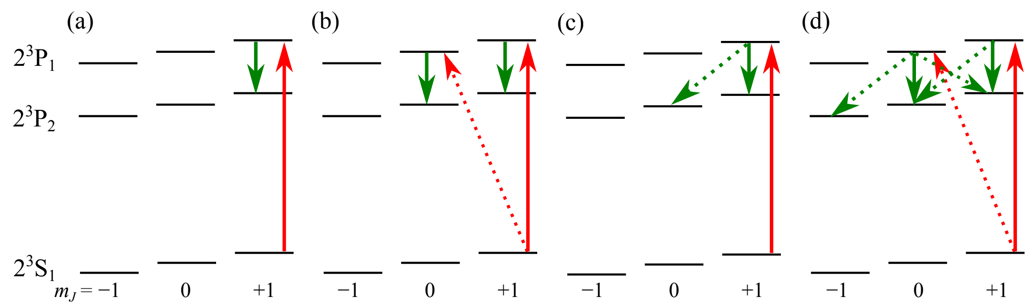

Figure 4.8: Imperfect polarization. Panel (a) shows the ideal experiment, where only intended transitions are driven. In (b), imperfect 1083-nm laser polarization drives the Δm_J=−1 transition. Panel (c) shows a microwave polarization imperfection causing the Δm_J=−1 transition. Both situations in (b) and (c) make the effective DC Zeeman shift rate different depending of the level of the polarization imperfection. Panel (d) shows possible transitions when both laser and microwave polarizations are misaligned. There could be a possible interference effect due to a recombination of excitation paths in (d). The dashed lines indicate the unintended transitions.

4.3 Imperfect Laser and Microwave Polarization

Figure 4.8(a) shows the ideal experiment where both the 1083-nm laser and microwave drive only intended transitions ($2^3S_1(m_J$=+1)-to-$2^3P_1(m_J$=+1) and $2^3P_1(m_J$=+1)-to-$2^3P_2(m_J$=+1)). When the polarizations of the laser and microwave fields are not perfectly aligned with the quantization axis of atoms (set by the direction of applied magnetic field), unintended transitions (Δm_J=±1) are also weakly driven, and these transitions could cause systematic shifts of linecentres. This section describes the effects due to the imperfect polarizations of the laser and microwave fields.

4.3.1 Imperfect 1083-nm laser polarization

Figure 4.8(b) shows the possible transitions driven by the 1083-nm laser whose polarization is not perfectly aligned with the quantization axis of the atoms. Imperfect 1083-nm laser polarization excites atoms in the $2^3S_1(m_J{=}+1)$ state to both the $2^3P_1(m_J{=}0)$ and $2^3P_1(m_J{=}+1)$ states prior to the FOSOF experiment sequence. The microwave then drives both the $2^3P_1(m_J{=}0)$-to-$2^3P_2(m_J{=}0)$ and $2^3P_1(m_J{=}+1)$-to-$2^3P_2(m_J{=}+1)$ transitions. These two microwave transitions have different quadratic Zeeman shift rates ($0.5283\,\mathrm{kHz/G^2}$ and $0.4295\,\mathrm{kHz/G^2}$, respectively [33, 54]), and thus the effective DC Zeeman shift depends on the fractional population in $2^3P_1(m_J{=}0)$ (due to the unintended laser excitation). In order to ensure a well-defined DC Zeeman shift, a high purity in the 1083-nm laser polarization is required.

The polarization of the laser is checked by the method described in Section 2.8. A large magnetic field is applied around the experiment region and the strengths of possible transitions are observed while scanning the 1083-nm laser tuned to the 2^3S_1-to-2^3P_1 transition. The 1083-nm laser power and pulse duration are increased (by a factor of 10) to exaggerate the effect of the wrong polarization. Figure 4.9 shows an averaged oscilloscope trace of the ionization signal during such a frequency scan of the 1083-nm laser. It shows a slight sign of a left-over population in $m_J{=}-1$

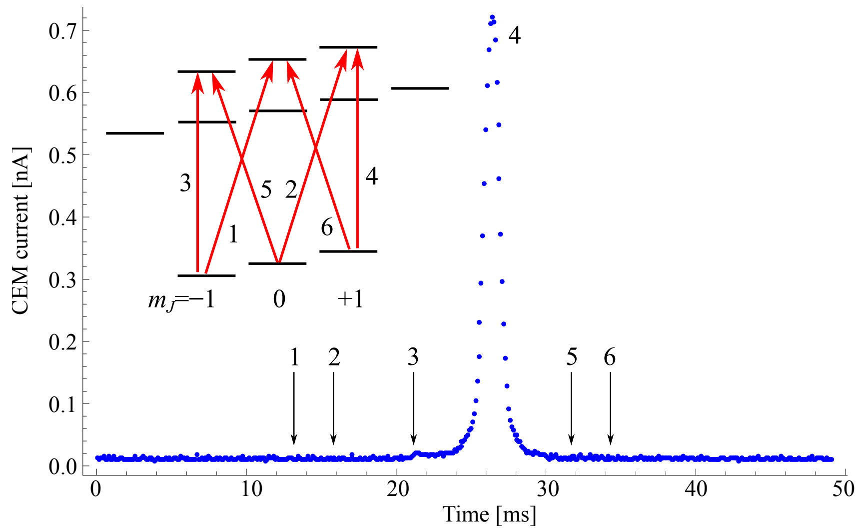

Figure 4.9: 1083-nm laser polarization test. The inset shows possible transitions. The arrows indicate the positions at which transitions are expected to appear. A small sign of a $2^3\mathrm{S}_1(m_J{=}{-1})$-to-$2^3\mathrm{P}_1(m_J{=}{-1})$ transition is seen on the plot, but the unintended $\Delta m_J{=}\pm1$ transitions are not seen on this scale.

state from optical pumping, but no sign of wrong polarization is observed (multiple peaks at different locations are expected when the polarization is imperfect, refer to Figures 2.17 and 2.18). To test this further, an AOM was used to tune the laser frequency, and the size of the FOSOF amplitude was measured at frequencies where transitions due to the wrong polarization are expected. The amplitude of these signals was measured to an accuracy of 0.1 % of the main FOSOF amplitude, and no sign of unintended transitions were detected.

For a typical experiment, the applied magnetic field is 5 G, causing the intended and unintended transitions to be separated by 10 MHz. The spectral width of the 15-ns 1083-nm laser pulse is 67 MHz, so both transitions are within the spectral width. Assuming 0.1 % as the highest limit of the polarization component driving the unintended transitions, 0.09 % relative population between the $2^3\mathrm{P}_1(m_J{=}{+1})$ and $2^3\mathrm{P}_1(m_J{=}0)$ states is expected at 5-G field (since the power of the laser pulse drops by 10 % at 10 MHz away from resonance). The effect of the 0.09 % relative population to the quadratic Zeeman shift rate is small. Comparison of linecentres between low and high fields shows no inconsistency (Table 4.2), which further indicates that there is no effect due to imperfect laser polarization.

4.3.2 Imperfect Microwave Polarization

Figure 4.8(c) shows possible transitions in the case of imperfect microwave polarization. The microwaves drive the $\Delta m_J{=}{-1}$ transition ($2^3\mathrm{P}_1(m_J{=}{+1})$-to-$2^3\mathrm{P}_2(m_J{=}0)$ transition) with its unintended polarization component. The signal due to the unintended transition causes a linecentre shift. Due to the curvature of the microwave magnetic field inside the coaxial airline (refer to Figure 4.2), the unintended polarization component is always present.

In [33], Borbely discusses the method of observing the effect due to the neighbouring transitions, by tuning the size of the applied magnetic field such that the SOF signals from the neighbouring transitions are either in phase or 90 degrees out of phase with the main SOF signal. When two signals are in phase, the addition of the signals causes no shift in linecentre. Signals that are 90 degrees out of phase maximize the effect of neighbouring transition. Comparison between the two experiments sets a limit on the size of possible shifts. In this experiment, the same method was used to test for possible effects, and no inconsistency was found between linecentres obtained in the two types of experiments. Also, the effect of neighbouring transition is expected to be smaller for larger magnetic fields. For a larger magnetic field, the neighbouring Δm_J=$\pm$1 transitions become more off-resonant (due to the first-order Zeeman effect) from the intended transition, suppressing the signal due to the unintended transition. The consistency of linecentres obtained at different magnetic fields supports the fact that imperfect microwave field polarization was not an issue in the present measurement.

4.3.3 Imperfect Laser and Microwave Polarization

Figure 4.8(d) shows the situation where both the laser and microwave have imperfect polarization components. In this situation, atoms starting from the $2^3\mathrm{S}_1(m_J{=}{+}1)$ are excited to both $2^3\mathrm{P}_1(m_J{=}{+}1)$ and $2^3\mathrm{P}_1(m_J{=}0)$ states. Imperfect microwave polarization drives Δm_J=$\pm$1 and Δm_J=0 transitions. In this situation, in addition to the linecentre shift due to the effects discussed in earlier sections, a quantum-mechanical interference due to recombination of excitation paths could be significant. This effect is also expected to be strongly dependent on the applied magnetic field. A large applied magnetic field suppresses the recombination channel, and, again, the consistency of linecentres at different magnetic fields indicates that the effect is not significant for the present work.

4.3.4 Conclusion on Effects due to Imperfect Laser and Microwave Polarizations

All effects described in this section are strongly dependent on the size of applied magnetic field, and they are most directly tested by comparing measured linecentres at different applied fields. Table 4.2 shows the summary of experimental results for different magnetic field settings. Consistency of linecentres demonstrated in Table 4.2 verifies that the effects due to imperfect polarizations are smaller than the level of precision of the current experiment. The effect of imperfect polarization would be expected to change sign for the m_J=+1 experiment (such as shown in Figure 4.8) and the analogous m_J=−1 experiment. Linecentres from the m_J=+1 and m_J=−1 experiments show a difference of (+8±17) Hz. The difference is consistent with zero, and it indicates that the size of any potential polarization related shifts are smaller than the final quoted uncertainty of 25 Hz for the current work.

4.4 Effect of Microwave Fields on Rydberg Atoms

There is a concern for possible linecentre shifts due to 18^3P_2 Rydberg atoms being influenced by the microwave fields. During the travel from the 2^3P-to18^3P excitation location to the ionizer, the Rydberg atoms are exposed to multiple microwave pulses. A particular concern is that the microwaves drive high-n Rydberg transitions due to the 0.22-ns pulse of microwave electric field discussed in Section 4.2.2. The matrix elements of electric dipole Rydberg transitions are large, and this causes a large power broadening of transitions. This broadening, along with the spectral width of 4.5 GHz due to the 0.22-ns duration of these pulses, allows transitions to be driven even when the applied microwave frequency is far off-resonance from the Rydberg transitions. Since these microwave pulses are in the FOSOF microwave configuration (alternating between $f + \delta f$ and $f - \delta f$), it is imaginable that the microwave transitions between Rydberg states could cause sinusoidally changing signals and add an additional phase onto the main FOSOF signal. The added phase could lead to a systematic shift. The effect of additional microwave pulses on the Rydberg atoms (and therefore on the detected ion signal) is investigated by performing three different experiments.

4.4.1 Downstream- vs. Upstream-Experiment Location

One test for microwave pulses affecting Rydberg atoms, is to change the position of the laser excitations within the microwave region. Figure 4.10 shows the two locations used for this test. During the travel between the excitation location to the ionizer, Rydberg atoms experience multiple microwave pulses. Table 4.6 summarizes

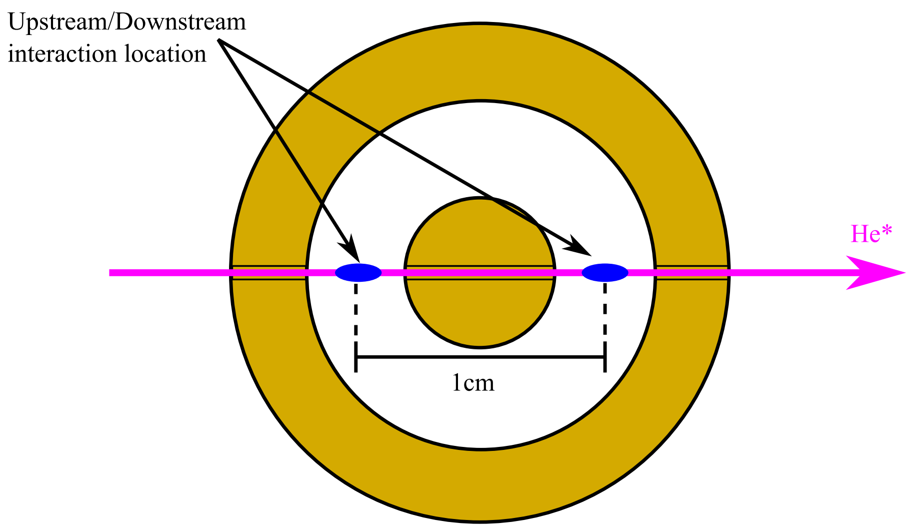

Figure 4.10: Upstream and downstream interaction locations.

the expected average number of microwave pulses that atoms experience during the travel. From the geometry of the 14-mm coaxial airline described in Sections 2.11.2.3 and 4.2.1, atoms spend average time of 1.81 μs and 11.1 μs after being excited to the Rydberg state at the downstream and upstream locations, respectively. The number of pulses seen by the atoms during the travel decreases for larger value of T due to a lower duty cycle. When atoms are excited at the upstream location, the atoms see a significantly larger number of pulses during the flight (as seen on Table 4.6). Experiments are performed at the upstream location with the timing parameters T=300 ns, and D=100 ns, and the result is compared to the result of identical experiment performed at the downstream location. The test revealed no inconsistency between data taken at the downstream and upstream locations, with

Pulse separation T [ns]	Pulse duration D [ns]	Number of pulses $N_{downstream}$	Number of pulses $N_{upstream}$
300	100	4.5	27.7
400	100	3.6	22.2
500	100	3.0	18.5
600	100	2.6	15.9
700	100	2.3	13.9
800	100	2.0	12.3
900	100	1.8	11.1

Table 4.6: Average number of microwave pulses experienced by the atoms for different pulse separations T for experiments taking place at the downstream and upstream locations.

a difference between the linecentres of (3±9)Hz.

4.4.2 Detection States

The 1532-nm diode laser driving the 4^3D-to-18^3P transition has a wide tuning range, and can be tuned to the 4^3D-to-18^3F transition. The 18^3F state can be used instead of 18^3P state as a detection state to test for a detection-state-dependent effect. The 18^3P and 18^3F states behave differently (including having different resonant frequencies for driving allowed transitions) when exposed to DC or AC electric field. The 18^3F state is more susceptible to the external DC electric field; whereas, the 18^3P state, because of its larger energy defect, does not shift (or mix with other states) as readily. A comparison between measurements using the 18^3F and 18^3P state shows a linecentre difference of (28±24) Hz. The level of consistency between

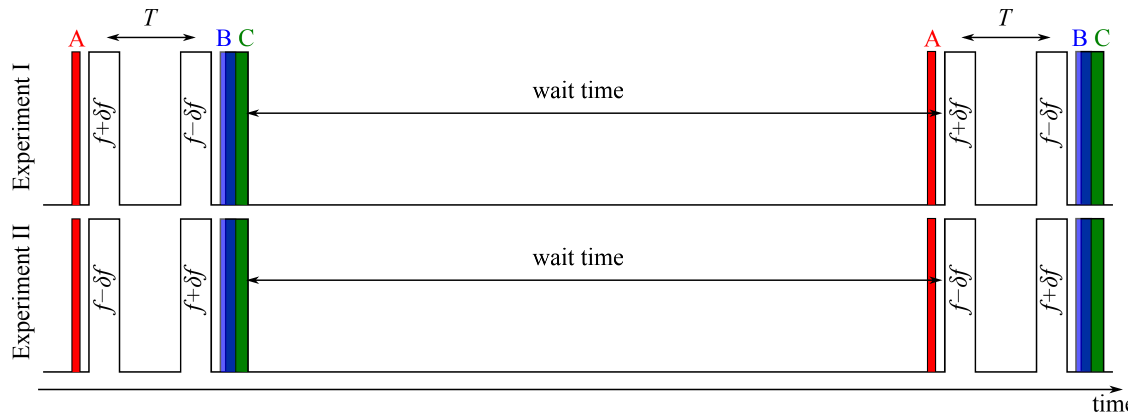

Figure 4.11: Low duty cycle experiment timing. The coloured rectangles represent the laser pulses (1083-, 447-, 1532-nm lasers), and the rectangles with labels $f + \delta f$ and $f + \delta f$ represent the microwave pulses. Experiment reversal is done by switching microwave pulse timings, and it causes a phase offset between two experiments, leading to a systematic shift.

the 18^3P and 18^3F data adds to our confidence that the interaction between the microwaves and the Rydberg atoms does not cause a shift.

4.4.3 Low Duty Cycle Experiments

Low duty cycle experiments (as shown in Figure 4.11) are performed as another test for the possible effect of microwave pulses on the Rydberg atoms. Reducing the duty cycle temporally separates subsequent experiments further apart, and reduces the number of microwave pulses seen by the Rydberg atoms. It is possible to set the duty cycle such that all atoms are completely cleared from the microwave region before the subsequent experiment cycle starts. This ensures that the linecentres obtained are not influenced by the additional microwave pulses.

Figure 4.11 illustrates the timing of the low duty-cycle experiment for the FOSOF experiment I and II. Unlike the normal operation of the FOSOF experiment where the laser pulse timings are shifted to switch between experiment I and II, timing of microwave pulses also must be switched for the low duty-cycle experiments. This type of experiment reversal is not ideal since it causes the microwave switches to operate differently for experiments I and II. The result is that experiments I and II no longer form a perfect reversal and there is a net phase shift in the average FOSOF signal from the two experiments. The effect of imperfect experiment reversal is tested by mixing the CW output of the microwave generator with the microwave pulses used in the experiment. The interference between two signals generates a sine wave which mimics a FOSOF signal, and its phase with respect to the FOSOF beat reference signal is monitored during the experiment reversal. It was found that the experiment reversals at lower duty cycles do not lead to a perfect cancellation of phase shifts, and consequently, the measured linecentres at low duty cycles are inconsistent with linecentres measured at normal duty cycle. It was, however, possible to correct the linecentre obtained at a particular duty cycle by the phase offset observed from the beating the pulses with CW microwaves (as described above) during this test. Correcting for the observed phase shifts, a consistency in linecentres was restored. The consistency was tested to a precision of 100 Hz. The precision of the performed test is not at the level of the current experiment; however, the origin of the systematic effect due to imperfect experiment reversal at low-duty cycle is well understood, and this test complements the tests of Sections 4.4.1 and 4.4.2.

4.4.4 Conclusion for the Effect of Microwave Fields on Rydberg Atoms

Three different experiments described in this section test the possible systematic effect due to the Rydberg atoms being influenced by the additional microwave pulses. A comparison between downstream/upstream experiments along with the consistency demonstrated in Section 4.2.5 for different pulse separations rules out the possibility of additional pulses affecting the linecentres. All other tests are also consistent with Rydberg atoms playing no significant role in the current measurement.

4.5 Laser Light Shifts

Overlap between laser pulses and microwave pulses during the experiment cycle could lead to a linecentre shift due to a light shift (AC Stark shift due to the electric fields of the laser light). The 1083- and 447-nm lasers driving 2^3S_1-to-2^3P_1 and 2^3P_2-to-2^3D_3, respectively, could shift the 2^3P_1-to-2^3P_2 transition if the laser light and microwaves temporally overlap. Overlap of the 1532-nm laser with the microwave pulse is less of a concern because this laser is not directly related to transitions involving 2^3P_1 and 2^3P_2 states.

Experiments with different laser-pulse timings and laser powers were performed to test for the possible effect of light shifts, as described below.

4.5.1 Experiments with Varied Laser Pulse Timings

Figure 4.12 shows the timing diagrams of three experiments performed to test the effect due to the overlap between the laser pulses and microwave pulses. Laser pulse timings are changed in each of the experiments shown in the figure. In Figure 4.12(a), the 1083-nm laser pulse is shifted by 30 ns earlier in time, separating it further away in time from the microwave pulse. AOM pulsing has a ringing effect caused by the RF pulse reflections inside the AOM crystal. This effect leaves an unsuppressed laser power for some time even after the pulse is turned off [33]. By separating the pulse further from the microwave pulse, any effect associated with the overlap of the tail of the 1083-nm laser can be suppressed.

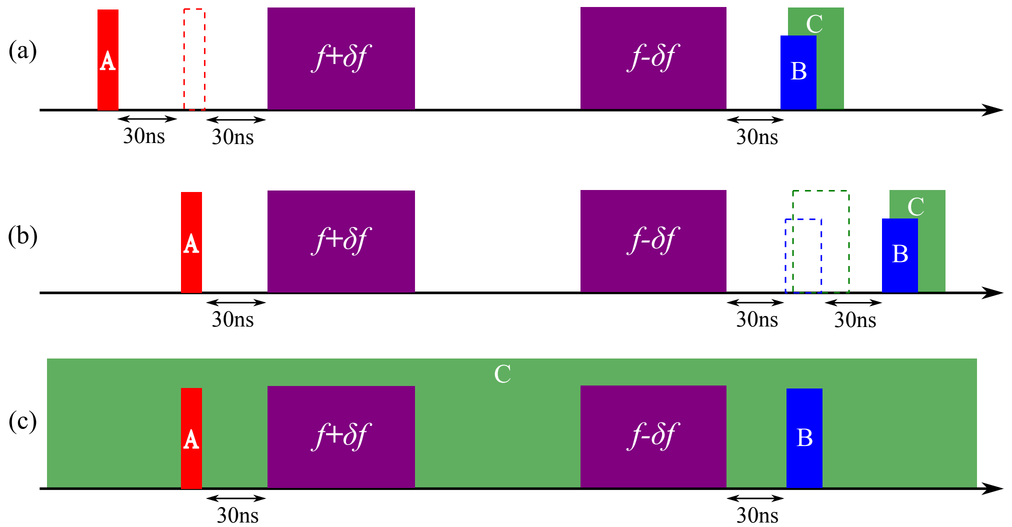

Figure 4.12: Experiments with varied laser pulses timings. The rectangles represent the laser and microwave pulses used for the experiment. 1083-nm laser pulse (laser A), 447-nm laser pulse (laser B), and 1532-nm laser pulse (laser C) are represented as the red, blue, and green rectangles, respectively. The purple rectangles represent the microwave pulses.

Figure 4.12(b) shows another experiment timing where the detection laser pulses are shifted by 30 ns later in time, again making them further away from the microwave pulse. Since the 447-nm laser pulse starts after the second microwave pulse, and the time between the laser pulse and next microwave pulse (the first pulse of the next experiment cycle) is over 100 ns (even further for larger pulse separation settings), the ringing effect is not a concern in this case. The overlap of the rising edge of the 447-nm detection laser with the falling-edge of the second microwave pulse is tested with this experiment.

Figure 4.12(c) shows the experiment that tests the overlap of 1532-nm laser with the microwave pulses. In this experiment, the 1532-nm laser simply runs in the CW mode. The laser overlaps with both microwave pulses. If there is any effect on the 2^3P_1-to-2^3P_2 transition due to the 1532-nm laser, the effect is greatly exaggerated in this experiment.

4.5.2 Experiments with Different Laser Powers

An AOM spatially separates the undiffracted and first-order diffracted paths, making the overlap of the two paths very unlikely. However, if there is an imperfect separation of the two paths, it causes a small laser power to be always present during the experiment, which could induce a light shift. In the previous section (Section 4.5.1), experiments to test the laser-microwave overlap are discussed. These experiments, however, do not test the light shift due to the presence of the unintended CW laser power during the experiment. In order to test for this effect, the 1083- and 447-nm laser powers are reduced to 10 % and 12.5 % of the typical operating power, respectively. Two experiments were performed separately to avoid significant reduction of signal-to-noise ratio. In one experiment, 1083-nm laser power is reduced, leaving the 447-nm laser power unchanged. In the other experiment, the 447-nm laser power is reduced, and the 1083-nm laser power is unchanged.

Experiment	Linecentre ν_{exp} [Hz]	$\Delta\nu$ [Hz]
447-nm laser +30ns	2 291 176 566(34)	−24
1083-nm laser -30ns	2 291 176 568(33)	−22
1532-nm laser CW	2 291 176 583(24)	−7
10 % 1083-nm laser power	2 291 176 603(22)	+13
12.5 % 447-nm laser power	2 291 176 572(38)	−18

Table 4.7: Summary of experimental results testing laser light shifts. $\Delta\nu = \nu_{\mathrm{exp}} - \nu_{12}$ is the difference between the measured linecentre ν_{exp} and the final measured result of $\nu_{12} = 2\,291\,176\,590\,\mathrm{Hz}$. One standard deviation uncertainties are shown in parentheses.

4.5.3 Conclusion for Laser Light Shifts

Five different experiments are performed to test for light shifts. Table 4.7 summarizes the results of the five experiments. Results from the three timing experiments reveal no inconsistencies in measured linecentres. The differences in measured linecentres with respect to the final measured result of 2 291 176 590 Hz are (-22±33) Hz, (-24±34) Hz, and (-7±24) Hz for experiments with varied 1083-nm laser pulse timing, varied 447-nm laser pulse timing, and CW-mode 1532-nm laser, respectively. Comparison of the experimental results with different laser powers showed differences of (+13±22) Hz and (-18±38) Hz for the reduced 1083- and 447-nm laser powers, respectively. These differences are consistent with zero. The (unlikely) possibility of having any light-shift-related systematic effect is suppressed to the level of agreement demonstrated in these experiments.

4.6 First-Order Doppler Shifts

In the present experiment, the microwave propagation directions intersect perpendicularly with an atomic beam. Imperfect alignment of the microwave region with respect to the atomic beam axis leads to a shift in linecentre due to the first-order Doppler shift. The Doppler shift can be written as

$$\Delta\nu_{\mathrm{Doppler}} = \nu_0 \beta \Delta\theta, \tag{4.8}$$

where ν_0 is the frequency of the microwave, $\Delta\nu_{\mathrm{Doppler}}$ is the shift in frequency, $\beta = \frac{v}{c}$ where v is the average speed of the atoms, c is the speed of light in vacuum, and $\Delta\theta$ is the angle at which the atoms intersect with the microwave (where $\Delta\theta = 0$ is defined by the atomic and microwave propagation directions being perpendicular). The entire system is aligned using a surveyor's scope, and the maximum deviation from the perfect alignment angle is very conservatively estimated to be less than 5 mrad (including the size of the slit at the microwave region and its distance from the helium source). The shift due to the first-order Doppler effect in this experiment is expected to be small because of the slow atomic speed (1100 m/s) and the small microwave frequency. The upper limit of the first-order Doppler shift is 42 Hz using Equation 4.8. However, a reflection of the microwave from the short ensures that the effect on the measured linecentres is much smaller than this 42-Hz limit for the present experiment. Even with the assumption of a 1 % power difference between the forward and reverse going microwaves, the 42 Hz estimate becomes 0.42 Hz, and is completely negligible.

4.7 Time-Base Correction

The time base of the Wiltron microwave generator is used to synchronize instruments for the experiment. The 10-MHz clock output of the Wiltron generator is daisy chained to other instruments that require clock synchronization and monitored at the end of the chain using a frequency counter (TTi960) referenced to a Rb frequency standard (FE-5680A). The frequency of the Rb clock is checked against a GPS disciplined clock (Trimble Thunderbolt E) on a weekly basis, to ensure that there is no frequency drift of the Rb clock over time. The Rb clock frequency stayed extremely stable over the course of data acquisition. The clock frequency of the Wiltron generator, monitored over the entire data acquisition, is shown in Figure 4.13. The time-base correction is calculated by the fractional deviation of the generator clock frequency from the 10 MHz Rb clock frequency,

$$\Delta\nu_{\text{time base}} = \frac{10\text{MHz(Wiltron)} - 10\text{MHz}}{10\text{MHz}} \times 2.291\text{GHz}. \tag{4.9}$$

The typical time-base correction applied to the measured linecentre is 4.5 kHz. The clock frequency drifted by maximum 0.015 ppm over the period of data acquisition which corresponds to the time-base correction drift of 30 Hz. Since the time base

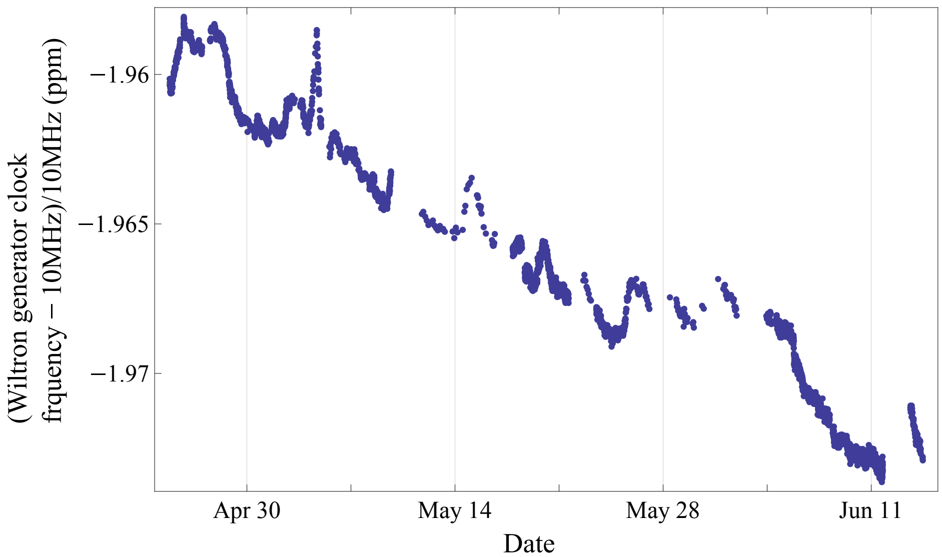

Figure 4.13: Wiltron clock frequency drift

is measured very accurately, the corrections are also known very accurately, and the uncertainties in these corrections are very small compared to the 25-Hz final uncertainty of our measurement.

4.8 Analysis-Related Systematic Effects

To test for possible analysis-related systematic effects, the data analysis was repeated with different data restrictions. Additionally, SOF signals were reconstructed using FOSOF data, and the entire data set was re-analyzed based on SOF fits. Details on results based on different analysis parameters are discussed in this section.

4.8.1 Saturation Restriction PD^2: Linearity of Power Extrapolation

The linecentre shifts discussed in Section 4.2 become more significant for higher powers. The shifts discussed in that section were linear in power; however, a nonlinear behaviour in linecentre shifts was observed for powers approaching the saturation of the transition. To avoid the effects of this nonlinearity only the linecentres taken at the lowest powers are included in the analysis. Additionally, the maximum power P_{max} included is varied to ensure that no systematic shifts are present due to the nonlinearity in the extrapolation of the linecentres to zero power. The criteria for choosing P_{max} is based on the saturation parameter PD^2, which determines the degree of the transition for a particular combination of P and D. The maximum value of PD^2 used in the experiment was $0.9\,\text{W}\mu\text{s}^2$. The entire data analysis was repeated with different $P_{\text{max}}D^2$ restriction (0.9, 0.75, 0.6, 0.45, and $0.3\,\text{W}\mu\text{s}^2$) to check the linearity of the extrapolation. The analysis results with different $P_{\text{max}}D^2$ restrictions are compared in Table 4.8. The consistent results in the table verifies that the extrapolation is not affected by the nonlinearity for the powers used in the analysis.

Saturation restriction PD^2 [Wμs^2]	Linecentre ν_{exp} [Hz]	$\Delta\nu$ [Hz]
0.3	2 291 176 588(21)	−2
0.45	2 291 176 592(16)	+3
0.6	2 291 176 602(13)	+12
0.75	2 291 176 590(11)	0
0.9	2 291 176 590(11)	0

Table 4.8: Summary of analysis results from different saturation restrictions $P_{\text{max}}D^2$. $\Delta\nu = \nu_{\text{exp}} - \nu_{12}$ is the difference between the measured linecentre and the final measured result of $\nu_{12} = 2\,291\,176\,590$ Hz. The result from the analysis using $P_{\text{max}}D^2$=0.75 Wμs^2 was used to quote the final measured result, so the difference to $\Delta\nu$ is zero. The saturation restriction used for quoting the final measured result (0.75 Wμs^2) is highlighted in gray.

4.8.2 Frequency Range of the FOSOF Fits

The envelope width ($\frac{1}{D}$) of the FOSOF signal (see Figure 3.4) was used to set the frequency range used in data acquisition. Data were typically collected over the range between $(f_0 - 1/(2D) - 2.5)$ MHz and $(f_0 + 1/(2D) + 2.5)$ MHz. Different frequency ranges (full range, $|f - f_0| < \frac{1}{2D}$, $|f - f_0| < \frac{1}{4D}$, and $|f - f_0| < \frac{1}{8D}$) are used to fit the collected data, and obtained linecentres are analyzed. Figure 4.14 shows FOSOF data at different powers and corresponding fits. The frequency ranges

Pulse duration [ns]	Full range [MHz]	$1/(2D)$ range [MHz]	$1/(4D)$ range [MHz]	$1/(8D)$ range [MHz]
50	25	20	12.5	10
100	15	5	2.5	1.25
125	13	4	2	1
150	11.7	3.3	1.7	0.8
200	10	2.5	1.25	0.625

Table 4.9: Frequency range used for fitting the data. The frequency ranges vary from 0.625 to 25 MHz.

Fit range	Linecentre ν_{exp} [Hz]	$\Delta\nu$ [Hz]
Full range	2 291 176 590(12)	0
$1/(2D)$	2 291 176 590(11)	0
$1/(4D)$	2 291 176 615(14)	+25
$1/(8D)$	2 291 176 595(16)	+6

Table 4.10: Analysis results with different fit ranges. $\Delta\nu = \nu_{\text{exp}} - \nu_{12}$ is the difference from the final measured result of $\nu_{12} = 2\,291\,176\,590\,\text{Hz}$. The analysis range of $1/2D$ is used to quote the final measured result and is highlighted in gray. The results shown are from a reanalysis of the entire data set used in this work.

used for each analysis are indicated with gray bands. Table 4.9 summarizes the frequency ranges used for fitting. Results obtained from different fitting ranges are compared in Table 4.10. The results reveal no significant inconsistency amongst the analysis results.

4.8.3 SOF Reconstruction Using FOSOF Data

The amplitude of the FOSOF signal along with corresponding phase information can be used to reconstruct SOF signals from the FOSOF experiment data. To do this, the FOSOF amplitude is multiplied by the cosine of $\overline{\Delta\theta}$. Simulations were performed for both the SOF and FOSOF experiments, and a small deviation between the two types of measurement was found. A small offset in the linecentre extrapolation (to zero microwave power) was predicted for the case of the SOF experiment, whereas the FOSOF linecentres extrapolate exactly to the atomic resonance (f_0) in these simulations. The SOF signal for the current measurement was reconstructed from

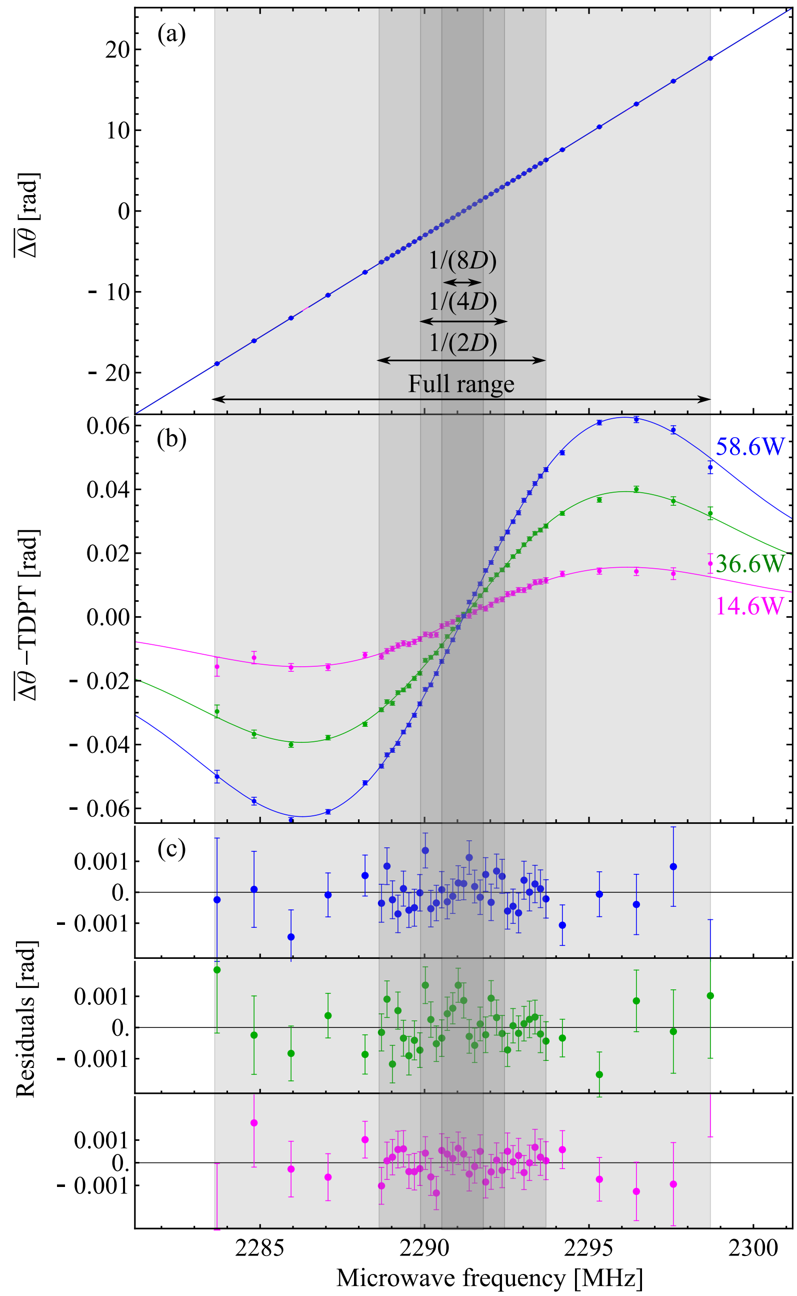

Figure 4.14: Illustration of fit ranges used for data analysis. The figure shows a full range fit to a (T,D)=(400,100) ns data. The gray bands indicate the different fit ranges used in the analysis. The different powers are unresolved in panel (a)

each FOSOF data run and was re-fit with the SOF lineshape of Equation 3.12. Obtained linecentres are extrapolated to zero microwave power. The averaged linecentre slightly deviates from the result of FOSOF experiment. Two values differ (when averaged over the entire data set) by (60±42) Hz, where the uncertainty is dominated by the SOF average linecentre.

4.9 Other Tests for Possible Systematic Effects

As described in Section 2.12, various experimental parameters are monitored over the course of data acquisition. Most of the logged parameters are not expected to be related to any systematic effects. However, if a correlation between the measured linecentres and logged parameter were found, further systematic studies would be required. Table 4.11 shows linecentre differences and their associated uncertainties for different logged parameters, and also shows the parameter ranges. Linecentres as a function of each parameter given in the table are fit to a linear model, and the difference from the minimum parameter value to the maximum parameter value is determined. In all cases, no significant shifts are found.

The source operation parameters are tested by changing the driving current and temperature. When the current is changed, the source operates differently (the atomic flux changes, and the relative production efficiencies of UV photons, singlet- and triplet-metastable helium atoms also changes). The source temperature tests

Parameter	Δ [Hz]	Uncertainty [Hz]	Minimum value	Maximum value
Source current	-4	12	10.0 mA	25.0 mA
Source temperature	$+24$	53	$-158\,^{\circ}$C	$+30\,^{\circ}$C
Chamber pressure	-7	53	3×10^{-9} torr	6.7×10^{-8} torr
Offset frequency	$+45$	23	-2800 Hz	+2800 Hz
2DMOT	-22	33	OFF	ON
m_J state	$+8$	17	-1	$+1$
B_x-coil current	$+3$	10	-16.3 mA	-11.0 mA
B_y-coil current	$+3$	11	57.2 mA	60.8 mA
B_z-coil current	$+7$	11	144.1 mA	147.5 mA
Ambient temperature	-18	16	26.1 C°	31.9 C°
Run start time	$+1$	9	0 day	43.6 days

Table 4.11: Table of linecentre comparisons for tests of other systematic effects. Δ denotes the difference in linecentres between the miminum and maximum values of parameters.

for atomic-speed-dependent effects.

Currents to all background magnetic field cancelling coils (B_x, B_y and B_z in Table 4.11) are monitored. A variation in linecentres with these coil currents tests for laser- and microwave-polarization effects.

Ambient temperature could cause small variation in electrical length of the microwave system, causing instability in microwave system operation. This may cause shifts discussed in Section 4.2.5. If there is any time-dependent effect such as magnetization of system components close to the experiment region and degradation of microwave components over time, it should show up in the run start time parameter. No significant deviations in linecentres are found from the comparisons (shown in Table 4.11).

4.9.1 Offset-Frequency Correction

The two microwave generators used in the current experiment have different frequency resolutions. The Wiltron microwave generator has a resolution of 0.1 Hz, whereas the HP generator frequency can only be set in steps of 1 kHz. Because of this limitation, the frequency f is nominally set by the HP generator, and the offset frequency $f + 2\delta f$ is set by the Wiltron generator (as opposed to setting the two frequencies symmetrically to $f - \delta f$ and $f + \delta f$, as was described in 2.11.1.2). Therefore, the offset frequency δf needs to be added to the measured linecentres in order to obtain the true FOSOF resonance position. The typical offset frequency used in the experiment is $2\delta f = 280$ Hz. Linecentres with offset frequencies ranging from -2.8 kHz to $+2.8$ kHz are also used to test for any possible systematic effects. Consistent linecentres are observed within the range of offset frequencies, eliminating the possibility of offset-frequency-dependent shifts, as shown in Table 4.11.

4.9.2 Pressure Shifts

The typical operating vacuum pressure inside the main experiment chamber is 3×10^{-9} torr and is dominated by the helium gas load from the metastable helium source. To set a limit for the size of a possible pressure shift, the pressure was increased to 6.7×10^{-8} torr and the linecentre was measured at that pressure. Since atoms may behave differently when colliding with gas molecules other than helium, it was important to keep the experimental environment as similar as possible to the normal operating environment in performing this experiment. Therefore, the pressure was increased by slowing down the turbo pump at the main experiment chamber instead of leaking gas into the chamber using a leak valve. This method ensures that the fractional composition of the residual gas is unchanged when the pressure is increased. The measured linecentres at the two pressures showed a difference of (-7±53) Hz, which is consistent with zero. Since the pressure shift is expected to grow linearly with pressure, the limit on the pressure shift at 3×10^{-9} torr (where the main data were taken) is 3 Hz.

4.9.3 Atomic Beam Intensity

The test for the pressure shift (Section 4.9.2) only concerns collisions of helium atoms with the background gas. In the current experiment, a 2DMOT is used to intensify the atomic beam. A high density of atoms could, though unlikely, cause a systematic shift due to collisions of atoms within the beam. Atoms within the beam collide with others due to the transverse and longitudinal velocity spread. To test for this possible systematic effect, linecentres are measured with or without operation of the 2DMOT. Results from the two experiments shows a difference of (-22±33) Hz. Another test performed with different source driving current (which reduces the atomic flux by a factor of 2) also shows no sign of linecentre shift, with a difference of (-3±12) Hz.

4.9.4 Microwave Amplitude Variation due to Travelling Atoms

During the experiment cycle, atoms travel a small distance inside the coaxial airline. As described in Section 4.2.1, the amplitude of the field varies as $1/|r|$ (r is measured from the central axis of the coaxial airline). Atoms see different pulse amplitudes for the two microwave pulses due to the difference in positions at which atoms experience the first and second microwave pulses. Figure 4.15(a) illustrates the $1/|r|$ field variation inside the coaxial airline, and Figures 4.15(b) and 4.15(c) show the pulse amplitudes seen by the atoms as a function of time for the upstream and downstream locations. The variation is as large as 20 % for the largest pulse separation T used in the current experiment.

No shift was expected from the field amplitude imbalance. The consistency of experimental results with different pulse separations T (demonstrated in Section 4.2.5) verifies that this effect does not contribute to a shift in linecentres. The experiment described in Section 4.4.1 also tests for this effect because atoms travel closer to (upstream) or further from (downstream) the inner conductor so that the field imbalance is reversed, as seen in Figures 4.15(b) and 4.15(c).

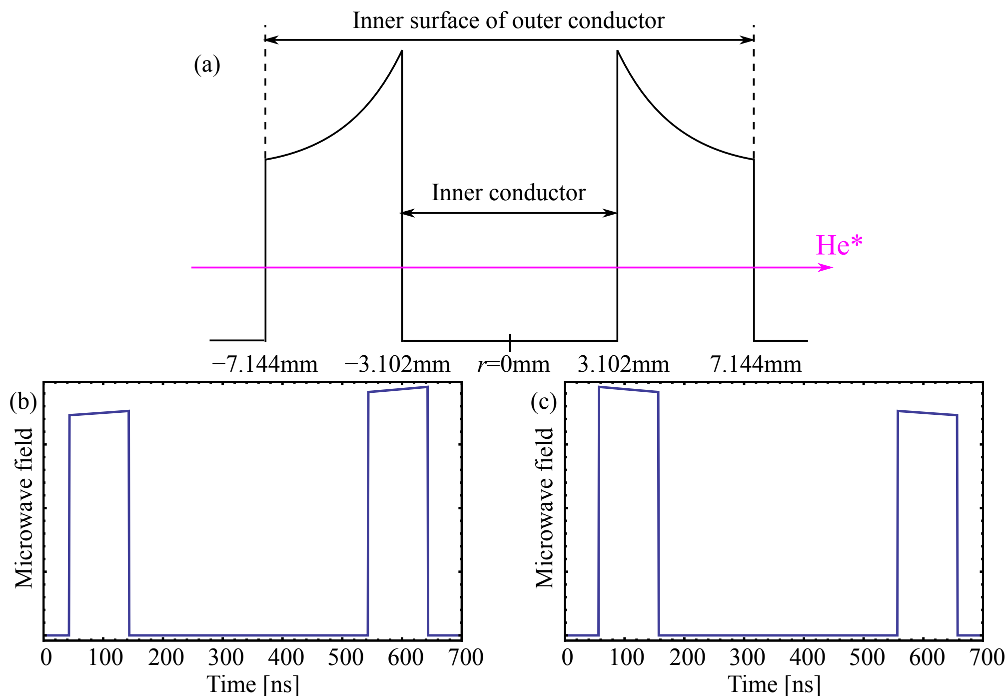

Figure 4.15: Microwave field strength variation inside the coaxial airline. (a) shows the field variation inside the coaxial airline as a function of distance. The pink arrow indicates the helium atoms moving to the right of the figure. (b) and (c) show the field strength variation seen by the atoms during one experiment cycle with (T,D)=(500,100) ns for upstream and downstream experiment locations, respectively.

5 Conclusion

The 2^3P_1-to-2^3P_2 fine-structure interval in atomic helium was measured using the frequency-offset separated-oscillatory-fields (FOSOF) technique. This work was the first demonstration of the FOSOF technique. An outstanding signal-to-noise ratio was achieved by employing a two-dimensional magneto-optical trap and a Stark-ionization detection scheme (described in Chapter 2). Collected data were fit to an analytic solution derived in Chapter 3. The quality of the fit confirmed that the experimental data were well described by the theoretical prediction (Figures 3.7 through 3.12). The excellent signal-to-noise ratio allowed for a very extensive study of systematic effects. A wide range of experimental parameters was investigated. A systematic effect pertaining to the microwave pulse imperfection was found during the experiment (Section 4.2.4), and was dealt with by extrapolating our measurements to zero microwave power (Section 4.2.5). A significant quantity of data was necessary to understand the systematic effects described in Chapter 4.

Table 5.1 shows the summary of measured linecentres with different experimental

Experimental Parameter	Parameter Detail	Linecentre ν_{exp} [Hz]	$\Delta\nu$ [Hz]	Section
Magnetic Field Direction	$+\hat{z}$	2 291 176 593(12)	+3	4.1
	$-\hat{z}$	2 291 176 592(13)	+2	
Magnetic Field Magnitude	$\|B\| < 5$	2 291 176 596(11)	−6	4.1, 4.3
	$5 \leq \|B\| \leq 10$	2 291 176 592(16)	+2	
	$\|B\| > 10$	2 291 176 567(62)	−23	
Timing Parameter (T, D)	(300, 50)	2 291 176 582(44)	+8	4.2.5
	(300, 100)	2 291 176 602(13)	+12	
	(300, 150)	2 291 176 612(24)	+22	
	(375, 125)	2 291 176 593(35)	+3	
	(400, 50)	2 291 176 584(40)	−6	
	(400, 100)	2 291 176 593(15)	+3	
	(400, 200)	2 291 176 564(35)	−26	
	(450, 150)	2 291 176 675(27)	−15	
	(500, 50)	2 291 176 565(46)	−25	
	(500, 100)	2 291 176 580(19)	−10	
	(500, 125)	2 291 176 618(27)	+26	
	(600, 50)	2 291 176 525(61)	−65	
	(600, 100)	2 291 176 602(30)	+12	
	(600, 150)	2 291 176 574(39)	−16	
	(600, 200)	2 291 176 576(68)	−14	
	(700, 100)	2 291 176 529(22)	−61	
	(800, 100)	2 291 176 612(50)	+22	
	(900, 100)	2 291 176 609(83)	+19	
Average of T Parameters	300	2 291 176 577(13)	+13	4.2.5
	400	2 291 176 592(15)	+2	
	500	2 291 176 591(17)	+1	
	600	2 291 176 589(26)	−1	
Average of D Parameters	50	2 291 176 591(38)	−1	4.2.5
	100	2 291 176 590(12)	+0.2	
	125	2 291 176 607(25)	+17	
	150	2 291 176 600(20)	+10	
	200	2 291 176 563(35)	−27	
Saturation Restriction PD^2	> 0.30	2 291 176 592(21)	−2	4.8.1
	> 0.45	2 291 176 592(16)	+2	
	> 0.60	2 291 176 602(13)	+12	
	> 0.75	2 291 176 590(11)	0	
	> 0.90	2 291 176 590(11)	+0.1	
Detection m_J State	$m_J = +1$	2 291 176 594(12)	+4	4.3.3
	$m_J = -1$	2 291 176 586(13)	−4	
Analysis Range	Full Range	2 291 176 590(12)	0	4.8.2
	$\|f - f_0\| <1/2D$	2 291 176 590(11)	0	
	$\|f - f_0\| <1/4D$	2 291 176 615(13)	+25	
	$\|f - f_0\| <1/8D$	2 291 176 595(16)	+5	
Laser Parameters	447-nm laser timing	2 291 176 566(34)	−24	4.5
	1083-nm laser timing	2 291 176 568(33)	−22	
	Low 1083-nm laser power	2 291 176 603(22)	+13	
	Low 447-nm laser power	2 291 176 572(38)	−18	
	CW 1532-nm laser	2 291 176 583(24)	−7	
Atomic Beam Intensity	2DMOT OFF	2 291 176 617(36)	+27	4.9.3
Rydberg State Detection	18F	2 291 176 625(29)	+35	4.4

Table 5.1: Summary of experimental parameters. $\Delta\nu = \nu_{\text{exp}} - \nu_{12}$ is the difference between the measured linecentre ν_{exp} and the final measured result of $\nu_{12} = 2\,291\,176\,590\,\text{Hz}$. One standard deviation uncertainties are shown in parentheses.

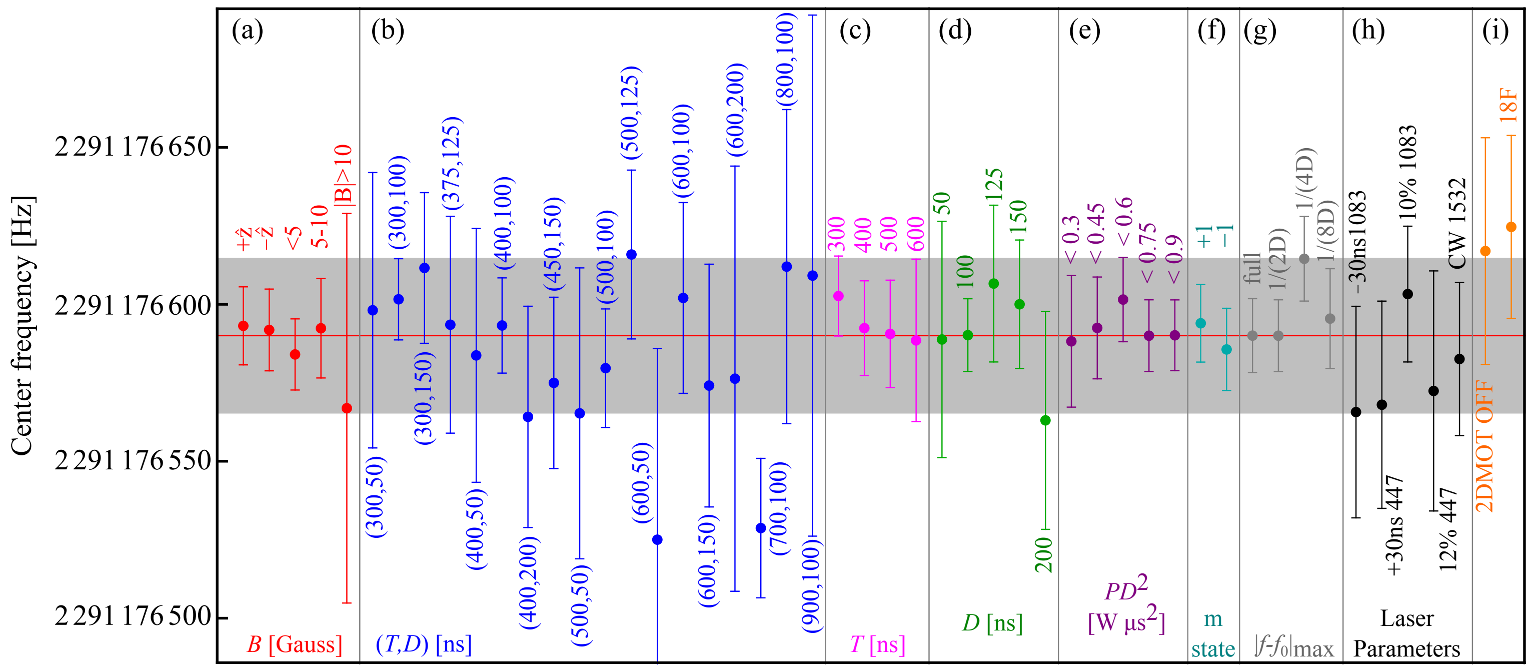

Figure 5.1: Summary of experiment parameters. (a) shows the measured linecentres with different magnetic fields. (b) through (d) are the measured linecentres with different timing parameters of the experiment. (e) and (g) are the linecentres resulting from analysis with different data restrictions. (h) shows the linecentres with different laser parameters. (f) and (i) show auxiliary data with different optical pumping and detection states, as well as the effect of turning off the 2DMOT. From the variations seen on the plot, a conservative 25-Hz uncertainty (gray band) is assigned to the final measured result of 2 291 176 590 Hz.

parameters. Figure 5.1 shows the plot of the measured linecentres listed in Table 5.1. The gray band is the 25-Hz uncertainty band for the current measurement. Excellent consistency amongst various experimental parameters is demonstrated.

A weighted average of all data presented in Table A.2 using the normalized weights in column 15 gives the final measured result. The final result of this work is 2 291 176 590(25) Hz. A conservative estimate of 25 Hz was assigned to the final measured result by observing the spread of measured linecentres obtained with different experimental parameters shown in Figure 5.1. Even though the final result quotes an uncertainty of 25 Hz, a total statistical uncertainty of < 2 Hz was achieved. This measurement is completely limited by the systematic uncertainty, and there is a possibility of improving the precision by another order of magnitude if all systematic effects are well understood.

Figure 5.2 shows the statistical distributions of linecentres. The histogram was obtained by taking the differences between the individual linecentres and the final measured result and dividing this difference (column 13 of Table A.2) by the total uncertainty (column 14 of Table A.2) of the individual measurement. The histogram shows an excellent agreement with a normal distribution.

Table 5.2 shows recent measurements of the 2^3P_1-to-2^3P_2 transition. Major systematic corrections are applied to laser spectroscopy results due to newly discovered quantum interference effects [57]. Figure 5.3 shows the comparison of the theoretical

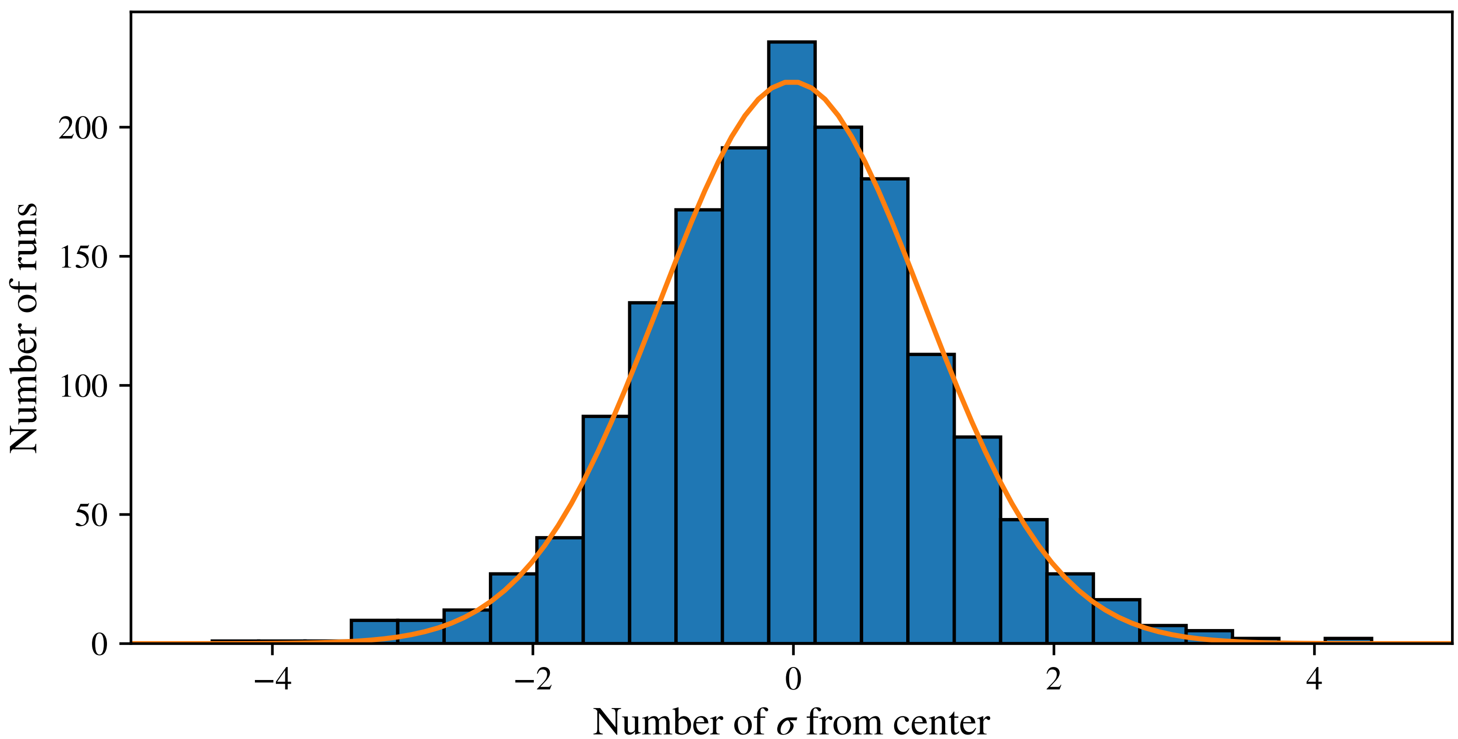

Figure 5.2: Statistical distribution of linecentres.

Research group	Experiment type	Quoted value [Hz]	Corrected values [Hz]	Correction type
Shiner, et al. [31]	Laser Spectroscopy	2 291 176 900(1000)	2 291 177 100(1000)	Quantum interference [57]
Gabrielse, et al. [30]	Laser Spectroscopy	2 291 175 590(510)	2 291 176 790(1100)	Quantum interference [59]
Hessels, et al. [27]	Microwave Spectroscopy	2 291 177 530(350)	2 291 176 655(660)	Reanalysis based on P/T [19]
Hu, et al. [58]	Laser Spectroscopy	2 291 177 690(360)		
Hu, et al. [29]	Laser Spectroscopy	2 291 177 560(190)		
This work [46]	Microwave Spectroscopy	2 291 176 590(25)		

Table 5.2: Recent measurements of the $2^3\mathrm{P}_1$-to-$2^3\mathrm{P}_2$ transition with new systematic corrections. For the most recent results of the combined ν_{02} transition, refer to [29] and [60]

calculation and experimental measurements of the $2^3\mathrm{P}_1$-to-$2^3\mathrm{P}_2$ transition. Our result is slightly smaller (1.5 times the estimated theoretical uncertainty) than the best theoretical prediction. It disagrees with recent laser measurements by Hu, et al. [29, 58] by 4.9 and 2.9 times their uncertainties. The SOF measurement by Hessels, et al. [27] has been reanalyzed based on the P/T linecentre extrapolation discussed in Section 4.2.5 [19]. The reanalyzed result agrees with the present measurement. This measurement is the most precise measurement to date of a helium fine-structure interval, and represents a major advance in this precision. This work sets the stage for a new level of accuracy for this fine structure, which, when combined with more precise theory, could provide <1 ppb tests of the physics and constants relevant to the interval—including a precise determination of the fine-structure constant, the most precise test of multi-electron QED, and tests for physics beyond the Standard Model.

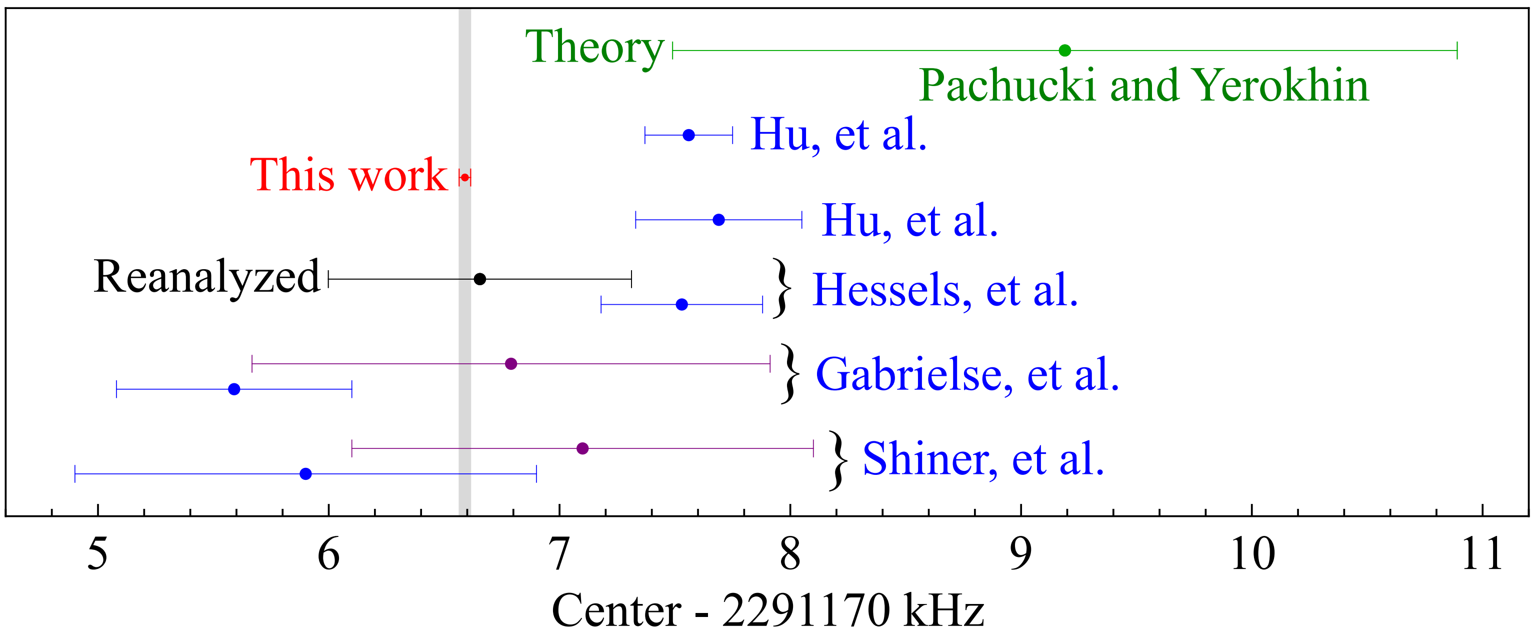

Figure 5.3: Comparison of recent measurements of the 2^3P_1-to-2^3P_2 transition. The blue points indicate values quoted by the research groups. The purple points are the results with quantum interference correction included. The black point is the reanalyzed result of [27] based on P/T extrapolation discussed in Section 4.2.5. The green point indicates the theoretical calculation of [26]. The red point is the current work. The plotted values are also given in Table 5.2.

Bibliography

[1] D. Hanneke, S. Fogwell, and G. Gabrielse. New measurement of the electron magnetic moment and the fine structure constant. *Physical Review Letters*, 100(12):1–4, 2008.

[2] R. Parker, C. Yu, Z Weicheng, E. Brian, and H. Müller. Measurement of the fine structure constant as a test of the Standard Model. *Science*, 360(6385):191–195, 2018.

[3] R. Bouchendira, P. Cladé, S. Guellati-Khélifa, F. Nez, and F. Biraben. New determination of the fine structure constant and test of the quantum electrodynamics. *Physical Review Letters*, 106(8):7–10, 2011.

[4] G. Gabrielse, S. F. Hoogerheide, J. Dorr, and E. Novitski. *Fundamental physics in particle traps*. Springer, New York, 2014.

[5] Y. Kahn, G. Krnjaic, S. Mishra-Sharma, and M.P. Tait. Light weakly coupled axial forces: Models, constraints, and projections. *Journal of High Energy*

Physics, 2017(5):0–33, 2017.

[6] Y. Lan, C. Kuan, B. Estey, D. English, J. M. Brown, M. A. Hohensee, and H. Müller. A clock directly linking time to a particle's mass. *Science*, 338(August):1321–1324, 2013.

[7] C. Schwartz. Fine structure of helium. *Physical Review*, 134(5A), 1964.

[8] W. E. Lamb. Measurement of the fine structure separation 3^3P_1-3^3P_2 for the helium atom. *Physical Review*, 105:1354–1358, 1957.

[9] F. D. Colegrove, P. A. Franken, R. R. Lewis, and R. H. Sands. Novel method of spectroscopy with applications to precision fine structure measurements. *Physical Review Letters*, 3(9):420–422, 1959.

[10] S. A. Lewis, F. M. J. Pichanick, and V. W. Hughes. Experiments on the 2^3P state of helium. II. Measurements of the Zeeman effect. *Physical Review A*, 7, 1969.

[11] M. Lewis. The fine structure constant from helium fine structure. *Physics Letters A*, 58(2):125–126, 1976.

[12] M. L. Lewis and P. H. Serafino. Second-order contributions to the fine structure of helium from all intermediate states. *Physical Review A*, 18(8), 1978.

[13] W. Frieze, E. A. Hinds, and V. W. Hughes. Experiments on the 2^3P state of helium. IV. Measurement of the 2^3P_0-2^3P_2 fine-structure interval. *Physical Review A*, 24(1), 1981.

[14] G.W.F. Drake. New variational techniques for the 1*snd* states of helium. *Physical Review Letters*, 59(14):1549–1552, 1987.

[15] D. Shiner, R. Dixson, and P. Zhao. Precise measurement of the Lamb shift and fine structure of the 2S-2P transition in tripiet heium. *Physical Review Letters*, 67(17):2339–2342, 1991.

[16] T. Zhang. Corrections to $O(\alpha^7(\ln\alpha)mc^2)$ fine-structure splittings and $O(\alpha^6(\ln\alpha)mc^2)$ energy levels in helium. *Physical Review A*, 54(2):1252–1312, 1996.

[17] F Marin, A Bramati, E Giacobino, T Zhang, J Poizat, J Roch, and F. Cedex. High precision calculation of fine structure splittings in helium and He-like ions. *Physical Review Letters*, 75(25):4606–4609, 1995.

[18] K. Pachucki and J. Sapirstein. Contributions to helium fine structure of order mα^7. *Journal of Physics B: Atomic, Molecular and Optical Physics*, 33(23):5297–5305, 2000.

[19] K. Kato, T. D. G. Skinner, and E. A. Hessels. Ultrahigh-precision measurement of the $n = 2$ triplet P fine structure of atomic helium using frequency-offset separated oscillatory fields. *Physical Review Letters*, 121(14):143002, 2018.

[20] J. S. Sims and S. A. Hagstrom. High-precision Hy-Cl variational calculations for the ground state of neutral helium and helium-like ions. *International Journal of Quantum Chemistry*, 90(6):1600–1609, 2002.

[21] G. W. F. Drake and D. C. Morton. A Multiplet table for neutral helium ($^4\mathrm{He}_I$) with transition rates. *The Astrophysical Journal Supplement Series*, 170(1):251–260, 2007.

[22] R. S. van Dyck, C. E. Johnson, and H. A. Shugart. Radiative lifetime of the $2^1\mathrm{S}_0$ metastable state of helium. *Physical Review A*, 4(4):1327, 1971.

[23] S. S. Hodgman, R. G. Dall, L. J. Byron, K. G.H. Baldwin, S. J. Buckman, and A. G. Truscott. Metastable helium: A new determination of the longest atomic excited-state lifetime. *Physical Review Letters*, 103(5):6–9, 2009.

[24] Felicia A. Corsaro. Fine structure of the $2^3\mathrm{P}$ state of the helium atom. *The Journal of Chemical Physics*, 58(7):2851, 1973.

[25] P. Zhang, X. Zhong, C. Yan, and Y. Shi. Precision calculation of fine structure in helium and Li^+. *Chinese Physics B*, 24(3):033101, 2015.

[26] K. Pachucki and V. A. Yerokhin. Fine structure of heliumlike ions and determination of the fine structure constant. *Physical Review Letters*, 104(7):7–10, 2010.

[27] J. S. Borbely, M. C. George, L. D. Lombardi, M. Weel, D. W. Fitzakerley, and E. A. Hessels. Separated oscillatory-field microwave measurement of the 2^3P_1-2^3P_2 fine-structure interval of atomic helium. *Physical Review A - Atomic, Molecular, and Optical Physics*, 79(6):1–4, 2009.

[28] M. C. George, L. D. Lombardi, and E. A. Hessels. Precision microwave measurement of the 2^3P_1-2^3P_0 interval in atomic helium: A determination of the fine-structure constant. *Physical Review Letters*, 87(17):173002, 2001.

[29] X. Zheng, Y. R. Sun, J. J. Chen, W. Jiang, K. Pachucki, and S. M. Hu. Laser spectroscopy of the fine-structure splitting in the 2^3P_J levels of ^{4}He. *Physical Review Letters*, 118(6):1–5, 2017.

[30] T. Zelevinsky, D. Farkas, and G. Gabrielse. Precision measurement of the three 2^3P_J helium fine structure intervals. *Physical Review Letters*, 95(20):4–7, 2005.

[31] J. Castillega, D. Livingston, A. Sanders, and D. Shiner. Precise measurement of the $J = 1$ to $J = 2$ fine structure interval in the 2^3P state of helium. *Physical Review Letters*, 84(19):4321–4, 2000.

[32] M. Smiciklas and D. Shiner. Determination of the fine structure constant using helium fine structure. *Physical Review Letters*, 105(12):1–4, 2010.

[33] J. S. Borbely. *Separated Oscillatory Field Microwave Measurement of the n=2 $^3P_1$ to n=2 $^3P_2$ Fine Structure Interval of Helium*. PhD thesis, York University, 2009.

[34] A. C. Vutha and E. A. Hessels. Frequency-offset separated oscillatory fields. *Physical Review A - Atomic, Molecular, and Optical Physics*, 92(5):1–6, 2015.

[35] M. J. Verheijen, H. C. W. Beijerinck, L. H. A. M. Van Moll, J. Driessen, and N. F. Verster. A discharge excited supersonic source of metastable rare gas atoms. *Journal of Physics E: Scientific Instruments*, 17(10):904–910, 1984.

[36] P. G. A. Theuws, H. C. W. Beijerinck, N. F. Verster, and D. C. Schram. A hollow cathode arc as a high intensity beam source for ground state and metastable noble gas atoms in the eV translational energy range. *Journal of Physics E: Scientific Instruments*, 15(5):573–579, 1982.

[37] J. A. Swansson, R. G. Dall, and A. G. Truscott. An intense cold beam of metastable helium. *Applied Physics B: Lasers and Optics*, 86(3):485–489, 2007.

[38] M. Baker, A. J. Palmer, and R. T. Sang. A high flux metastable atomic discharge source with three-dimensional translation. *Measurement Science and Technology*, 14(4), 2003.

[39] E. A. Donley, T. P. Heavner, F. Levi, M. O. Tataw, and S. R. Jefferts. Double-pass acousto-optic modulator system. *Review of Scientific Instruments*, 76(6):3–8, 2005.

[40] H. Beica. Improved Laser Locking Techniques for Realizing an Enhanced Measurement of the Helium 2 Triplet P Fine Structure. Master's thesis, York University, 2013.

[41] M. L. Harris, S. L. Cornish, A. Tripathi, and I. G. Hughes. Optimization of sub-Doppler DAVLL on the rubidium D2 line. *Journal of Physics B: Atomic, Molecular and Optical Physics*, 41(8), 2008.

[42] G. W. Choi and H. R. Noh. Sub-Doppler DAVLL spectra of the D1 line of rubidium: A theoretical and experimental study. *Journal of Physics B: Atomic, Molecular and Optical Physics*, 48(11), 2015.

[43] B. Cheron, H. Gilles, J. Hamel, O. Moreau, and H. Sorel. Laser frequency stabilization using Zeeman effect. *Journal de Physique III*, 4(3):401–406, 1994.

[44] K. Razdan and D. A. Van Baak. Demonstrating optical beat notes through heterodyne experiments. *American Journal of Physics*, 70(10):1061–1067, 2002.

[45] M. Weel and A. Kumarakrishnan. Laser-frequency stabilization using a lock-in amplifier. *Canadian Journal of Physics*, 80(12):1449–1458, 2002.

[46] K. Kato, D. W. Fitzakerley, M. George, A. Vutha, M. Weel, C. Storry, T. Kirchner, and E. A. Hessels. Selective detection of metastable helium atoms by elastic scattering collisions. *Physical Review A*, 86(1), 2012.

[47] J. Foot. *Atomic physics*. Oxford University Press, 2005.

[48] H. J. Metcalf and P. Straten. *Laser cooling and trapping*. Springer, 1999.

[49] S. Zhang, J. F. Chen, C. Liu, S. Zhou, M. M. T. Loy, G. K. L. Wong, and S. Du. A dark-line two-dimensional magneto-optical trap of ^{85}Rb atoms with high optical depth. *Review of Scientific Instruments*, 83(7):073102, 2012.

[50] J. Abbott. Parametric design of tri-axial nested Helmholtz coils. *Review of Scientific Instruments*, 86(5), 2015.

[51] N. F. Ramsey. A molecular beam resonance method with separated oscillating fields. *Physical Review*, 78(6):695–699, 1950.

[52] Zürich Instruments. Principles of lock-in detection and the state of the art Zurich Instruments. *White Paper*, (November):1–10, 2016.

[53] C. W. Fabjan and F. M. Pipkin. Resonance-narrowed-Lamb-shift measurement in Hydrogen, n =3. *Physical Review A*, 6:556–570, 1971.

[54] L. D. Lombardi. *Progress Towards a Separated Oscillatory Fields Measurement of the 2^3P_1-to-2^3P_2 Fine-Structure Interval of Atomic Helium.* PhD thesis, York University, 2009.

[55] J. D. Jackson. *Classical Electrodynamics.* John Wiley and Sons, inc., third edition, 1998.

[56] M. C. George. *Precision Measurements of the $n = 2^3P$ Intervals of Atomic Helium: A Determination of the Fine-Structure Constant.* PhD thesis, York University, 2003.

[57] A. Marsman, M. Horbatsch, and E. A. Hessels. Shifts due to distant neighboring resonances for laser measurements of $2^3\mathrm{S}_1$-to-$2^3\mathrm{P}_J$ transitions of helium. *Physical Review A - Atomic, Molecular, and Optical Physics*, 86(4):2–5, 2012.

[58] G. P. Feng, X. Zheng, Y. R. Sun, and S. M. Hu. Laser-spectroscopy measurement of the fine-structure splitting $2^3\mathrm{P}_1$-$2^3\mathrm{P}_2$ of ^{4}He. *Physical Review A - Atomic, Molecular, and Optical Physics*, 91(3):1–5, 2015.

[59] A. Marsman, M. Horbatsch, and E. A. Hessels. Quantum interference effects in saturated absorption spectroscopy of $n = 2$ triplet-helium fine structure. *Physical Review A*, 91(6):062506, 2015.

[60] A. Marsman, M. Horbatsch, and E. A. Hessels. The effect of quantum-mechanical interference on precise measurements of the n = 2 triplet P fine structure of helium. *Journal of Physical and Chemical Reference Data*, 44(3), 2015.

A Table of Data Runs

Identifier	Acronym	Description
NR	Normal Run	Normal experiment running parameter
LB	Large B	$\lvert B \rvert > 10$ applied to the experiment
PR	Power Restriction	Data with $PD^2 > 0.9$
PRLB	Power Restriction Large B	Data with $PD^2 > 0.9$ and $\lvert B \rvert > 10$ applied to the experiment
FDET	F DETection	18F detection experiment
CWLC	CW Laser C	CW 1532-nm laser experiment
LLAP	Low Laser A Power	Reduced 1083-nm laser power
LLBP	Low Laser B Power	Reduced 447-nm laser power
LAT	Laser A Timing	Varied 1083-nm laser timing
LBT	Laser B Timing	Varied 447-nm laser timing
MOT0	MOT OFF	2DMOT turned off
UP	UPstream	Experiment performed at upstream location
UPLB	UPstream Large B	Experiment performed at upstream location with large B applied

Table A.1: Data identifier table. The table describes the interpretation of the last column in Table A.2.

Table A.2: Table of data runs. Each row is a weighted average of repeated runs. Experiment type is specified in Data Type column. Uncertainties are highlighted in gray. Columns 7 and 13 are with respect to the final measured result of 2 291 176 590 Hz

1	2	3	4	5	6	7	8	9	10	11	12	13	14	15	16
Run Number N_{run}	Pulse Separation T [ns]	Pulse Duration D [ns]	Microwave Power P [W]	Magnetic Field B [Gauss]	Polarizer Angle θ_{pol} [degree]	Fit Linecentre ν_{fit} [Hz]	Fit Uncertainty $\Delta\nu_{\mathrm{fit}}$ [Hz]	DC Zeeman Correction $\mathrm{DC_B}$ [Hz]	Zeeman Uncertainty $\Delta\mathrm{DC_B}$ [Hz]	Slope Correction SC [Hz]	Slope Uncertainty ΔSC [Hz]	Corrected Linecentre ν_0 [Hz]	Total uncertainty $\Delta\nu_0$ [Hz]	Weights wts. [%]	Data Type
1	300	100	15	4.762	260	10069	110	-9765	9.8	98	2	206	111	0.32	NR
2	300	100	52.5	4.762	260	10102	84	-9766	14.7	371	13	-35	87	0.00	NR
3	300	100	60	4.762	260	10151	91	-9765	15	428	16	-42	94	0.00	NR
4	300	100	7.5	4.762	260	9687	137	-9765	14.4	46	2	-124	137	0.03	NR
5	300	100	74.25	4.762	260	10284	38	-9765	9.8	528	13	-9	41	0.00	NR
6	300	100	52.5	-4.762	260	10117	67	-9758	9.8	374	9	-16	68	0.14	NR
7	300	100	22.5	-4.762	260	9920	81	-9758	9.8	154	4	9	82	0.50	NR
8	300	100	30	-4.762	260	9890	103	-9758	11.8	208	6	-76	104	0.05	NR
9	300	100	74.25	-4.762	260	10358	56	-9757	9.8	529	13	73	58	0.00	NR
10	300	100	45	4.762	260	10035	71	-9766	9.8	318	8	-48	72	0.26	NR
11	300	100	22.5	4.762	260	9928	88	-9766	9.8	153	4	9	89	0.42	NR
12	300	100	7.5	-4.762	260	9770	87	-9757	9.8	46	1	-33	87	0.61	NR
13	300	100	37.5	-4.762	260	10073	58	-9759	9.8	259	6	55	59	0.63	NR
14	300	100	60	-4.762	260	10115	44	-9758	9.8	422	10	-65	46	0.03	NR
15	300	100	30	4.762	260	10008	74	-9765	9.8	206	5	36	75	0.48	NR
16	300	100	15	-4.762	260	9908	108	-9758	9.8	98	2	52	108	0.34	NR
17	300	100	37.5	4.762	260	9949	57	-9767	9.8	259	6	-77	58	0.65	NR
18	300	100	45	-4.762	260	10075	59	-9756	9.8	315	8	4	61	0.39	NR
19	400	100	7.5	-4.762	260	9908	133	-9757	9.8	35	1	116	133	0.27	NR
20	400	100	7.5	-4.762	260	9905	122	-9758	9.8	34	1	113	122	0.32	NR
21	400	100	7.5	-4.762	260	9764	140	-9758	9.8	34	1	-28	140	0.24	NR
22	500	125	7.5	3.81	260	6227	211	-6250	6.2	32	6	-55	211	0.11	NR
23	500	125	7.5	3.81	260	6270	143	-6250	6.2	32	6	-12	143	0.25	NR
24	500	125	7.5	3.81	260	6484	230	-6250	6.2	32	6	202	230	0.09	NR
25	500	125	15	-3.81	260	6343	101	-6243	6.2	70	12	29	102	0.17	NR
26	500	125	15	-3.81	260	6313	160	-6243	6.2	70	12	-1	161	0.07	NR
27	500	125	15	-3.81	260	6348	128	-6243	6.2	70	12	35	129	0.11	NR
28	500	125	74.25	3.81	260	6535	125	-6250	6.2	380	66	-94	141	0.00	PR
29	400	100	74.25	-4.762	260	10090	95	-9757	9.8	406	10	-73	96	0.02	NR
30	400	100	30	-4.762	260	9906	89	-9759	9.8	158	4	-10	90	0.40	NR
31	400	100	52.5	-4.762	260	10007	86	-9757	9.8	282	7	-32	86	0.23	NR
32	400	100	22.5	4.762	260	9905	88	-9765	9.8	116	3	24	89	0.48	NR
33	400	100	74.25	4.762	260	10118	66	-9763	9.8	405	10	-50	68	0.05	NR
34	400	100	60	-4.762	260	10109	65	-9758	9.8	327	8	24	66	0.29	NR
35	500	125	60	3.81	260	6580	126	-6249	6.2	309	53	22	137	0.00	PR
36	500	125	74.25	-3.81	260	6468	113	-6244	6.2	384	67	-159	131	0.00	PR
37	400	100	22.5	-4.762	260	9933	120	-9759	15.4	116	4	58	121	0.00	NR
38	400	100	45	-4.762	260	10135	93	-9757	9.8	242	6	136	94	0.25	NR
39	500	125	52.5	3.81	260	6463	108	-6250	6.2	268	46	-55	118	0.00	PR
40	500	125	22.5	3.81	260	6341	113	-6250	6.2	109	19	-17	115	0.00	NR
41	500	125	15	3.81	260	6475	137	-6250	6.3	70	12	155	137	0.09	NR
42	500	125	15	3.81	260	6374	142	-6249	6.2	70	12	54	143	0.09	NR
43	500	125	15	3.81	260	6135	152	-6249	6.2	70	12	-184	153	0.08	NR
44	400	100	7.5	4.762	260	9699	140	-9766	9.8	34	1	-101	140	0.24	NR
45	400	100	7.5	4.762	260	9544	146	-9765	9.8	34	1	-255	147	0.22	NR
46	400	100	7.5	4.762	260	9969	161	-9766	9.8	34	1	169	161	0.18	NR
47	400	100	37.5	-4.762	260	10053	86	-9759	9.8	197	5	97	87	0.37	NR
48	500	125	52.5	-3.81	260	6529	124	-6244	6.2	264	46	22	133	0.00	PR
49	500	125	30	-3.81	260	6555	125	-6244	6.2	148	26	163	127	0.00	NR
50	500	125	37.5	-3.81	260	6336	87	-6243	6.2	187	32	-94	93	0.00	NR
51	400	100	15	-4.762	260	9616	97	-9757	9.8	74	2	-215	97	0.45	NR
52	400	100	15	-4.762	260	9831	131	-9758	9.8	74	2	0	132	0.25	NR
53	400	100	15	-4.762	260	9680	166	-9757	9.8	74	2	-150	166	0.15	NR
54	500	125	30	3.81	260	6334	88	-6250	6.3	148	26	-64	92	0.00	NR
55	500	125	45	3.81	260	6535	129	-6250	6.3	225	39	60	135	0.00	NR
56	400	100	30	4.762	260	9950	78	-9765	9.8	156	4	29	79	0.53	NR
57	500	125	60	-3.81	260	6387	161	-6243	6.2	304	53	-160	169	0.00	PR
58	500	125	22.5	-3.81	260	6468	114	-6244	6.2	109	19	115	116	0.00	NR
59	500	125	45	-3.81	260	6545	165	-6244	6.2	225	39	75	169	0.00	NR
60	400	100	15	4.762	260	9736	96	-9765	9.8	74	2	-103	96	0.46	NR
61	400	100	60	4.762	260	10089	78	-9766	9.8	322	8	1	79	0.20	NR
62	500	125	7.5	-3.81	260	5848	238	-6244	6.2	32	6	-428	238	0.09	NR
63	500	125	7.5	-3.81	260	5742	170	-6244	6.2	32	6	-534	171	0.17	NR
64	500	125	7.5	-3.81	260	5993	208	-6244	6.2	32	6	-283	209	0.11	NR
65	500	125	37.5	3.81	260	6432	74	-6251	6.3	186	32	-4	81	0.00	NR
66	400	100	45	4.762	260	9946	97	-9766	9.8	238	6	-57	97	0.24	NR
67	400	100	52.5	4.762	260	9976	75	-9767	9.8	279	7	-70	76	0.31	NR
68	400	100	37.5	4.762	260	9879	84	-9765	9.8	198	5	-84	85	0.38	NR
69	300	100	67.5	4.762	260	10284	51	-9766	9.8	477	11	40	53	0.00	NR
70	400	100	67.5	-4.762	260	10099	83	-9759	9.8	368	9	-28	84	0.10	NR
71	400	100	67.5	4.762	260	10229	74	-9765	9.8	368	9	95	75	0.12	NR
72	300	100	67.5	-4.762	260	10216	49	-9759	9.8	478	11	-21	51	0.00	NR
73	500	125	67.5	3.81	260	6687	145	-6250	6.2	347	60	90	157	0.00	PR
74	500	125	67.5	-3.81	260	6720	137	-6244	6.2	348	60	128	150	0.00	PR
75	300	100	74.25	-4.762	260	10274	67	-9757	9.8	541	13	-24	69	0.00	LBT

Continued on next page

Table A.2 Continued from previous page

N_{run}	T [ns]	D [ns]	P [W]	B [Gauss]	θ_{pol} [deg.]	ν_{fit} [Hz]	$\Delta\nu_{\mathrm{fit}}$ [Hz]	$\mathrm{DC_B}$ [Hz]	$\Delta\mathrm{DC_B}$ [Hz]	SC [Hz]	ΔSC [Hz]	ν_0 [Hz]	$\Delta\nu_0$ [Hz]	wts. [%]	Data Type
76	300	100	74.25	-4.762	260	10070	142	-9763	9.8	541	13	-235	142	0.00	LBT
77	300	100	74.25	-4.762	260	10451	99	-9757	9.8	542	13	153	100	0.00	LBT
78	300	100	74.25	-4.762	260	10259	70	-9757	9.8	542	13	-40	72	0.00	LBT
79	300	100	74.25	-4.762	260	10120	88	-9758	9.8	542	13	-179	89	0.00	LBT
80	300	100	74.25	-4.762	260	10311	106	-9756	9.8	542	13	13	107	0.00	LBT
81	300	100	74.25	-4.762	260	10296	138	-9757	9.8	541	13	-2	139	0.00	LBT
82	300	100	74.25	-4.762	260	10203	100	-9759	9.8	542	13	-98	101	0.00	LBT
83	300	100	74.25	-4.762	260	10094	131	-9757	9.8	542	13	-204	132	0.00	LBT
84	300	100	74.25	-4.762	260	10481	84	-9757	9.8	542	13	182	86	0.00	LBT
85	300	100	74.25	-4.762	260	10239	115	-9758	9.8	541	13	-59	116	0.00	LAT
86	300	100	74.25	-4.762	260	10337	76	-9762	9.8	541	13	34	78	0.00	LAT
87	300	100	74.25	-4.762	260	10234	135	-9757	9.8	541	13	-63	136	0.00	LAT
88	300	100	74.25	-4.762	260	10181	75	-9758	9.8	540	13	-117	77	0.00	LAT
89	300	100	74.25	-4.762	260	10488	103	-9759	9.8	540	13	190	104	0.00	LAT
90	300	100	74.25	-4.762	260	10294	89	-9758	9.8	539	13	-3	91	0.00	LAT
91	300	100	74.25	-4.762	260	10381	130	-9757	9.8	539	13	85	131	0.00	LAT
92	300	100	74.25	-4.762	260	10205	68	-9758	9.8	539	13	-91	70	0.00	LAT
93	300	100	74.25	-4.762	260	10282	143	-9757	9.8	539	13	-13	144	0.00	LAT
94	300	100	74.25	-4.762	260	10267	73	-9757	9.8	539	13	-29	75	0.00	LAT
95	300	50	67.5	9.524	170	39194	80	-38982	39	165	32	47	94	0.00	NR
96	300	50	15	-9.524	170	39121	115	-38971	39	32	6	118	121	0.00	NR
97	300	50	67.5	-9.524	170	38968	70	-38972	39	163	32	-168	86	0.00	NR
98	300	50	52.5	9.524	170	38993	91	-38984	39	126	25	-117	102	0.00	NR
99	300	50	7.5	9.524	170	39058	165	-38985	39	14	3	59	170	0.00	NR
100	300	50	22.5	-9.524	170	38964	79	-38972	39	50	10	-57	89	0.00	NR
101	300	50	15	9.524	170	39258	125	-38986	39	32	6	240	131	0.00	NR
102	300	50	7.5	-9.524	170	38943	145	-38969	39	14	3	-40	151	0.00	NR
103	300	50	60	-9.524	170	39195	97	-38969	39	142	28	83	108	0.00	NR
104	300	50	22.5	9.524	170	39031	76	-38986	39	50	10	-5	86	0.00	NR
105	300	50	52.5	-9.524	170	39060	62	-38969	39	124	24	-34	77	0.00	NR
106	300	50	30	-9.524	170	39125	98	-38968	39	68	13	89	107	0.00	NR
107	300	50	37.5	9.524	170	38987	131	-38987	39	87	17	-87	138	0.00	NR
108	300	50	74.25	-9.524	170	39070	67	-38969	39	179	35	-78	85	0.00	NR
109	300	50	45	9.524	170	39167	127	-38986	39	106	21	75	134	0.00	NR
110	300	50	37.5	-9.524	170	38859	92	-38969	39	87	17	-197	101	0.00	NR
111	300	50	45	-9.524	170	39072	86	-38968	39	105	21	-2	96	0.00	NR
112	300	50	60	9.524	170	39266	118	-38987	39	142	28	137	127	0.00	NR
113	300	50	30	9.524	170	39283	93	-38987	39	68	13	228	101	0.00	NR
114	300	50	74.25	9.524	170	39040	77	-38986	39	179	35	-124	93	0.00	NR
115	400	200	60	-7.143	170	23641	107	-21964	22	976	199	702	227	0.00	PR
116	300	150	7.5	-3.175	170	4448	72	-4354	4.4	84	9	10	73	0.92	NR
117	400	200	67.5	-7.143	170	24036	96	-21963	22	1076	219	996	240	0.00	PR
118	300	100	15	19.048	170	156004	102	-155952	156	101	2	-50	187	0.00	LB
119	400	200	22.5	7.143	170	22355	94	-21979	22	356	72	21	121	0.00	PR
120	400	200	37.5	-7.143	170	22721	109	-21964	22	602	122	155	165	0.00	PR
121	400	200	7.5	7.143	170	22006	138	-21978	22	111	23	-83	142	0.00	NR
122	300	150	15	3.175	170	4599	54	-4360	4.4	178	20	61	57	0.00	NR
123	300	150	52.5	3.175	170	5226	47	-4360	4.4	647	72	219	86	0.00	PR
124	400	200	60	7.143	170	23463	96	-21978	22	964	196	521	219	0.00	PR
125	300	150	37.5	3.175	170	4888	80	-4361	4.4	465	52	63	96	0.00	PR
126	400	200	7.5	-7.143	170	21906	129	-21963	22	110	22	-167	133	0.00	NR
127	300	150	74.25	-3.175	170	6011	67	-4355	4.4	909	101	747	121	0.00	PR
128	300	150	45	-3.175	170	5056	53	-4353	4.4	562	62	141	82	0.00	PR
129	600	100	15	-4.762	170	9941	238	-9757	9.8	48	1	136	238	0.08	NR
130	300	150	67.5	3.175	170	5633	53	-4359	4.4	828	92	446	106	0.00	PR
131	400	200	74.25	-7.143	170	24565	93	-21962	22	1185	241	1418	259	0.00	PR
132	300	150	7.5	3.175	170	4399	84	-4359	4.4	84	9	-44	85	0.65	NR
133	400	200	15	-7.143	170	22043	70	-21963	22	230	47	-150	87	0.00	NR
134	400	200	37.5	7.143	170	22558	121	-21979	22	600	122	-21	173	0.00	PR
135	300	150	60	-3.175	170	5428	50	-4353	4.4	742	82	334	96	0.00	PR
136	300	150	37.5	-3.175	170	4875	69	-4352	4.4	464	52	58	86	0.00	PR
137	300	150	60	3.175	170	5382	59	-4360	4.4	743	83	280	101	0.00	PR
138	400	200	67.5	7.143	170	24039	98	-21978	22	1085	221	975	243	0.00	PR
139	400	200	22.5	-7.143	170	22139	72	-21964	22	359	73	-183	105	0.00	PR
140	300	150	52.5	-3.175	170	5083	61	-4354	4.4	651	72	78	95	0.00	PR
141	400	200	15	7.143	170	22173	108	-21979	22	235	48	-41	120	0.00	NR
142	300	150	15	-3.175	170	4625	47	-4354	4.4	179	20	93	51	0.00	NR
143	400	200	30	7.143	170	22459	47	-21980	22	481	98	-2	111	0.00	PR
144	400	200	45	-7.143	170	22809	84	-21965	22	724	147	121	171	0.00	PR
145	300	150	45	3.175	170	4993	63	-4360	4.4	557	62	75	89	0.00	PR
146	300	150	22.5	-3.175	170	4594	44	-4353	4.4	275	31	-34	54	0.00	NR
147	300	150	74.25	3.175	170	5906	58	-4360	4.4	908	101	638	116	0.00	PR
148	400	200	52.5	7.143	170	23311	102	-21978	22	846	172	487	201	0.00	PR
149	400	200	30	-7.143	170	22400	62	-21963	22	483	98	-45	118	0.00	PR
150	400	200	52.5	-7.143	170	23214	99	-21963	22	848	173	403	200	0.00	PR
151	300	150	22.5	3.175	170	4552	56	-4361	4.4	276	31	-85	64	0.00	NR
152	300	150	30	-3.175	170	4764	49	-4354	4.4	371	41	40	64	0.00	NR
153	300	100	15	-19.048	170	155925	63	-155915	155.9	101	2	-91	168	0.00	LB
154	400	200	74.25	7.143	170	24533	98	-21983	22	1185	241	1365	261	0.00	PR
155	400	200	45	7.143	170	22789	115	-21977	22	735	150	76	190	0.00	PR
156	300	150	67.5	-3.175	170	5640	57	-4354	4.4	836	93	450	109	0.00	PR
157	600	100	74.25	-4.762	170	10154	115	-9758	9.8	285	7	110	116	0.13	NR
158	300	150	30	3.175	170	4739	50	-4359	4.4	371	41	9	65	0.00	NR
159	700	100	67.5	-4.762	170	10088	159	-9757	9.8	221	5	110	159	0.10	NR
160	700	100	67.5	-4.762	170	9835	196	-9758	9.8	222	5	-144	196	0.07	NR
161	700	100	67.5	4.762	170	10015	295	-9767	9.8	223	5	25	295	0.03	NR
162	700	100	67.5	4.762	170	9715	223	-9767	9.8	224	5	-276	223	0.05	NR
163	600	100	52.5	4.762	170	10042	136	-9766	9.8	197	5	79	137	0.15	NR
164	600	100	60	4.762	170	9963	102	-9765	9.8	226	5	-27	102	0.23	NR
165	600	100	15	-4.762	170	9871	302	-9759	9.8	48	1	64	302	0.05	NR
166	600	100	22.5	-4.762	170	10067	192	-9759	9.8	77	2	231	192	0.11	NR
167	600	100	52.5	-4.762	170	9815	119	-9758	9.8	196	5	-139	120	0.19	NR
168	600	100	15	4.762	170	9738	302	-9766	9.8	50	1	-78	302	0.05	NR
169	600	100	30	4.762	170	9409	151	-9767	9.8	107	3	-465	151	0.17	NR
170	600	100	30	-4.762	170	9943	152	-9759	9.8	106	3	79	152	0.17	NR
171	600	100	22.5	4.762	170	9919	211	-9765	9.8	77	2	77	211	0.09	NR
172	600	100	60	-4.762	170	9939	112	-9759	9.8	223	5	-43	112	0.20	NR
173	600	100	37.5	4.762	170	10091	189	-9765	9.8	135	3	192	189	0.10	NR

Continued on next page

Table A.2 Continued from previous page

N_{run}	T [ns]	D [ns]	P [W]	B [Gauss]	θ_{pol} [deg.]	ν_{fit} [Hz]	$\Delta\nu_{\mathrm{fit}}$ [Hz]	$\mathrm{DC_B}$ [Hz]	$\Delta\mathrm{DC_B}$ [Hz]	SC [Hz]	ΔSC [Hz]	ν_0 [Hz]	$\Delta\nu_0$ [Hz]	wts. [%]	Data Type
174	600	100	45	4.762	170	9850	138	-9765	9.8	164	4	-79	138	0.17	NR
175	600	100	45	-4.762	170	9815	125	-9759	9.8	164	4	-108	125	0.20	NR
176	300	150	26.25	-3.175	170	4690	79	-4355	4.4	323	36	12	87	0.00	NR
177	300	150	18.75	3.175	170	4620	79	-4358	4.4	229	25	32	83	0.00	NR
178	300	150	11.25	-3.175	170	4411	139	-4354	4.4	133	15	-77	140	0.10	NR
179	300	150	3.75	3.175	170	4598	219	-4359	4.4	40	4	199	219	0.14	NR
180	300	150	3.75	-3.175	170	4822	227	-4355	4.4	40	4	428	227	0.14	NR
181	300	150	26.25	3.175	170	4741	98	-4358	4.4	321	36	62	104	0.00	NR
182	300	150	18.75	-3.175	170	4473	94	-4354	4.4	228	25	-110	98	0.00	NR
183	300	150	11.25	3.175	170	4422	106	-4358	4.4	133	15	-69	107	0.17	NR
184	400	200	18.75	7.143	170	22221	74	-21981	22	294	60	-54	98	0.00	NR
185	400	200	11.25	-7.143	170	22036	105	-21966	22	170	35	-100	113	0.00	NR
186	400	200	11.25	7.143	170	22105	114	-21978	22	169	34	-42	121	0.00	NR
187	400	200	3.75	-7.143	170	21727	229	-21968	22	51	10	-292	230	0.00	NR
188	400	200	18.75	7.143	170	22515	109	-21978	22	292	59	246	126	0.00	NR
189	400	200	3.75	7.143	170	21948	230	-21976	22	52	11	-80	231	0.00	NR
190	700	100	37.5	4.762	170	10058	169	-9766	9.8	116	3	176	169	0.13	NR
191	700	100	37.5	-4.762	170	9751	185	-9760	9.8	115	3	-124	186	0.11	NR
192	400	50	74.25	-12.762	260	70046	169	-70002	70	138	27	-94	185	0.00	LB
193	400	50	22.5	5.762	260	14219	124	-14278	14.3	36	7	-95	125	0.00	NR
194	400	50	45	-8.762	260	33415	153	-33013	33	78	15	323	158	0.00	NR
195	400	50	7.5	4.762	260	9948	229	-9766	9.8	10	2	172	229	0.08	NR
196	400	50	37.5	-7.762	260	26023	101	-25929	25.9	64	12	30	105	0.00	NR
197	400	50	15	4.762	260	9657	174	-9766	9.8	23	4	-132	175	0.10	NR
198	400	50	67.5	-11.762	260	59584	130	-59498	59.5	120	24	-34	145	0.00	LB
199	400	50	22.5	-5.762	260	14501	199	-14271	14.3	36	7	194	199	0.00	NR
200	400	50	67.5	11.762	260	59535	140	-59511	59.5	121	24	-96	154	0.00	LB
201	400	50	7.5	-4.762	260	9783	237	-9762	9.8	10	2	11	237	0.07	NR
202	400	50	30	6.762	260	19834	151	-19705	19.7	49	10	79	153	0.00	NR
203	400	50	37.5	7.762	260	25948	141	-25937	25.9	63	12	-53	144	0.00	NR
204	400	50	30	-6.762	260	19940	137	-19698	19.7	50	10	192	138	0.00	NR
205	400	50	52.5	9.762	260	40983	164	-40954	41	91	18	-61	170	0.00	NR
206	400	50	15	-4.762	260	9871	187	-9760	9.8	22	4	88	187	0.08	NR
207	400	50	60	-10.762	260	49884	217	-49840	49.8	105	21	-60	224	0.00	LB
208	400	50	74.25	12.762	260	70297	137	-70017	70	135	26	145	156	0.00	LB
209	400	50	52.5	-9.762	260	41024	190	-40946	40.9	92	18	-13	195	0.00	NR
210	400	50	60	10.762	260	49959	165	-49850	49.8	106	21	3	173	0.00	LB
211	400	50	45	8.762	260	33144	121	-33024	33	77	15	43	126	0.00	NR
212	600	150	22.5	7.143	260	21938	143	-21978	22	135	15	-175	146	0.00	NR
213	500	50	7.5	9.762	260	41894	425	-40956	41	8	1	931	427	0.00	NR
214	500	50	37.5	-9.762	260	40917	275	-40947	40.9	50	10	-79	279	0.00	NR
215	600	150	18.75	-7.143	260	21876	207	-21968	22	111	12	-203	209	0.00	NR
216	600	150	11.25	-7.143	260	22668	264	-21969	22	63	7	636	265	0.00	NR
217	500	50	60	-9.762	260	41310	274	-40946	40.9	84	16	280	278	0.00	NR
218	600	150	33.75	-7.143	260	22320	158	-21970	22	208	23	141	161	0.00	PR
219	500	50	7.5	-9.762	260	41350	442	-40948	40.9	8	2	394	444	0.00	NR
220	600	150	7.5	7.143	260	22502	304	-21976	22	40	4	486	305	0.00	NR
221	600	150	18.75	7.143	260	21967	130	-21978	22	110	12	-122	133	0.00	NR
222	600	150	15	7.143	260	21801	239	-21977	22	87	10	-263	240	0.00	NR
223	600	150	30	-7.143	260	22679	170	-21970	22	183	20	526	173	0.00	NR
224	500	50	22.5	-9.762	260	40620	338	-40948	40.9	28	6	-356	340	0.00	NR
225	500	50	15	9.762	260	41149	358	-40960	41	18	3	171	360	0.00	NR
226	600	150	11.25	7.143	260	22162	198	-21978	22	62	7	122	199	0.00	NR
227	600	150	3.75	-7.143	260	22516	429	-21968	22	18	2	530	430	0.00	NR
228	500	50	30	-9.762	260	40920	238	-40946	40.9	39	8	-65	242	0.00	NR
229	500	50	45	9.762	260	41057	235	-40959	41	60	12	37	238	0.00	NR
230	600	150	26.25	7.143	260	22228	140	-21979	22	158	18	91	142	0.00	NR
231	500	50	15	-9.762	260	40641	304	-40945	40.9	18	3	-321	307	0.00	NR
232	500	50	52.5	-9.762	260	40619	308	-40946	40.9	71	14	-398	311	0.00	NR
233	500	50	52.5	9.762	260	41167	252	-40961	41	72	14	135	256	0.00	NR
234	500	50	67.5	9.762	260	40696	215	-40961	41	96	19	-361	219	0.00	NR
235	500	50	45	-9.762	260	41066	298	-40946	40.9	61	12	59	301	0.00	NR
236	600	150	30	7.143	260	22279	145	-21978	22	183	20	118	148	0.00	NR
237	500	50	37.5	9.762	260	41169	174	-40961	41	50	10	158	179	0.00	NR
238	500	50	60	9.762	260	41487	172	-40961	41	83	16	442	177	0.00	NR
239	600	150	15	-7.143	260	22245	216	-21969	22	87	10	190	217	0.00	NR
240	600	150	7.5	-7.143	260	22002	344	-21969	22	40	4	-7	345	0.00	NR
241	600	150	3.75	7.143	260	21754	552	-21979	22	17	2	-243	552	0.00	NR
242	500	50	74.25	9.762	260	41041	201	-40961	41	105	21	-24	206	0.00	NR
243	500	50	74.25	-9.762	260	40757	297	-40944	40.9	107	21	-294	300	0.00	NR
244	600	150	22.5	-7.143	260	21947	186	-21968	22	134	15	-155	188	0.00	NR
245	500	50	30	9.762	260	40763	246	-40960	41	39	8	-236	250	0.00	NR
246	600	150	33.75	7.143	260	22293	114	-21979	22	207	23	108	119	0.00	PR
247	500	50	22.5	9.762	260	41115	269	-40958	41	28	5	129	273	0.00	NR
248	500	50	67.5	-9.762	260	40648	219	-40948	40.9	95	19	-395	223	0.00	NR
249	600	150	26.25	-7.143	260	21935	318	-21966	22	159	18	-190	320	0.00	NR
250	375	125	74.25	7.62	260	25737	62	-25005	25	491	85	241	108	0.00	PR
251	375	125	52.5	7.62	260	25445	76	-25005	25	344	60	96	100	0.00	PR
252	375	125	7.5	7.62	260	25111	104	-25004	25	43	7	64	108	0.00	NR
253	375	125	60	7.62	260	25510	68	-25006	25	391	68	113	99	0.00	PR
254	375	125	37.5	-7.62	260	25242	117	-24996	25	243	42	3	127	0.00	NR
255	375	125	30	7.62	260	25093	116	-25009	25	192	33	-108	123	0.00	NR
256	375	125	67.5	7.62	260	25552	81	-25008	25	443	77	100	114	0.00	PR
257	375	125	52.5	-7.62	260	25486	91	-24997	25	345	60	144	112	0.00	PR
258	375	125	60	-7.62	260	25547	105	-24994	25	394	68	159	128	0.00	PR
259	375	125	37.5	7.62	260	25241	82	-25006	25	242	42	-6	96	0.00	NR
260	375	125	22.5	-7.62	260	25192	78	-24994	25	141	24	56	86	0.00	NR
261	375	125	22.5	7.62	260	25148	82	-25006	25	141	24	1	89	0.00	NR
262	375	125	15	7.62	260	25040	109	-25005	25	91	16	-56	113	0.00	NR
263	375	125	74.25	-7.62	260	25681	86	-24995	25	489	85	197	123	0.00	PR
264	375	125	7.5	-7.62	260	24906	132	-24995	25	43	7	-131	135	0.00	NR
265	375	125	67.5	-7.62	260	25498	87	-24993	25	443	77	62	118	0.00	PR
266	375	125	45	-7.62	260	25264	105	-24993	25	294	51	-23	119	0.00	NR
267	375	125	15	-7.62	260	25265	102	-24994	25	92	16	180	107	0.00	NR
268	375	125	45	7.62	260	25300	93	-25006	25	291	50	3	109	0.00	NR
269	375	125	30	-7.62	260	25243	125	-24993	25	192	33	57	131	0.00	NR
270	600	200	74.25	7.62	260	26667	217	-25005	25	799	163	863	272	0.00	PR
271	600	200	52.5	7.62	260	25810	285	-25006	25	561	114	244	308	0.00	PR

Continued on next page

Table A.2 Continued from previous page

N_{run}	T [ns]	D [ns]	P [W]	B [Gauss]	θ_{pol} [deg.]	ν_{fit} [Hz]	$\Delta\nu_{\mathrm{fit}}$ [Hz]	$\mathrm{DC_B}$ [Hz]	$\Delta\mathrm{DC_B}$ [Hz]	SC [Hz]	ΔSC [Hz]	ν_0 [Hz]	$\Delta\nu_0$ [Hz]	wts. [%]	Data Type
272	600	200	15	7.62	260	25213	240	-25009	25	151	31	53	243	0.00	NR
273	600	200	15	-7.62	260	25062	357	-24994	25	150	31	-82	359	0.00	NR
274	600	200	45	-7.62	260	25530	338	-24992	25	479	97	60	353	0.00	PR
275	600	200	37.5	-7.62	260	25079	359	-24995	25	401	82	-317	369	0.00	PR
276	600	200	60	7.62	260	26187	192	-25010	25	645	131	532	234	0.00	PR
277	600	200	37.5	7.62	260	25434	269	-25006	25	402	82	27	282	0.00	PR
278	600	200	74.25	-7.62	260	26903	235	-24993	25	800	163	1110	287	0.00	PR
279	600	200	45	7.62	260	25358	302	-25008	25	487	99	-137	319	0.00	PR
280	600	200	22.5	7.62	260	25168	188	-25009	25	236	48	-77	195	0.00	PR
281	600	200	67.5	7.62	260	26771	299	-25006	25	727	148	1037	335	0.00	PR
282	600	200	7.5	-7.62	260	24624	459	-24994	25	71	14	-441	460	0.00	NR
283	600	200	74.25	7.62	260	27172	206	-25011	25	803	163	1357	264	0.00	PR
284	600	200	74.25	7.62	260	26840	299	-25007	25	802	163	1030	341	0.00	PR
285	600	200	45	7.62	260	25542	363	-25007	25	483	98	52	377	0.00	PR
286	600	200	45	7.62	260	26129	330	-25007	25	481	98	640	345	0.00	PR
287	450	150	45	-3.175	260	4861	123	-4355	4.4	370	41	136	130	0.00	PR
288	450	150	45	-3.175	260	4732	116	-4356	4.4	369	41	7	123	0.00	PR
289	600	200	74.25	-7.62	260	26853	221	-24993	25	802	163	1058	276	0.00	PR
290	600	200	74.25	-7.62	260	27152	271	-24994	25	805	164	1354	317	0.00	PR
291	450	150	67.5	3.175	260	5208	89	-4362	4.4	565	63	282	109	0.00	PR
292	450	150	67.5	3.175	260	5026	102	-4361	4.4	563	63	101	120	0.00	PR
293	600	200	45	-7.62	260	25576	319	-24991	25	484	99	101	335	0.00	PR
294	600	200	74.25	-7.62	260	26457	353	-24993	25	801	163	663	390	0.00	PR
295	600	200	74.25	-7.62	260	26550	275	-24993	25	805	164	752	321	0.00	PR
296	600	200	74.25	7.62	260	26723	259	-25008	25	804	164	912	308	0.00	PR
297	600	200	74.25	7.62	260	26247	293	-25008	25	804	164	435	336	0.00	PR
298	600	200	45	7.62	260	25669	317	-25009	25	485	99	175	333	0.00	PR
299	600	200	45	7.62	260	25726	325	-25008	25	481	98	237	341	0.00	PR
300	600	200	52.5	7.62	260	26078	306	-25007	25	564	115	506	328	0.00	PR
301	600	200	52.5	7.62	260	25765	272	-25009	25	564	115	192	296	0.00	PR
302	600	200	30	-7.62	260	25280	438	-24994	25	315	64	-28	443	0.00	PR
303	600	200	30	-7.62	260	25747	386	-24996	25	314	64	437	392	0.00	PR
304	600	200	60	-7.62	260	26365	284	-24993	25	644	131	729	314	0.00	PR
305	600	200	60	-7.62	260	26151	339	-24992	25	646	131	513	364	0.00	PR
306	450	150	45	-3.175	260	4731	149	-4356	4.4	370	41	5	154	0.00	PR
307	450	150	45	-3.175	260	5047	140	-4356	4.4	369	41	321	146	0.00	PR
308	450	150	67.5	-3.175	260	5067	124	-4355	4.4	560	62	153	139	0.00	PR
309	450	150	67.5	-3.175	260	4932	101	-4356	4.4	561	62	15	119	0.00	PR
310	450	150	60	-3.175	260	5042	96	-4355	4.4	498	55	190	111	0.00	PR
311	450	150	60	-3.175	260	4934	120	-4356	4.4	498	55	80	132	0.00	PR
312	600	200	37.5	7.62	260	26093	366	-25009	25	398	81	686	376	0.00	PR
313	600	200	37.5	7.62	260	25677	341	-25009	25	398	81	269	351	0.00	PR
314	450	150	15	-3.175	260	4291	159	-4355	4.4	114	13	-178	160	0.12	NR
315	450	150	15	-3.175	260	4418	135	-4356	4.4	114	13	-52	136	0.16	NR
316	600	200	22.5	7.62	260	25066	227	-25008	25	231	47	-173	233	0.00	PR
317	600	200	22.5	7.62	260	25648	251	-25010	25	231	47	407	256	0.00	PR
318	450	150	37.5	-3.175	260	4414	134	-4355	4.4	301	33	-243	138	0.00	PR
319	450	150	37.5	-3.175	260	4673	160	-4356	4.4	300	33	17	164	0.00	PR
320	450	150	60	3.175	260	4912	88	-4361	4.4	490	54	61	103	0.00	PR
321	450	150	60	3.175	260	5013	104	-4362	4.4	491	55	160	118	0.00	PR
322	600	200	67.5	7.62	260	26301	245	-25009	25	720	146	572	287	0.00	PR
323	600	200	67.5	7.62	260	26425	223	-25008	25	723	147	694	268	0.00	PR
324	450	150	15	3.175	260	4533	116	-4362	4.4	114	13	56	117	0.22	NR
325	450	150	15	3.175	260	4590	110	-4362	4.4	114	13	114	111	0.25	NR
326	600	200	67.5	-7.62	260	25613	343	-24991	25	720	146	-97	374	0.00	PR
327	600	200	67.5	-7.62	260	26440	262	-24991	25	723	147	726	302	0.00	PR
328	450	150	30	-3.175	260	4719	160	-4356	4.4	241	27	123	162	0.00	NR
329	450	150	30	-3.175	260	4869	117	-4355	4.4	240	27	275	120	0.00	NR
330	450	150	7.5	-3.175	260	4791	171	-4355	4.4	53	6	383	171	0.22	NR
331	450	150	7.5	-3.175	260	4653	211	-4355	4.4	53	6	245	211	0.14	NR
332	450	150	45	3.175	260	4984	114	-4362	4.4	362	40	260	121	0.00	PR
333	450	150	45	3.175	260	4656	117	-4361	4.4	364	40	-69	124	0.00	PR
334	600	200	45	-7.62	260	25411	412	-24994	25	475	97	-57	423	0.00	PR
335	600	200	45	-7.62	260	25311	294	-24993	25	475	97	-157	311	0.00	PR
336	600	200	7.5	7.62	260	24223	542	-25009	25	69	14	-856	543	0.00	NR
337	600	200	7.5	7.62	260	24917	480	-25011	25	69	14	-162	480	0.00	NR
338	600	200	15	-7.62	260	24719	462	-24994	25	148	30	-422	464	0.00	NR
339	600	200	15	-7.62	260	25291	497	-24993	25	148	30	149	499	0.00	NR
340	600	200	30	7.62	260	25157	440	-25011	25	311	63	-165	445	0.00	PR
341	600	200	30	7.62	260	25769	279	-25011	25	312	63	447	287	0.00	PR
342	600	200	37.5	-7.62	260	25403	364	-24996	25	392	80	15	373	0.00	PR
343	600	200	37.5	-7.62	260	25305	393	-24996	25	393	80	-85	402	0.00	PR
344	450	150	52.5	3.175	260	4985	96	-4363	4.4	426	47	195	108	0.00	PR
345	450	150	52.5	3.175	260	4900	111	-4362	4.4	427	47	112	121	0.00	PR
346	450	150	74.25	-3.175	260	5294	95	-4355	4.4	612	68	327	117	0.00	PR
347	450	150	74.25	-3.175	260	5499	84	-4355	4.4	615	68	530	109	0.00	PR
348	450	150	22.5	3.175	260	4441	113	-4362	4.4	177	20	-98	114	0.00	NR
349	450	150	22.5	3.175	260	4550	88	-4362	4.4	176	20	13	91	0.00	NR
350	600	200	7.5	-7.62	260	25761	520	-24994	25	69	14	697	521	0.00	NR
351	600	200	7.5	-7.62	260	25228	512	-24994	25	69	14	165	512	0.00	NR
352	450	150	52.5	-3.175	260	4771	113	-4355	4.4	425	47	-9	123	0.00	PR
353	450	150	52.5	-3.175	260	4917	101	-4355	4.4	428	48	134	112	0.00	PR
354	600	200	22.5	-7.62	260	25107	436	-24992	25	232	47	-117	439	0.00	PR
355	600	200	22.5	-7.62	260	25391	254	-24993	25	230	47	169	259	0.00	PR
356	450	150	67.5	3.175	260	5092	91	-4363	4.4	551	61	179	110	0.00	PR
357	450	150	67.5	3.175	260	5168	114	-4362	4.4	554	62	252	130	0.00	PR
358	450	150	37.5	3.175	260	4615	122	-4362	4.4	302	34	-50	127	0.00	PR
359	450	150	37.5	3.175	260	4739	122	-4362	4.4	302	34	75	127	0.00	PR
360	450	150	74.25	3.175	260	5453	108	-4362	4.4	613	68	478	128	0.00	PR
361	450	150	74.25	3.175	260	5183	107	-4363	4.4	617	69	204	127	0.00	PR
362	600	200	60	7.62	260	25678	412	-25011	25	644	131	23	433	0.00	PR
363	600	200	60	7.62	260	26199	307	-25012	25	642	131	545	334	0.00	PR
364	600	200	52.5	-7.62	260	26042	377	-24994	25	561	114	487	394	0.00	PR
365	600	200	52.5	-7.62	260	26171	339	-24992	25	559	114	619	358	0.00	PR
366	450	150	22.5	-3.175	260	4547	100	-4355	4.4	176	20	16	102	0.00	NR
367	450	150	22.5	-3.175	260	4357	117	-4355	4.4	176	20	-174	118	0.00	NR
368	600	200	15	7.62	260	25457	280	-25010	25	149	30	298	283	0.00	NR
369	600	200	15	7.62	260	25333	296	-25010	25	149	30	175	298	0.00	NR

Continued on next page

Table A.2 Continued from previous page

N_{run}	T [ns]	D [ns]	P [W]	B [Gauss]	θ_{pol} [deg.]	ν_{fit} [Hz]	$\Delta\nu_{\text{fit}}$ [Hz]	DC_{B} [Hz]	$\Delta\text{DC}_{\text{B}}$ [Hz]	SC [Hz]	ΔSC [Hz]	ν_0 [Hz]	$\Delta\nu_0$ [Hz]	wts. [%]	Data Type
370	450	150	30	3.175	260	4573	170	-4362	4.4	239	27	-29	172	0.00	NR
371	450	150	30	3.175	260	4478	122	-4362	4.4	240	27	-124	125	0.00	NR
372	800	100	74.25	-4.762	260	9984	383	-9759	9.8	212	5	13	383	0.02	NR
373	800	100	74.25	-4.762	260	9862	264	-9759	9.8	212	5	-109	265	0.04	NR
374	800	100	74.25	-4.762	260	10345	296	-9760	9.8	212	5	373	296	0.03	NR
375	800	100	74.25	-4.762	260	9697	408	-9759	9.8	213	5	-275	408	0.02	NR
376	800	100	74.25	-4.762	260	9439	338	-9759	9.8	213	5	-533	338	0.02	NR
377	800	100	74.25	-4.762	260	9903	379	-9760	9.8	213	5	-70	379	0.02	NR
378	800	100	74.25	-4.762	260	9606	381	-9759	9.8	213	5	-366	382	0.02	NR
379	800	100	74.25	4.762	260	10265	266	-9771	9.8	213	5	281	266	0.04	NR
380	800	100	74.25	4.762	260	9603	280	-9770	9.8	213	5	-380	280	0.03	NR
381	800	100	74.25	4.762	260	9643	265	-9771	9.8	213	5	-341	265	0.04	NR
382	800	100	74.25	4.762	260	9796	267	-9770	9.8	213	5	-188	267	0.04	NR
383	800	100	74.25	4.762	260	10073	271	-9770	9.8	213	5	90	271	0.04	NR
384	800	100	74.25	4.762	260	10057	226	-9769	9.8	213	5	75	226	0.05	NR
385	300	50	15	9.524	170	38880	242	-38984	39	30	6	-133	245	0.00	NR
386	300	50	52.5	-9.524	170	39080	96	-38965	39	119	23	-5	106	0.00	NR
387	300	50	60	9.524	170	39092	125	-38987	39	138	27	-32	134	0.00	NR
388	300	50	67.5	-9.524	170	39026	100	-38968	39	157	31	-99	111	0.00	NR
389	300	50	67.5	9.524	170	39138	112	-38986	39	157	31	-5	122	0.00	NR
390	300	50	37.5	-9.524	170	39076	151	-38967	39	82	16	26	156	0.00	NR
391	300	50	45	-9.524	170	39057	101	-38968	39	100	20	-12	110	0.00	NR
392	300	50	30	9.524	170	39099	186	-38986	39	65	13	49	190	0.00	NR
393	300	50	15	-9.524	170	38872	198	-38969	39	30	6	-127	202	0.00	NR
394	300	50	74.25	-9.524	170	39212	95	-38967	39	175	34	71	108	0.00	NR
395	300	50	74.25	9.524	170	39325	122	-38986	39	175	34	163	133	0.00	NR
396	300	50	22.5	-9.524	170	38982	140	-38969	39	47	9	-34	145	0.00	NR
397	300	50	37.5	9.524	170	39185	148	-38988	39	83	16	114	154	0.00	NR
398	300	50	52.5	9.524	170	39443	133	-38986	39	119	23	337	140	0.00	NR
399	300	50	60	-9.524	170	39038	94	-38972	39	138	27	-71	105	0.00	NR
400	300	50	7.5	-9.524	170	38730	328	-38967	39	14	3	-251	330	0.00	NR
401	300	50	22.5	9.524	170	39005	202	-38989	39	47	9	-30	206	0.00	NR
402	300	50	45	9.524	170	38999	158	-38985	39	101	20	-87	164	0.00	NR
403	300	50	30	-9.524	170	38984	149	-38968	39	65	13	-50	154	0.00	NR
404	300	50	7.5	9.524	170	39338	387	-38985	39	14	3	340	389	0.00	NR
405	450	150	26.25	-3.175	170	4582	109	-4356	4.4	209	23	17	112	0.00	NR
406	450	150	30	-3.175	170	4472	91	-4355	4.4	242	27	-125	95	0.00	NR
407	450	150	3.75	3.175	170	4413	287	-4360	4.4	25	3	28	287	0.10	NR
408	450	150	18.75	3.175	170	4322	124	-4359	4.4	146	16	-183	126	0.08	NR
409	450	150	30	3.175	170	4498	103	-4360	4.4	240	27	-102	107	0.00	NR
410	450	150	11.25	-3.175	170	4397	118	-4357	4.4	84	9	-43	118	0.34	NR
411	450	150	18.75	-3.175	170	4551	127	-4356	4.4	146	16	48	128	0.07	NR
412	450	150	3.75	-3.175	170	4067	276	-4355	4.4	25	3	-312	276	0.10	NR
413	450	150	11.25	3.175	170	4304	194	-4360	4.4	84	9	-139	194	0.13	NR
414	450	150	15	-3.175	170	4480	119	-4355	4.4	116	13	9	120	0.20	NR
415	450	150	7.5	-3.175	170	4071	173	-4355	4.4	54	6	-338	173	0.21	NR
416	450	150	22.5	3.175	170	4656	133	-4360	4.4	177	20	119	134	0.00	NR
417	450	150	22.5	-3.175	170	4577	85	-4356	4.4	177	20	45	87	0.00	NR
418	450	150	26.25	3.175	170	4451	128	-4359	4.4	208	23	-116	130	0.00	NR
419	450	150	15	3.175	170	4183	142	-4359	4.4	114	13	-291	142	0.15	NR
420	500	125	45	3.175	170	4587	94	-4361	4.4	221	38	5	102	0.00	NR
421	375	125	22.5	3.175	170	4591	127	-4361	4.4	142	25	88	130	0.00	NR
422	500	125	30	-3.175	170	4638	157	-4355	4.4	145	25	139	159	0.00	NR
423	500	125	15	-3.175	170	4660	169	-4356	4.4	68	12	237	169	0.12	NR
424	500	125	30	3.175	170	4767	112	-4361	4.4	144	25	262	115	0.00	NR
425	375	125	37.5	-3.175	170	4593	74	-4356	4.4	238	41	-2	85	0.00	NR
426	500	125	45	-3.175	170	4581	104	-4355	4.4	220	38	6	111	0.00	NR
427	375	125	22.5	-3.175	170	4623	131	-4354	4.4	140	24	128	133	0.00	NR
428	375	125	45	-3.175	170	4665	89	-4356	4.4	289	50	20	103	0.00	NR
429	375	125	15	-3.175	170	4324	132	-4355	4.4	91	16	-123	133	0.08	NR
430	375	125	15	3.175	170	4522	157	-4361	4.4	91	16	70	158	0.06	NR
431	500	125	15	3.175	170	4672	201	-4361	4.4	67	12	244	201	0.09	NR
432	500	125	7.5	-3.175	170	4556	244	-4355	4.4	31	5	170	244	0.11	NR
433	500	125	7.5	3.175	170	4002	305	-4361	4.4	31	5	-390	305	0.07	NR
434	500	125	37.5	3.175	170	4690	113	-4361	4.4	182	31	147	117	0.00	NR
435	375	125	30	3.175	170	4612	119	-4361	4.4	191	33	60	124	0.00	NR
436	375	125	7.5	-3.175	170	4446	187	-4355	4.4	42	7	48	187	0.16	NR
437	500	125	22.5	-3.175	170	4493	136	-4355	4.4	105	18	33	138	0.01	NR
438	500	125	22.5	3.175	170	4433	145	-4361	4.4	104	18	-33	146	0.01	NR
439	375	125	37.5	3.175	170	4530	108	-4362	4.4	237	41	-68	116	0.00	NR
440	500	125	37.5	-3.175	170	4485	111	-4355	4.4	181	31	-51	116	0.00	NR
441	375	125	7.5	3.175	170	4409	234	-4362	4.4	42	7	5	234	0.10	NR
442	375	125	30	-3.175	170	4463	99	-4355	4.4	187	32	-80	104	0.00	NR
443	375	125	45	3.175	170	4686	114	-4362	4.4	286	50	38	125	0.00	NR
444	600	200	3.75	7.143	170	22046	716	-21981	22	31	6	33	716	0.00	NR
445	600	200	18.75	-7.143	170	22278	209	-21967	22	186	38	125	214	0.00	NR
446	600	150	7.5	6.35	170	17731	401	-17384	17.4	38	4	308	402	0.00	NR
447	600	150	30	-6.35	170	17328	169	-17373	17.4	178	20	-223	171	0.00	NR
448	600	200	11.25	-7.143	170	22249	358	-21968	22	107	22	175	359	0.00	NR
449	600	150	26.25	6.35	170	17698	171	-17384	17.4	153	17	161	173	0.00	NR
450	600	150	11.25	-6.35	170	17563	293	-17372	17.4	60	7	131	294	0.00	NR
451	600	150	11.25	6.35	170	17024	279	-17383	17.4	60	7	-419	279	0.00	NR
452	600	200	3.75	-7.143	170	21938	673	-21967	22	31	6	-60	674	0.00	NR
453	600	150	26.25	-6.35	170	17087	190	-17371	17.4	153	17	-438	191	0.00	NR
454	600	150	33.75	-6.35	170	17533	178	-17372	17.4	201	22	-40	180	0.00	PR
455	600	150	33.75	6.35	170	17349	114	-17384	17.4	202	22	-236	117	0.00	PR
456	600	150	7.5	-6.35	170	17330	304	-17372	17.4	38	4	-80	304	0.00	NR
457	600	150	22.5	-6.35	170	17217	193	-17371	17.4	130	14	-284	194	0.00	NR
458	600	200	18.75	7.143	170	22248	240	-21981	22	186	38	81	244	0.00	NR
459	600	150	18.75	-6.35	170	17178	227	-17372	17.4	107	12	-300	228	0.00	NR
460	600	150	3.75	6.35	170	17881	544	-17384	17.4	17	2	480	544	0.00	NR
461	600	150	15	6.35	170	17831	222	-17385	17.4	82	9	364	222	0.00	NR
462	600	150	3.75	-6.35	170	17878	439	-17370	17.4	17	2	491	439	0.00	NR
463	600	150	30	6.35	170	17537	204	-17385	17.4	176	20	-24	206	0.00	NR
464	600	200	11.25	7.143	170	22118	276	-21981	22	106	22	31	277	0.00	NR
465	600	150	18.75	6.35	170	17379	246	-17385	17.4	106	12	-112	247	0.00	NR
466	600	150	15	-6.35	170	17477	206	-17371	17.4	83	9	22	207	0.00	NR
467	600	150	22.5	6.35	170	16849	214	-17385	17.4	129	14	-665	215	0.00	NR

Continued on next page

Table A.2 Continued from previous page

N_{run}	T [ns]	D [ns]	P [W]	B [Gauss]	θ_{pol} [deg.]	ν_{fit} [Hz]	$\Delta\nu_{\mathrm{fit}}$ [Hz]	$\mathrm{DC_B}$ [Hz]	$\Delta\mathrm{DC_B}$ [Hz]	SC [Hz]	ΔSC [Hz]	ν_0 [Hz]	$\Delta\nu_0$ [Hz]	wts. [%]	Data Type
468	300	100	60	-4.762	170	10168	77	-9759	9.8	410	10	-1	79	0.02	NR
469	300	100	52.5	4.762	170	10258	91	-9771	9.8	357	9	129	92	0.10	NR
470	300	100	7.5	4.762	170	9944	170	-9771	9.8	44	1	129	171	0.16	NR
471	300	100	67.5	-4.762	170	10236	63	-9758	9.8	463	11	15	65	0.00	NR
472	300	100	15	-4.762	170	10078	79	-9759	9.8	96	2	223	79	0.64	NR
473	300	100	52.5	-4.762	170	10028	70	-9758	9.8	358	9	-88	71	0.16	NR
474	300	100	30	4.762	170	10113	90	-9770	9.8	202	5	140	90	0.33	NR
475	300	100	67.5	4.762	170	10356	71	-9770	9.8	467	11	119	72	0.00	NR
476	300	100	22.5	-4.762	170	9943	76	-9758	9.8	149	4	37	77	0.57	NR
477	300	100	45	4.762	170	10110	82	-9770	9.8	306	7	34	83	0.21	NR
478	300	100	7.5	-4.762	170	9882	148	-9758	9.8	45	1	79	149	0.21	NR
479	300	100	30	-4.762	170	10090	83	-9758	9.8	199	5	132	83	0.40	NR
480	300	100	22.5	4.762	170	9897	91	-9769	9.8	147	4	-19	92	0.40	NR
481	300	100	60	4.762	170	10270	89	-9769	9.8	409	10	93	91	0.02	NR
482	300	100	37.5	4.762	170	10025	90	-9769	9.8	253	6	3	91	0.25	NR
483	300	100	37.5	-4.762	170	10025	90	-9760	9.8	252	6	12	91	0.25	NR
484	300	100	74.25	4.762	170	10279	54	-9769	9.8	514	12	-4	56	0.00	NR
485	300	100	15	4.762	170	9808	123	-9768	9.8	95	2	-55	124	0.26	NR
486	300	100	74.25	-4.762	170	10242	66	-9760	9.8	514	12	-33	68	0.00	NR
487	300	100	45	-4.762	170	10093	82	-9759	9.8	306	7	28	83	0.21	NR
488	400	200	18.75	-4.762	260	9849	184	-9758	9.8	279	57	-188	192	0.00	NR
489	400	200	15	-4.762	260	10181	173	-9758	9.8	220	45	204	179	0.00	NR
490	400	200	18.75	4.762	260	9909	133	-9771	9.8	278	57	-140	145	0.00	NR
491	400	200	22.5	-4.762	260	9983	167	-9758	9.8	337	69	-112	180	0.00	PR
492	400	200	22.5	4.762	260	10131	159	-9770	9.8	337	69	24	173	0.00	PR
493	400	200	15	4.762	260	9946	181	-9770	9.8	221	45	-45	187	0.00	NR
494	400	200	7.5	-4.762	260	9758	309	-9757	9.8	105	21	-104	309	0.00	NR
495	400	200	7.5	-4.762	260	10003	241	-9760	9.8	104	21	139	242	0.00	NR
496	400	200	7.5	-4.762	260	9902	264	-9758	9.8	105	21	40	265	0.00	NR
497	400	200	3.75	4.762	260	9825	359	-9769	9.8	49	10	6	359	0.00	NR
498	400	200	3.75	4.762	260	9541	272	-9767	9.8	49	10	-275	272	0.00	NR
499	400	200	3.75	4.762	260	9751	423	-9767	9.8	48	10	-64	423	0.00	NR
500	400	200	3.75	-4.762	260	9511	381	-9760	9.8	49	10	-298	382	0.00	NR
501	400	200	3.75	-4.762	260	10283	381	-9761	9.8	49	10	473	382	0.00	NR
502	400	200	3.75	-4.762	260	10156	312	-9759	9.8	49	10	347	313	0.00	NR
503	400	200	7.5	4.762	260	9672	179	-9768	9.8	103	21	-199	180	0.00	NR
504	400	200	7.5	4.762	260	9878	255	-9768	9.8	104	21	6	256	0.00	NR
505	400	200	7.5	4.762	260	10089	304	-9767	9.8	105	21	217	305	0.00	NR
506	400	200	11.25	4.762	260	9665	171	-9767	9.8	162	33	-264	174	0.00	NR
507	400	200	11.25	-4.762	260	10096	254	-9760	9.8	162	33	174	257	0.00	NR
508	400	50	22.5	-9.524	170	38970	595	-38970	39	35	7	-35	597	0.00	NR
509	400	50	22.5	-9.524	170	38136	410	-38967	39	35	7	-866	412	0.00	NR
510	400	50	22.5	-9.524	170	39522	363	-38971	39	35	7	516	365	0.00	NR
511	400	50	45	9.524	170	39386	373	-38986	39	76	15	324	375	0.00	NR
512	400	50	15	-9.524	170	39108	372	-38969	39	23	4	117	374	0.00	NR
513	400	50	15	-9.524	170	38769	508	-38968	39	22	4	-221	509	0.00	NR
514	400	50	15	-9.524	170	38906	421	-38969	39	22	4	-85	423	0.00	NR
515	400	50	37.5	9.524	170	39168	378	-38987	39	61	12	120	380	0.00	NR
516	400	50	60	9.524	170	38865	255	-38988	39	102	20	-226	259	0.00	NR
517	400	50	22.5	9.524	170	39365	496	-38989	39	35	7	341	498	0.00	NR
518	400	50	60	-9.524	170	38863	177	-38966	39	103	20	-206	183	0.00	NR
519	400	50	30	-9.524	170	39202	402	-38970	39	49	10	184	404	0.00	NR
520	400	50	15	9.524	170	38878	482	-38989	39	22	4	-133	484	0.00	NR
521	400	50	52.5	9.524	170	39805	257	-38988	39	88	17	729	261	0.00	NR
522	400	50	52.5	-9.524	170	38668	257	-38968	39	89	17	-389	261	0.00	NR
523	400	50	45	-9.524	170	38844	327	-38967	39	75	15	-197	330	0.00	NR
524	400	50	37.5	-9.524	170	38114	288	-38967	39	62	12	-914	291	0.00	NR
525	400	50	30	9.524	170	38647	388	-38990	39	48	10	-391	390	0.00	NR
526	400	50	74.25	9.524	170	39084	279	-38986	39	131	26	-33	283	0.00	NR
527	400	50	74.25	-9.524	170	39127	251	-38966	39	132	26	29	255	0.00	NR
528	400	50	7.5	-9.524	170	39026	758	-38968	39	10	2	49	759	0.00	NR
529	400	50	7.5	-9.524	170	37378	779	-38968	39	10	2	-1600	780	0.00	NR
530	400	50	7.5	-9.524	170	38174	953	-38966	39	10	2	-802	953	0.00	NR
531	400	50	7.5	9.524	170	39012	1052	-38986	39	10	2	16	1053	0.00	NR
532	400	50	67.5	9.524	170	39395	240	-38987	39	116	23	292	244	0.00	NR
533	400	50	67.5	-9.524	170	38901	235	-38965	39	118	23	-182	239	0.00	NR
534	500	50	37.5	-9.524	170	38931	494	-38965	39	49	10	-83	496	0.00	NR
535	500	50	37.5	-9.524	170	39256	621	-38965	39	49	10	242	622	0.00	NR
536	500	50	15	-9.524	170	38487	612	-38965	39	17	3	-495	613	0.00	NR
537	500	50	15	-9.524	170	39124	610	-38968	39	17	3	139	611	0.00	NR
538	500	50	15	-9.524	170	37309	648	-38966	39	17	3	-1674	649	0.00	NR
539	500	50	37.5	9.524	170	38844	698	-38987	39	48	9	-191	699	0.00	NR
540	500	50	37.5	9.524	170	39782	654	-38988	39	48	9	746	655	0.00	NR
541	500	50	7.5	9.524	170	41516	3953	-38985	39	7	1	2523	3953	0.00	NR
542	500	50	7.5	9.524	170	43204	3272	-38988	39	7	1	4208	3272	0.00	NR
543	500	50	7.5	9.524	170	36901	4066	-38987	39	7	1	-2094	4066	0.00	NR
544	500	100	37.5	4.762	170	10050	312	-9770	9.8	151	4	129	312	0.04	NR
545	500	100	37.5	4.762	170	9390	315	-9769	9.8	153	4	-533	315	0.03	NR
546	500	100	15	-4.762	170	8609	627	-9758	9.8	57	1	-1206	627	0.01	NR
547	500	100	15	-4.762	170	9684	590	-9759	9.8	57	1	-132	590	0.02	NR
548	500	100	15	-4.762	170	9982	482	-9760	9.8	57	1	165	482	0.02	NR
549	500	50	7.5	-9.524	170	35979	1110	-38967	39	7	1	-2995	1111	0.00	NR
550	500	50	7.5	-9.524	170	40591	1558	-38966	39	7	1	1618	1559	0.00	NR
551	500	50	7.5	-9.524	170	38835	2051	-38966	39	7	1	-138	2052	0.00	NR
552	500	100	52.5	-4.762	170	10080	291	-9758	9.8	217	5	106	291	0.03	NR
553	500	100	52.5	-4.762	170	9720	258	-9757	9.8	220	5	-257	258	0.04	NR
554	500	100	22.5	-4.762	170	9524	366	-9757	9.8	89	2	-323	366	0.03	NR
555	500	100	22.5	-4.762	170	9447	543	-9759	9.8	89	2	-401	543	0.01	NR
556	500	100	22.5	-4.762	170	9863	491	-9758	9.8	89	2	16	491	0.01	NR
557	500	50	22.5	-9.524	170	38602	614	-38967	39	27	5	-393	616	0.00	NR
558	500	50	22.5	-9.524	170	39789	633	-38966	39	27	5	795	634	0.00	NR
559	500	50	22.5	-9.524	170	39370	507	-38966	39	27	5	376	508	0.00	NR
560	500	50	67.5	9.524	170	38022	589	-38987	39	94	18	-1059	591	0.00	NR
561	500	50	67.5	9.524	170	39061	616	-38988	39	94	18	-22	618	0.00	NR
562	500	100	45	4.762	170	10009	417	-9769	9.8	187	4	53	417	0.02	NR
563	500	100	45	4.762	170	9564	316	-9770	9.8	187	4	-393	317	0.03	NR
564	500	50	30	9.524	170	39414	777	-38985	39	38	8	390	778	0.00	NR
565	500	50	30	9.524	170	39502	827	-38988	39	38	8	476	827	0.00	NR

Continued on next page

Table A.2 Continued from previous page

N_{run}	T [ns]	D [ns]	P [W]	B [Gauss]	θ_{pol} [deg.]	ν_{fit} [Hz]	$\Delta\nu_{\mathrm{fit}}$ [Hz]	$\mathrm{DC_B}$ [Hz]	$\Delta\mathrm{DC_B}$ [Hz]	SC [Hz]	ΔSC [Hz]	ν_0 [Hz]	$\Delta\nu_0$ [Hz]	wts. [%]	Data Type
566	500	50	60	-9.524	170	38400	478	-38967	39	82	16	-649	480	0.00	NR
567	500	50	60	-9.524	170	38665	405	-38964	39	82	16	-381	408	0.00	NR
568	500	100	67.5	-4.762	170	9748	300	-9758	9.8	289	7	-299	300	0.02	NR
569	500	100	67.5	-4.762	170	10138	221	-9760	9.8	290	7	88	222	0.03	NR
570	500	100	74.25	4.762	170	9896	275	-9769	9.8	323	8	-196	275	0.02	NR
571	500	100	74.25	4.762	170	9782	240	-9769	9.8	325	8	-312	240	0.02	NR
572	500	50	22.5	9.524	170	39119	600	-38988	39	28	6	103	601	0.00	NR
573	500	50	22.5	9.524	170	38564	567	-38988	39	28	5	-451	568	0.00	NR
574	500	50	22.5	9.524	170	38744	666	-38988	39	27	5	-272	667	0.00	NR
575	500	100	45	-4.762	170	9944	362	-9758	9.8	187	5	-1	362	0.02	NR
576	500	100	45	-4.762	170	10027	343	-9759	9.8	188	5	80	343	0.02	NR
577	500	100	7.5	-4.762	170	10204	650	-9759	9.8	26	1	419	650	0.01	NR
578	500	100	7.5	-4.762	170	10928	745	-9757	9.8	26	1	1144	745	0.01	NR
579	500	100	7.5	-4.762	170	9296	796	-9756	9.8	26	1	-486	797	0.01	NR
580	500	50	45	9.524	170	39059	569	-38987	39	60	12	13	570	0.00	NR
581	500	50	45	9.524	170	39511	558	-38989	39	60	12	462	560	0.00	NR
582	500	50	52.5	9.524	170	38811	448	-38988	39	71	14	-248	450	0.00	NR
583	500	50	52.5	9.524	170	39858	666	-38986	39	71	14	801	667	0.00	NR
584	500	100	67.5	4.762	170	10028	272	-9771	9.8	291	7	-34	272	0.02	NR
585	500	100	67.5	4.762	170	9911	293	-9769	9.8	292	7	-151	293	0.02	NR
586	500	100	30	-4.762	170	10507	363	-9760	9.8	124	3	623	363	0.03	NR
587	500	100	30	-4.762	170	9494	405	-9757	9.8	123	3	-386	405	0.02	NR
588	500	100	22.5	4.762	170	10084	459	-9770	9.8	90	2	225	459	0.02	NR
589	500	100	22.5	4.762	170	9614	455	-9769	9.8	90	2	-245	455	0.02	NR
590	500	100	22.5	4.762	170	9345	601	-9768	9.8	90	2	-513	601	0.01	NR
591	500	100	37.5	-4.762	170	10083	317	-9756	9.8	155	4	172	318	0.03	NR
592	500	100	37.5	-4.762	170	9973	346	-9759	9.8	156	4	58	346	0.03	NR
593	500	50	52.5	-9.524	170	38586	433	-38966	39	72	14	-451	435	0.00	NR
594	500	50	52.5	-9.524	170	39085	478	-38965	39	72	14	49	480	0.00	NR
595	500	50	30	-9.524	170	39223	606	-38966	39	39	8	219	607	0.00	NR
596	500	50	30	-9.524	170	38598	647	-38966	39	39	8	-407	648	0.00	NR
597	500	50	45	-9.524	170	38390	492	-38964	39	60	12	-635	493	0.00	NR
598	500	50	45	-9.524	170	38841	581	-38965	39	60	12	-184	582	0.00	NR
599	500	50	74.25	-9.524	170	38348	406	-38966	39	107	21	-725	408	0.00	NR
600	500	50	74.25	-9.524	170	38152	345	-38968	39	107	21	-923	348	0.00	NR
601	500	100	74.25	-4.762	170	9682	279	-9758	9.8	325	8	-400	280	0.01	NR
602	500	100	74.25	-4.762	170	9927	247	-9759	9.8	326	8	-158	247	0.02	NR
603	500	50	60	9.524	170	38457	480	-38988	39	84	17	-615	482	0.00	NR
604	500	50	60	9.524	170	39107	391	-38987	39	84	17	36	393	0.00	NR
605	500	50	74.25	9.524	170	39102	366	-38987	39	108	21	7	368	0.00	NR
606	500	50	74.25	9.524	170	38624	512	-38986	39	108	21	-470	514	0.00	NR
607	500	100	52.5	4.762	170	9864	348	-9769	11.4	225	6	-130	348	0.01	NR
608	500	100	52.5	4.762	170	10254	382	-9767	9.8	224	5	263	382	0.02	NR
609	500	100	15	4.762	170	9851	635	-9766	9.8	58	1	27	635	0.01	NR
610	300	150	60	-3.175	260	5265	67	-4354	4.4	716	80	194	104	0.00	PR
611	300	150	15	-3.175	260	4364	125	-4354	4.4	172	19	-162	126	0.00	NR
612	300	150	22.5	3.175	260	4584	98	-4360	4.4	261	29	-38	102	0.00	NR
613	300	150	7.5	3.175	260	4378	145	-4360	4.4	81	9	-62	146	0.23	NR
614	300	150	52.5	3.175	260	5207	77	-4360	4.4	621	69	226	104	0.00	PR
615	300	150	3.75	3.175	260	4488	216	-4359	4.4	39	4	90	216	0.15	NR
616	300	150	30	3.175	260	4845	72	-4359	4.4	350	39	137	82	0.00	NR
617	300	150	67.5	-3.175	260	5539	68	-4354	4.4	804	89	381	113	0.00	PR
618	300	150	15	3.175	260	4663	94	-4359	4.4	173	19	132	96	0.00	NR
619	300	150	37.5	3.175	260	4869	66	-4359	4.4	443	49	67	82	0.00	PR
620	300	150	45	3.175	260	5032	76	-4359	4.4	535	59	139	96	0.00	PR
621	300	150	7.5	-3.175	260	4120	172	-4355	4.4	82	9	-317	172	0.16	NR
622	300	150	45	-3.175	260	5054	70	-4354	4.4	534	59	166	92	0.00	PR
623	300	150	52.5	-3.175	260	5167	58	-4354	4.4	627	70	186	91	0.00	PR
624	300	150	11.25	-3.175	260	4431	127	-4355	4.4	127	14	-51	128	0.14	NR
625	300	150	74.25	-3.175	260	5847	68	-4355	4.4	896	100	596	121	0.00	PR
626	300	150	22.5	-3.175	260	4432	70	-4354	4.4	267	30	-189	76	0.00	NR
627	300	150	26.25	-3.175	260	4688	100	-4354	4.4	310	34	24	106	0.00	NR
628	300	150	37.5	-3.175	260	4766	73	-4355	4.4	443	49	-32	88	0.00	PR
629	300	150	30	-3.175	260	4727	86	-4355	4.4	353	39	19	95	0.00	NR
630	300	150	60	3.175	260	5434	53	-4358	4.4	718	80	357	96	0.00	PR
631	300	150	18.75	3.175	260	4573	98	-4359	4.4	219	24	-6	101	0.00	NR
632	300	150	3.75	-3.175	260	4433	195	-4354	4.4	39	4	40	195	0.19	NR
633	300	150	18.75	-3.175	260	4420	93	-4355	4.4	217	24	-152	96	0.00	NR
634	300	150	74.25	3.175	260	5881	69	-4359	4.4	896	100	626	121	0.00	PR
635	300	150	26.25	3.175	260	4827	93	-4359	4.4	312	35	156	99	0.00	NR
636	300	150	11.25	3.175	260	4691	111	-4358	4.4	128	14	205	112	0.18	NR
637	300	150	67.5	3.175	260	5738	71	-4357	4.4	814	90	566	115	0.00	PR
638	300	50	52.5	-9.524	260	39095	107	-38972	39	122	24	1	116	0.00	NR
639	300	50	74.25	9.524	260	39228	87	-38979	39	177	35	71	101	0.00	NR
640	300	50	30	9.524	260	38937	102	-38979	39	66	13	-108	110	0.00	NR
641	300	50	22.5	-9.524	260	38940	150	-38977	39	48	9	-85	155	0.00	NR
642	300	50	37.5	9.524	260	39163	113	-38980	39	83	16	99	120	0.00	NR
643	300	50	7.5	-9.524	260	38688	294	-38976	39	14	3	-303	297	0.00	NR
644	300	50	45	9.524	260	39152	115	-38980	39	101	20	71	123	0.00	NR
645	300	50	60	-9.524	260	39116	121	-38978	39	139	27	-1	130	0.00	NR
646	300	50	30	-9.524	260	39191	169	-38977	39	66	13	148	174	0.00	NR
647	300	50	22.5	9.524	260	38891	163	-38980	39	48	9	-136	168	0.00	NR
648	300	50	74.25	-9.524	260	39202	88	-38972	39	176	35	54	102	0.00	NR
649	300	50	67.5	9.524	260	39049	69	-38979	39	159	31	-88	85	0.00	NR
650	300	50	15	9.524	260	39112	168	-38978	39	31	6	103	173	0.00	NR
651	300	50	74.25	9.524	260	39114	73	-38980	39	176	35	-42	89	0.00	NR
652	300	50	60	9.524	260	39137	86	-38982	39	139	27	16	99	0.00	NR
653	300	50	7.5	9.524	260	39102	228	-38982	39	14	3	106	231	0.00	NR
654	300	50	15	-9.524	260	39351	237	-38977	39	30	6	343	241	0.00	NR
655	300	50	52.5	-9.524	260	39257	123	-38975	39	120	24	163	131	0.00	NR
656	300	50	37.5	-9.524	260	39161	127	-38978	39	84	16	99	134	0.00	NR
657	300	50	52.5	9.524	260	39045	112	-38979	39	120	24	-54	121	0.00	NR
658	300	50	67.5	-9.524	260	39047	114	-38975	39	159	31	-87	124	0.00	NR
659	300	50	45	-9.524	260	39102	143	-38975	39	103	20	24	149	0.00	NR
660	600	50	52.5	-9.524	260	38953	172	-38975	39	61	12	-83	176	0.00	NR
661	500	100	52.5	-4.762	260	10017	160	-9762	9.8	225	5	29	160	0.09	NR
662	500	100	52.5	-4.762	260	9784	128	-9762	9.8	226	5	-204	128	0.15	NR
663	500	100	22.5	-4.762	260	9726	148	-9762	9.8	91	2	-127	149	0.18	NR

Continued on next page

Table A.2 Continued from previous page

N_{run}	T [ns]	D [ns]	P [W]	B [Gauss]	θ_{pol} [deg.]	ν_{fit} [Hz]	$\Delta\nu_{\mathrm{fit}}$ [Hz]	$\mathrm{DC_B}$ [Hz]	$\Delta\mathrm{DC_B}$ [Hz]	SC [Hz]	ΔSC [Hz]	ν_0 [Hz]	$\Delta\nu_0$ [Hz]	wts. [%]	Data Type
664	500	100	22.5	-4.762	260	9846	133	-9762	9.8	92	2	-7	133	0.23	NR
665	500	100	74.25	-4.762	260	9948	151	-9761	9.8	331	8	-143	152	0.05	NR
666	500	100	74.25	-4.762	260	9997	148	-9761	9.8	333	8	-98	149	0.05	NR
667	600	50	30	9.524	260	38703	242	-38976	39	33	6	-306	245	0.00	NR
668	600	50	74.25	-9.524	260	38725	239	-38977	39	92	18	-345	243	0.00	NR
669	500	100	7.5	-4.762	260	9449	294	-9763	9.8	27	1	-342	294	0.05	NR
670	500	100	7.5	-4.762	260	10203	300	-9763	9.8	27	1	413	300	0.05	NR
671	500	100	30	-4.762	260	9963	163	-9763	9.8	125	3	75	163	0.14	NR
672	500	100	30	-4.762	260	9618	199	-9762	9.8	126	3	-270	199	0.09	NR
673	500	100	60	-4.762	260	10058	193	-9762	9.8	261	6	35	194	0.05	NR
674	500	100	60	-4.762	260	10235	191	-9763	9.8	262	6	210	191	0.05	NR
675	600	50	30	-9.524	260	38537	296	-38976	39	33	6	-472	298	0.00	NR
676	500	100	37.5	-4.762	260	10104	267	-9764	9.8	157	4	183	267	0.05	NR
677	500	100	45	4.762	260	9680	253	-9762	9.8	199	5	-280	254	0.04	NR
678	500	100	45	4.762	260	9940	211	-9762	9.8	198	5	-20	211	0.06	NR
679	500	100	60	4.762	260	9964	178	-9762	9.8	270	6	-67	179	0.06	NR
680	500	100	60	4.762	260	9862	185	-9763	9.8	270	6	-171	185	0.06	NR
681	500	100	15	4.762	260	10311	190	-9762	9.8	60	1	489	191	0.12	NR
682	500	100	15	4.762	260	9460	166	-9762	9.8	60	1	-362	166	0.16	NR
683	500	100	52.5	-4.762	260	10107	195	-9764	9.8	229	5	114	195	0.06	NR
684	500	100	52.5	-4.762	260	10049	167	-9764	9.8	229	5	56	168	0.08	NR
685	500	100	74.25	4.762	260	10046	187	-9760	9.8	334	8	-48	187	0.03	NR
686	500	100	74.25	4.762	260	9707	133	-9759	9.8	335	8	-387	133	0.06	NR
687	500	100	52.5	4.762	260	9954	200	-9759	9.8	232	6	-37	200	0.06	NR
688	500	100	52.5	4.762	260	9964	181	-9761	9.8	231	6	-28	181	0.07	NR
689	500	100	30	4.762	260	10237	188	-9760	9.8	128	3	349	188	0.10	NR
690	500	100	30	4.762	260	10380	276	-9760	9.8	127	3	492	277	0.05	NR
691	500	100	22.5	4.762	260	9737	165	-9759	9.8	93	2	-115	165	0.15	NR
692	500	100	22.5	4.762	260	9650	167	-9760	9.8	93	2	-202	167	0.14	NR
693	500	100	45	-4.762	260	10366	204	-9763	9.8	193	5	411	204	0.07	NR
694	500	100	45	-4.762	260	9954	165	-9763	9.8	194	5	-2	165	0.10	NR
695	500	100	7.5	4.762	260	9367	435	-9761	9.8	27	1	-421	435	0.02	NR
696	500	100	7.5	4.762	260	9431	306	-9762	9.8	27	1	-358	306	0.05	NR
697	600	50	74.25	9.524	260	38802	182	-38972	39	93	18	-263	187	0.00	NR
698	500	100	15	-4.762	260	9550	250	-9764	9.8	60	1	-274	250	0.07	NR
699	500	100	15	-4.762	260	9921	314	-9764	9.8	60	1	98	314	0.05	NR
700	500	100	37.5	4.762	260	10130	165	-9762	9.8	160	4	207	166	0.12	NR
701	500	100	37.5	4.762	260	10044	210	-9761	9.8	161	4	122	210	0.07	NR
702	500	100	67.5	4.762	260	10172	125	-9762	9.8	301	7	109	125	0.10	NR
703	500	100	67.5	4.762	260	9995	196	-9762	9.8	302	7	-68	197	0.04	NR
704	600	50	52.5	9.524	260	39000	223	-38973	39	62	12	-35	227	0.00	NR
705	500	100	67.5	-4.762	260	10170	137	-9764	9.8	298	7	108	138	0.08	NR
706	500	100	67.5	-4.762	260	9935	146	-9763	9.8	299	7	-128	147	0.07	NR
707	400	100	7.5	-4.762	170	9945	125	-9762	9.8	35	1	148	126	0.30	NR
708	375	125	52.5	-3.81	170	6732	83	-6248	6.2	347	60	136	103	0.00	PR
709	400	100	45	-4.762	170	10125	93	-9762	9.8	242	6	122	94	0.25	NR
710	400	100	37.5	-4.762	170	9901	88	-9762	9.8	201	5	-62	89	0.35	NR
711	400	100	37.5	4.762	170	10186	146	-9763	9.8	201	5	222	146	0.13	NR
712	400	100	30	-4.762	170	10057	122	-9762	9.8	160	4	134	122	0.22	NR
713	400	100	45	4.762	170	10050	99	-9762	9.8	246	6	42	100	0.22	NR
714	400	100	15	4.762	170	9938	105	-9762	9.8	76	2	100	106	0.38	NR
715	500	50	7.5	-9.524	170	38377	245	-38978	39	8	2	-609	248	0.00	NR
716	600	50	30	-9.524	170	38991	243	-38977	39	33	6	-18	246	0.00	NR
717	500	50	15	-9.524	170	38455	174	-38978	39	18	4	-541	179	0.00	NR
718	600	50	74.25	9.524	170	39009	205	-38982	39	91	18	-63	210	0.00	NR
719	400	100	30	4.762	170	9985	97	-9763	9.8	158	4	64	97	0.34	NR
720	400	100	7.5	4.762	170	10056	132	-9764	9.8	34	1	258	132	0.27	NR
721	600	50	52.5	-9.524	170	38921	200	-38979	39	61	12	-118	204	0.00	NR
722	500	50	7.5	9.524	170	39050	312	-38982	39	8	2	60	315	0.00	NR
723	500	100	30	-4.762	170	9955	113	-9763	9.8	125	3	67	113	0.28	NR
724	500	125	52.5	3.81	170	6642	148	-6249	6.2	264	46	129	155	0.00	PR
725	400	100	22.5	-4.762	170	9869	82	-9762	9.8	115	3	-8	82	0.56	NR
726	400	100	74.25	-4.762	170	10102	80	-9761	9.8	402	10	-61	82	0.04	NR
727	375	125	52.5	3.81	170	6743	63	-6248	6.2	344	60	151	87	0.00	PR
728	400	100	15	-4.762	170	9868	132	-9761	9.8	73	2	33	133	0.24	NR
729	400	100	67.5	-4.762	170	10192	60	-9762	9.8	361	9	69	62	0.22	NR
730	500	100	60	4.762	170	9948	161	-9762	9.8	260	6	-74	162	0.08	NR
731	400	100	52.5	4.762	170	10262	95	-9764	9.8	279	7	219	96	0.19	NR
732	600	50	30	9.524	170	38954	332	-38980	39	33	6	-59	334	0.00	NR
733	400	100	67.5	4.762	170	10171	80	-9763	9.8	364	9	44	81	0.11	NR
734	400	100	52.5	-4.762	170	10049	91	-9762	9.8	281	7	6	92	0.21	NR
735	500	100	60	-4.762	170	10022	117	-9761	9.8	262	6	-1	118	0.14	NR
736	450	150	7.5	-3.175	170	4500	161	-4356	4.4	55	6	88	161	0.24	NR
737	600	50	74.25	-9.524	170	39037	157	-38978	39	91	18	-32	163	0.00	NR
738	400	100	60	-4.762	170	10089	71	-9763	9.8	321	8	5	72	0.25	NR
739	400	100	22.5	4.762	170	10006	126	-9762	9.8	114	3	130	126	0.24	NR
740	600	50	52.5	9.524	170	39124	208	-38979	39	61	12	84	212	0.00	NR
741	500	100	7.5	-4.762	170	9630	182	-9762	9.8	26	1	-159	183	0.14	NR
742	400	100	74.25	4.762	170	10171	85	-9764	9.8	400	10	8	86	0.04	NR
743	500	50	67.5	-9.524	170	39269	167	-38976	39	97	19	196	172	0.00	NR
744	400	100	60	4.762	170	9984	93	-9765	9.8	319	8	-99	94	0.15	NR
745	450	150	37.5	-3.175	170	4571	103	-4357	4.4	304	34	-91	109	0.00	PR
746	450	150	37.5	3.175	170	4736	92	-4357	4.4	306	34	74	98	0.00	PR
747	500	125	52.5	-3.81	170	6719	100	-6248	6.2	263	45	208	110	0.00	PR
748	600	200	7.5	-7.143	170	22165	227	-21972	22	71	14	122	229	0.00	NR
749	600	200	7.5	7.143	170	21805	209	-21970	22	71	15	-236	211	0.00	NR
750	600	200	15	7.143	170	22259	192	-21971	22	154	31	134	196	0.00	NR
751	600	200	15	-7.143	170	21961	163	-21976	22	152	31	-167	168	0.00	NR
752	600	100	30	-4.762	260	10086	388	-9764	9.8	105	3	217	388	0.02	NR
753	600	100	45	-4.762	260	10040	381	-9764	9.8	162	4	114	381	0.02	NR
754	600	100	60	4.762	260	10127	213	-9761	9.8	220	5	147	213	0.05	NR
755	600	100	22.5	-4.762	260	9336	291	-9764	9.8	77	2	-505	291	0.05	NR
756	600	100	67.5	4.762	260	10104	143	-9764	9.8	247	6	92	144	0.10	NR
757	600	100	15	-4.762	260	9800	285	-9760	9.8	48	1	-8	285	0.05	NR
758	600	100	30	4.762	260	10089	268	-9766	9.8	102	2	221	269	0.05	NR
759	600	100	22.5	-4.762	260	9783	154	-9760	9.8	74	2	-51	154	0.18	NR
760	600	100	52.5	4.762	260	9847	196	-9769	9.8	186	4	-108	196	0.08	NR
761	600	100	45	4.762	260	9862	187	-9768	9.8	157	4	-62	187	0.09	NR

Continued on next page

Table A.2 Continued from previous page

N_{run}	T [ns]	D [ns]	P [W]	B [Gauss]	θ_{pol} [deg.]	ν_{fit} [Hz]	$\Delta\nu_{\mathrm{fit}}$ [Hz]	$\mathrm{DC_B}$ [Hz]	$\Delta\mathrm{DC_B}$ [Hz]	SC [Hz]	ΔSC [Hz]	ν_0 [Hz]	$\Delta\nu_0$ [Hz]	wts. [%]	Data Type
762	600	100	52.5	-4.762	260	10009	276	-9761	9.8	185	4	63	276	0.04	NR
763	600	100	67.5	-4.762	260	10281	232	-9761	9.8	245	6	275	233	0.04	NR
764	600	100	7.5	-4.762	260	10886	488	-9761	9.8	21	0	1104	488	0.02	NR
765	600	100	45	-4.762	260	10200	291	-9760	9.8	156	4	284	291	0.04	NR
766	600	100	74.25	-4.762	260	9743	188	-9760	9.8	272	7	-289	189	0.05	NR
767	600	100	30	-4.762	260	9480	321	-9760	9.8	102	2	-383	322	0.04	NR
768	600	100	15	4.762	260	10398	464	-9770	9.8	47	1	582	465	0.02	NR
769	600	100	60	4.762	260	10066	237	-9771	9.8	212	5	83	237	0.04	NR
770	600	100	15	4.762	260	10133	229	-9771	9.8	46	1	316	229	0.08	NR
771	600	100	37.5	-4.762	260	10189	454	-9759	9.8	127	3	303	454	0.02	NR
772	600	100	22.5	4.762	260	9560	219	-9771	9.8	72	2	-284	219	0.09	NR
773	600	100	7.5	4.762	260	9739	435	-9771	9.8	20	0	-51	435	0.03	NR
774	600	100	60	-4.762	260	10390	312	-9758	9.8	209	5	422	312	0.03	NR
775	600	100	37.5	4.762	260	9843	355	-9772	9.8	126	3	-55	355	0.03	NR
776	600	100	74.25	-4.762	260	10601	243	-9759	9.8	267	6	575	243	0.03	NR
777	600	100	74.25	4.762	260	10326	173	-9771	9.8	268	6	287	173	0.06	NR
778	500	50	15	-9.524	260	39111	281	-38966	39	16	3	128	283	0.00	NR
779	500	50	60	-9.524	260	39189	109	-38968	39	81	16	140	117	0.00	NR
780	500	50	15	9.524	260	39099	202	-38995	39	16	3	89	206	0.00	NR
781	500	50	74.25	-9.524	260	39085	120	-38967	39	104	20	14	128	0.00	NR
782	500	50	37.5	-9.524	260	39060	147	-38965	39	47	9	48	152	0.00	NR
783	500	50	67.5	9.524	260	38970	103	-39000	39	92	18	-122	112	0.00	NR
784	500	50	67.5	-9.524	260	39238	91	-38966	39	92	18	180	100	0.00	NR
785	500	50	7.5	-9.524	260	38848	458	-38969	39	6	1	-127	460	0.00	NR
786	500	50	52.5	-9.524	260	38906	97	-38967	39	68	13	-129	105	0.00	NR
787	500	50	22.5	9.524	260	38886	136	-38996	39	26	5	-136	142	0.00	NR
788	500	50	22.5	-9.524	260	38731	204	-38965	39	25	5	-260	208	0.00	NR
789	500	50	30	9.524	260	38918	187	-38997	39	36	7	-115	191	0.00	NR
790	500	50	37.5	9.524	260	39170	130	-38996	39	46	9	128	136	0.00	NR
791	500	50	45	9.524	260	38945	149	-38996	39	57	11	-108	155	0.00	NR
792	500	50	52.5	9.524	260	38971	103	-38998	39	68	13	-95	111	0.00	NR
793	500	50	74.25	9.524	260	39187	65	-39000	39	103	20	84	79	0.00	NR
794	500	50	45	-9.524	260	38906	104	-38967	39	58	11	-119	112	0.00	NR
795	500	50	60	9.524	260	39106	113	-39001	39	80	16	25	121	0.00	NR
796	500	50	30	-9.524	260	39175	200	-38968	39	36	7	171	204	0.00	NR
797	500	50	7.5	9.524	260	38374	387	-39000	39	6	1	-632	389	0.00	NR
798	500	100	67.5	-4.762	260	10016	95	-9758	9.8	280	7	-22	96	0.19	NR
799	500	100	22.5	4.762	260	9841	82	-9773	9.8	84	2	-16	83	0.60	NR
800	500	100	15	4.762	260	9725	128	-9773	9.8	53	1	-101	129	0.27	NR
801	500	100	52.5	-4.762	260	9877	79	-9756	9.8	213	5	-92	80	0.40	NR
802	500	100	52.5	4.762	260	10029	72	-9774	9.8	214	5	41	73	0.49	NR
803	500	100	7.5	4.762	260	9989	145	-9773	9.8	24	1	192	145	0.23	NR
804	500	100	30	4.762	260	9840	103	-9773	9.8	115	3	-48	103	0.35	NR
805	500	100	30	-4.762	260	9944	92	-9757	9.8	115	3	72	92	0.44	NR
806	500	100	37.5	4.762	260	10128	83	-9773	9.8	147	4	208	84	0.48	NR
807	500	100	45	4.762	260	10001	68	-9772	9.8	180	4	49	69	0.64	NR
808	500	100	22.5	-4.762	260	9605	127	-9756	9.8	84	2	-235	127	0.26	NR
809	500	100	15	-4.762	260	10013	133	-9756	9.8	53	1	205	133	0.25	NR
810	500	100	7.5	-4.762	260	9801	238	-9756	9.8	24	1	21	238	0.08	NR
811	500	100	37.5	-4.762	260	10005	92	-9756	9.8	146	4	103	92	0.40	NR
812	500	100	45	-4.762	260	9864	98	-9756	9.8	179	4	-71	98	0.31	NR
813	500	100	67.5	4.762	260	10091	69	-9773	9.8	281	7	37	70	0.37	NR
814	600	200	18.75	-7.143	260	22104	252	-21967	22	184	37	-47	256	0.00	NR
815	600	200	3.75	-7.143	260	20317	1020	-21969	22	30	6	-1682	1020	0.00	NR
816	700	100	67.5	-4.762	260	10092	230	-9760	9.8	209	5	123	231	0.05	NR
817	700	100	37.5	4.762	260	10293	406	-9772	9.8	109	3	412	407	0.02	NR
818	700	100	74.25	4.762	260	9884	180	-9772	9.8	234	6	-121	181	0.07	NR
819	600	200	18.75	7.143	260	22104	234	-21984	22	186	38	-66	238	0.00	NR
820	700	100	74.25	-4.762	260	10647	261	-9760	9.8	235	6	652	262	0.03	NR
821	600	200	11.25	-7.143	260	21765	355	-21968	22	106	22	-309	357	0.00	NR
822	700	100	67.5	4.762	260	9787	254	-9772	9.8	211	5	-195	254	0.04	NR
823	600	200	11.25	7.143	260	22877	879	-21982	22	105	21	791	880	0.00	NR
824	700	100	37.5	-4.762	260	10057	496	-9760	9.8	109	3	188	496	0.01	NR
825	600	200	11.25	7.143	260	22140	437	-21985	22	106	22	49	438	0.00	NR
826	600	50	37.5	-9.524	260	38876	340	-38969	39	40	8	-133	343	0.00	NR
827	450	150	18.75	-3.175	260	4543	140	-4357	4.4	142	16	45	141	0.07	NR
828	450	150	11.25	-3.175	260	4582	202	-4356	4.4	81	9	145	202	0.12	NR
829	450	150	18.75	3.175	260	4433	131	-4363	4.4	142	16	-72	132	0.08	NR
830	600	50	60	-9.524	260	38931	300	-38969	39	68	13	-106	303	0.00	NR
831	600	50	45	9.524	260	39028	395	-38992	39	49	10	-14	397	0.00	NR
832	450	150	11.25	3.175	260	4850	206	-4364	4.4	81	9	404	206	0.11	NR
833	450	150	3.75	3.175	260	4062	395	-4363	4.4	24	3	-325	395	0.06	NR
834	600	50	52.5	-9.524	260	38790	393	-38968	39	58	11	-235	395	0.00	NR
835	450	150	7.5	-3.175	260	3946	223	-4356	4.4	52	6	-462	224	0.13	NR
836	600	50	52.5	9.524	260	38920	299	-38989	39	59	11	-128	302	0.00	NR
837	600	50	15	-9.524	260	39662	798	-38971	39	13	3	678	799	0.00	NR
838	600	50	45	-9.524	260	38697	322	-38970	39	49	10	-323	324	0.00	NR
839	450	150	7.5	3.175	260	4586	204	-4364	4.4	52	6	170	204	0.15	NR
840	450	150	26.25	-3.175	260	4575	102	-4356	4.4	204	23	15	105	0.00	NR
841	450	150	26.25	3.175	260	4603	123	-4363	4.4	205	23	35	125	0.00	NR
842	450	150	3.75	-3.175	260	4236	378	-4356	4.4	24	3	-144	378	0.06	NR
843	600	50	67.5	-9.524	260	38858	239	-38968	39	78	15	-189	242	0.00	NR
844	600	50	15	9.524	260	38405	730	-38990	39	14	3	-599	731	0.00	NR
845	600	50	67.5	9.524	260	39241	218	-38994	39	78	15	169	222	0.00	NR
846	600	50	22.5	-9.524	260	38564	325	-38970	39	22	4	-428	328	0.00	NR
847	600	50	37.5	9.524	260	39222	237	-38990	39	40	8	192	240	0.00	NR
848	600	50	22.5	9.524	260	39311	470	-38991	39	22	4	298	472	0.00	NR
849	600	50	60	9.524	260	39374	231	-38991	39	68	13	315	235	0.00	NR
850	500	100	74.25	4.762	260	9787	106	-9771	9.8	320	8	-304	107	0.11	NR
851	700	100	74.25	4.762	260	10115	200	-9770	9.8	235	6	110	200	0.06	NR
852	700	100	74.25	-4.762	260	10406	196	-9761	9.8	236	6	409	196	0.06	NR
853	500	100	74.25	-4.762	260	10127	102	-9761	9.8	325	8	41	103	0.12	NR
854	600	50	74.25	-9.524	260	39511	335	-38966	39	91	18	454	338	0.00	NR
855	600	200	3.75	-7.143	260	21263	1130	-21970	22	31	6	-737	1130	0.00	NR
856	500	100	30	-4.762	170	10053	115	-9759	9.8	122	3	173	115	0.28	NR
857	500	100	7.5	-4.762	170	9693	251	-9759	9.8	25	1	-91	251	0.08	NR
858	600	50	60	9.524	170	38972	430	-38992	39	69	14	-90	432	0.00	NR
859	600	100	74.25	-4.762	170	10064	160	-9759	9.8	274	7	31	161	0.07	NR

Continued on next page

Table A.2 Continued from previous page

N_{run}	T [ns]	D [ns]	P [W]	B [Gauss]	θ_{pol} [deg.]	ν_{fit} [Hz]	$\Delta\nu_{\mathrm{fit}}$ [Hz]	$\mathrm{DC_B}$ [Hz]	$\Delta\mathrm{DC_B}$ [Hz]	SC [Hz]	ΔSC [Hz]	ν_0 [Hz]	$\Delta\nu_0$ [Hz]	wts. [%]	Data Type
860	600	100	67.5	-4.762	170	9978	233	-9760	9.8	248	6	-30	233	0.04	NR
861	600	100	7.5	-4.762	170	9997	543	-9760	9.8	21	0	217	543	0.02	NR
862	600	50	67.5	9.524	170	39630	391	-38989	39	79	16	562	394	0.00	NR
863	600	50	45	9.524	170	38706	573	-38990	39	50	10	-334	575	0.00	NR
864	600	50	67.5	-9.524	170	38858	218	-38969	39	79	16	-191	222	0.00	NR
865	450	150	7.5	-3.175	170	4172	272	-4357	4.4	53	6	-237	272	0.08	NR
866	600	50	22.5	9.524	170	39230	658	-38989	39	22	4	219	659	0.00	NR
867	600	50	45	-9.524	170	39007	368	-38969	39	49	10	-12	370	0.00	NR
868	600	100	37.5	4.762	170	10313	333	-9772	9.8	128	3	413	333	0.03	NR
869	600	100	7.5	4.762	170	9108	631	-9771	9.8	20	0	-683	632	0.02	NR
870	700	100	74.25	4.762	170	10411	289	-9773	9.8	236	6	403	289	0.03	NR
871	500	50	15	-9.524	170	38734	342	-38970	39	17	3	-253	344	0.00	NR
872	700	100	74.25	-4.762	170	9760	250	-9760	9.8	236	6	-237	250	0.04	NR
873	600	50	15	-9.524	170	39397	660	-38968	39	14	3	415	661	0.00	NR
874	600	50	60	-9.524	170	39297	320	-38968	39	69	13	261	322	0.00	NR
875	600	100	67.5	4.762	170	9856	228	-9772	9.8	245	6	-161	228	0.04	NR
876	600	50	22.5	-9.524	170	38333	502	-38968	39	23	4	-657	504	0.00	NR
877	600	50	15	9.524	170	42317	1489	-38991	39	14	3	3311	1489	0.00	NR
878	600	50	37.5	-9.524	170	38040	528	-38967	39	40	8	-967	529	0.00	NR
879	400	200	18.75	7.143	170	22437	159	-21986	22	282	57	169	171	0.00	NR
880	600	50	37.5	9.524	170	39752	735	-38990	39	41	8	721	736	0.00	NR
881	500	125	22.5	4.286	170	7867	283	-7915	7.9	105	18	-154	284	0.00	NR
882	400	200	7.5	-6.548	170	18340	233	-18456	18.5	105	21	-221	235	0.00	NR
883	500	100	37.5	5.238	170	11964	249	-11819	11.8	154	4	-9	250	0.03	NR
884	300	50	37.5	19.048	170	156481	207	-155965	156	81	16	435	260	0.00	LB
885	300	100	22.5	3.968	170	6995	120	-6799	6.8	148	4	49	121	0.39	NR
886	400	50	60	-8.929	170	34514	155	-34330	34.3	103	20	82	161	0.00	NR
887	300	150	7.5	2.381	170	2256	207	-2465	2.5	81	9	-290	207	0.14	NR
888	300	100	22.5	-5.556	170	13467	101	-13267	13.3	149	4	51	102	0.06	NR
889	300	150	7.5	-15.875	170	108177	190	-108269	108.3	81	9	-173	219	0.00	LB
890	300	50	37.5	-19.048	170	156152	156	-155924	155.9	81	16	147	221	0.00	LB
891	300	100	22.5	-19.048	170	156022	118	-155928	155.9	147	4	-53	195	0.00	LB
892	400	50	60	-19.048	170	156136	186	-155926	155.9	102	20	108	244	0.00	LB
893	300	100	7.5	5.556	170	13329	240	-13282	13.3	44	1	3	241	0.03	NR
894	300	100	7.5	-3.968	170	6732	191	-6788	6.8	44	1	-100	192	0.18	NR
895	300	50	45	-19.048	170	156011	152	-155921	155.9	98	19	-8	219	0.00	LB
896	300	50	37.5	-10.317	170	45825	135	-45815	45.8	81	16	-71	143	0.00	LB
897	300	50	45	-10.317	170	45969	149	-45807	45.8	98	19	64	157	0.00	LB
898	400	50	60	8.929	170	34309	256	-34348	34.3	102	20	-141	259	0.00	NR
899	300	100	15	3.968	170	6647	141	-6797	6.8	95	2	-246	142	0.31	NR
900	500	100	37.5	4.286	170	8018	200	-7914	7.9	153	4	-50	200	0.12	NR
901	600	150	37.5	3.571	170	5495	568	-5497	5.5	226	25	-229	569	0.00	PR
902	400	200	15	16.667	170	119262	312	-119375	119.4	220	45	-333	337	0.00	LB
903	400	100	22.5	5.357	170	12568	143	-12368	12.4	111	3	89	143	0.09	NR
904	300	50	45	-8.73	170	32850	104	-32767	32.8	99	19	-16	111	0.00	NR
905	300	100	7.5	-19.048	170	156048	208	-155925	155.9	44	1	79	260	0.00	LB
906	400	100	22.5	19.048	170	156076	323	-155972	156	110	3	-6	359	0.00	LB
907	500	125	22.5	-4.286	170	8381	236	-7906	7.9	104	18	371	237	0.00	NR
908	300	150	7.5	-2.381	170	2505	167	-2459	2.5	79	9	-33	167	0.23	NR
909	400	100	30	19.048	170	155927	182	-155969	156	150	4	-191	239	0.00	LB
910	300	150	15	2.381	170	2581	133	-2466	2.5	168	19	-52	134	0.08	NR
911	300	50	45	19.048	170	156293	189	-155967	156	98	19	227	246	0.00	LB
912	400	200	15	7.738	170	26037	248	-25805	25.8	219	45	14	253	0.00	NR
913	300	150	15	-3.968	170	6833	110	-6789	6.8	168	19	-124	112	0.00	NR
914	300	100	7.5	-5.556	170	13552	208	-13267	13.3	44	1	241	209	0.04	NR
915	500	125	22.5	15.24	170	99681	413	-99903	99.9	104	18	-325	426	0.00	LB
916	400	100	22.5	-19.048	170	156155	151	-155929	155.9	110	3	117	217	0.00	LB
917	300	100	7.5	3.968	170	6880	242	-6799	6.8	44	1	37	242	0.12	NR
918	600	150	37.5	2.778	170	2974	514	-3333	3.3	224	25	-582	515	0.00	PR
919	400	100	22.5	-5.357	170	12393	144	-12352	12.4	110	3	-69	144	0.09	NR
920	300	50	37.5	8.73	170	32784	158	-32788	32.8	81	16	-84	162	0.00	NR
921	400	200	7.5	-7.738	170	25501	236	-25782	25.8	104	21	-385	239	0.00	NR
922	600	150	37.5	15.875	170	108932	546	-108313	108.3	224	25	395	557	0.00	PRLB
923	400	200	7.5	6.548	170	17658	315	-18475	18.5	104	21	-921	316	0.00	NR
924	300	50	37.5	-8.73	170	32733	149	-32765	32.8	81	16	-113	153	0.00	NR
925	300	100	15	5.556	170	13741	117	-13282	13.3	95	2	364	118	0.09	NR
926	300	100	15	-5.556	170	13421	160	-13265	13.3	95	2	62	161	0.05	NR
927	400	200	15	-5.357	170	12351	184	-12351	12.4	219	45	-219	189	0.00	NR
928	300	100	15	-19.048	170	155729	194	-155918	155.9	95	2	-284	249	0.00	LB
929	300	100	22.5	5.556	170	13645	117	-13284	13.3	147	4	215	118	0.04	NR
930	300	100	15	-3.968	170	6873	105	-6788	6.8	95	2	-10	105	0.57	NR
931	600	150	37.5	-15.875	170	107741	430	-108269	108.3	226	25	-755	445	0.00	PRLB
932	600	150	37.5	-2.778	170	3658	416	-3327	3.3	227	25	104	416	0.00	PR
933	300	50	45	8.73	170	32982	129	-32786	32.8	99	20	97	134	0.00	NR
934	300	50	37.5	10.317	170	45610	152	-45834	45.8	82	16	-306	160	0.00	LB
935	400	200	7.5	16.667	170	119634	390	-119380	119.4	106	22	148	409	0.00	LB
936	300	150	7.5	-3.968	170	7237	170	-6790	6.8	81	9	366	170	0.10	NR
937	300	50	45	10.317	170	45888	157	-45835	45.8	100	20	-47	165	0.00	LB
938	300	150	15	-2.381	170	2784	127	-2459	2.5	171	19	154	129	0.08	NR
939	300	150	7.5	3.968	170	7235	182	-6798	6.8	81	9	357	183	0.09	NR
940	500	100	37.5	-4.286	170	7799	178	-7904	7.9	156	4	-261	178	0.15	NR
941	300	100	7.5	19.048	170	155736	252	-155972	156	45	1	-281	297	0.00	LB
942	400	100	22.5	-4.167	170	7661	110	-7473	7.5	112	3	76	110	0.46	NR
943	400	200	15	-16.667	170	119390	230	-119330	119.3	222	45	-163	263	0.00	LB
944	500	100	37.5	-5.238	170	11570	239	-11810	11.8	154	4	-393	239	0.03	NR
945	300	100	22.5	-3.968	170	7028	79	-6787	6.8	147	4	94	79	0.91	NR
946	400	200	7.5	-16.667	170	119381	414	-119334	119.3	104	21	-57	431	0.00	LB
947	400	200	7.5	7.738	170	25942	466	-25804	25.8	104	21	34	467	0.00	NR
948	400	200	15	5.357	170	12664	185	-12367	12.4	219	45	77	191	0.00	NR
949	600	150	37.5	-3.571	170	5154	415	-5488	5.5	225	25	-560	415	0.00	PR
950	500	100	37.5	-19.048	170	155981	328	-155921	155.9	154	4	-94	363	0.00	LB
951	300	100	22.5	19.048	170	156342	167	-155978	156	147	4	217	229	0.00	LB
952	300	150	15	15.875	170	108619	146	-108309	108.3	168	19	142	183	0.00	LB
953	400	100	22.5	4.167	170	7525	203	-7483	7.5	110	3	-68	203	0.13	NR
954	500	125	22.5	-15.24	170	99963	363	-99869	99.9	104	18	-10	377	0.00	LB
955	400	100	30	-4.167	170	7809	126	-7473	7.5	150	4	186	126	0.32	NR
956	400	50	60	10.119	170	44303	188	-44021	44	101	20	181	194	0.00	LB
957	400	200	15	-7.738	170	25528	181	-25784	25.8	220	45	-475	188	0.00	NR

Continued on next page

Table A.2 Continued from previous page

N_{run}	T [ns]	D [ns]	P [W]	B [Gauss]	θ_{pol} [deg.]	ν_{fit} [Hz]	$\Delta\nu_{\mathrm{fit}}$ [Hz]	$\mathrm{DC_B}$ [Hz]	$\Delta\mathrm{DC_B}$ [Hz]	SC [Hz]	ΔSC [Hz]	ν_0 [Hz]	$\Delta\nu_0$ [Hz]	wts. [%]	Data Type
958	400	100	30	5.357	170	12359	126	-12366	12.4	151	4	-157	127	0.08	NR
959	500	125	22.5	3.333	170	4977	289	-4787	4.8	104	18	86	289	0.00	NR
960	400	100	30	-19.048	170	155870	153	-155926	155.9	150	4	-206	218	0.00	LB
961	400	100	30	4.167	170	7725	157	-7482	7.5	151	4	92	157	0.21	NR
962	500	125	22.5	-3.333	170	4508	195	-4778	4.8	104	18	-374	196	0.00	NR
963	500	100	37.5	19.048	170	156390	366	-155972	156	153	4	265	398	0.00	LB
964	400	50	60	19.048	170	156074	186	-155981	156	102	20	-10	244	0.00	LB
965	400	100	30	-5.357	170	12514	144	-12354	12.4	151	4	9	145	0.06	NR
966	400	50	60	-10.119	170	43912	133	-44000	44	102	20	-190	141	0.00	LB
967	300	150	15	3.968	170	6949	139	-6798	6.8	169	19	-18	140	0.00	NR
968	300	100	15	19.048	170	156193	187	-155970	156	95	2	128	244	0.00	LB
969	300	150	15	-15.875	170	108405	117	-108272	108.3	168	19	-36	161	0.00	LB
970	300	150	7.5	15.875	170	108003	207	-108310	108.3	80	9	-387	234	0.00	LB
971	300	100	71.25	-33.334	260	477897	88	-477397	477.4	487	12	13	486	0.00	LB
972	300	100	71.25	-33.334	260	477871	77	-477422	477.4	490	12	-41	484	0.00	LB
973	300	100	71.25	-33.334	260	478014	80	-477415	477.4	492	12	107	484	0.00	LB
974	300	100	71.25	-14.286	260	88329	67	-87783	87.8	492	12	54	111	0.00	LB
975	300	100	71.25	-14.286	260	88317	86	-87772	87.8	493	12	52	124	0.00	LB
976	300	100	71.25	-14.286	260	88329	69	-87771	87.8	493	12	64	112	0.00	LB
977	300	100	71.25	19.048	260	156476	61	-155968	156	494	12	15	168	0.00	LB
978	300	100	71.25	19.048	260	156541	67	-155974	156	492	12	75	170	0.00	LB
979	300	100	71.25	19.048	260	156448	51	-155964	156	492	12	-7	165	0.00	LB
980	300	100	71.25	-28.572	260	351142	67	-350615	350.6	492	12	35	357	0.00	LB
981	300	100	71.25	-28.572	260	351126	83	-350616	350.6	492	12	19	360	0.00	LB
982	300	100	71.25	-28.572	260	351198	54	-350615	350.6	492	12	91	355	0.00	LB
983	300	100	71.25	-4.762	260	10355	58	-9767	9.8	492	12	96	60	0.00	NR
984	300	100	71.25	-4.762	260	10157	63	-9763	9.8	492	12	-98	65	0.00	NR
985	300	100	71.25	-4.762	260	10224	69	-9762	9.8	493	12	-31	71	0.00	NR
986	300	100	71.25	-19.048	260	156456	82	-155924	155.9	493	12	38	176	0.00	LB
987	300	100	71.25	-19.048	260	156486	51	-155925	155.9	493	12	68	165	0.00	LB
988	300	100	71.25	-19.048	260	156545	71	-155925	155.9	494	12	126	172	0.00	LB
989	300	100	71.25	28.572	260	351124	66	-350665	350.7	494	12	-35	357	0.00	LB
990	300	100	71.25	28.572	260	351184	66	-350678	350.7	494	12	12	357	0.00	LB
991	300	100	71.25	28.572	260	351250	65	-350677	350.7	494	12	79	357	0.00	LB
992	300	150	7.5	-2.381	260	2572	140	-2462	2.5	79	9	31	140	0.33	NR
993	400	200	15	-7.738	260	25862	156	-25786	25.8	217	44	-141	164	0.00	NR
994	300	150	7.5	-15.875	260	108369	163	-108270	108.3	78	9	22	196	0.00	LB
995	300	150	15	15.875	260	108304	136	-108306	108.3	163	18	-165	174	0.00	LB
996	300	150	15	2.381	260	2556	82	-2465	2.5	164	18	-73	84	0.25	NR
997	400	100	30	-5.357	260	12496	129	-12356	12.4	147	4	-7	130	0.08	NR
998	300	150	15	-3.968	260	7158	87	-6788	6.8	164	18	206	89	0.00	NR
999	400	100	30	-19.048	260	155922	189	-155924	155.9	148	4	-150	245	0.00	LB
1000	400	50	60	-8.929	260	34595	156	-34334	34.3	101	20	160	161	0.00	NR
1001	300	100	7.5	-3.968	260	7192	163	-6788	6.8	43	1	361	163	0.26	NR
1002	400	100	30	5.357	260	12649	97	-12364	12.4	147	4	138	98	0.14	NR
1003	500	100	37.5	-19.048	260	156023	276	-155920	155.9	151	4	-47	317	0.00	LB
1004	300	50	45	19.048	260	156293	98	-155963	156	98	19	233	185	0.00	LB
1005	400	200	7.5	-7.738	260	25469	233	-25788	25.8	102	21	-420	235	0.00	NR
1006	500	100	37.5	-5.238	260	12084	211	-11810	11.8	151	4	123	211	0.04	NR
1007	600	150	37.5	2.778	260	3304	256	-3331	3.3	223	25	-251	257	0.00	PR
1008	300	50	45	10.317	260	45863	111	-45829	45.8	98	19	-64	122	0.00	LB
1009	400	200	15	-5.357	260	12498	177	-12355	12.4	216	44	-73	183	0.00	NR
1010	400	100	30	19.048	260	156000	113	-155962	156	149	4	-111	193	0.00	LB
1011	400	100	22.5	5.357	260	12458	116	-12366	12.4	109	3	-18	117	0.13	NR
1012	400	200	15	-16.667	260	119099	239	-119336	119.3	217	44	-454	271	0.00	LB
1013	300	150	15	-2.381	260	2625	98	-2460	2.5	166	18	-1	100	0.16	NR
1014	400	100	22.5	4.167	260	7468	169	-7479	7.5	110	3	-122	169	0.19	NR
1015	600	150	37.5	-15.875	260	109232	503	-108269	108.3	226	25	737	515	0.00	PRLB
1016	300	100	22.5	-3.968	260	6767	88	-6790	6.8	146	4	-170	88	0.73	NR
1017	400	200	7.5	16.667	260	119464	216	-119373	119.4	104	21	-13	247	0.00	LB
1018	400	200	7.5	-6.548	260	18378	191	-18459	18.5	103	21	-184	193	0.00	NR
1019	300	100	22.5	3.968	260	6913	95	-6796	6.8	145	3	-28	96	0.63	NR
1020	600	150	37.5	-3.571	260	5652	370	-5489	5.5	225	25	-61	371	0.00	PR
1021	400	100	22.5	-5.357	260	12520	127	-12354	12.4	110	3	56	128	0.11	NR
1022	500	125	22.5	4.286	260	7897	221	-7913	7.9	103	18	-120	222	0.00	NR
1023	300	50	37.5	-8.73	260	32778	135	-32767	32.8	81	16	-70	140	0.00	NR
1024	500	125	22.5	-15.24	260	100833	305	-99865	99.9	104	18	864	322	0.00	LB
1025	300	150	15	-15.875	260	108524	141	-108271	108.3	167	19	86	179	0.00	LB
1026	300	50	45	-19.048	260	156052	138	-155929	155.9	99	19	25	209	0.00	LB
1027	300	100	7.5	3.968	260	6626	131	-6798	6.8	44	1	-216	132	0.40	NR
1028	300	150	7.5	15.875	260	108497	162	-108309	108.3	79	9	108	195	0.00	LB
1029	300	100	7.5	-5.556	260	13591	165	-13269	13.3	44	1	277	166	0.07	NR
1030	600	150	37.5	15.875	260	108444	349	-108305	108.3	224	25	-85	366	0.00	PRLB
1031	500	100	37.5	-4.286	260	8337	190	-7907	7.9	153	4	277	191	0.13	NR
1032	400	50	60	10.119	260	44312	153	-44021	44	102	20	189	161	0.00	LB
1033	300	50	45	-8.73	260	32855	118	-32769	32.8	99	19	-12	124	0.00	NR
1034	300	50	37.5	-10.317	260	46056	148	-45809	45.8	81	16	166	155	0.00	LB
1035	300	100	7.5	5.556	260	13314	198	-13279	13.3	44	1	-9	198	0.05	NR
1036	300	100	22.5	-5.556	260	13504	109	-13268	13.3	145	3	92	110	0.05	NR
1037	500	100	37.5	19.048	260	155995	201	-155959	156	152	4	-117	255	0.00	LB
1038	600	150	37.5	-2.778	260	4031	319	-3328	3.3	225	25	478	320	0.00	PR
1039	300	50	45	8.73	260	32926	138	-32785	32.8	98	19	43	143	0.00	NR
1040	600	150	37.5	3.571	260	5619	260	-5496	5.5	225	25	-102	261	0.00	PR
1041	300	100	15	-3.968	260	7080	131	-6788	6.8	95	2	198	131	0.37	NR
1042	300	100	22.5	19.048	260	156067	89	-155959	156	146	4	-38	180	0.00	LB
1043	300	50	37.5	-19.048	260	155987	148	-155934	155.9	81	16	-28	216	0.00	LB
1044	300	100	7.5	19.048	260	156027	206	-155969	156	44	1	14	258	0.00	LB
1045	500	100	37.5	4.286	260	7857	141	-7916	7.9	153	4	-212	142	0.24	NR
1046	400	200	15	5.357	260	12500	204	-12364	12.4	219	45	-83	209	0.00	NR
1047	500	125	22.5	3.333	260	5314	164	-4786	4.8	105	18	423	165	0.00	NR
1048	300	100	15	-19.048	260	155966	152	-155926	155.9	95	2	-56	217	0.00	LB
1049	400	50	60	-19.048	260	155819	166	-155932	155.9	102	20	-215	228	0.00	LB
1050	400	200	7.5	7.738	260	26281	196	-25805	25.8	105	21	371	199	0.00	NR
1051	300	100	22.5	-19.048	260	155797	134	-155927	155.9	146	4	-276	206	0.00	LB
1052	400	100	30	-4.167	260	7568	123	-7474	7.5	150	4	-56	123	0.34	NR
1053	500	125	22.5	-4.286	260	7861	262	-7905	7.9	104	18	-149	263	0.00	NR
1054	400	200	15	16.667	260	119339	180	-119373	119.4	218	44	-253	220	0.00	LB
1055	300	150	7.5	2.381	260	2498	159	-2465	2.5	79	9	-47	159	0.25	NR

Continued on next page

Table A.2 Continued from previous page

N_{run}	T [ns]	D [ns]	P [W]	B [Gauss]	θ_{pol} [deg.]	ν_{fit} [Hz]	$\Delta\nu_{\mathrm{fit}}$ [Hz]	$\mathrm{DC_B}$ [Hz]	$\Delta\mathrm{DC_B}$ [Hz]	SC [Hz]	ΔSC [Hz]	ν_0 [Hz]	$\Delta\nu_0$ [Hz]	wts. [%]	Data Type
1056	500	125	22.5	-3.333	260	4746	253	-4779	4.8	104	18	-137	254	0.00	NR
1057	500	125	22.5	15.24	260	100121	277	-99904	99.9	104	18	113	295	0.00	LB
1058	500	100	37.5	5.238	260	11976	176	-11821	11.8	153	4	2	176	0.05	NR
1059	400	200	15	7.738	260	26098	139	-25799	25.8	219	44	81	148	0.00	NR
1060	300	100	22.5	5.556	260	13507	104	-13280	13.3	146	4	82	105	0.06	NR
1061	300	50	37.5	10.317	260	45750	110	-45831	45.8	81	16	-162	120	0.00	LB
1062	300	100	15	5.556	260	13404	105	-13280	13.3	95	2	30	106	0.11	NR
1063	400	200	7.5	6.548	260	18451	274	-18472	18.5	105	21	-126	276	0.00	NR
1064	400	50	60	-10.119	260	44282	147	-43998	44	103	20	181	155	0.00	LB
1065	300	150	7.5	-3.968	260	6878	130	-6788	6.8	80	9	10	131	0.17	NR
1066	300	50	37.5	19.048	260	156046	122	-155968	156	81	16	-2	199	0.00	LB
1067	300	100	15	-5.556	260	13345	118	-13270	13.3	94	2	-19	119	0.09	NR
1068	300	100	15	19.048	260	156032	113	-155971	156	94	2	-33	192	0.00	LB
1069	400	100	22.5	-19.048	260	156365	207	-155928	155.9	109	3	328	259	0.00	LB
1070	300	150	7.5	3.968	260	7074	133	-6798	6.8	79	9	198	134	0.17	NR
1071	300	150	15	3.968	260	7012	109	-6797	6.8	166	18	49	111	0.00	NR
1072	300	100	7.5	-19.048	260	155906	217	-155924	155.9	44	1	-62	267	0.00	LB
1073	400	50	60	19.048	260	156003	152	-155973	156	101	20	-71	219	0.00	LB
1074	400	100	22.5	-4.167	260	7717	123	-7473	7.5	110	3	133	123	0.37	NR
1075	300	50	37.5	8.73	260	32918	94	-32785	32.8	81	16	52	101	0.00	NR
1076	400	100	22.5	19.048	260	155987	155	-155961	156	112	3	-86	220	0.00	LB
1077	300	100	15	3.968	260	6850	126	-6799	6.8	96	2	-46	127	0.39	NR
1078	400	200	7.5	-16.667	260	119350	359	-119335	119.3	105	21	-90	379	0.00	LB
1079	400	100	30	4.167	260	7611	74	-7481	7.5	152	4	-22	75	0.93	NR
1080	400	50	60	8.929	260	34323	137	-34345	34.3	104	20	-126	143	0.00	NR
1081	300	50	45	-10.317	260	45998	140	-45811	45.8	101	20	86	149	0.00	LB
1082	300	100	71.25	9.524	260	39530	49	-38999	39	500	12	32	64	0.00	NR
1083	300	100	71.25	9.524	260	39475	54	-38993	39	500	12	-18	68	0.00	NR
1084	300	100	71.25	9.524	260	39400	75	-38993	39	501	12	-94	85	0.00	NR
1085	300	100	71.25	-4.762	260	10203	44	-9761	9.8	500	12	-59	46	0.00	NR
1086	300	100	71.25	-4.762	260	10276	75	-9760	9.8	500	12	15	77	0.00	NR
1087	300	100	71.25	-4.762	260	10306	54	-9761	9.8	500	12	46	56	0.00	NR
1088	300	100	71.25	-23.81	260	244045	70	-243528	243.5	500	12	17	254	0.00	LB
1089	300	100	71.25	-23.81	260	244125	68	-243553	243.6	500	12	72	253	0.00	LB
1090	300	100	71.25	-23.81	260	244029	88	-243546	243.5	500	12	-17	259	0.00	LB
1091	300	100	71.25	-9.524	260	39607	55	-38978	39	500	12	129	69	0.00	NR
1092	300	100	71.25	-9.524	260	39448	59	-38972	39	499	12	-23	72	0.00	NR
1093	300	100	71.25	-9.524	260	39604	58	-38967	39	498	12	139	71	0.00	NR
1094	300	100	71.25	23.81	260	244260	60	-243601	243.6	498	12	160	251	0.00	LB
1095	300	100	71.25	23.81	260	244186	51	-243607	243.6	498	12	80	249	0.00	LB
1096	300	100	71.25	23.81	260	244091	56	-243602	243.6	498	12	-8	250	0.00	LB
1097	300	100	71.25	14.286	260	88324	53	-87809	87.8	498	12	18	103	0.00	LB
1098	300	100	71.25	14.286	260	88364	57	-87800	87.8	498	12	66	106	0.00	LB
1099	300	100	71.25	14.286	260	88286	56	-87802	87.8	498	12	-14	105	0.00	LB
1100	300	100	71.25	4.762	260	10242	63	-9773	9.8	498	12	-29	65	0.00	NR
1101	300	100	71.25	4.762	260	10222	34	-9771	9.8	498	12	-47	37	0.00	NR
1102	300	100	71.25	4.762	260	10338	63	-9771	9.8	499	12	69	65	0.00	NR
1103	300	100	71.25	28.572	260	351262	75	-350653	350.7	499	12	109	359	0.00	LB
1104	300	100	71.25	28.572	260	351305	69	-350694	350.7	500	12	112	358	0.00	LB
1105	300	100	71.25	28.572	260	351196	52	-350680	350.7	500	12	15	355	0.00	LB
1106	300	100	71.25	33.334	260	477993	56	-477481	477.5	504	12	8	481	0.00	LB
1107	300	100	71.25	33.334	260	477948	55	-477472	477.5	503	12	-27	481	0.00	LB
1108	300	100	71.25	33.334	260	477899	71	-477481	477.5	505	12	-86	483	0.00	LB
1109	900	100	74.25	4.762	170	11504	877	-9772	9.8	183	4	1549	877	0.00	NR
1110	900	100	74.25	-4.762	170	10379	544	-9758	9.8	182	4	439	544	0.01	NR
1111	900	100	74.25	-4.762	170	9766	415	-9759	9.8	181	4	-174	415	0.02	NR
1112	900	100	74.25	4.762	170	10054	781	-9772	9.8	181	4	101	782	0.00	NR
1113	900	100	74.25	4.762	170	10616	628	-9772	9.8	182	4	662	628	0.01	NR
1114	900	100	74.25	-4.762	170	9927	1261	-9758	9.8	182	4	-13	1261	0.00	NR
1115	900	100	74.25	-4.762	170	9765	381	-9756	9.8	182	4	-173	381	0.02	NR
1116	900	100	74.25	4.762	170	9865	842	-9772	9.8	183	4	-89	842	0.01	NR
1117	900	100	74.25	-4.762	170	9864	385	-9757	9.8	183	4	-76	385	0.02	NR
1118	900	100	74.25	4.762	170	10059	804	-9773	9.8	183	4	103	804	0.01	NR
1119	900	100	74.25	-4.762	170	9379	496	-9757	9.8	184	4	-561	497	0.02	NR
1120	900	100	74.25	4.762	170	11310	734	-9772	9.8	184	4	1354	734	0.01	NR
1121	900	100	74.25	4.762	170	10477	754	-9772	9.8	184	4	521	754	0.01	NR
1122	900	100	74.25	-4.762	170	10420	396	-9756	9.8	184	4	480	397	0.02	NR
1123	900	100	74.25	4.762	170	9335	2359	-9772	9.8	183	4	-619	2359	0.00	NR
1124	900	100	74.25	4.762	170	8277	1240	-9772	9.8	184	4	-1678	1240	0.00	NR
1125	900	100	74.25	-4.762	170	9632	453	-9757	9.8	184	4	-309	453	0.02	NR
1126	900	100	74.25	-4.762	170	10888	450	-9757	9.8	184	4	947	450	0.01	NR
1127	900	100	74.25	4.762	260	9911	408	-9771	9.8	185	4	-45	408	0.02	NR
1128	900	100	74.25	-4.762	260	8872	450	-9760	9.8	183	4	-1071	450	0.01	NR
1129	900	100	74.25	-4.762	260	9673	692	-9760	9.8	184	4	-271	692	0.01	NR
1130	900	100	74.25	4.762	260	10517	550	-9770	9.8	184	4	563	550	0.01	NR
1131	900	100	74.25	4.762	260	9875	571	-9770	9.8	184	4	-79	571	0.01	NR
1132	800	100	74.25	-4.762	170	9617	316	-9761	9.8	205	5	-349	317	0.03	NR
1133	800	100	74.25	4.762	170	10132	377	-9770	9.8	205	5	157	377	0.02	NR
1134	800	100	74.25	-4.762	170	10305	334	-9761	9.8	206	5	338	334	0.02	NR
1135	800	100	74.25	4.762	170	10047	382	-9770	9.8	206	5	71	383	0.02	NR
1136	800	100	74.25	4.762	170	10030	341	-9770	9.8	207	5	53	342	0.02	NR
1137	800	100	74.25	-4.762	170	10255	316	-9761	9.8	207	5	286	316	0.03	NR
1138	800	100	74.25	-4.762	170	11309	462	-9761	9.8	207	5	1341	462	0.01	NR
1139	800	100	74.25	4.762	170	9995	388	-9769	9.8	207	5	19	388	0.02	NR
1140	900	100	74.25	-4.762	260	9546	837	-9759	9.8	183	4	-396	837	0.00	NR
1141	900	100	74.25	4.762	260	9519	461	-9773	9.8	183	4	-437	461	0.01	NR
1142	900	100	74.25	4.762	260	10543	487	-9774	9.8	184	4	586	487	0.01	NR
1143	800	100	74.25	4.762	260	8905	770	-9773	9.8	204	5	-1071	770	0.01	NR
1144	800	100	74.25	-4.762	260	9504	326	-9758	9.8	204	5	-459	326	0.02	NR
1145	800	100	74.25	-4.762	260	9706	383	-9759	9.8	205	5	-258	383	0.02	NR
1146	800	100	74.25	-4.762	260	9402	401	-9760	9.8	206	5	-563	401	0.02	NR
1147	300	100	67.5	-4.762	260	10033	165	-9724	9.7	461	11	-151	166	0.00	UP
1148	300	100	67.5	-4.762	260	10028	157	-9723	9.7	462	11	-157	158	0.00	UP
1149	300	100	67.5	-4.762	260	10291	154	-9723	9.7	463	11	105	154	0.00	UP
1150	300	100	15	-4.762	260	10251	198	-9724	9.7	91	2	437	198	0.00	UP
1151	300	100	15	-4.762	260	9822	196	-9724	9.7	90	2	9	196	0.00	UP
1152	300	100	15	-4.762	260	9965	266	-9723	9.7	90	2	152	266	0.00	UP
1153	300	100	60	-4.762	260	10051	148	-9723	9.7	401	10	-73	148	0.00	UP

Continued on next page

Table A.2 Continued from previous page

N_{run}	T [ns]	D [ns]	P [W]	B [Gauss]	θ_{pol} [deg.]	ν_{fit} [Hz]	$\Delta\nu_{\mathrm{fit}}$ [Hz]	$\mathrm{DC_B}$ [Hz]	$\Delta\mathrm{DC_B}$ [Hz]	SC [Hz]	ΔSC [Hz]	ν_0 [Hz]	$\Delta\nu_0$ [Hz]	wts. [%]	Data Type
1154	300	100	60	-4.762	260	9918	142	-9722	9.7	404	10	-209	143	0.00	UP
1155	300	100	60	-4.762	260	10195	132	-9723	9.7	407	10	65	133	0.00	UP
1156	300	100	37.5	-14.286	260	87812	243	-87515	87.5	248	6	48	258	0.00	UPLB
1157	300	100	37.5	-14.286	260	87720	244	-87525	87.5	248	6	-53	260	0.00	UPLB
1158	300	100	37.5	-14.286	260	87296	258	-87524	87.5	247	6	-475	273	0.00	UPLB
1159	300	100	67.5	14.286	260	88147	193	-87656	87.7	457	11	34	212	0.00	UPLB
1160	300	100	67.5	14.286	260	87943	195	-87651	87.7	459	11	-168	214	0.00	UPLB
1161	300	100	67.5	14.286	260	88021	170	-87647	87.6	460	11	-86	192	0.00	UPLB
1162	300	100	15	4.762	260	10042	203	-9766	9.8	92	2	184	203	0.00	UP
1163	300	100	15	4.762	260	9813	189	-9766	9.8	91	2	-44	190	0.00	UP
1164	300	100	15	4.762	260	10055	249	-9765	9.8	91	2	200	250	0.00	UP
1165	300	100	22.5	-14.286	260	87785	218	-87524	87.5	140	3	121	235	0.00	UPLB
1166	300	100	22.5	-14.286	260	87382	247	-87529	87.5	140	3	-286	262	0.00	UPLB
1167	300	100	22.5	-14.286	260	87314	296	-87523	87.5	140	3	-349	309	0.00	UPLB
1168	300	100	67.5	-14.286	260	88048	147	-87530	87.5	452	11	66	171	0.00	UPLB
1169	300	100	67.5	-14.286	260	87956	220	-87524	87.5	458	11	-26	237	0.00	UPLB
1170	300	100	67.5	-14.286	260	88309	196	-87522	87.5	459	11	329	215	0.00	UPLB
1171	300	100	7.5	-14.286	260	87679	490	-87526	87.5	42	1	111	498	0.00	UPLB
1172	300	100	7.5	-14.286	260	87657	515	-87526	87.5	41	1	90	523	0.00	UPLB
1173	300	100	7.5	-14.286	260	87626	528	-87529	87.5	41	1	56	536	0.00	UPLB
1174	300	100	74.25	-14.286	260	88266	212	-87524	87.5	496	12	245	229	0.00	UPLB
1175	300	100	74.25	-14.286	260	88121	145	-87527	87.5	506	12	88	170	0.00	UPLB
1176	300	100	74.25	-14.286	260	88090	224	-87521	87.5	509	12	59	241	0.00	UPLB
1177	300	100	60	-14.286	260	87996	200	-87524	87.5	407	10	65	218	0.00	UPLB
1178	300	100	60	-14.286	260	87995	194	-87524	87.5	406	10	65	213	0.00	UPLB
1179	300	100	60	-14.286	260	88062	210	-87524	87.5	405	10	132	228	0.00	UPLB
1180	300	100	60	4.762	260	10179	117	-9768	9.8	405	10	6	118	0.00	UP
1181	300	100	60	4.762	260	9951	156	-9766	9.8	405	10	-221	157	0.00	UP
1182	300	100	60	4.762	260	10106	144	-9766	9.8	405	10	-65	144	0.00	UP
1183	300	100	7.5	-4.762	260	10729	511	-9723	9.7	42	1	965	511	0.00	UP
1184	300	100	7.5	-4.762	260	9759	372	-9723	9.7	41	1	-5	372	0.00	UP
1185	300	100	7.5	-4.762	260	9794	415	-9722	9.7	41	1	31	415	0.00	UP
1186	300	100	30	4.762	260	9670	197	-9766	9.8	188	5	-284	198	0.00	UP
1187	300	100	30	4.762	260	10008	177	-9765	9.8	189	5	54	178	0.00	UP
1188	300	100	30	4.762	260	9601	257	-9766	9.8	189	5	-354	257	0.00	UP
1189	300	100	52.5	14.286	260	88157	205	-87650	87.7	344	8	162	223	0.00	UPLB
1190	300	100	52.5	14.286	260	87880	204	-87658	87.7	346	8	-124	222	0.00	UPLB
1191	300	100	52.5	14.286	260	87880	196	-87651	87.7	346	8	-117	215	0.00	UPLB
1192	300	100	15	14.286	260	88286	271	-87654	87.7	90	2	541	285	0.00	UPLB
1193	300	100	15	14.286	260	87642	226	-87654	87.7	90	2	-102	242	0.00	UPLB
1194	300	100	15	14.286	260	88139	282	-87655	87.7	89	2	396	295	0.00	UPLB
1195	300	100	30	-4.762	260	9447	224	-9723	9.7	190	5	-466	224	0.00	UP
1196	300	100	30	-4.762	260	10020	258	-9723	9.7	190	5	108	258	0.00	UP
1197	300	100	30	-4.762	260	9894	260	-9723	9.7	190	5	-19	260	0.00	UP
1198	300	100	37.5	-4.762	260	9793	255	-9723	9.7	241	6	-170	255	0.00	UP
1199	300	100	37.5	-4.762	260	9637	185	-9722	9.7	242	6	-326	186	0.00	UP
1200	300	100	37.5	-4.762	260	10200	227	-9723	9.7	242	6	235	228	0.00	UP
1201	300	100	52.5	4.762	260	10010	153	-9765	9.8	346	8	-101	153	0.00	UP
1202	300	100	52.5	4.762	260	10023	142	-9765	9.8	347	8	-90	142	0.00	UP
1203	300	100	52.5	4.762	260	9944	182	-9765	9.8	347	8	-167	183	0.00	UP
1204	300	100	7.5	14.286	260	87318	393	-87658	87.7	43	1	-382	403	0.00	UPLB
1205	300	100	7.5	14.286	260	87739	337	-87654	87.7	42	1	43	349	0.00	UPLB
1206	300	100	7.5	14.286	260	86738	396	-87658	87.7	42	1	-962	405	0.00	UPLB
1207	300	100	60	14.286	260	87622	155	-87654	87.7	397	10	-429	178	0.00	UPLB
1208	300	100	60	14.286	260	88240	168	-87652	87.7	402	10	186	190	0.00	UPLB
1209	300	100	60	14.286	260	88168	151	-87654	87.7	403	10	111	175	0.00	UPLB
1210	300	100	45	4.762	260	9878	158	-9768	9.8	296	7	-185	158	0.00	UP
1211	300	100	45	4.762	260	10002	200	-9767	9.8	295	7	-60	200	0.00	UP
1212	300	100	45	4.762	260	10047	188	-9766	9.8	295	7	-14	188	0.00	UP
1213	300	100	45	14.286	260	87890	190	-87653	87.7	294	7	-57	209	0.00	UPLB
1214	300	100	45	14.286	260	87867	233	-87658	87.7	295	7	-85	249	0.00	UPLB
1215	300	100	45	14.286	260	88103	184	-87658	87.7	294	7	150	204	0.00	UPLB
1216	300	100	74.25	4.762	260	9938	145	-9768	9.8	502	12	-332	146	0.00	UP
1217	300	100	74.25	4.762	260	10183	166	-9766	9.8	504	12	-87	167	0.00	UP
1218	300	100	74.25	4.762	260	10151	156	-9765	9.8	505	12	-119	157	0.00	UP
1219	300	100	74.25	14.286	260	87935	134	-87652	87.7	506	12	-223	161	0.00	UPLB
1220	300	100	74.25	14.286	260	88194	231	-87657	87.7	506	12	30	247	0.00	UPLB
1221	300	100	74.25	14.286	260	88345	156	-87656	87.7	507	12	183	180	0.00	UPLB
1222	300	100	30	-14.286	260	87270	311	-87526	87.5	195	5	-451	323	0.00	UPLB
1223	300	100	30	-14.286	260	88692	674	-87524	87.5	193	5	974	680	0.00	UPLB
1224	300	100	30	-14.286	260	87983	711	-87523	87.5	192	5	268	716	0.00	UPLB
1225	300	100	30	14.286	260	87192	400	-87655	87.7	192	5	-655	410	0.00	UPLB
1226	300	100	30	14.286	260	87780	249	-87658	87.7	192	5	-70	264	0.00	UPLB
1227	300	100	30	14.286	260	88016	292	-87658	87.7	192	5	167	305	0.00	UPLB
1228	300	100	67.5	4.762	260	10037	165	-9768	9.8	453	11	-184	166	0.00	UP
1229	300	100	67.5	4.762	260	10202	178	-9766	9.8	456	11	-20	178	0.00	UP
1230	300	100	67.5	4.762	260	10035	166	-9766	9.8	457	11	-189	167	0.00	UP
1231	300	100	37.5	14.286	260	87684	271	-87647	87.6	245	6	-208	285	0.00	UPLB
1232	300	100	37.5	14.286	260	87837	242	-87653	87.7	243	6	-60	257	0.00	UPLB
1233	300	100	37.5	14.286	260	88397	215	-87657	87.7	243	6	497	233	0.00	UPLB
1234	300	100	22.5	4.762	260	9901	163	-9767	9.8	141	3	-6	164	0.00	UP
1235	300	100	22.5	4.762	260	9876	156	-9766	9.8	141	3	-30	156	0.00	UP
1236	300	100	22.5	4.762	260	9885	141	-9766	9.8	140	3	-22	141	0.00	UP
1237	300	100	45	-4.762	260	10078	199	-9722	9.7	294	7	63	200	0.00	UP
1238	300	100	45	-4.762	260	10324	122	-9722	9.7	294	7	308	122	0.00	UP
1239	300	100	45	-4.762	260	10121	192	-9722	9.7	295	7	103	193	0.00	UP
1240	300	100	52.5	-14.286	260	88338	286	-87520	87.5	347	8	471	299	0.00	UPLB
1241	300	100	52.5	-14.286	260	87835	247	-87517	87.5	348	8	-30	262	0.00	UPLB
1242	300	100	52.5	-14.286	260	87927	242	-87525	87.5	348	8	55	257	0.00	UPLB
1243	300	100	22.5	14.286	260	88113	194	-87658	87.7	141	3	313	213	0.00	UPLB
1244	300	100	22.5	14.286	260	87778	182	-87660	87.7	140	3	-22	202	0.00	UPLB
1245	300	100	22.5	14.286	260	87513	179	-87659	87.7	140	3	-286	199	0.00	UPLB
1246	300	100	45	-14.286	260	87488	263	-87517	87.5	293	7	-323	277	0.00	UPLB
1247	300	100	45	-14.286	260	88040	289	-87526	87.5	294	7	220	302	0.00	UPLB
1248	300	100	45	-14.286	260	87659	271	-87523	87.5	294	7	-159	285	0.00	UPLB
1249	300	100	22.5	-4.762	260	9814	213	-9723	9.7	141	3	-50	214	0.00	UP
1250	300	100	22.5	-4.762	260	9697	169	-9722	9.7	140	3	-165	169	0.00	UP
1251	300	100	22.5	-4.762	260	9979	210	-9722	9.7	140	3	118	210	0.00	UP

Continued on next page

Table A.2 Continued from previous page

N_{run}	T [ns]	D [ns]	P [W]	B [Gauss]	θ_{pol} [deg.]	ν_{fit} [Hz]	$\Delta\nu_{\mathrm{fit}}$ [Hz]	$\mathrm{DC_B}$ [Hz]	$\Delta\mathrm{DC_B}$ [Hz]	SC [Hz]	ΔSC [Hz]	ν_0 [Hz]	$\Delta\nu_0$ [Hz]	wts. [%]	Data Type
1252	300	100	74.25	-4.762	260	10252	186	-9721	9.7	499	12	32	187	0.00	UP
1253	300	100	74.25	-4.762	260	10015	165	-9722	9.7	502	12	-208	166	0.00	UP
1254	300	100	74.25	-4.762	260	10114	165	-9722	9.7	503	12	-111	166	0.00	UP
1255	300	100	15	-14.286	260	87941	351	-87519	87.5	91	2	331	362	0.00	UPLB
1256	300	100	15	-14.286	260	87470	338	-87521	87.5	90	2	-141	349	0.00	UPLB
1257	300	100	15	-14.286	260	87573	296	-87517	87.5	90	2	-35	308	0.00	UPLB
1258	300	100	7.5	4.762	260	9880	306	-9767	9.8	42	1	71	306	0.00	UP
1259	300	100	7.5	4.762	260	9507	254	-9766	9.8	42	1	-301	254	0.00	UP
1260	300	100	7.5	4.762	260	9518	366	-9765	9.8	42	1	-289	366	0.00	UP
1261	300	100	52.5	-4.762	260	10078	210	-9723	9.7	346	8	9	210	0.00	UP
1262	300	100	52.5	-4.762	260	9970	239	-9723	9.7	349	8	-102	240	0.00	UP
1263	300	100	52.5	-4.762	260	9953	198	-9723	9.7	350	8	-119	198	0.00	UP
1264	300	100	37.5	4.762	260	9968	190	-9764	9.8	245	6	-42	190	0.00	UP
1265	300	100	37.5	4.762	260	10149	189	-9764	9.8	244	6	140	189	0.00	UP
1266	300	100	37.5	4.762	260	9609	253	-9765	9.8	244	6	-400	253	0.00	UP
1267	300	100	74.25	-14.286	260	88071	168	-87523	87.5	496	12	51	190	0.00	UPLB
1268	300	100	74.25	9.524	260	39468	141	-38939	38.9	500	12	29	146	0.00	UP
1269	300	100	74.25	-4.762	260	10325	217	-9723	9.7	499	12	103	217	0.00	UP
1270	300	100	74.25	14.286	260	88046	161	-87649	87.6	500	12	-103	183	0.00	UPLB
1271	300	100	74.25	19.048	260	156395	139	-155689	155.7	503	12	203	209	0.00	UPLB
1272	300	100	74.25	-23.81	260	243599	152	-242934	242.9	502	12	163	287	0.00	UPLB
1273	300	100	74.25	23.81	260	244117	150	-243146	243.1	502	12	469	286	0.00	UPLB
1274	300	100	74.25	-9.524	260	39403	163	-38856	38.9	502	12	45	168	0.00	UP
1275	300	100	74.25	28.572	260	351134	168	-349983	350	503	12	648	388	0.00	UPLB
1276	300	100	74.25	4.762	260	10154	144	-9771	9.8	503	12	-120	144	0.00	UP
1277	300	100	74.25	-28.572	260	350475	192	-349716	349.7	503	12	255	399	0.00	UPLB
1278	300	100	74.25	-19.048	260	156260	178	-155518	155.5	503	12	239	237	0.00	UPLB
1279	300	100	60	14.286	170	88294	212	-87655	87.7	403	10	235	230	0.00	UPLB
1280	300	100	60	14.286	170	88024	237	-87654	87.7	402	10	-32	253	0.00	UPLB
1281	300	100	60	14.286	170	88449	165	-87655	87.7	402	10	393	187	0.00	UPLB
1282	300	100	45	14.286	170	87823	252	-87654	87.7	296	7	-127	267	0.00	UPLB
1283	300	100	45	14.286	170	88177	279	-87660	87.7	294	7	223	293	0.00	UPLB
1284	300	100	45	14.286	170	88034	240	-87657	87.7	293	7	84	255	0.00	UPLB
1285	300	100	67.5	-4.762	170	10184	139	-9723	9.7	453	11	7	140	0.00	UP
1286	300	100	67.5	-4.762	170	9997	125	-9724	9.7	456	11	-182	126	0.00	UP
1287	300	100	67.5	-4.762	170	10194	102	-9723	9.7	457	11	14	103	0.00	UP
1288	300	100	67.5	4.762	170	10440	155	-9766	9.8	456	11	218	156	0.00	UP
1289	300	100	67.5	4.762	170	10350	132	-9766	9.8	454	11	130	133	0.00	UP
1290	300	100	67.5	4.762	170	10165	193	-9765	9.8	453	11	-54	193	0.00	UP
1291	300	100	52.5	-4.762	170	10011	146	-9722	9.7	347	8	-59	146	0.00	UP
1292	300	100	52.5	-4.762	170	9996	116	-9723	9.7	345	8	-72	117	0.00	UP
1293	300	100	52.5	-4.762	170	10207	160	-9722	9.7	345	8	140	160	0.00	UP
1294	300	100	15	14.286	170	87825	232	-87653	87.7	89	2	82	248	0.00	UPLB
1295	300	100	15	14.286	170	88261	225	-87654	87.7	88	2	519	241	0.00	UPLB
1296	300	100	15	14.286	170	87856	244	-87648	87.6	88	2	121	259	0.00	UPLB
1297	300	100	15	-4.762	170	9972	161	-9723	9.7	87	2	162	161	0.00	UP
1298	300	100	15	-4.762	170	9772	173	-9723	9.7	87	2	-38	173	0.00	UP
1299	300	100	15	-4.762	170	9857	167	-9723	9.7	87	2	47	167	0.00	UP
1300	300	100	22.5	-4.762	170	9739	114	-9722	9.7	137	3	-120	114	0.00	UP
1301	300	100	22.5	-4.762	170	9763	143	-9723	9.7	137	3	-97	143	0.00	UP
1302	300	100	22.5	-4.762	170	9907	127	-9721	9.7	137	3	49	127	0.00	UP
1303	300	100	60	-4.762	170	10173	141	-9722	9.7	393	9	57	142	0.00	UP
1304	300	100	60	-4.762	170	10195	176	-9722	9.7	401	10	72	176	0.00	UP
1305	300	100	60	-4.762	170	9980	115	-9723	9.7	403	10	-146	116	0.00	UP
1306	300	100	22.5	4.762	170	10119	110	-9765	9.8	141	3	213	110	0.00	UP
1307	300	100	22.5	4.762	170	9695	144	-9765	9.8	139	3	-209	144	0.00	UP
1308	300	100	22.5	4.762	170	9743	196	-9764	9.8	139	3	-160	196	0.00	UP
1309	300	100	45	4.762	170	9972	187	-9766	9.8	293	7	-86	188	0.00	UP
1310	300	100	45	4.762	170	10140	207	-9765	9.8	294	7	81	208	0.00	UP
1311	300	100	45	4.762	170	10141	155	-9765	9.8	294	7	82	155	0.00	UP
1312	300	100	74.25	-14.286	170	87822	171	-87520	87.5	500	12	-198	192	0.00	UPLB
1313	300	100	74.25	-14.286	170	87996	124	-87524	87.5	501	12	-29	152	0.00	UPLB
1314	300	100	74.25	-14.286	170	88140	174	-87525	87.5	503	12	111	196	0.00	UPLB
1315	300	100	37.5	14.286	170	88214	195	-87657	87.7	245	6	312	214	0.00	UPLB
1316	300	100	37.5	14.286	170	88111	271	-87652	87.7	243	6	216	285	0.00	UPLB
1317	300	100	37.5	14.286	170	87960	288	-87658	87.7	242	6	60	301	0.00	UPLB
1318	300	100	60	4.762	170	10127	174	-9766	9.8	399	10	-38	175	0.00	UP
1319	300	100	60	4.762	170	10097	160	-9766	9.8	401	10	-69	161	0.00	UP
1320	300	100	60	4.762	170	10362	182	-9765	9.8	401	10	196	183	0.00	UP
1321	300	100	30	-4.762	170	9709	172	-9722	9.7	192	5	-205	173	0.00	UP
1322	300	100	30	-4.762	170	10061	189	-9722	9.7	191	5	149	190	0.00	UP
1323	300	100	30	-4.762	170	9653	194	-9722	9.7	190	5	-259	195	0.00	UP
1324	300	100	52.5	14.286	170	87709	195	-87646	87.6	345	8	-282	214	0.00	UPLB
1325	300	100	52.5	14.286	170	88184	222	-87649	87.6	346	8	188	239	0.00	UPLB
1326	300	100	52.5	14.286	170	88721	175	-87652	87.7	346	8	723	196	0.00	UPLB
1327	300	100	74.25	-4.762	170	10306	135	-9724	9.7	499	12	84	136	0.00	UP
1328	300	100	74.25	-4.762	170	9877	129	-9723	9.7	500	12	-346	130	0.00	UP
1329	300	100	74.25	-4.762	170	10046	158	-9722	9.7	502	12	-178	159	0.00	UP
1330	300	100	74.25	4.762	170	10180	155	-9765	9.8	502	12	-87	155	0.00	UP
1331	300	100	74.25	4.762	170	10218	172	-9765	9.8	502	12	-50	173	0.00	UP
1332	300	100	74.25	4.762	170	10146	198	-9766	9.8	502	12	-122	198	0.00	UP
1333	300	100	30	-14.286	170	87730	268	-87520	87.5	192	5	18	282	0.00	UPLB
1334	300	100	30	-14.286	170	87297	248	-87524	87.5	190	5	-417	263	0.00	UPLB
1335	300	100	30	-14.286	170	87733	199	-87522	87.5	190	5	22	217	0.00	UPLB
1336	300	100	74.25	14.286	170	87878	191	-87652	87.7	499	12	-273	210	0.00	UPLB
1337	300	100	74.25	14.286	170	88156	208	-87652	87.7	502	12	1	226	0.00	UPLB
1338	300	100	74.25	14.286	170	87986	206	-87652	87.7	502	12	-168	224	0.00	UPLB
1339	300	100	45	-14.286	170	87634	237	-87529	87.5	295	7	-189	252	0.00	UPLB
1340	300	100	45	-14.286	170	88091	188	-87527	87.5	293	7	270	208	0.00	UPLB
1341	300	100	45	-14.286	170	87707	213	-87529	87.5	292	7	-114	230	0.00	UPLB
1342	300	100	37.5	4.762	170	9949	172	-9767	9.8	241	6	-58	173	0.00	UP
1343	300	100	37.5	4.762	170	9830	248	-9765	9.8	240	6	-175	248	0.00	UP
1344	300	100	37.5	4.762	170	10055	194	-9764	9.8	240	6	51	195	0.00	UP
1345	300	100	30	4.762	170	10050	262	-9765	9.8	189	5	95	263	0.00	UP
1346	300	100	30	4.762	170	10049	166	-9765	9.8	189	5	95	166	0.00	UP
1347	300	100	30	4.762	170	10146	282	-9765	9.8	189	5	192	282	0.00	UP
1348	300	100	60	-14.286	170	87923	165	-87518	87.5	397	10	7	187	0.00	UPLB
1349	300	100	60	-14.286	170	88030	166	-87523	87.5	399	10	109	188	0.00	UPLB

Continued on next page

Table A.2 Continued from previous page

N_{run}	T [ns]	D [ns]	P [W]	B [Gauss]	θ_{pol} [deg.]	ν_{fit} [Hz]	$\Delta\nu_{\mathrm{fit}}$ [Hz]	$\mathrm{DC_B}$ [Hz]	$\Delta\mathrm{DC_B}$ [Hz]	SC [Hz]	ΔSC [Hz]	ν_0 [Hz]	$\Delta\nu_0$ [Hz]	wts. [%]	Data Type
1350	300	100	60	-14.286	170	87666	182	-87528	87.5	399	10	-260	202	0.00	UPLB
1351	300	100	22.5	14.286	170	87949	217	-87654	87.7	139	3	157	234	0.00	UPLB
1352	300	100	22.5	14.286	170	88271	157	-87651	87.7	138	3	482	180	0.00	UPLB
1353	300	100	22.5	14.286	170	88315	212	-87655	87.7	138	3	522	229	0.00	UPLB
1354	300	100	22.5	-14.286	170	87316	139	-87526	87.5	138	3	-347	165	0.00	UPLB
1355	300	100	22.5	-14.286	170	87899	154	-87522	87.5	138	3	239	177	0.00	UPLB
1356	300	100	22.5	-14.286	170	87600	214	-87521	87.5	138	3	-59	231	0.00	UPLB
1357	300	100	37.5	-14.286	170	87529	206	-87526	87.5	239	6	-236	224	0.00	UPLB
1358	300	100	37.5	-14.286	170	88133	196	-87524	87.5	240	6	369	214	0.00	UPLB
1359	300	100	37.5	-14.286	170	87682	219	-87524	87.5	240	6	-82	236	0.00	UPLB
1360	300	100	15	4.762	170	9642	192	-9767	9.8	90	2	-214	192	0.00	UP
1361	300	100	15	4.762	170	10016	192	-9766	9.8	90	2	161	192	0.00	UP
1362	300	100	15	4.762	170	9717	201	-9766	9.8	90	2	-139	201	0.00	UP
1363	300	100	15	-14.286	170	87436	179	-87522	87.5	90	2	-176	200	0.00	UPLB
1364	300	100	15	-14.286	170	87613	164	-87527	87.5	90	2	-3	186	0.00	UPLB
1365	300	100	15	-14.286	170	87837	182	-87521	87.5	90	2	226	202	0.00	UPLB
1366	300	100	37.5	-4.762	170	9629	202	-9724	9.7	240	6	-335	203	0.00	UP
1367	300	100	37.5	-4.762	170	9672	196	-9723	9.7	241	6	-293	197	0.00	UP
1368	300	100	37.5	-4.762	170	9894	189	-9723	9.7	241	6	-71	189	0.00	UP
1369	300	100	7.5	4.762	170	9921	299	-9765	9.8	42	1	114	299	0.00	UP
1370	300	100	7.5	4.762	170	9361	278	-9765	9.8	42	1	-446	278	0.00	UP
1371	300	100	7.5	4.762	170	10042	234	-9764	9.8	42	1	237	234	0.00	UP
1372	300	100	7.5	-4.762	170	9746	259	-9722	9.7	42	1	-18	259	0.00	UP
1373	300	100	7.5	-4.762	170	9475	201	-9723	9.7	41	1	-289	202	0.00	UP
1374	300	100	7.5	-4.762	170	9833	265	-9721	9.7	41	1	70	265	0.00	UP
1375	300	100	52.5	-14.286	170	87999	169	-87521	87.5	339	8	139	191	0.00	UPLB
1376	300	100	52.5	-14.286	170	87877	159	-87521	87.5	341	8	14	182	0.00	UPLB
1377	300	100	52.5	-14.286	170	87908	158	-87521	87.5	342	8	45	181	0.00	UPLB
1378	300	100	52.5	4.762	170	10220	196	-9766	9.8	342	8	112	196	0.00	UP
1379	300	100	52.5	4.762	170	9737	197	-9766	9.8	343	8	-372	197	0.00	UP
1380	300	100	52.5	4.762	170	10037	148	-9765	9.8	343	8	-71	148	0.00	UP
1381	300	100	30	14.286	170	88226	268	-87651	87.7	191	5	384	282	0.00	UPLB
1382	300	100	30	14.286	170	88073	270	-87652	87.7	191	5	230	284	0.00	UPLB
1383	300	100	30	14.286	170	88037	319	-87648	87.6	190	5	199	331	0.00	UPLB
1384	300	100	67.5	-14.286	170	88090	135	-87529	87.5	446	11	114	161	0.00	UPLB
1385	300	100	67.5	-14.286	170	87958	139	-87523	87.5	449	11	-14	165	0.00	UPLB
1386	300	100	67.5	-14.286	170	88039	141	-87528	87.5	448	11	62	166	0.00	UPLB
1387	300	100	7.5	-14.286	170	87420	307	-87527	87.5	43	1	-149	319	0.00	UPLB
1388	300	100	7.5	-14.286	170	87442	291	-87528	87.5	42	1	-129	304	0.00	UPLB
1389	300	100	7.5	-14.286	170	87472	249	-87523	87.5	43	1	-93	264	0.00	UPLB
1390	300	100	7.5	14.286	170	88394	422	-87652	87.7	43	1	699	431	0.00	UPLB
1391	300	100	7.5	14.286	170	87217	332	-87652	87.7	42	1	-477	344	0.00	UPLB
1392	300	100	7.5	14.286	170	88243	398	-87650	87.6	43	1	550	407	0.00	UPLB
1393	300	100	67.5	14.286	170	88181	250	-87652	87.7	452	11	78	265	0.00	UPLB
1394	300	100	67.5	14.286	170	87937	212	-87649	87.6	456	11	-167	230	0.00	UPLB
1395	300	100	67.5	14.286	170	88416	214	-87645	87.6	458	11	313	231	0.00	UPLB
1396	300	100	45	-4.762	170	10017	207	-9727	9.7	299	7	-10	207	0.00	UP
1397	300	100	45	-4.762	170	9833	185	-9726	9.7	299	7	-192	186	0.00	UP
1398	300	100	45	-4.762	170	10142	158	-9724	9.7	298	7	120	159	0.00	UP
1399	300	100	22.5	4.762	170	9908	128	-9763	9.8	143	3	1	128	0.00	UP
1400	300	100	22.5	4.762	170	10124	151	-9763	9.8	143	3	218	151	0.00	UP
1401	300	100	22.5	14.286	170	88030	188	-87648	87.6	143	3	239	207	0.00	UPLB
1402	300	100	22.5	14.286	170	87854	248	-87652	87.7	142	3	59	263	0.00	UPLB
1403	300	100	60	-4.762	170	10188	179	-9725	9.7	399	10	63	179	0.00	UP
1404	300	100	60	-4.762	170	9868	143	-9724	9.7	401	10	-258	144	0.00	UP
1405	300	100	7.5	-14.286	170	87894	291	-87525	87.5	43	1	326	303	0.00	UPLB
1406	300	100	7.5	-14.286	170	87496	367	-87527	87.5	43	1	-74	378	0.00	UPLB
1407	300	100	74.25	-14.286	170	87993	145	-87530	87.5	502	12	-39	170	0.00	UPLB
1408	300	100	74.25	-14.286	170	88180	197	-87530	87.5	507	12	143	216	0.00	UPLB
1409	300	100	7.5	4.762	170	10001	228	-9764	9.8	43	1	194	228	0.00	UP
1410	300	100	7.5	4.762	170	10023	213	-9763	9.8	43	1	216	213	0.00	UP
1411	300	100	45	-14.286	170	87766	184	-87524	87.5	298	7	-56	204	0.00	UPLB
1412	300	100	45	-14.286	170	87726	244	-87529	87.5	300	7	-102	260	0.00	UPLB
1413	300	100	37.5	-14.286	170	87939	293	-87526	87.5	248	6	165	305	0.00	UPLB
1414	300	100	37.5	-14.286	170	87879	213	-87529	87.5	248	6	102	230	0.00	UPLB
1415	300	100	67.5	-4.762	170	10103	158	-9726	9.7	457	11	-79	159	0.00	UP
1416	300	100	67.5	-4.762	170	10084	140	-9725	9.7	457	11	-98	141	0.00	UP
1417	300	100	30	4.762	170	10173	181	-9764	9.8	195	5	214	181	0.00	UP
1418	300	100	30	4.762	170	9594	190	-9763	9.8	194	5	-364	190	0.00	UP
1419	300	100	30	-4.762	170	9919	219	-9724	9.7	195	5	1	219	0.00	UP
1420	300	100	30	-4.762	170	10037	227	-9725	9.7	194	5	118	228	0.00	UP
1421	300	100	74.25	14.286	170	88167	194	-87644	87.6	502	12	21	213	0.00	UPLB
1422	300	100	74.25	14.286	170	87942	181	-87651	87.7	504	12	-212	201	0.00	UPLB
1423	300	100	52.5	14.286	170	87908	213	-87647	87.6	351	8	-90	231	0.00	UPLB
1424	300	100	52.5	14.286	170	87852	261	-87648	87.6	350	8	-146	275	0.00	UPLB
1425	300	100	7.5	-4.762	170	9856	222	-9725	9.7	43	1	88	222	0.00	UP
1426	300	100	7.5	-4.762	170	9663	293	-9724	9.7	43	1	-105	293	0.00	UP
1427	300	100	45	-4.762	170	9977	177	-9724	9.7	298	7	-45	177	0.00	UP
1428	300	100	45	-4.762	170	9892	188	-9725	9.7	299	7	-131	189	0.00	UP
1429	300	100	37.5	-4.762	170	9993	170	-9725	9.7	247	6	20	171	0.00	UP
1430	300	100	37.5	-4.762	170	9823	188	-9725	9.7	247	6	-149	189	0.00	UP
1431	300	100	67.5	4.762	170	10374	149	-9764	9.8	456	11	154	150	0.00	UP
1432	300	100	67.5	4.762	170	10011	176	-9765	9.8	456	11	-210	177	0.00	UP
1433	300	100	67.5	-14.286	170	88307	183	-87524	87.5	455	11	329	203	0.00	UPLB
1434	300	100	67.5	-14.286	170	87421	190	-87526	87.5	456	11	-560	209	0.00	UPLB
1435	300	100	15	4.762	170	10060	192	-9765	9.8	91	2	203	192	0.00	UP
1436	300	100	15	4.762	170	9991	195	-9764	9.8	90	2	137	195	0.00	UP
1437	300	100	52.5	-14.286	170	87832	278	-87527	87.5	344	8	-39	292	0.00	UPLB
1438	300	100	52.5	-14.286	170	88156	159	-87530	87.5	347	8	280	182	0.00	UPLB
1439	300	100	15	14.286	170	87991	292	-87646	87.6	91	2	253	305	0.00	UPLB
1440	300	100	15	14.286	170	87731	288	-87648	87.6	91	2	-8	301	0.00	UPLB
1441	300	100	60	14.286	170	88093	198	-87644	87.6	395	9	54	217	0.00	UPLB
1442	300	100	60	14.286	170	88217	235	-87648	87.6	398	10	171	251	0.00	UPLB
1443	300	100	45	4.762	170	9854	237	-9765	9.8	296	7	-206	237	0.00	UP
1444	300	100	45	4.762	170	10100	218	-9763	9.8	295	7	42	219	0.00	UP
1445	300	100	30	14.286	170	87859	273	-87646	87.6	192	5	20	287	0.00	UPLB
1446	300	100	30	14.286	170	87671	319	-87642	87.6	192	5	-164	331	0.00	UPLB
1447	300	100	15	-14.286	170	87875	190	-87526	87.5	91	2	258	209	0.00	UPLB

Continued on next page

Table A.2 Continued from previous page

$N_{\rm run}$	T [ns]	D [ns]	P [W]	B [Gauss]	$\theta_{\rm pol}$ [deg.]	$\nu_{\rm fit}$ [Hz]	$\Delta\nu_{\rm fit}$ [Hz]	$\rm DC_B$ [Hz]	$\Delta\rm DC_B$ [Hz]	SC [Hz]	ΔSC [Hz]	ν_0 [Hz]	$\Delta\nu_0$ [Hz]	wts. [%]	Data Type
1448	300	100	15	-14.286	170	87589	254	-87527	87.5	91	2	-29	269	0.00	UPLB
1449	300	100	37.5	14.286	170	88404	307	-87652	87.7	244	6	508	319	0.00	UPLB
1450	300	100	37.5	14.286	170	87483	273	-87649	87.6	245	6	-411	287	0.00	UPLB
1451	300	100	60	4.762	170	10156	179	-9765	9.8	401	10	-10	179	0.00	UP
1452	300	100	60	4.762	170	10195	158	-9764	9.8	403	10	28	158	0.00	UP
1453	300	100	60	-14.286	170	87733	147	-87524	87.5	403	10	-194	171	0.00	UPLB
1454	300	100	60	-14.286	170	88039	218	-87528	87.5	403	10	108	235	0.00	UPLB
1455	300	100	22.5	-14.286	170	87793	213	-87528	87.5	143	3	122	230	0.00	UPLB
1456	300	100	22.5	-14.286	170	87552	178	-87530	87.5	143	3	-121	198	0.00	UPLB
1457	300	100	15	-4.762	170	9842	192	-9726	9.7	92	2	24	192	0.00	UP
1458	300	100	15	-4.762	170	9685	167	-9726	9.7	92	2	-133	167	0.00	UP
1459	300	100	67.5	14.286	170	88015	215	-87645	87.6	454	11	-84	232	0.00	UPLB
1460	300	100	67.5	14.286	170	87967	211	-87648	87.6	457	11	-138	228	0.00	UPLB
1461	300	100	74.25	-4.762	170	10205	166	-9726	9.7	503	12	-25	167	0.00	UP
1462	300	100	74.25	-4.762	170	10182	141	-9725	9.7	502	12	-45	142	0.00	UP
1463	300	100	52.5	4.762	170	9779	142	-9763	9.8	350	8	-334	143	0.00	UP
1464	300	100	52.5	4.762	170	10327	207	-9764	9.8	348	8	215	208	0.00	UP
1465	300	100	7.5	14.286	170	89415	414	-87648	87.6	43	1	1724	423	0.00	UPLB
1466	300	100	7.5	14.286	170	87817	445	-87648	87.6	43	1	126	454	0.00	UPLB
1467	300	100	37.5	4.762	170	9936	220	-9766	9.8	244	6	-74	221	0.00	UP
1468	300	100	37.5	4.762	170	10521	201	-9763	9.8	245	6	512	201	0.00	UP
1469	300	100	30	-14.286	170	87640	281	-87526	87.5	195	5	-81	294	0.00	UPLB
1470	300	100	30	-14.286	170	87800	327	-87524	87.5	194	5	82	339	0.00	UPLB
1471	300	100	52.5	-4.762	170	9962	178	-9727	9.7	349	8	-114	179	0.00	UP
1472	300	100	52.5	-4.762	170	10121	166	-9724	9.7	350	8	47	167	0.00	UP
1473	300	100	22.5	-4.762	170	9853	151	-9726	9.7	143	3	-15	151	0.00	UP
1474	300	100	22.5	-4.762	170	9926	161	-9725	9.7	143	3	59	162	0.00	UP
1475	300	100	45	14.286	170	87886	309	-87644	87.6	296	7	-54	321	0.00	UPLB
1476	300	100	45	14.286	170	88067	329	-87643	87.6	298	7	126	340	0.00	UPLB
1477	300	100	74.25	4.762	170	10298	157	-9764	9.8	505	12	29	158	0.00	UP
1478	300	100	74.25	4.762	170	10361	131	-9763	9.8	505	12	92	132	0.00	UP
1479	400	100	30	14.286	170	88349	426	-87645	87.6	148	4	556	435	0.00	UPLB
1480	300	100	15	-14.286	170	87442	258	-87532	87.5	92	2	-181	272	0.00	UPLB
1481	300	100	15	-14.286	170	87641	191	-87530	87.5	92	2	19	210	0.00	UPLB
1482	300	100	22.5	4.762	170	10023	184	-9763	9.8	142	3	118	184	0.00	UP
1483	300	100	22.5	4.762	170	9530	211	-9763	9.8	142	3	-375	211	0.00	UP
1484	400	100	74.25	-4.762	170	10033	242	-9725	9.7	389	9	-82	242	0.00	UP
1485	400	100	74.25	-4.762	170	9961	248	-9726	9.7	392	9	-157	248	0.00	UP
1486	400	100	60	-4.762	170	9769	265	-9724	9.7	312	7	-267	265	0.00	UP
1487	400	100	60	-4.762	170	9769	181	-9725	9.7	311	7	-267	181	0.00	UP
1488	400	100	52.5	4.762	170	10570	270	-9763	9.8	270	6	537	270	0.00	UP
1489	400	100	52.5	4.762	170	10045	306	-9763	9.8	269	6	13	306	0.00	UP
1490	300	100	15	4.762	170	9961	241	-9763	9.8	92	2	105	241	0.00	UP
1491	300	100	15	4.762	170	9724	221	-9762	9.8	92	2	-130	221	0.00	UP
1492	300	100	67.5	-14.286	170	87723	228	-87534	87.5	455	11	-266	244	0.00	UPLB
1493	300	100	67.5	-14.286	170	87963	217	-87531	87.5	457	11	-25	234	0.00	UPLB
1494	300	100	37.5	4.762	170	9306	190	-9765	9.8	246	6	-705	190	0.00	UP
1495	300	100	37.5	4.762	170	10053	223	-9764	9.8	245	6	43	223	0.00	UP
1496	400	100	74.25	4.762	170	10412	248	-9763	9.8	391	9	259	249	0.00	UP
1497	400	100	74.25	4.762	170	10220	263	-9763	9.8	393	9	65	263	0.00	UP
1498	300	100	7.5	-14.286	170	87763	419	-87531	87.5	43	1	189	428	0.00	UPLB
1499	300	100	7.5	-14.286	170	86407	566	-87528	87.5	43	1	-1163	573	0.00	UPLB
1500	300	100	37.5	-14.286	170	87550	297	-87530	87.5	244	6	-225	309	0.00	UPLB
1501	300	100	37.5	-14.286	170	87419	396	-87536	87.5	246	6	-362	405	0.00	UPLB
1502	400	100	52.5	-4.762	170	10475	324	-9728	9.7	268	6	479	324	0.00	UP
1503	400	100	52.5	-4.762	170	10116	248	-9726	9.7	268	6	122	248	0.00	UP
1504	300	100	37.5	14.286	170	87889	307	-87643	87.6	246	6	-1	319	0.00	UPLB
1505	300	100	37.5	14.286	170	88374	451	-87647	87.6	246	6	481	460	0.00	UPLB
1506	300	100	60	14.286	170	88139	269	-87646	87.6	402	10	90	283	0.00	UPLB
1507	300	100	60	14.286	170	88222	240	-87646	87.6	403	10	173	256	0.00	UPLB
1508	300	100	22.5	-14.286	170	87577	240	-87531	87.5	143	3	-97	255	0.00	UPLB
1509	300	100	22.5	-14.286	170	87408	198	-87532	87.5	143	3	-267	217	0.00	UPLB
1510	400	100	45	-4.762	170	9978	256	-9727	9.7	226	5	25	257	0.00	UP
1511	400	100	45	-4.762	170	9889	244	-9726	9.7	227	5	-64	245	0.00	UP
1512	300	100	74.25	-14.286	170	87700	188	-87530	87.5	507	12	-338	207	0.00	UPLB
1513	300	100	74.25	-14.286	170	88051	197	-87534	87.5	505	12	13	216	0.00	UPLB
1514	400	100	37.5	-4.762	170	10168	373	-9727	9.7	187	4	254	373	0.00	UP
1515	400	100	37.5	-4.762	170	9911	342	-9726	9.7	186	4	-1	342	0.00	UP
1516	400	100	22.5	-4.762	170	10006	191	-9725	9.7	107	3	174	191	0.00	UP
1517	400	100	22.5	-4.762	170	9974	212	-9725	9.7	107	3	142	212	0.00	UP
1518	400	100	7.5	-4.762	170	9448	551	-9724	9.7	32	1	-307	551	0.00	UP
1519	400	100	7.5	-4.762	170	9359	452	-9724	9.7	32	1	-397	452	0.00	UP
1520	300	100	15	14.286	170	87644	380	-87647	87.6	93	2	-95	390	0.00	UPLB
1521	300	100	15	14.286	170	88308	276	-87648	87.6	93	2	567	289	0.00	UPLB
1522	400	100	30	-4.762	170	10277	353	-9726	9.7	148	4	403	354	0.00	UP
1523	400	100	30	-4.762	170	9825	311	-9726	9.7	148	4	-49	311	0.00	UP
1524	300	100	67.5	14.286	170	88000	208	-87647	87.6	456	11	-104	226	0.00	UPLB
1525	300	100	67.5	14.286	170	88391	256	-87650	87.6	457	11	284	271	0.00	UPLB
1526	300	100	52.5	-14.286	170	87904	197	-87529	87.5	351	8	23	216	0.00	UPLB
1527	300	100	52.5	-14.286	170	87815	257	-87528	87.5	351	8	-64	272	0.00	UPLB
1528	300	100	74.25	14.286	170	88477	247	-87647	87.6	504	12	327	262	0.00	UPLB
1529	300	100	74.25	14.286	170	88220	190	-87657	87.7	503	12	60	210	0.00	UPLB
1530	300	100	7.5	14.286	170	88720	454	-87650	87.7	43	1	1026	462	0.00	UPLB
1531	300	100	7.5	14.286	170	88349	428	-87652	87.7	43	1	654	437	0.00	UPLB
1532	300	100	22.5	14.286	170	87235	339	-87646	87.6	144	3	-554	350	0.00	UPLB
1533	300	100	22.5	14.286	170	87778	319	-87645	87.6	144	3	-10	331	0.00	UPLB
1534	300	100	7.5	4.762	170	9921	220	-9765	9.8	43	1	113	220	0.00	UP
1535	300	100	7.5	4.762	170	9689	378	-9764	9.8	43	1	-118	378	0.00	UP
1536	300	100	30	4.762	170	9849	280	-9764	9.8	194	5	-108	280	0.00	UP
1537	300	100	30	4.762	170	10483	227	-9764	9.8	195	5	524	227	0.00	UP
1538	300	100	52.5	14.286	170	87788	189	-87647	87.6	349	8	-208	209	0.00	UPLB
1539	300	100	52.5	14.286	170	88049	253	-87646	87.6	350	8	53	268	0.00	UPLB
1540	400	100	15	-4.762	170	9757	331	-9726	9.7	69	2	-38	331	0.00	UP
1541	400	100	15	-4.762	170	10052	346	-9725	9.7	69	2	258	346	0.00	UP
1542	300	100	45	4.762	170	10397	221	-9762	9.8	295	7	339	222	0.00	UP
1543	300	100	45	4.762	170	9988	245	-9763	9.8	297	7	-71	245	0.00	UP
1544	300	100	45	14.286	170	88076	286	-87642	87.6	297	7	137	299	0.00	UPLB
1545	300	100	45	14.286	170	88388	260	-87644	87.6	297	7	447	274	0.00	UPLB

Continued on next page

Table A.2 Continued from previous page

N_{run}	T [ns]	D [ns]	P [W]	B [Gauss]	θ_{pol} [deg.]	ν_{fit} [Hz]	$\Delta\nu_{\mathrm{fit}}$ [Hz]	$\mathrm{DC_B}$ [Hz]	$\Delta\mathrm{DC_B}$ [Hz]	SC [Hz]	ΔSC [Hz]	ν_0 [Hz]	$\Delta\nu_0$ [Hz]	wts. [%]	Data Type
1546	300	100	30	-14.286	170	88022	343	-87528	87.5	194	5	301	354	0.00	UPLB
1547	300	100	30	-14.286	170	87855	281	-87531	87.5	194	5	130	295	0.00	UPLB
1548	300	100	45	-14.286	170	87883	228	-87528	87.5	296	7	59	244	0.00	UPLB
1549	300	100	45	-14.286	170	87957	296	-87525	87.5	297	7	135	308	0.00	UPLB
1550	400	100	67.5	-4.762	170	10125	170	-9727	9.7	350	8	48	171	0.00	UP
1551	400	100	67.5	-4.762	170	9886	196	-9725	9.7	352	8	-191	197	0.00	UP
1552	400	100	60	4.762	170	10562	289	-9763	9.8	310	7	489	290	0.00	UP
1553	400	100	60	4.762	170	10189	299	-9764	9.8	309	7	116	300	0.00	UP
1554	300	100	30	14.286	170	87747	369	-87644	87.6	195	5	-92	380	0.00	UPLB
1555	300	100	30	14.286	170	88118	344	-87648	87.6	194	5	277	355	0.00	UPLB
1556	400	100	67.5	4.762	170	9886	298	-9764	9.8	350	8	-228	299	0.00	UP
1557	400	100	67.5	4.762	170	10260	259	-9763	9.8	352	8	145	260	0.00	UP
1558	300	100	60	-14.286	170	87864	175	-87527	87.5	404	10	-67	196	0.00	UPLB
1559	300	100	60	-14.286	170	88011	194	-87528	87.5	404	10	79	213	0.00	UPLB
1560	300	100	74.25	14.286	170	88438	224	-87655	87.7	498	12	284	241	0.00	UPLB
1561	300	100	74.25	14.286	170	88376	242	-87653	87.7	499	12	225	258	0.00	UPLB
1562	300	100	22.5	4.762	170	9929	142	-9766	9.8	138	3	24	143	0.00	UP
1563	300	100	22.5	4.762	170	9744	196	-9765	9.8	138	3	-158	196	0.00	UP
1564	300	100	74.25	-4.762	170	10538	199	-9723	9.7	494	12	321	200	0.00	UP
1565	300	100	74.25	-4.762	170	10132	164	-9722	9.7	498	12	-88	165	0.00	UP
1566	300	100	60	14.286	170	88048	263	-87647	87.6	398	10	3	277	0.00	UPLB
1567	300	100	60	14.286	170	88139	278	-87652	87.7	396	10	90	292	0.00	UPLB
1568	300	100	67.5	-4.762	170	10137	158	-9725	9.7	449	11	-37	159	0.00	UP
1569	300	100	67.5	-4.762	170	10126	143	-9723	9.7	449	11	-46	144	0.00	UP
1570	300	100	52.5	-14.286	170	87536	229	-87525	87.5	345	8	-334	245	0.00	UPLB
1571	300	100	52.5	-14.286	170	87795	196	-87525	87.5	343	8	-73	215	0.00	UPLB
1572	300	100	74.25	4.762	170	10383	159	-9766	9.8	498	12	119	159	0.00	UP
1573	300	100	74.25	4.762	170	10385	134	-9766	9.8	500	12	119	135	0.00	UP
1574	300	100	67.5	-14.286	170	88255	159	-87524	87.5	451	11	281	182	0.00	UPLB
1575	300	100	67.5	-14.286	170	88075	250	-87524	87.5	451	11	100	265	0.00	UPLB
1576	300	100	7.5	-14.286	170	87632	358	-87526	87.5	41	1	65	368	0.00	UPLB
1577	300	100	7.5	-14.286	170	86862	351	-87527	87.5	41	1	-706	362	0.00	UPLB
1578	300	100	37.5	14.286	170	87740	250	-87652	87.7	238	6	-150	265	0.00	UPLB
1579	300	100	37.5	14.286	170	88333	379	-87651	87.7	239	6	443	389	0.00	UPLB
1580	300	100	7.5	4.762	170	9796	270	-9766	9.8	41	1	-11	270	0.00	UP
1581	300	100	7.5	4.762	170	10156	229	-9765	9.8	41	1	351	229	0.00	UP
1582	300	100	52.5	4.762	170	10206	198	-9764	9.8	340	8	102	199	0.00	UP
1583	300	100	52.5	4.762	170	9843	176	-9765	9.8	343	8	-265	177	0.00	UP
1584	300	100	45	14.286	170	88611	272	-87648	87.6	291	7	673	286	0.00	UPLB
1585	300	100	45	14.286	170	87771	210	-87654	87.7	290	7	-174	228	0.00	UPLB
1586	300	100	15	-4.762	170	10003	206	-9725	9.7	88	2	190	207	0.00	UP
1587	300	100	15	-4.762	170	9672	172	-9723	9.7	88	2	-138	172	0.00	UP
1588	300	100	30	-4.762	170	9956	268	-9722	9.7	186	4	47	269	0.00	UP
1589	300	100	30	-4.762	170	9861	195	-9723	9.7	186	4	-48	196	0.00	UP
1590	300	100	7.5	14.286	170	88318	354	-87650	87.6	41	1	628	365	0.00	UPLB
1591	300	100	7.5	14.286	170	87629	334	-87648	87.6	40	1	-59	345	0.00	UPLB
1592	300	100	37.5	-4.762	170	10048	269	-9726	9.7	234	6	88	269	0.00	UP
1593	300	100	37.5	-4.762	170	10164	172	-9725	9.7	236	6	203	172	0.00	UP
1594	300	100	15	-14.286	170	87919	242	-87524	87.5	88	2	307	258	0.00	UPLB
1595	300	100	15	-14.286	170	87506	213	-87525	87.5	88	2	-107	230	0.00	UPLB
1596	300	100	37.5	4.762	170	9828	226	-9767	9.8	236	6	-175	226	0.00	UP
1597	300	100	37.5	4.762	170	9946	198	-9765	9.8	236	6	-56	198	0.00	UP
1598	300	100	52.5	14.286	170	88042	246	-87650	87.7	339	8	53	261	0.00	UPLB
1599	300	100	52.5	14.286	170	88180	214	-87654	87.7	340	8	186	232	0.00	UPLB
1600	300	100	22.5	14.286	170	88016	223	-87652	87.7	138	3	226	240	0.00	UPLB
1601	300	100	30	-4.762	170	9537	186	-9724	9.7	189	5	-375	186	0.00	UP
1602	300	100	30	-4.762	170	9957	234	-9723	9.7	189	5	45	234	0.00	UP
1603	300	100	60	-4.762	170	9924	139	-9722	9.7	390	9	-188	140	0.00	UP
1604	300	100	60	-4.762	170	10197	189	-9723	9.7	392	9	83	190	0.00	UP
1605	400	100	15	4.762	170	9744	228	-9765	9.8	67	2	-88	228	0.00	UP
1606	400	100	15	4.762	170	9693	265	-9765	9.8	67	2	-139	265	0.00	UP
1607	400	100	22.5	-4.762	170	9860	227	-9722	9.7	104	3	34	227	0.00	UP
1608	400	100	22.5	-4.762	170	9783	176	-9723	9.7	104	3	-44	176	0.00	UP
1609	300	100	37.5	4.762	170	10052	191	-9766	9.8	239	6	48	191	0.00	UP
1610	300	100	37.5	4.762	170	10321	186	-9765	9.8	239	6	316	186	0.00	UP
1611	400	100	60	4.762	170	9839	172	-9766	9.8	301	7	-227	173	0.00	UP
1612	400	100	60	4.762	170	9992	181	-9765	9.8	302	7	-75	182	0.00	UP
1613	400	100	30	-4.762	170	9602	339	-9722	9.7	144	3	-264	340	0.00	UP
1614	400	100	30	-4.762	170	10124	314	-9722	9.7	143	3	259	314	0.00	UP
1615	300	100	15	-4.762	170	9751	213	-9722	9.7	90	2	-61	213	0.00	UP
1616	300	100	15	-4.762	170	9835	167	-9723	9.7	89	2	23	167	0.00	UP
1617	300	100	67.5	-4.762	170	10057	169	-9721	9.7	443	11	-107	170	0.00	UP
1618	300	100	67.5	-4.762	170	10051	193	-9722	9.7	445	11	-116	194	0.00	UP
1619	300	100	7.5	4.762	170	9693	235	-9764	9.8	42	1	-113	235	0.00	UP
1620	300	100	7.5	4.762	170	9842	341	-9764	9.8	41	1	36	341	0.00	UP
1621	300	100	52.5	-4.762	170	9971	150	-9721	9.7	339	8	-90	151	0.00	UP
1622	300	100	52.5	-4.762	170	9701	161	-9723	9.7	341	8	-362	162	0.00	UP
1623	300	100	60	4.762	170	10219	173	-9764	9.8	392	9	63	173	0.00	UP
1624	300	100	60	4.762	170	10293	225	-9764	9.8	392	9	137	225	0.00	UP
1625	300	100	7.5	-4.762	170	10365	302	-9722	9.7	42	1	601	302	0.00	UP
1626	300	100	7.5	-4.762	170	9718	246	-9722	9.7	41	1	-46	246	0.00	UP
1627	300	100	22.5	-4.762	170	10022	157	-9722	9.7	138	3	162	158	0.00	UP
1628	300	100	22.5	-4.762	170	9807	149	-9722	9.7	138	3	-53	149	0.00	UP
1629	300	100	60	-4.762	170	10179	135	-9723	9.7	390	9	66	135	0.00	UP
1630	300	100	60	-4.762	170	10322	145	-9723	9.7	391	9	208	146	0.00	UP
1631	400	100	45	-4.762	170	10062	238	-9722	9.7	221	5	119	238	0.00	UP
1632	400	100	45	-4.762	170	10037	207	-9722	9.7	221	5	94	208	0.00	UP
1633	400	100	74.25	-4.762	170	10110	210	-9722	9.7	379	9	9	211	0.00	UP
1634	400	100	74.25	-4.762	170	10101	193	-9722	9.7	381	9	-3	194	0.00	UP
1635	400	100	67.5	4.762	170	9915	235	-9764	9.8	344	8	-194	235	0.00	UP
1636	400	100	67.5	4.762	170	10238	229	-9764	9.8	344	8	130	230	0.00	UP
1637	300	100	67.5	4.762	170	9955	137	-9765	9.8	446	11	-256	138	0.00	UP
1638	300	100	67.5	4.762	170	10000	124	-9766	9.8	452	11	-217	125	0.00	UP
1639	400	100	45	4.762	170	9767	245	-9765	9.8	227	5	-225	245	0.00	UP
1640	400	100	45	4.762	170	9607	274	-9765	9.8	225	5	-383	274	0.00	UP
1641	400	100	7.5	-4.762	170	9380	374	-9722	9.7	31	1	-372	374	0.00	UP
1642	400	100	7.5	-4.762	170	9873	287	-9723	9.7	31	1	119	287	0.00	UP
1643	400	100	7.5	4.762	170	9558	462	-9766	9.8	30	1	-238	462	0.00	UP

Continued on next page

Table A.2 Continued from previous page

N_{run}	T [ns]	D [ns]	P [W]	B [Gauss]	θ_{pol} [deg.]	ν_{fit} [Hz]	$\Delta\nu_{\mathrm{fit}}$ [Hz]	$\mathrm{DC_B}$ [Hz]	$\Delta\mathrm{DC_B}$ [Hz]	SC [Hz]	ΔSC [Hz]	ν_0 [Hz]	$\Delta\nu_0$ [Hz]	wts. [%]	Data Type
1644	400	100	7.5	4.762	170	9366	408	-9765	9.8	30	1	-429	408	0.00	UP
1645	400	100	52.5	4.762	170	10089	188	-9766	9.8	258	6	65	188	0.00	UP
1646	400	100	52.5	4.762	170	10342	268	-9765	9.8	261	6	316	268	0.00	UP
1647	300	100	45	4.762	170	10111	205	-9766	9.8	291	7	54	205	0.00	UP
1648	300	100	45	4.762	170	10067	224	-9766	9.8	292	7	9	225	0.00	UP
1649	400	100	22.5	4.762	170	10141	196	-9765	9.8	105	3	271	197	0.00	UP
1650	400	100	22.5	4.762	170	10069	172	-9765	9.8	105	3	199	172	0.00	UP
1651	300	100	37.5	-4.762	170	10001	199	-9721	9.7	239	6	40	199	0.00	UP
1652	300	100	37.5	-4.762	170	10146	200	-9720	9.7	239	6	186	200	0.00	UP
1653	300	100	52.5	4.762	170	9977	183	-9765	9.8	342	8	-131	184	0.00	UP
1654	300	100	52.5	4.762	170	9968	177	-9764	9.8	342	8	-139	178	0.00	UP
1655	300	100	37.5	4.762	170	9803	172	-9765	9.8	240	6	-202	172	0.00	UP
1656	300	100	37.5	4.762	170	9933	183	-9765	9.8	239	6	-71	183	0.00	UP
1657	300	100	74.25	4.762	170	10318	179	-9766	9.8	494	12	57	180	0.00	UP
1658	300	100	74.25	4.762	170	10196	130	-9766	9.8	496	12	-67	131	0.00	UP
1659	400	100	74.25	4.762	170	10453	259	-9766	9.8	383	9	305	260	0.00	UP
1660	400	100	74.25	4.762	170	10135	178	-9765	9.8	382	9	-12	178	0.00	UP
1661	300	100	30	4.762	170	9845	199	-9766	9.8	190	5	-111	199	0.00	UP
1662	300	100	30	4.762	170	9866	215	-9765	9.8	187	5	-86	215	0.00	UP
1663	300	100	45	-4.762	170	9904	161	-9722	9.7	287	7	-105	161	0.00	UP
1664	300	100	45	-4.762	170	10072	198	-9721	9.7	287	7	64	198	0.00	UP
1665	400	100	15	4.762	170	9757	250	-9766	9.8	66	2	-75	250	0.00	UP
1666	400	100	15	4.762	170	9374	255	-9766	9.8	66	2	-457	255	0.00	UP
1667	400	100	15	-4.762	170	10002	240	-9721	9.7	65	2	216	240	0.00	UP
1668	400	100	15	-4.762	170	9625	221	-9722	9.7	65	2	-162	221	0.00	UP
1669	400	100	37.5	4.762	170	10122	260	-9765	9.8	178	4	178	260	0.00	UP
1670	400	100	37.5	4.762	170	10104	279	-9766	9.8	179	4	159	279	0.00	UP
1671	400	100	52.5	-4.762	170	10010	210	-9721	9.7	257	6	32	211	0.00	UP
1672	400	100	52.5	-4.762	170	9824	218	-9721	9.7	259	6	-156	219	0.00	UP
1673	400	100	60	4.762	170	10079	220	-9766	9.8	299	7	14	221	0.00	UP
1674	400	100	60	4.762	170	9930	221	-9766	9.8	299	7	-136	221	0.00	UP
1675	300	100	22.5	4.762	170	9982	182	-9766	9.8	137	3	80	183	0.00	UP
1676	300	100	22.5	4.762	170	9918	185	-9766	9.8	136	3	16	185	0.00	UP
1677	300	100	30	-4.762	170	9839	184	-9721	9.7	186	4	-68	184	0.00	UP
1678	300	100	30	-4.762	170	9722	178	-9721	9.7	186	4	-185	178	0.00	UP
1679	400	100	30	-4.762	170	9979	293	-9720	9.7	140	3	119	294	0.00	UP
1680	400	100	30	-4.762	170	10183	242	-9722	9.7	140	3	321	242	0.00	UP
1681	400	100	22.5	-4.762	170	9559	211	-9721	9.7	102	2	-265	211	0.00	UP
1682	400	100	22.5	-4.762	170	9629	179	-9722	9.7	102	2	-195	179	0.00	UP
1683	400	100	30	4.762	170	9812	257	-9766	9.8	140	3	-95	257	0.00	UP
1684	400	100	30	4.762	170	10680	315	-9767	9.8	140	3	773	315	0.00	UP
1685	300	100	74.25	-4.762	170	10087	140	-9721	9.7	489	12	-123	141	0.00	UP
1686	300	100	74.25	-4.762	170	10186	122	-9721	9.7	495	12	-30	123	0.00	UP
1687	400	100	37.5	-4.762	170	9999	286	-9722	9.7	183	4	94	286	0.00	UP
1688	400	100	37.5	-4.762	170	9214	197	-9722	9.7	181	4	-689	197	0.00	UP
1689	300	100	15	4.762	170	10192	146	-9766	9.8	89	2	338	146	0.00	UP
1690	300	100	15	4.762	170	9926	233	-9766	9.8	88	2	72	233	0.00	UP
1691	400	100	67.5	-4.762	170	9743	179	-9721	9.7	338	8	-316	180	0.00	UP
1692	400	100	67.5	-4.762	170	10032	163	-9722	9.7	340	8	-30	163	0.00	UP
1693	400	100	60	-4.762	170	10036	184	-9721	9.7	299	7	16	185	0.00	UP
1694	400	100	60	-4.762	170	10129	171	-9723	9.7	299	7	106	172	0.00	UP
1695	900	100	74.25	4.762	170	10039	561	-9772	9.8	182	4	85	561	0.01	NR
1696	900	100	74.25	4.762	170	10681	559	-9771	9.8	182	4	728	559	0.01	NR
1697	900	100	74.25	-4.762	170	9836	317	-9761	9.8	182	4	-106	317	0.03	NR
1698	900	100	74.25	-4.762	170	9651	392	-9760	9.8	180	4	-290	392	0.02	NR
1699	900	100	74.25	-4.762	170	9452	339	-9761	9.8	180	4	-489	339	0.03	NR
1700	900	100	74.25	-4.762	170	10438	383	-9761	9.8	179	4	498	384	0.02	NR
1701	900	100	74.25	4.762	170	9951	570	-9772	9.8	180	4	0	570	0.01	NR
1702	900	100	74.25	4.762	170	10449	454	-9773	9.8	181	4	496	454	0.01	NR
1703	300	100	74.25	-3.175	170	4780	50	-4355	4.4	507	12	-82	52	1.33	NR
1704	300	100	60	3.175	170	4786	74	-4365	4.4	404	10	17	74	0.83	NR
1705	300	100	74.25	3.175	170	4951	64	-4364	4.4	507	12	80	66	0.81	NR
1706	300	100	30	3.175	170	4557	81	-4363	4.4	195	5	-1	81	1.06	NR
1707	300	100	60	-3.175	170	4782	61	-4356	4.4	406	10	20	62	1.24	NR
1708	300	100	67.5	3.175	170	4857	57	-4363	4.4	462	11	32	58	1.22	NR
1709	300	100	22.5	6.349	170	17579	70	-17388	17.4	142	3	48	72	0.00	NR
1710	300	100	52.5	-6.349	170	17687	63	-17372	17.4	351	8	-36	66	0.00	NR
1711	300	100	52.5	6.349	170	17795	56	-17388	17.4	354	8	53	59	0.00	NR
1712	300	100	37.5	-3.175	170	4662	73	-4356	4.4	247	6	60	73	1.22	NR
1713	300	100	60	6.349	170	17791	66	-17388	17.4	404	10	-2	69	0.00	NR
1714	300	100	60	-6.349	170	17664	48	-17371	17.4	406	10	-114	52	0.00	NR
1715	300	100	15	6.349	170	17482	82	-17388	17.4	90	2	4	84	0.00	NR
1716	300	100	37.5	3.175	170	4664	72	-4365	4.4	240	6	59	72	1.27	NR
1717	300	100	37.5	-6.349	170	17597	66	-17372	17.4	241	6	-16	68	0.00	NR
1718	300	100	22.5	-3.175	170	4494	46	-4356	4.4	139	3	-1	47	3.56	NR
1719	300	100	37.5	6.349	170	17685	81	-17386	17.4	239	6	60	83	0.00	NR
1720	300	100	74.25	-6.349	170	17828	60	-17375	17.4	499	12	-46	64	0.00	NR
1721	300	100	52.5	3.175	170	4616	87	-4364	4.4	347	8	-95	87	0.68	NR
1722	300	100	7.5	-3.175	170	4606	96	-4356	4.4	41	1	208	96	0.96	NR
1723	300	100	52.5	-3.175	170	4587	58	-4355	4.4	340	8	-108	58	1.67	NR
1724	300	100	22.5	-6.349	170	17471	48	-17372	17.4	138	3	-39	51	0.00	NR
1725	300	100	15	3.175	170	4356	71	-4365	4.4	89	2	-98	72	1.65	NR
1726	300	100	30	-6.349	170	17639	104	-17369	17.4	187	4	82	105	0.00	NR
1727	300	100	67.5	6.349	170	17876	48	-17390	17.4	447	11	39	52	0.00	NR
1728	300	100	30	6.349	170	17548	91	-17391	17.4	191	5	-34	93	0.00	NR
1729	300	100	67.5	-6.349	170	17838	63	-17370	17.4	448	11	20	66	0.00	NR
1730	300	100	15	-6.349	170	17520	83	-17371	17.4	90	2	58	84	0.00	NR
1731	300	100	74.25	6.349	170	17825	56	-17390	17.4	500	12	-65	60	0.00	NR
1732	300	100	67.5	-3.175	170	4815	44	-4355	4.4	457	11	2	45	1.95	NR
1733	300	100	15	-3.175	170	4438	54	-4355	4.4	91	2	-8	54	2.97	NR
1734	300	100	30	-3.175	170	4520	124	-4355	4.4	191	5	-26	124	0.46	NR
1735	400	100	22.5	5.06	170	11415	115	-11054	11.1	106	3	255	115	0.22	NR
1736	400	100	7.5	5.06	170	11109	227	-11055	11.1	31	1	24	227	0.07	NR
1737	500	50	45	-9.762	170	41159	146	-40945	40.9	57	11	157	152	0.00	NR
1738	400	100	45	5.06	170	11288	77	-11055	11.1	220	5	13	78	0.24	NR
1739	375	125	15	-7.62	170	24989	67	-24995	25	84	15	-89	73	0.00	NR
1740	400	100	15	-5.06	170	10953	148	-11039	11	66	2	-152	148	0.15	NR
1741	500	50	30	-9.762	170	40906	154	-40943	40.9	35	7	-73	160	0.00	NR

Continued on next page

Table A.2 Continued from previous page

N_{run}	T [ns]	D [ns]	P [W]	B [Gauss]	θ_{pol} [deg.]	ν_{fit} [Hz]	$\Delta\nu_{\mathrm{fit}}$ [Hz]	$\mathrm{DC_B}$ [Hz]	$\Delta\mathrm{DC_B}$ [Hz]	SC [Hz]	ΔSC [Hz]	ν_0 [Hz]	$\Delta\nu_0$ [Hz]	wts. [%]	Data Type
1742	300	100	15	-5.159	170	11526	106	-11467	11.5	87	2	-29	107	0.24	NR
1743	500	50	67.5	-9.762	170	41254	135	-40943	40.9	90	18	222	142	0.00	NR
1744	400	100	30	5.06	170	11270	101	-11056	11.1	141	3	74	101	0.24	NR
1745	300	50	30	9.921	170	42183	171	-42351	42.4	59	12	-228	177	0.00	NR
1746	500	125	7.5	-3.81	170	6326	177	-6242	6.2	28	5	56	177	0.17	NR
1747	300	50	52.5	9.921	170	42658	150	-42351	42.4	109	21	198	158	0.00	NR
1748	500	50	60	-9.762	170	40949	138	-40945	40.9	78	15	-73	145	0.00	NR
1749	375	125	30	-7.62	170	25186	57	-24993	25	176	31	16	69	0.00	NR
1750	300	50	37.5	9.921	170	42662	152	-42351	42.4	76	15	235	158	0.00	NR
1751	300	100	60	-5.159	170	11956	75	-11466	11.5	395	9	95	77	0.00	NR
1752	500	125	15	-3.81	170	6375	102	-6241	6.2	64	11	70	103	0.23	NR
1753	300	100	22.5	-5.159	170	11620	71	-11466	11.5	138	3	15	72	0.42	NR
1754	375	125	7.5	7.62	170	25009	135	-25021	25	39	7	-51	137	0.00	NR
1755	400	200	15	4.762	170	10001	71	-9775	9.8	207	42	18	83	0.00	NR
1756	400	200	3.75	-4.762	170	9599	123	-9758	9.8	46	9	-205	123	0.03	NR
1757	300	50	7.5	9.921	170	42271	399	-42353	42.4	12	2	-94	401	0.00	NR
1758	500	125	37.5	-3.81	170	6315	76	-6241	6.2	171	30	-97	82	0.00	NR
1759	400	100	52.5	-5.06	170	11295	95	-11038	11	263	6	-6	95	0.11	NR
1760	500	125	7.5	3.81	170	6119	182	-6255	6.3	29	5	-166	182	0.16	NR
1761	400	200	7.5	-4.762	170	9980	75	-9757	9.8	99	20	125	79	0.00	NR
1762	400	200	11.25	4.762	170	10036	86	-9774	9.8	151	31	111	92	0.00	NR
1763	500	50	7.5	-9.762	170	40841	364	-40941	40.9	7	1	-107	366	0.00	NR
1764	500	50	37.5	-9.762	170	41054	143	-40942	40.9	46	9	66	149	0.00	NR
1765	300	100	22.5	5.159	170	11685	107	-11485	11.5	138	3	61	108	0.18	NR
1766	300	100	45	-5.159	170	11706	72	-11466	11.5	290	7	-51	73	0.05	NR
1767	300	50	60	-9.921	170	42387	106	-42317	42.3	130	26	-60	117	0.00	NR
1768	400	100	52.5	5.06	170	11239	88	-11057	11.1	262	6	-80	89	0.12	NR
1769	375	125	30	7.62	170	25300	56	-25022	25	180	31	98	69	0.00	NR
1770	375	125	22.5	7.62	170	25237	98	-25021	25	132	23	84	103	0.00	NR
1771	300	50	30	-9.921	170	42157	126	-42318	42.3	61	12	-222	133	0.00	NR
1772	500	50	45	9.762	170	41064	180	-40977	41	57	11	31	185	0.00	NR
1773	500	125	15	3.81	170	6382	119	-6255	6.3	63	11	63	120	0.17	NR
1774	300	50	67.5	9.921	170	42594	101	-42351	42.4	148	29	95	113	0.00	NR
1775	400	100	30	-5.06	170	10981	107	-11038	11	144	3	-202	108	0.21	NR
1776	400	100	67.5	5.06	170	11295	78	-11056	11.1	344	8	-106	79	0.00	NR
1777	300	50	52.5	-9.921	170	42458	102	-42314	42.3	113	22	32	112	0.00	NR
1778	500	50	52.5	-9.762	170	41051	126	-40940	40.9	68	13	43	133	0.00	NR
1779	300	100	37.5	5.159	170	11780	96	-11487	11.5	240	6	53	97	0.09	NR
1780	500	50	22.5	-9.762	170	41250	222	-40940	40.9	26	5	284	226	0.00	NR
1781	500	50	52.5	9.762	170	40672	167	-40977	41	67	13	-372	173	0.00	NR
1782	300	100	30	5.159	170	11537	78	-11486	11.5	189	5	-138	79	0.25	NR
1783	400	200	18.75	4.762	170	10047	61	-9775	9.8	264	54	8	82	0.00	NR
1784	400	200	18.75	-4.762	170	9964	58	-9758	9.8	264	54	-58	79	0.00	NR
1785	300	100	52.5	5.159	170	11957	67	-11484	11.5	339	8	134	68	0.00	NR
1786	500	50	7.5	9.762	170	40427	571	-40976	41	7	1	-556	573	0.00	NR
1787	375	125	37.5	-7.62	170	25219	54	-24994	25	223	39	2	71	0.00	NR
1788	300	50	7.5	-9.921	170	42306	347	-42318	42.3	12	2	-24	350	0.00	NR
1789	400	100	37.5	5.06	170	11049	111	-11057	11.1	177	4	-185	111	0.16	NR
1790	500	125	30	3.81	170	6298	69	-6255	6.3	132	23	-90	73	0.00	NR
1791	500	50	37.5	9.762	170	41034	320	-40975	41	45	9	14	323	0.00	NR
1792	375	125	22.5	-7.62	170	25176	68	-24993	25	131	23	52	76	0.00	NR
1793	500	125	30	-3.81	170	6501	89	-6241	6.2	134	23	125	92	0.00	NR
1794	500	125	37.5	3.81	170	6346	223	-6256	6.3	170	30	-80	225	0.00	NR
1795	500	50	60	9.762	170	41069	164	-40970	41	78	15	20	170	0.00	NR
1796	375	125	15	7.62	170	25211	122	-25017	25	84	15	110	125	0.00	NR
1797	300	100	45	5.159	170	11790	51	-11482	11.5	284	7	25	53	0.14	NR
1798	300	100	15	5.159	170	11698	106	-11482	11.5	88	2	128	107	0.24	NR
1799	300	100	7.5	5.159	170	11501	177	-11480	11.5	42	1	-21	178	0.10	NR
1800	400	200	11.25	-4.762	170	9910	68	-9760	9.8	154	31	-4	76	0.00	NR
1801	300	50	67.5	-9.921	170	42403	68	-42319	42.3	149	29	-65	85	0.00	NR
1802	300	100	7.5	-5.159	170	11619	173	-11469	11.5	42	1	107	173	0.11	NR
1803	500	50	15	9.762	170	41001	322	-40974	41	16	3	11	324	0.00	NR
1804	300	100	30	-5.159	170	11679	81	-11469	11.5	185	4	26	82	0.23	NR
1805	400	100	67.5	-5.06	170	11491	60	-11040	11	342	8	109	62	0.00	NR
1806	300	50	37.5	-9.921	170	42465	135	-42323	42.3	79	16	62	143	0.00	NR
1807	300	100	67.5	-5.159	170	11967	57	-11470	11.5	451	11	47	59	0.00	NR
1808	300	50	15	9.921	170	42175	249	-42344	42.3	28	6	-198	253	0.00	NR
1809	400	200	7.5	4.762	170	9860	105	-9772	9.8	100	20	-13	108	0.00	NR
1810	300	50	60	9.921	170	42527	136	-42343	42.3	130	26	54	145	0.00	NR
1811	500	50	30	9.762	170	40849	314	-40969	41	37	7	-157	317	0.00	NR
1812	500	50	67.5	9.762	170	41344	145	-40973	41	91	18	280	152	0.00	NR
1813	300	50	45	-9.921	170	42390	100	-42319	42.3	95	19	-25	111	0.00	NR
1814	300	100	67.5	5.159	170	11992	67	-11483	11.5	450	11	58	69	0.00	NR
1815	400	100	7.5	-5.06	170	10692	187	-11040	11	31	1	-379	187	0.11	NR
1816	400	100	60	5.06	170	11259	100	-11054	11.1	305	7	-100	100	0.04	NR
1817	300	50	37.5	9.921	170	42571	147	-42349	42.3	79	16	143	154	0.00	NR
1818	300	50	15	-9.921	170	42316	164	-42320	42.3	29	6	-32	169	0.00	NR
1819	400	200	7.5	-4.762	170	9747	121	-9760	9.8	101	21	-115	123	0.00	NR
1820	300	100	60	5.159	170	11952	57	-11483	11.5	397	10	72	59	0.00	NR
1821	500	50	22.5	9.762	170	40858	210	-40971	41	27	5	-140	214	0.00	NR
1822	400	100	37.5	-5.06	170	11125	128	-11043	11	184	4	-102	129	0.12	NR
1823	500	125	22.5	3.81	170	6493	76	-6252	6.3	101	18	140	78	0.00	NR
1824	400	100	60	-5.06	170	11285	79	-11043	11	306	7	-64	80	0.07	NR
1825	500	125	37.5	3.81	170	6535	100	-6252	6.3	177	31	106	105	0.00	NR
1826	300	100	37.5	-5.159	170	11785	82	-11470	11.5	246	6	70	83	0.12	NR
1827	400	100	15	5.06	170	11392	208	-11053	11.1	70	2	270	209	0.07	NR
1828	400	200	15	4.762	170	9951	86	-9772	9.8	214	44	-35	97	0.00	NR
1829	500	125	22.5	-3.81	170	6578	91	-6243	6.2	99	17	235	93	0.00	NR
1830	400	100	22.5	-5.06	170	11300	101	-11041	11	104	3	155	101	0.28	NR
1831	400	200	3.75	4.762	170	9785	146	-9772	9.8	46	9	-33	147	0.02	NR
1832	300	50	22.5	-9.921	170	42293	138	-42322	42.3	43	9	-73	145	0.00	NR
1833	300	50	45	9.921	170	42547	139	-42348	42.3	93	18	106	146	0.00	NR
1834	400	100	45	-5.06	170	11342	86	-11040	11	221	5	81	87	0.20	NR
1835	500	50	52.5	-9.762	170	40961	162	-40946	40.9	68	13	-53	167	0.00	NR
1836	375	125	37.5	7.62	170	25209	80	-25017	25	223	39	-31	93	0.00	NR
1837	375	125	7.5	-7.62	170	24884	107	-24995	25	39	7	-151	110	0.00	NR
1838	500	50	15	-9.762	170	40918	254	-40948	40.9	16	3	-46	257	0.00	NR
1839	300	100	52.5	-5.159	170	11776	70	-11468	11.5	336	8	-28	72	0.00	NR

Continued on next page

Table A.2 Continued from previous page

N_{run}	T [ns]	D [ns]	P [W]	B [Gauss]	θ_{pol} [deg.]	ν_{fit} [Hz]	$\Delta\nu_{\mathrm{fit}}$ [Hz]	$\mathrm{DC_B}$ [Hz]	$\Delta\mathrm{DC_B}$ [Hz]	SC [Hz]	ΔSC [Hz]	ν_0 [Hz]	$\Delta\nu_0$ [Hz]	wts. [%]	Data Type
1840	400	200	18.75	-7.143	260	22100	80	-21968	22	262	53	-129	99	0.00	NR
1841	400	100	52.5	5.06	260	11140	61	-11054	11.1	258	6	-173	62	0.28	NR
1842	400	200	11.25	-7.143	260	22024	74	-21967	22	151	31	-94	83	0.00	NR
1843	300	100	67.5	5.159	260	11919	64	-11483	11.5	440	11	-3	66	0.00	NR
1844	400	50	60	9.524	260	38801	104	-38995	39	99	19	-292	113	0.00	NR
1845	300	50	22.5	9.921	260	42520	186	-42351	42.4	44	9	124	191	0.00	NR
1846	300	50	30	9.921	260	42391	129	-42348	42.3	60	12	-18	136	0.00	NR
1847	400	100	22.5	-5.06	260	11168	113	-11040	11	105	3	23	114	0.22	NR
1848	400	200	7.5	7.143	260	22221	96	-21989	22	98	20	134	101	0.00	NR
1849	300	50	7.5	-9.921	260	42554	370	-42317	42.3	12	2	225	372	0.00	NR
1850	400	200	18.75	7.143	260	22206	71	-21988	22	264	54	-46	92	0.00	NR
1851	400	50	52.5	9.524	260	39055	80	-39001	39	85	17	-30	91	0.00	NR
1852	400	100	45	-5.06	260	11300	90	-11041	11	221	5	38	91	0.18	NR
1853	400	100	30	-5.06	260	11050	99	-11040	11	144	3	-133	99	0.25	NR
1854	400	100	15	5.06	260	11232	145	-11055	11.1	67	2	110	145	0.16	NR
1855	300	100	37.5	5.159	260	11648	75	-11482	11.5	239	6	-74	76	0.16	NR
1856	400	100	30	5.06	260	11236	97	-11055	11.1	144	3	38	98	0.25	NR
1857	300	50	15	-9.921	260	42744	292	-42317	42.3	28	5	400	295	0.00	NR
1858	300	50	7.5	9.921	260	42396	294	-42349	42.3	12	2	34	297	0.00	NR
1859	400	100	37.5	5.06	260	11213	94	-11055	11.1	180	4	-22	94	0.22	NR
1860	300	100	7.5	-5.159	260	11784	146	-11467	11.5	42	1	275	146	0.15	NR
1861	300	100	45	-5.159	260	11755	74	-11467	11.5	288	7	0	75	0.06	NR
1862	300	50	22.5	-9.921	260	42436	240	-42320	42.3	44	9	72	244	0.00	NR
1863	300	100	45	5.159	260	11852	77	-11484	11.5	289	7	80	78	0.05	NR
1864	300	50	37.5	-9.921	260	42381	184	-42319	42.3	77	15	-15	189	0.00	NR
1865	400	50	37.5	-9.524	260	38783	141	-38970	39	58	11	-245	147	0.00	NR
1866	400	50	7.5	9.524	260	39076	293	-38996	39	9	2	71	296	0.00	NR
1867	300	50	45	9.921	260	42252	139	-42348	42.3	93	18	-189	147	0.00	NR
1868	300	100	22.5	5.159	260	11722	104	-11482	11.5	139	3	101	104	0.20	NR
1869	300	50	52.5	-9.921	260	42512	130	-42320	42.3	111	22	82	138	0.00	NR
1870	400	100	15	-5.06	260	11112	181	-11040	11	67	2	4	181	0.10	NR
1871	300	100	60	5.159	260	11811	64	-11482	11.5	390	9	-62	65	0.00	NR
1872	400	100	7.5	5.06	260	10833	168	-11054	11.1	31	1	-252	169	0.13	NR
1873	400	50	7.5	-9.524	260	39491	401	-38969	39	9	2	513	403	0.00	NR
1874	400	50	45	-9.524	260	38585	124	-38970	39	70	14	-454	131	0.00	NR
1875	300	100	7.5	5.159	260	11510	177	-11483	11.5	41	1	-14	177	0.10	NR
1876	300	100	52.5	-5.159	260	11808	62	-11468	11.5	338	8	2	63	0.00	NR
1877	400	50	37.5	9.524	260	38999	123	-38995	39	58	11	-54	130	0.00	NR
1878	300	100	15	-5.159	260	11666	127	-11468	11.5	89	2	109	127	0.17	NR
1879	300	50	52.5	9.921	260	42444	109	-42348	42.3	111	22	-14	119	0.00	NR
1880	400	50	30	-9.524	260	39047	191	-38969	39	45	9	34	195	0.00	NR
1881	400	200	11.25	7.143	260	22149	97	-21988	22	152	31	9	104	0.00	NR
1882	400	100	37.5	-5.06	260	11152	109	-11041	11	180	4	-69	110	0.16	NR
1883	300	50	30	-9.921	260	42067	189	-42317	42.3	61	12	-310	194	0.00	NR
1884	300	100	22.5	-5.159	260	11619	98	-11470	11.5	139	3	10	99	0.22	NR
1885	300	50	67.5	9.921	260	42572	98	-42347	42.3	147	29	77	111	0.00	NR
1886	400	50	67.5	-9.524	260	38995	119	-38968	39	113	22	-86	127	0.00	NR
1887	400	200	15	-7.143	260	22127	82	-21967	22	209	42	-49	95	0.00	NR
1888	300	100	15	5.159	260	11445	97	-11483	11.5	89	2	-127	98	0.29	NR
1889	300	100	37.5	-5.159	260	11736	73	-11468	11.5	238	6	30	74	0.17	NR
1890	300	100	67.5	-5.159	260	11984	68	-11468	11.5	441	11	75	70	0.00	NR
1891	300	100	30	5.159	260	11620	94	-11482	11.5	189	5	-51	95	0.17	NR
1892	400	50	60	-9.524	260	39121	109	-38971	39	98	19	53	117	0.00	NR
1893	300	50	60	9.921	260	42283	97	-42348	42.3	129	25	-194	109	0.00	NR
1894	400	50	45	9.524	260	39200	141	-38997	39	71	14	132	147	0.00	NR
1895	400	50	22.5	9.524	260	39158	136	-38999	39	32	6	127	141	0.00	NR
1896	400	100	22.5	5.06	260	11130	137	-11055	11.1	102	2	-27	138	0.15	NR
1897	400	100	7.5	-5.06	260	10909	247	-11040	11	30	1	-161	247	0.06	NR
1898	300	50	60	-9.921	260	42247	124	-42319	42.3	126	25	-198	133	0.00	NR
1899	400	100	45	5.06	260	11289	81	-11054	11.1	216	5	19	82	0.23	NR
1900	400	50	15	-9.524	260	38968	221	-38968	39	20	4	-20	224	0.00	NR
1901	400	50	67.5	9.524	260	39186	93	-38995	39	111	22	80	103	0.00	NR
1902	400	50	52.5	-9.524	260	39003	138	-38969	39	83	16	-50	145	0.00	NR
1903	400	100	60	-5.06	260	11538	76	-11042	11	295	7	202	77	0.10	NR
1904	300	50	45	-9.921	260	42487	182	-42320	42.3	93	18	75	188	0.00	NR
1905	400	50	15	9.524	260	39142	180	-38993	39	20	4	129	184	0.00	NR
1906	400	200	3.75	-7.143	260	22034	205	-21967	22	46	9	21	207	0.00	NR
1907	400	200	15	7.143	260	22126	67	-21987	22	206	42	-67	82	0.00	NR
1908	300	100	30	-5.159	260	11779	93	-11468	11.5	188	5	123	94	0.18	NR
1909	400	100	60	5.06	260	11314	70	-11054	11.1	298	7	-39	71	0.10	NR
1910	400	100	67.5	-5.06	260	11295	94	-11039	11	339	8	-84	95	0.00	NR
1911	300	100	60	-5.159	260	11713	69	-11468	11.5	388	9	-143	70	0.00	NR
1912	400	200	3.75	7.143	260	21960	165	-21987	22	45	9	-73	167	0.00	NR
1913	300	50	15	9.921	260	42407	228	-42349	42.3	27	5	32	232	0.00	NR
1914	400	50	30	9.524	260	38939	114	-38996	39	44	9	-102	121	0.00	NR
1915	400	100	67.5	5.06	260	11309	75	-11055	11.1	339	8	-84	77	0.00	NR
1916	300	50	67.5	-9.921	260	42511	120	-42322	42.3	147	29	42	131	0.00	NR
1917	300	100	52.5	5.159	260	11878	61	-11482	11.5	338	8	59	63	0.00	NR
1918	400	100	52.5	-5.06	260	11188	91	-11042	11	259	6	-113	92	0.12	NR
1919	400	50	22.5	-9.524	260	38729	183	-38972	39	32	6	-275	188	0.00	NR
1920	400	200	7.5	-7.143	260	22070	151	-21970	22	97	20	3	154	0.00	NR
1921	300	50	37.5	9.921	260	42411	123	-42344	42.3	76	15	-9	131	0.00	NR
1922	600	150	3.75	-6.35	260	18279	611	-17376	17.4	15	2	887	611	0.00	NR
1923	600	150	15	-6.35	260	17337	182	-17374	17.4	78	9	-114	183	0.00	NR
1924	600	150	18.75	-6.35	260	17238	247	-17374	17.4	100	11	-236	248	0.00	NR
1925	600	150	7.5	-6.35	260	17121	284	-17375	17.4	35	4	-289	285	0.00	NR
1926	600	150	11.25	6.35	260	17482	225	-17391	17.4	56	6	35	226	0.00	NR
1927	600	150	22.5	-6.35	260	17352	209	-17372	17.4	122	14	-142	210	0.00	NR
1928	600	150	26.25	6.35	260	17436	156	-17388	17.4	144	16	-96	158	0.00	NR
1929	600	150	3.75	6.35	260	17393	500	-17389	17.4	15	2	-11	500	0.00	NR
1930	600	150	7.5	6.35	260	17421	340	-17389	17.4	35	4	-2	341	0.00	NR
1931	600	150	11.25	-6.35	260	17440	280	-17372	17.4	56	6	11	280	0.00	NR
1932	600	150	26.25	-6.35	260	17555	173	-17374	17.4	143	16	38	175	0.00	NR
1933	600	150	22.5	6.35	260	17708	153	-17384	17.4	123	14	201	154	0.00	NR
1934	600	150	18.75	6.35	260	17601	153	-17384	17.4	103	11	114	155	0.00	NR
1935	600	150	15	6.35	260	17450	172	-17383	17.4	80	9	-13	173	0.00	NR
1936	800	100	60	4.762	260	9901	280	-9770	9.8	154	4	-23	280	0.04	NR
1937	800	100	60	4.762	260	10167	211	-9768	9.8	155	4	244	211	0.07	NR

Continued on next page

Table A.2 Continued from previous page

N_{run}	T [ns]	D [ns]	P [W]	B [Gauss]	θ_{pol} [deg.]	ν_{fit} [Hz]	$\Delta\nu_{\mathrm{fit}}$ [Hz]	$\mathrm{DC_B}$ [Hz]	$\Delta\mathrm{DC_B}$ [Hz]	SC [Hz]	ΔSC [Hz]	ν_0 [Hz]	$\Delta\nu_0$ [Hz]	wts. [%]	Data Type
1938	800	100	60	4.762	260	9824	217	-9769	9.8	155	4	-100	217	0.07	NR
1939	800	100	60	4.762	260	9831	372	-9769	9.8	154	4	-92	372	0.02	NR
1940	800	100	60	4.762	260	10217	270	-9769	9.8	154	4	295	270	0.05	NR
1941	800	100	60	-4.762	260	9973	333	-9765	9.8	154	4	55	334	0.03	NR
1942	800	100	60	-4.762	260	10606	391	-9765	9.8	154	4	687	391	0.02	NR
1943	800	100	60	-4.762	260	10493	343	-9765	9.8	155	4	573	343	0.03	NR
1944	800	100	60	-4.762	260	9723	379	-9764	9.8	155	4	-197	379	0.02	NR
1945	800	100	60	-4.762	260	10393	271	-9763	9.8	155	4	475	272	0.05	NR
1946	800	100	60	4.762	260	9873	361	-9773	9.8	152	4	-52	361	0.02	NR
1947	800	100	60	4.762	260	10130	272	-9769	9.8	154	4	207	272	0.05	NR
1948	800	100	60	4.762	260	10080	273	-9770	9.8	154	4	157	274	0.05	NR
1949	800	100	60	4.762	260	9755	272	-9770	9.8	155	4	-171	272	0.05	NR
1950	700	100	60	-4.762	260	10021	128	-9765	9.8	175	4	81	129	0.18	NR
1951	700	100	60	-4.762	260	9587	109	-9765	9.8	176	4	-354	110	0.25	NR
1952	700	100	60	-4.762	260	9876	181	-9765	9.8	176	4	-64	181	0.09	NR
1953	700	100	60	-4.762	260	9673	106	-9765	9.8	176	4	-267	106	0.27	NR
1954	700	100	60	-4.762	260	9778	142	-9764	9.8	175	4	-161	142	0.15	NR
1955	700	100	60	-4.762	260	9986	149	-9766	9.8	175	4	45	150	0.13	NR
1956	700	100	60	4.762	260	9984	128	-9768	9.8	175	4	41	129	0.18	NR
1957	700	100	60	4.762	260	10046	149	-9768	9.8	174	4	104	150	0.14	NR
1958	700	100	60	4.762	260	10141	174	-9767	9.8	175	4	199	174	0.10	NR
1959	700	100	60	4.762	260	10026	164	-9768	9.8	175	4	84	164	0.11	NR
1960	700	100	60	4.762	260	9725	186	-9768	9.8	175	4	-218	186	0.09	NR
1961	700	100	60	4.762	260	9966	120	-9768	9.8	176	4	21	120	0.21	NR
1962	900	100	60	4.762	260	9614	1372	-9771	9.8	140	3	-297	1372	0.00	NR
1963	700	100	60	4.762	260	9718	230	-9770	9.8	182	4	-235	230	0.05	NR
1964	700	100	60	-4.762	170	10156	158	-9764	9.8	182	4	210	158	0.12	NR
1965	700	100	60	-4.762	170	9996	220	-9762	9.8	182	4	52	220	0.06	NR
1966	700	100	60	-4.762	170	10259	163	-9763	9.8	181	4	315	163	0.11	NR
1967	700	100	60	-4.762	170	10048	136	-9764	9.8	181	4	103	137	0.16	NR
1968	700	100	60	4.762	170	9510	173	-9771	9.8	181	4	-442	173	0.10	NR
1969	700	100	60	4.762	170	9616	250	-9770	9.8	182	4	-336	250	0.05	NR
1970	700	100	60	4.762	170	9821	181	-9770	9.8	183	4	-132	181	0.09	NR
1971	700	100	60	4.762	170	9768	175	-9770	9.8	183	4	-185	176	0.09	NR
1972	700	100	60	4.762	170	9685	157	-9770	9.8	183	4	-268	157	0.12	NR
1973	700	100	60	4.762	170	10022	165	-9771	9.8	183	4	67	166	0.11	NR
1974	700	100	60	4.762	170	9548	174	-9771	9.8	183	4	-405	174	0.10	NR
1975	700	100	60	4.762	170	9506	210	-9772	9.8	182	4	-448	210	0.07	NR
1976	700	100	60	-4.762	170	10475	174	-9763	9.8	181	4	532	174	0.10	NR
1977	700	100	60	-4.762	170	10074	184	-9762	9.8	180	4	131	184	0.09	NR
1978	700	100	60	-4.762	170	10392	146	-9763	9.8	180	4	449	147	0.14	NR
1979	700	100	60	-4.762	170	10032	145	-9764	9.8	180	4	89	146	0.14	NR
1980	800	100	60	4.762	170	9767	676	-9770	9.8	158	4	-161	677	0.01	NR
1981	800	100	60	4.762	170	8894	628	-9770	9.8	159	4	-1034	628	0.01	NR
1982	800	100	60	4.762	170	10335	689	-9769	9.8	158	4	408	689	0.01	NR
1983	800	100	60	4.762	170	11328	1153	-9770	9.8	160	4	1398	1153	0.00	NR
1984	800	100	60	4.762	170	10689	708	-9771	9.8	160	4	758	708	0.01	NR
1985	800	100	60	4.762	170	9069	648	-9771	9.8	160	4	-863	648	0.01	NR
1986	900	100	60	4.762	170	9374	546	-9770	9.8	141	3	-537	546	0.01	NR
1987	900	100	60	-4.762	170	9896	422	-9764	9.8	140	3	-9	422	0.02	NR
1988	900	100	60	4.762	170	9399	1045	-9766	9.8	141	3	-509	1045	0.00	NR
1989	700	100	7.5	4.762	170	8972	1345	-9767	9.8	16	0	-811	1345	0.01	NR
1990	700	100	60	-4.762	170	9649	94	-9764	9.8	178	4	-293	95	0.33	NR
1991	700	100	15	-4.762	170	9790	302	-9765	9.8	38	1	-13	302	0.05	NR
1992	700	100	52.5	4.762	170	9936	165	-9766	9.8	153	4	16	165	0.12	NR
1993	700	100	45	-4.762	170	9637	120	-9764	9.8	130	3	-257	120	0.25	NR
1994	700	100	22.5	-4.762	170	9380	225	-9764	9.8	60	1	-444	225	0.08	NR
1995	700	100	37.5	4.762	170	10095	219	-9766	9.8	106	3	223	219	0.08	NR
1996	700	100	15	4.762	170	9679	362	-9767	9.8	38	1	-126	362	0.04	NR
1997	700	100	7.5	-4.762	170	9953	567	-9765	9.8	17	0	171	567	0.02	NR
1998	700	100	22.5	4.762	170	9497	263	-9767	9.8	60	1	-330	263	0.06	NR
1999	700	100	30	-4.762	170	9378	197	-9764	9.8	83	2	-469	197	0.11	NR
2000	700	100	60	4.762	170	9902	155	-9767	9.8	178	4	-43	155	0.12	NR
2001	700	100	30	4.762	170	9581	253	-9769	9.8	83	2	-271	253	0.06	NR
2002	700	100	37.5	-4.762	170	9717	137	-9764	9.8	106	3	-154	137	0.20	NR
2003	700	100	52.5	-4.762	170	9728	118	-9764	9.8	153	4	-189	119	0.24	NR
2004	700	100	45	4.762	170	9823	136	-9767	9.8	130	3	-74	136	0.19	NR
2005	700	100	52.5	4.762	260	9642	130	-9769	9.8	154	4	-281	130	0.19	NR
2006	700	100	45	4.762	260	9750	135	-9769	9.8	130	3	-149	135	0.19	NR
2007	700	100	60	-4.762	260	9910	130	-9765	9.8	179	4	-33	130	0.18	NR
2008	700	100	52.5	-4.762	260	10158	173	-9765	9.8	154	4	239	174	0.11	NR
2009	700	100	45	-4.762	260	10029	164	-9763	9.8	130	3	137	164	0.13	NR
2010	700	100	37.5	-4.762	260	9785	232	-9763	9.8	107	3	-85	232	0.07	NR
2011	700	100	37.5	4.762	260	9597	145	-9769	9.8	108	3	-280	145	0.18	NR
2012	700	100	60	4.762	260	10048	130	-9769	9.8	181	4	97	130	0.17	NR
2013	700	100	7.5	-4.762	260	11043	979	-9765	9.8	17	0	1261	979	0.01	NR
2014	700	100	7.5	-4.762	260	9968	970	-9765	9.8	16	0	186	970	0.01	NR
2015	700	100	22.5	-4.762	260	9834	326	-9763	9.8	59	1	12	326	0.04	NR
2016	700	100	30	-4.762	260	9447	264	-9764	9.8	81	2	-398	265	0.06	NR
2017	700	100	30	4.762	260	9793	128	-9770	9.8	81	2	-59	128	0.25	NR
2018	700	100	22.5	4.762	260	9939	244	-9770	9.8	59	1	110	244	0.07	NR
2019	700	100	7.5	4.762	260	9113	541	-9771	9.8	16	0	-674	541	0.02	NR
2020	700	100	7.5	4.762	260	9275	578	-9771	9.8	16	0	-512	578	0.02	NR
2021	700	100	15	-4.762	260	9956	403	-9763	9.8	37	1	156	403	0.03	NR
2022	700	100	15	-4.762	260	9393	424	-9765	9.8	37	1	-408	424	0.03	NR
2023	700	100	15	4.762	260	9459	285	-9771	9.8	37	1	-349	285	0.05	NR
2024	700	100	15	4.762	260	9975	313	-9770	9.8	37	1	168	313	0.05	NR
2025	900	100	60	4.762	260	9905	467	-9769	9.8	138	3	-2	467	0.02	NR
2026	300	100	74.25	4.762	260	10309	73	-9771	9.8	498	12	39	74	0.00	NR
2027	300	100	74.25	4.762	260	10300	79	-9772	9.8	500	12	29	80	0.00	NR
2028	300	100	74.25	-4.762	260	10187	73	-9765	9.8	501	12	-79	74	0.00	NR
2029	300	100	74.25	-4.762	260	10308	87	-9765	9.8	502	12	41	88	0.00	NR
2030	300	100	74.25	-4.762	260	10048	67	-9763	9.8	505	12	-220	69	0.00	NR
2031	300	100	74.25	-4.762	260	9923	76	-9764	9.8	506	12	-347	78	0.00	NR
2032	300	100	74.25	4.762	260	10282	81	-9769	9.8	506	12	6	82	0.00	NR
2033	300	100	74.25	-4.762	260	10065	93	-9765	9.8	506	12	-206	95	0.00	NR
2034	300	100	74.25	-4.762	260	10203	110	-9763	9.8	505	12	-65	111	0.00	NR
2035	300	100	74.25	-4.762	260	10258	94	-9764	9.8	504	12	-10	96	0.00	NR

Continued on next page

Table A.2 Continued from previous page

N_{run}	T [ns]	D [ns]	P [W]	B [Gauss]	θ_{pol} [deg.]	ν_{fit} [Hz]	$\Delta\nu_{\mathrm{fit}}$ [Hz]	$\mathrm{DC_B}$ [Hz]	$\Delta\mathrm{DC_B}$ [Hz]	SC [Hz]	ΔSC [Hz]	ν_0 [Hz]	$\Delta\nu_0$ [Hz]	wts. [%]	Data Type
2036	300	100	74.25	4.762	260	10324	103	-9771	9.8	504	12	48	104	0.00	NR
2037	300	100	74.25	-4.762	260	10287	85	-9763	9.8	504	12	20	87	0.00	NR
2038	300	100	74.25	4.762	260	10339	81	-9774	9.8	505	12	60	82	0.00	NR
2039	300	100	74.25	4.762	260	10358	76	-9772	9.8	505	12	81	78	0.00	NR
2040	300	100	74.25	-4.762	260	10193	98	-9763	9.8	505	12	-75	99	0.00	NR
2041	300	100	74.25	-4.762	260	10115	88	-9763	9.8	505	12	-153	89	0.00	NR
2042	300	100	74.25	4.762	260	10365	84	-9773	9.8	505	12	87	85	0.00	NR
2043	300	100	74.25	4.762	260	10291	83	-9772	9.8	505	12	14	84	0.00	NR
2044	300	100	74.25	-4.762	260	10087	80	-9763	9.8	505	12	-181	81	0.00	NR
2045	300	100	74.25	-4.762	260	10187	95	-9762	9.8	509	12	-84	96	0.00	NR
2046	300	100	74.25	4.762	260	10346	71	-9774	9.8	511	12	61	73	0.00	NR
2047	300	100	74.25	4.762	260	10315	86	-9771	9.8	512	12	32	87	0.00	NR
2048	300	100	74.25	4.762	260	10539	73	-9772	9.8	512	12	255	75	0.00	NR
2049	300	100	74.25	-4.762	260	10361	98	-9764	9.8	511	12	86	100	0.00	NR
2050	300	100	74.25	-4.762	260	10276	96	-9764	9.8	509	12	3	97	0.00	NR
2051	300	100	74.25	4.762	260	10263	85	-9772	9.8	508	12	-18	87	0.00	NR
2052	300	100	74.25	4.762	260	10620	77	-9773	9.8	508	12	339	78	0.00	NR
2053	300	100	74.25	4.762	260	10339	69	-9771	9.8	507	12	61	71	0.00	NR
2054	300	100	74.25	-4.762	260	10244	122	-9764	9.8	507	12	-28	123	0.00	NR
2055	300	100	74.25	4.762	260	10460	84	-9775	9.8	507	12	178	86	0.00	NR
2056	300	100	74.25	4.762	260	10486	74	-9773	9.8	507	12	206	75	0.00	NR
2057	300	100	74.25	4.762	260	10385	68	-9772	9.8	507	12	106	69	0.00	NR
2058	300	100	74.25	-4.762	260	10402	89	-9762	9.8	507	12	133	91	0.00	NR
2059	300	100	74.25	4.762	260	10351	61	-9773	9.8	507	12	71	63	0.00	NR
2060	300	100	74.25	-4.762	260	10659	383	-9763	9.8	505	12	391	383	0.00	MOT0
2061	300	100	74.25	-4.762	260	10239	313	-9762	9.8	505	12	-29	313	0.00	MOT0
2062	300	100	74.25	-4.762	260	10001	308	-9761	9.8	505	12	-265	308	0.00	MOT0
2063	300	100	74.25	-4.762	260	10615	335	-9762	9.8	505	12	348	335	0.00	MOT0
2064	300	100	74.25	-4.762	260	10428	412	-9763	9.8	505	12	161	412	0.00	MOT0
2065	300	100	74.25	-4.762	260	9819	341	-9762	9.8	505	12	-448	342	0.00	MOT0
2066	300	100	74.25	4.762	260	10248	328	-9772	9.8	505	12	-30	328	0.00	MOT0
2067	300	100	74.25	4.762	260	10376	368	-9772	9.8	505	12	99	368	0.00	MOT0
2068	300	100	74.25	4.762	260	10482	341	-9773	9.8	505	12	204	341	0.00	MOT0
2069	300	100	74.25	4.762	260	11515	437	-9773	9.8	505	12	1237	438	0.00	MOT0
2070	300	100	74.25	4.762	260	10309	518	-9773	9.8	505	12	32	518	0.00	MOT0
2071	300	100	74.25	4.762	260	10131	320	-9774	9.8	505	12	-148	321	0.00	MOT0
2072	300	100	74.25	4.762	260	10009	436	-9773	9.8	505	12	-270	436	0.00	MOT0
2073	300	100	74.25	4.762	260	10804	523	-9773	9.8	505	12	526	524	0.00	MOT0
2074	300	100	74.25	4.762	260	10517	484	-9773	9.8	505	12	239	484	0.00	MOT0
2075	300	100	74.25	-4.762	260	10712	427	-9763	9.8	505	12	444	427	0.00	MOT0
2076	300	100	74.25	-4.762	260	9976	420	-9762	9.8	505	12	-291	421	0.00	MOT0
2077	300	100	74.25	-4.762	260	10174	394	-9763	9.8	505	12	-94	394	0.00	MOT0
2078	300	100	74.25	4.762	260	10451	356	-9772	9.8	505	12	174	357	0.00	MOT0
2079	300	100	74.25	4.762	260	10258	344	-9773	9.8	505	12	-20	345	0.00	MOT0
2080	300	100	74.25	4.762	260	10366	355	-9773	9.8	505	12	87	355	0.00	MOT0
2081	300	100	74.25	-4.762	260	10182	396	-9762	9.8	505	12	-86	396	0.00	MOT0
2082	300	100	74.25	-4.762	260	10224	357	-9763	9.8	505	12	-44	357	0.00	MOT0
2083	300	100	74.25	-4.762	260	10395	383	-9763	9.8	505	12	127	384	0.00	MOT0
2084	300	100	74.25	4.762	260	10317	286	-9774	9.8	505	12	39	287	0.00	MOT0
2085	300	100	74.25	4.762	260	10734	306	-9774	9.8	505	12	455	307	0.00	MOT0
2086	300	100	74.25	4.762	260	9839	332	-9773	9.8	505	12	-439	333	0.00	MOT0
2087	300	100	74.25	4.762	260	10546	282	-9773	9.8	505	12	267	282	0.00	MOT0
2088	300	100	74.25	4.762	260	10673	343	-9772	9.8	505	12	395	343	0.00	MOT0
2089	300	100	74.25	4.762	260	10284	376	-9773	9.8	505	12	6	376	0.00	MOT0
2090	300	100	74.25	4.762	260	9934	367	-9773	9.8	506	12	-344	367	0.00	MOT0
2091	300	100	74.25	4.762	260	10566	325	-9773	9.8	506	12	287	325	0.00	MOT0
2092	300	100	74.25	4.762	260	10365	349	-9773	9.8	506	12	86	349	0.00	MOT0
2093	300	100	74.25	-4.762	260	10223	420	-9762	9.8	506	12	-45	420	0.00	MOT0
2094	300	100	74.25	-4.762	260	9897	371	-9763	9.8	506	12	-372	371	0.00	MOT0
2095	300	100	74.25	-4.762	260	9728	376	-9762	9.8	505	12	-540	376	0.00	MOT0
2096	300	100	74.25	-4.762	260	9885	456	-9762	9.8	505	12	-383	456	0.00	MOT0
2097	300	100	74.25	-4.762	260	10300	799	-9763	9.8	506	12	32	799	0.00	MOT0
2098	300	100	74.25	-4.762	260	10393	454	-9762	9.8	506	12	125	454	0.00	MOT0
2099	300	100	74.25	4.762	260	10973	325	-9773	9.8	506	12	693	325	0.00	MOT0
2100	300	100	74.25	4.762	260	9785	393	-9772	9.8	506	12	-493	393	0.00	MOT0
2101	300	100	74.25	4.762	260	10852	348	-9772	9.8	507	12	572	348	0.00	MOT0
2102	300	100	74.25	4.762	260	10873	325	-9773	9.8	507	12	593	325	0.00	MOT0
2103	300	100	74.25	4.762	260	11527	374	-9773	9.8	507	12	1247	374	0.00	MOT0
2104	300	100	74.25	4.762	260	10961	356	-9773	9.8	507	12	681	356	0.00	MOT0
2105	300	100	74.25	4.762	260	10557	380	-9774	9.8	507	12	277	380	0.00	MOT0
2106	300	100	74.25	4.762	260	9859	398	-9773	9.8	507	12	-421	398	0.00	MOT0
2107	300	100	74.25	4.762	260	10925	389	-9772	9.8	507	12	646	389	0.00	MOT0
2108	300	100	74.25	-4.762	260	9462	591	-9763	9.8	507	12	-808	591	0.00	MOT0
2109	300	100	74.25	-4.762	260	9237	717	-9763	9.8	507	12	-1033	717	0.00	MOT0
2110	300	100	74.25	-4.762	260	9369	456	-9762	9.8	507	12	-899	456	0.00	MOT0
2111	300	100	74.25	4.762	260	10521	494	-9773	9.8	507	12	241	494	0.00	MOT0
2112	300	100	74.25	4.762	260	10654	748	-9773	9.8	507	12	374	749	0.00	MOT0
2113	300	100	74.25	4.762	260	9955	696	-9772	9.8	508	12	-325	697	0.00	MOT0
2114	300	100	74.25	-4.762	260	9697	685	-9763	9.8	508	12	-574	685	0.00	MOT0
2115	300	100	74.25	-4.762	260	11245	664	-9761	9.8	508	12	976	664	0.00	MOT0
2116	300	100	74.25	-4.762	260	10875	426	-9762	9.8	509	12	605	426	0.00	MOT0
2117	300	100	74.25	-4.762	260	9871	368	-9762	9.8	509	12	-400	369	0.00	MOT0
2118	300	100	74.25	-4.762	260	9417	390	-9763	9.8	510	12	-855	390	0.00	MOT0
2119	300	100	74.25	-4.762	260	10381	447	-9762	9.8	510	12	110	447	0.00	MOT0
2120	300	100	74.25	-4.762	260	9966	300	-9761	9.8	510	12	-305	300	0.00	MOT0
2121	300	100	74.25	-4.762	260	9659	396	-9762	9.8	511	12	-614	397	0.00	MOT0
2122	300	100	74.25	-4.762	260	10120	423	-9763	9.8	512	12	-155	423	0.00	MOT0
2123	300	100	74.25	4.762	260	9803	302	-9772	9.8	512	12	-481	303	0.00	MOT0
2124	300	100	74.25	4.762	260	9822	351	-9773	9.8	512	12	-464	352	0.00	MOT0
2125	300	100	74.25	4.762	260	10958	361	-9772	9.8	512	12	674	362	0.00	MOT0
2126	300	100	74.25	-4.762	260	10548	373	-9761	9.8	512	12	275	374	0.00	MOT0
2127	300	100	74.25	-4.762	260	9960	371	-9763	9.8	515	12	-318	372	0.00	MOT0
2128	300	100	74.25	-4.762	260	9465	474	-9762	9.8	514	12	-811	474	0.00	MOT0
2129	300	100	74.25	-4.762	260	9352	413	-9762	9.8	514	12	-925	414	0.00	MOT0
2130	300	100	74.25	-4.762	260	10222	380	-9762	9.8	513	12	-52	380	0.00	MOT0
2131	300	100	74.25	-4.762	260	10019	404	-9762	9.8	512	12	-256	405	0.00	MOT0
2132	300	100	74.25	-4.762	260	9673	372	-9761	9.8	512	12	-601	372	0.00	MOT0

Continued on next page

Table A.2 Continued from previous page

N_{run}	T [ns]	D [ns]	P [W]	B [Gauss]	θ_{pol} [deg.]	ν_{fit} [Hz]	$\Delta\nu_{\mathrm{fit}}$ [Hz]	$\mathrm{DC_B}$ [Hz]	$\Delta\mathrm{DC_B}$ [Hz]	SC [Hz]	ΔSC [Hz]	ν_0 [Hz]	$\Delta\nu_0$ [Hz]	wts. [%]	Data Type
2133	300	100	74.25	-4.762	260	10451	430	-9762	9.8	513	12	176	430	0.00	MOT0
2134	300	100	74.25	-4.762	260	10504	417	-9762	9.8	513	12	229	417	0.00	MOT0
2135	300	100	74.25	4.762	260	10672	402	-9774	9.8	513	12	384	402	0.00	MOT0
2136	300	100	74.25	4.762	260	11269	366	-9773	9.8	514	12	981	366	0.00	MOT0
2137	300	100	74.25	4.762	260	9272	360	-9773	9.8	514	12	-1016	360	0.00	MOT0
2138	300	100	74.25	-4.762	260	9724	401	-9762	9.8	514	12	-552	401	0.00	MOT0
2139	300	100	74.25	-4.762	260	10000	495	-9763	9.8	513	12	-276	495	0.00	MOT0
2140	300	100	74.25	-4.762	260	9565	430	-9762	9.8	513	12	-711	430	0.00	MOT0
2141	300	100	74.25	-4.762	260	10382	455	-9762	9.8	514	12	105	455	0.00	MOT0
2142	300	100	74.25	-4.762	260	9902	412	-9762	9.8	514	12	-374	412	0.00	MOT0
2143	300	100	74.25	-4.762	260	9695	401	-9762	9.8	514	12	-581	401	0.00	MOT0
2144	300	100	74.25	-4.762	260	9886	463	-9762	9.8	508	12	-384	463	0.00	MOT0
2145	300	100	74.25	-4.762	260	10047	336	-9761	9.8	513	12	-226	337	0.00	MOT0
2146	300	100	74.25	-4.762	260	10209	418	-9761	9.8	511	12	-64	418	0.00	MOT0
2147	300	100	74.25	4.762	260	10592	378	-9774	9.8	512	12	306	378	0.00	MOT0
2148	300	100	74.25	4.762	260	10566	338	-9773	9.8	512	12	281	338	0.00	MOT0
2149	300	100	74.25	4.762	260	11327	412	-9773	9.8	513	12	1041	412	0.00	MOT0
2150	300	100	74.25	-4.762	260	9750	569	-9761	9.8	513	12	-523	569	0.00	MOT0
2151	300	100	74.25	-4.762	260	9429	401	-9762	9.8	512	12	-846	401	0.00	MOT0
2152	300	100	74.25	-4.762	260	9119	394	-9762	9.8	513	12	-1156	394	0.00	MOT0
2153	300	100	74.25	4.762	260	10378	428	-9774	9.8	513	12	92	428	0.00	MOT0
2154	300	100	74.25	4.762	260	10544	468	-9775	9.8	513	12	257	468	0.00	MOT0
2155	300	100	74.25	4.762	260	10481	410	-9772	9.8	513	12	196	411	0.00	MOT0
2156	300	100	74.25	-4.762	260	10434	435	-9762	9.8	512	12	160	435	0.00	MOT0
2157	300	100	74.25	-4.762	260	10221	334	-9762	9.8	512	12	-53	334	0.00	MOT0
2158	300	100	74.25	-4.762	260	10290	532	-9761	9.8	512	12	16	532	0.00	MOT0
2159	300	100	74.25	-4.762	260	11053	555	-9762	9.8	512	12	778	556	0.00	MOT0
2160	300	100	74.25	-4.762	260	10302	421	-9761	9.8	512	12	29	421	0.00	MOT0
2161	300	100	74.25	-4.762	260	9981	435	-9762	9.8	512	12	-293	435	0.00	MOT0
2162	300	100	74.25	-4.762	260	10051	494	-9762	9.8	512	12	-223	494	0.00	MOT0
2163	300	100	74.25	-4.762	260	10513	364	-9762	9.8	512	12	239	364	0.00	MOT0
2164	300	100	74.25	-4.762	260	10355	467	-9761	9.8	512	12	81	467	0.00	MOT0
2165	300	100	74.25	4.762	260	10205	404	-9774	9.8	512	12	-81	404	0.00	MOT0
2166	300	100	74.25	4.762	260	10079	482	-9774	9.8	512	12	-207	482	0.00	MOT0
2167	300	100	74.25	4.762	260	9437	361	-9774	9.8	512	12	-849	361	0.00	MOT0
2168	300	100	74.25	-4.762	260	10233	458	-9761	9.8	512	12	-40	458	0.00	MOT0
2169	300	100	74.25	-4.762	260	9917	444	-9762	9.8	512	12	-357	444	0.00	MOT0
2170	300	100	74.25	-4.762	260	9323	465	-9762	9.8	512	12	-951	465	0.00	MOT0
2171	300	100	74.25	4.762	260	11187	462	-9775	9.8	512	12	900	462	0.00	MOT0
2172	300	100	74.25	4.762	260	10869	398	-9774	9.8	512	12	583	398	0.00	MOT0
2173	300	100	74.25	4.762	260	10787	373	-9774	9.8	512	12	501	374	0.00	MOT0
2174	300	100	74.25	-4.762	260	10366	477	-9762	9.8	512	12	92	478	0.00	MOT0
2175	300	100	74.25	-4.762	260	10295	474	-9762	9.8	513	12	20	474	0.00	MOT0
2176	300	100	74.25	-4.762	260	9986	481	-9762	9.8	513	12	-289	481	0.00	MOT0
2177	300	100	74.25	-4.762	260	9807	601	-9762	9.8	513	12	-467	601	0.00	MOT0
2178	300	100	74.25	-4.762	260	10371	408	-9761	9.8	513	12	96	408	0.00	MOT0
2179	300	100	74.25	-4.762	260	10006	526	-9761	9.8	513	12	-268	526	0.00	MOT0
2180	300	100	74.25	4.762	260	11037	369	-9776	9.8	513	12	748	370	0.00	MOT0
2181	300	100	74.25	4.762	260	11220	441	-9774	9.8	513	12	934	442	0.00	MOT0
2182	300	100	74.25	4.762	260	10586	443	-9775	9.8	513	12	298	443	0.00	MOT0
2183	300	100	74.25	4.762	260	10709	489	-9774	9.8	513	12	422	489	0.00	MOT0
2184	300	100	74.25	4.762	260	11043	352	-9774	9.8	513	12	756	352	0.00	MOT0
2185	300	100	74.25	4.762	260	9981	424	-9773	9.8	513	12	-306	424	0.00	MOT0
2186	300	100	74.25	4.762	260	10783	478	-9774	9.8	514	12	496	479	0.00	MOT0
2187	300	100	74.25	4.762	260	10447	431	-9774	9.8	514	12	159	431	0.00	MOT0
2188	300	100	74.25	4.762	260	11095	446	-9774	9.8	514	12	807	447	0.00	MOT0
2189	300	100	74.25	4.762	260	11013	528	-9774	9.8	514	12	725	529	0.00	MOT0
2190	300	100	74.25	4.762	260	10365	338	-9775	9.8	514	12	76	338	0.00	MOT0
2191	300	100	74.25	4.762	260	10696	438	-9773	9.8	514	12	408	439	0.00	MOT0
2192	300	100	74.25	4.762	260	10016	390	-9774	9.8	514	12	-272	390	0.00	MOT0
2193	300	100	74.25	4.762	260	10951	377	-9775	9.8	513	12	663	378	0.00	MOT0
2194	300	100	74.25	4.762	260	10087	391	-9775	9.8	514	12	-201	391	0.00	MOT0
2195	300	100	74.25	4.762	260	10619	391	-9774	9.8	514	12	331	391	0.00	MOT0
2196	300	100	74.25	4.762	260	10510	424	-9775	9.8	515	12	221	424	0.00	MOT0
2197	300	100	74.25	4.762	260	10645	359	-9774	9.8	515	12	356	359	0.00	MOT0
2198	300	100	74.25	4.762	260	10547	477	-9774	9.8	515	12	258	478	0.00	MOT0
2199	300	100	74.25	4.762	260	10130	571	-9775	9.8	515	12	-159	571	0.00	MOT0
2200	300	100	74.25	4.762	260	10477	514	-9775	9.8	515	12	188	515	0.00	MOT0
2201	300	100	74.25	4.762	260	10351	301	-9774	9.8	515	12	62	302	0.00	MOT0
2202	300	100	74.25	4.762	260	10115	396	-9773	9.8	515	12	-173	396	0.00	MOT0
2203	300	100	74.25	4.762	260	10935	441	-9775	9.8	515	12	646	441	0.00	MOT0
2204	300	100	74.25	-4.762	260	10446	530	-9761	9.8	515	12	171	530	0.00	MOT0
2205	300	100	74.25	-4.762	260	10169	530	-9760	9.8	515	12	-106	530	0.00	MOT0
2206	300	100	74.25	-4.762	260	9882	447	-9762	9.8	515	12	-394	447	0.00	MOT0
2207	300	100	74.25	-4.762	260	10218	417	-9759	9.8	515	12	-57	417	0.00	MOT0
2208	300	100	74.25	-4.762	260	9862	434	-9760	9.8	516	12	-414	435	0.00	MOT0
2209	300	100	74.25	-4.762	260	10461	393	-9761	9.8	516	12	184	393	0.00	MOT0
2210	300	100	74.25	-4.762	260	9522	503	-9761	9.8	517	12	-755	503	0.00	MOT0
2211	300	100	74.25	-4.762	260	9917	497	-9760	9.8	517	12	-360	497	0.00	MOT0
2212	300	100	74.25	-4.762	260	10872	406	-9761	9.8	517	12	595	407	0.00	MOT0
2213	300	100	74.25	4.762	260	10592	87	-9774	9.8	518	12	300	89	0.00	FDET
2214	300	100	74.25	4.762	260	10288	114	-9773	9.8	519	12	-3	115	0.00	FDET
2215	300	100	74.25	4.762	260	10496	110	-9773	9.8	519	12	203	111	0.00	FDET
2216	300	100	74.25	-4.762	260	10127	113	-9762	9.8	518	12	-153	114	0.00	FDET
2217	300	100	74.25	-4.762	260	9939	87	-9763	9.8	519	12	-343	89	0.00	FDET
2218	300	100	74.25	-4.762	260	10049	75	-9764	9.8	519	12	-234	76	0.00	FDET
2219	300	100	74.25	4.762	260	10610	119	-9772	9.8	519	12	320	120	0.00	FDET
2220	300	100	74.25	4.762	260	10508	91	-9773	9.8	518	12	217	92	0.00	FDET
2221	300	100	74.25	4.762	260	10715	94	-9773	9.8	518	12	424	96	0.00	FDET
2222	300	100	74.25	4.762	260	10346	88	-9772	9.8	518	12	55	90	0.00	FDET
2223	300	100	74.25	4.762	260	10392	93	-9774	9.8	518	12	100	94	0.00	FDET
2224	300	100	74.25	4.762	260	10518	95	-9772	9.8	518	12	228	96	0.00	FDET
2225	300	100	74.25	-4.762	260	10223	101	-9762	9.8	518	12	-57	102	0.00	FDET
2226	300	100	74.25	-4.762	260	10206	91	-9762	9.8	518	12	-74	92	0.00	FDET
2227	300	100	74.25	-4.762	260	10056	93	-9762	9.8	518	12	-224	95	0.00	FDET
2228	300	100	74.25	-4.762	260	10037	280	-9763	9.8	515	12	-241	280	0.00	LLAP

Continued on next page

Table A.2 Continued from previous page

N_{run}	T [ns]	D [ns]	P [W]	B [Gauss]	θ_{pol} [deg.]	ν_{fit} [Hz]	$\Delta\nu_{\text{fit}}$ [Hz]	DC_{B} [Hz]	$\Delta\text{DC}_{\text{B}}$ [Hz]	SC [Hz]	ΔSC [Hz]	ν_0 [Hz]	$\Delta\nu_0$ [Hz]	wts. [%]	Data Type
2229	300	100	74.25	-4.762	260	10348	277	-9764	9.8	515	12	69	278	0.00	LLAP
2230	300	100	74.25	-4.762	260	10239	209	-9763	9.8	516	12	-40	210	0.00	LLAP
2231	300	100	74.25	-4.762	260	10246	190	-9764	9.8	516	12	-34	191	0.00	LLAP
2232	300	100	74.25	-4.762	260	10119	227	-9762	9.8	516	12	-159	227	0.00	LLAP
2233	300	100	74.25	-4.762	260	10278	204	-9764	9.8	516	12	-1	205	0.00	LLAP
2234	300	100	74.25	-4.762	260	10106	243	-9762	9.8	516	12	-173	244	0.00	LLAP
2235	300	100	74.25	-4.762	260	10208	248	-9763	9.8	515	12	-70	248	0.00	LLAP
2236	300	100	74.25	-4.762	260	10706	240	-9763	9.8	515	12	428	241	0.00	LLAP
2237	300	100	74.25	4.762	260	10008	255	-9771	9.8	515	12	-279	255	0.00	LLAP
2238	300	100	74.25	4.762	260	10481	146	-9772	9.8	515	12	194	147	0.00	LLAP
2239	300	100	74.25	4.762	260	10426	237	-9772	9.8	515	12	139	238	0.00	LLAP
2240	300	100	74.25	-4.762	260	10573	241	-9761	9.8	516	12	296	241	0.00	LLAP
2241	300	100	74.25	-4.762	260	10126	192	-9762	9.8	516	12	-152	192	0.00	LLAP
2242	300	100	74.25	-4.762	260	10557	219	-9762	9.8	516	12	279	220	0.00	LLAP
2243	300	100	74.25	4.762	260	10433	214	-9774	9.8	515	12	143	214	0.00	LLAP
2244	300	100	74.25	4.762	260	10325	218	-9774	9.8	515	12	36	219	0.00	LLAP
2245	300	100	74.25	4.762	260	10623	143	-9772	9.8	515	12	336	143	0.00	LLAP
2246	300	100	74.25	4.762	260	10419	151	-9773	9.8	516	12	131	152	0.00	LLAP
2247	300	100	74.25	4.762	260	10311	178	-9773	9.8	516	12	23	179	0.00	LLAP
2248	300	100	74.25	4.762	260	9842	192	-9773	9.8	516	12	-447	193	0.00	LLAP
2249	300	100	74.25	-4.762	260	10268	228	-9764	9.8	516	12	-12	228	0.00	LLAP
2250	300	100	74.25	-4.762	260	10462	282	-9763	9.8	515	12	184	282	0.00	LLAP
2251	300	100	74.25	-4.762	260	10218	256	-9765	9.8	515	12	-62	256	0.00	LLAP
2252	300	100	74.25	-4.762	260	10680	255	-9764	9.8	516	12	401	256	0.00	LLAP
2253	300	100	74.25	-4.762	260	9762	228	-9764	9.8	518	12	-520	229	0.00	LLAP
2254	300	100	74.25	-4.762	260	10256	232	-9762	9.8	518	12	-24	232	0.00	LLAP
2255	300	100	74.25	4.762	260	10001	235	-9772	9.8	517	12	-288	236	0.00	LLAP
2256	300	100	74.25	4.762	260	10480	273	-9772	9.8	517	12	191	274	0.00	LLAP
2257	300	100	74.25	4.762	260	10415	242	-9773	9.8	516	12	127	242	0.00	LLAP
2258	300	100	74.25	-4.762	260	9706	228	-9763	9.8	516	12	-572	228	0.00	LLAP
2259	300	100	74.25	-4.762	260	10119	241	-9764	9.8	516	12	-161	242	0.00	LLAP
2260	300	100	74.25	-4.762	260	10168	287	-9763	9.8	515	12	-110	288	0.00	LLAP
2261	300	100	74.25	4.762	260	10122	183	-9771	9.8	515	12	-165	184	0.00	LLAP
2262	300	100	74.25	4.762	260	10527	200	-9772	9.8	515	12	239	201	0.00	LLAP
2263	300	100	74.25	4.762	260	10849	237	-9772	9.8	515	12	563	237	0.00	LLAP
2264	300	100	74.25	-4.762	260	10709	358	-9763	9.8	515	12	431	358	0.00	LLAP
2265	300	100	74.25	-4.762	260	10210	254	-9763	9.8	515	12	-68	254	0.00	LLAP
2266	300	100	74.25	-4.762	260	10355	307	-9762	9.8	515	12	78	307	0.00	LLAP
2267	300	100	74.25	-4.762	260	10223	322	-9763	9.8	515	12	-55	323	0.00	LLAP
2268	300	100	74.25	-4.762	260	10431	254	-9764	9.8	515	12	152	255	0.00	LLAP
2269	300	100	74.25	-4.762	260	10274	214	-9764	9.8	515	12	-4	215	0.00	LLAP
2270	300	100	74.25	-4.762	260	9698	198	-9763	9.8	515	12	-580	199	0.00	LLAP
2271	300	100	74.25	-4.762	260	10425	250	-9764	9.8	515	12	147	250	0.00	LLAP
2272	300	100	74.25	-4.762	260	10299	259	-9762	9.8	515	12	22	259	0.00	LLAP
2273	300	100	74.25	-4.762	260	10038	274	-9764	9.8	515	12	-241	275	0.00	LLAP
2274	300	100	74.25	-4.762	260	10552	200	-9764	9.8	515	12	274	201	0.00	LLAP
2275	300	100	74.25	-4.762	260	9988	227	-9763	9.8	515	12	-290	228	0.00	LLAP
2276	300	100	74.25	4.762	260	10352	198	-9772	9.8	515	12	65	199	0.00	LLAP
2277	300	100	74.25	4.762	260	10845	229	-9772	9.8	515	12	557	229	0.00	LLAP
2278	300	100	74.25	4.762	260	10400	219	-9773	9.8	515	12	112	219	0.00	LLAP
2279	300	100	74.25	4.762	260	10357	215	-9772	9.8	515	12	71	216	0.00	LLAP
2280	300	100	74.25	4.762	260	10553	247	-9773	9.8	514	12	266	247	0.00	LLAP
2281	300	100	74.25	4.762	260	10670	175	-9772	9.8	515	12	383	176	0.00	LLAP
2282	300	100	74.25	4.762	260	10298	159	-9772	9.8	515	12	10	160	0.00	LLAP
2283	300	100	74.25	4.762	260	10382	212	-9773	9.8	515	12	94	213	0.00	LLAP
2284	300	100	74.25	4.762	260	10434	233	-9773	9.8	515	12	145	234	0.00	LLAP
2285	300	100	74.25	-4.762	260	9937	249	-9762	9.8	515	12	-341	249	0.00	LLAP
2286	300	100	74.25	-4.762	260	9994	186	-9763	9.8	515	12	-283	187	0.00	LLAP
2287	300	100	74.25	-4.762	260	10201	276	-9763	9.8	515	12	-77	276	0.00	LLAP
2288	300	100	74.25	-4.762	260	10102	262	-9762	9.8	515	12	-175	262	0.00	LLAP
2289	300	100	74.25	-4.762	260	10663	160	-9763	9.8	515	12	385	160	0.00	LLAP
2290	300	100	74.25	-4.762	260	10011	205	-9763	9.8	515	12	-267	206	0.00	LLAP
2291	300	100	74.25	4.762	260	10208	164	-9773	9.8	515	12	-79	165	0.00	LLAP
2292	300	100	74.25	4.762	260	10596	194	-9773	9.8	514	12	310	195	0.00	LLAP
2293	300	100	74.25	4.762	260	10425	213	-9774	9.8	513	12	137	214	0.00	LLAP
2294	300	100	74.25	4.762	260	10481	186	-9773	9.8	514	12	194	187	0.00	LLAP
2295	300	100	74.25	4.762	260	10238	203	-9772	9.8	514	12	-49	204	0.00	LLAP
2296	300	100	74.25	4.762	260	10098	264	-9774	9.8	515	12	-190	264	0.00	LLAP
2297	300	100	74.25	4.762	260	10211	211	-9774	9.8	514	12	-78	211	0.00	LLAP
2298	300	100	74.25	4.762	260	10038	245	-9775	9.8	514	12	-251	246	0.00	LLAP
2299	300	100	74.25	4.762	260	10580	204	-9774	9.8	514	12	292	204	0.00	LLAP
2300	300	100	74.25	-4.762	260	10691	253	-9763	9.8	514	12	414	254	0.00	LLAP
2301	300	100	74.25	-4.762	260	10434	263	-9761	9.8	514	12	159	264	0.00	LLAP
2302	300	100	74.25	-4.762	260	10297	224	-9762	9.8	514	12	22	225	0.00	LLAP
2303	300	100	74.25	-4.762	260	10421	197	-9762	9.8	514	12	144	198	0.00	LLAP
2304	300	100	74.25	-4.762	260	10359	218	-9762	9.8	514	12	83	219	0.00	LLAP
2305	300	100	74.25	-4.762	260	10613	204	-9762	9.8	514	12	337	204	0.00	LLAP
2306	300	100	74.25	4.762	260	10245	196	-9773	9.8	514	12	-41	196	0.00	LLAP
2307	300	100	74.25	4.762	260	10093	201	-9774	9.8	514	12	-195	201	0.00	LLAP
2308	300	100	74.25	4.762	260	10007	183	-9774	9.8	515	12	-282	184	0.00	LLAP
2309	300	100	74.25	4.762	260	10157	143	-9773	9.8	515	12	-131	144	0.00	LLAP
2310	300	100	74.25	4.762	260	10188	184	-9773	9.8	514	12	-99	184	0.00	LLAP
2311	300	100	74.25	4.762	260	10622	149	-9774	9.8	514	12	334	149	0.00	LLAP
2312	300	100	74.25	-4.762	260	10490	188	-9762	9.8	514	12	214	189	0.00	LLAP
2313	300	100	74.25	-4.762	260	10071	213	-9761	9.8	514	12	-205	214	0.00	LLAP
2314	300	100	74.25	-4.762	260	10213	204	-9762	9.8	514	12	-63	205	0.00	LLAP
2315	300	100	74.25	4.762	260	10214	200	-9773	9.8	514	12	-73	201	0.00	LLAP
2316	300	100	74.25	4.762	260	10404	231	-9775	9.8	514	12	116	232	0.00	LLAP
2317	300	100	74.25	4.762	260	10349	170	-9774	9.8	514	12	62	170	0.00	LLAP
2318	300	100	74.25	4.762	260	10158	226	-9773	9.8	514	12	-129	226	0.00	LLAP
2319	300	100	74.25	4.762	260	10104	194	-9773	9.8	513	12	-182	195	0.00	LLAP
2320	300	100	74.25	4.762	260	10397	176	-9773	9.8	513	12	111	177	0.00	LLAP
2321	300	100	74.25	4.762	260	10214	154	-9773	9.8	513	12	-72	154	0.00	LLAP
2322	300	100	74.25	4.762	260	10315	162	-9773	9.8	513	12	29	163	0.00	LLAP
2323	300	100	74.25	4.762	260	10165	181	-9773	9.8	513	12	-120	182	0.00	LLAP

Continued on next page

Table A.2 Continued from previous page

N_{run}	T [ns]	D [ns]	P [W]	B [Gauss]	θ_{pol} [deg.]	ν_{fit} [Hz]	$\Delta\nu_{\mathrm{fit}}$ [Hz]	$\mathrm{DC_B}$ [Hz]	$\Delta\mathrm{DC_B}$ [Hz]	SC [Hz]	ΔSC [Hz]	ν_0 [Hz]	$\Delta\nu_0$ [Hz]	wts. [%]	Data Type
2324	300	100	74.25	4.762	260	10346	199	-9773	9.8	514	12	59	199	0.00	LLAP
2325	300	100	74.25	4.762	260	10134	183	-9773	9.8	514	12	-153	184	0.00	LLAP
2326	300	100	74.25	4.762	260	10138	179	-9773	9.8	513	12	-148	180	0.00	LLAP
2327	300	100	74.25	-4.762	260	10408	184	-9762	9.8	513	12	132	185	0.00	LLAP
2328	300	100	74.25	-4.762	260	10013	255	-9762	9.8	514	12	-262	256	0.00	LLAP
2329	300	100	74.25	-4.762	260	10388	156	-9762	9.8	514	12	113	157	0.00	LLAP
2330	300	100	74.25	-4.762	260	10597	259	-9761	9.8	514	12	323	259	0.00	LLAP
2331	300	100	74.25	-4.762	260	9969	278	-9762	9.8	514	12	-307	278	0.00	LLAP
2332	300	100	74.25	-4.762	260	10107	217	-9762	9.8	514	12	-169	218	0.00	LLAP
2333	300	100	74.25	4.762	260	10369	199	-9774	9.8	514	12	82	200	0.00	LLAP
2334	300	100	74.25	4.762	260	10420	191	-9774	9.8	513	12	133	192	0.00	LLAP
2335	300	100	74.25	4.762	260	10308	199	-9775	9.8	513	12	20	200	0.00	LLAP
2336	300	100	74.25	-4.762	260	10535	222	-9762	9.8	513	12	260	222	0.00	LLAP
2337	300	100	74.25	4.762	260	9967	221	-9773	9.8	514	12	-320	222	0.00	LLAP
2338	300	100	74.25	4.762	260	10390	211	-9774	9.8	514	12	102	212	0.00	LLAP
2339	300	100	74.25	4.762	260	10220	227	-9775	9.8	514	12	-69	228	0.00	LLAP
2340	300	100	74.25	4.762	260	10532	188	-9774	9.8	513	12	244	189	0.00	LLAP
2341	300	100	74.25	4.762	260	10427	211	-9774	9.8	514	12	139	212	0.00	LLAP
2342	300	100	74.25	4.762	260	10370	217	-9774	9.8	514	12	82	217	0.00	LLAP
2343	300	100	74.25	4.762	260	10573	196	-9774	9.8	513	12	286	196	0.00	LLAP
2344	300	100	74.25	4.762	260	10442	200	-9774	9.8	513	12	154	201	0.00	LLAP
2345	300	100	74.25	4.762	260	10262	186	-9773	9.8	514	12	-25	186	0.00	LLAP
2346	300	100	74.25	4.762	260	10288	214	-9774	9.8	514	12	0	214	0.00	LLAP
2347	300	100	74.25	4.762	260	10567	227	-9774	9.8	514	12	279	228	0.00	LLAP
2348	300	100	74.25	4.762	260	10031	215	-9773	9.8	514	12	-256	216	0.00	LLAP
2349	300	100	74.25	-4.762	260	10161	233	-9762	9.8	513	12	-115	233	0.00	LLAP
2350	300	100	74.25	-4.762	260	10174	221	-9761	9.8	514	12	-100	222	0.00	LLAP
2351	300	100	74.25	-4.762	260	10684	217	-9760	9.8	514	12	411	217	0.00	LLAP
2352	300	100	74.25	-4.762	260	10218	207	-9760	9.8	514	12	-56	208	0.00	LLAP
2353	300	100	74.25	-4.762	260	10209	173	-9761	9.8	514	12	-66	174	0.00	LLAP
2354	300	100	74.25	-4.762	260	10277	263	-9761	9.8	513	12	3	264	0.00	LLAP
2355	300	100	74.25	-4.762	260	10328	158	-9761	9.8	513	12	54	159	0.00	LLAP
2356	300	100	74.25	-4.762	260	10177	244	-9761	9.8	513	12	-97	244	0.00	LLAP
2357	300	100	74.25	-4.762	260	10721	267	-9760	9.8	513	12	447	267	0.00	LLAP
2358	300	100	74.25	-4.762	260	10379	251	-9761	9.8	513	12	105	252	0.00	LLAP
2359	300	100	74.25	-4.762	260	10585	246	-9761	9.8	513	12	311	246	0.00	LLAP
2360	300	100	74.25	-4.762	260	10325	203	-9760	9.8	513	12	52	203	0.00	LLAP
2361	300	100	74.25	-4.762	260	10346	266	-9761	9.8	513	12	72	266	0.00	LLAP
2362	300	100	74.25	-4.762	260	10022	306	-9760	9.8	513	12	-251	307	0.00	LLAP
2363	300	100	74.25	-4.762	260	10217	175	-9761	9.8	514	12	-58	176	0.00	LLAP
2364	300	100	74.25	4.762	260	10286	162	-9775	9.8	514	12	-3	163	0.00	LLAP
2365	300	100	74.25	4.762	260	10640	227	-9774	9.8	514	12	351	228	0.00	LLAP
2366	300	100	74.25	4.762	260	10405	188	-9776	9.8	514	12	115	188	0.00	LLAP
2367	300	100	74.25	4.762	260	10025	153	-9775	9.8	514	12	-264	153	0.00	LLAP
2368	300	100	74.25	4.762	260	10039	181	-9775	9.8	514	12	-250	181	0.00	LLAP
2369	300	100	74.25	4.762	260	10432	232	-9775	9.8	514	12	143	232	0.00	LLAP
2370	300	100	74.25	-4.762	260	10145	202	-9761	9.8	514	12	-130	203	0.00	LLAP
2371	300	100	74.25	-4.762	260	10135	226	-9760	9.8	514	12	-139	226	0.00	LLAP
2372	300	100	74.25	-4.762	260	10117	227	-9760	9.8	513	12	-156	228	0.00	LLAP
2373	300	100	74.25	4.762	260	10078	153	-9776	9.8	513	12	-212	154	0.00	LLAP
2374	300	100	74.25	4.762	260	10504	203	-9775	9.8	513	12	216	203	0.00	LLAP
2375	300	100	74.25	4.762	260	10212	208	-9775	9.8	513	12	-76	208	0.00	LLAP
2376	300	100	74.25	4.762	260	10315	224	-9775	9.8	513	12	27	225	0.00	LLAP
2377	300	100	74.25	4.762	260	10463	209	-9776	9.8	513	12	174	210	0.00	LLAP
2378	300	100	74.25	4.762	260	10095	258	-9776	9.8	513	12	-194	258	0.00	LLAP
2379	300	100	74.25	-4.762	260	10293	231	-9759	9.8	513	12	20	231	0.00	LLAP
2380	300	100	74.25	-4.762	260	9907	193	-9760	9.8	513	12	-366	194	0.00	LLAP
2381	300	100	74.25	-4.762	260	10241	253	-9760	9.8	513	12	-33	254	0.00	LLAP
2382	300	100	74.25	4.762	260	10529	224	-9775	9.8	513	12	241	225	0.00	LLAP
2383	300	100	74.25	4.762	260	10455	199	-9776	9.8	513	12	166	200	0.00	LLAP
2384	300	100	74.25	4.762	260	10149	257	-9775	9.8	513	12	-138	257	0.00	LLAP
2385	300	100	74.25	4.762	260	10001	209	-9776	9.8	513	12	-287	209	0.00	LLAP
2386	300	100	74.25	4.762	260	10046	184	-9775	9.8	513	12	-242	185	0.00	LLAP
2387	300	100	74.25	4.762	260	10289	218	-9775	9.8	513	12	1	219	0.00	LLAP
2388	300	100	74.25	-4.762	260	9743	254	-9759	9.8	513	12	-529	254	0.00	LLAP
2389	300	100	74.25	-4.762	260	9810	230	-9760	9.8	513	12	-463	231	0.00	LLAP
2390	300	100	74.25	-4.762	260	9882	214	-9759	9.8	513	12	-391	215	0.00	LLAP
2391	300	100	74.25	-4.762	260	10410	209	-9761	9.8	513	12	136	209	0.00	LLAP
2392	300	100	74.25	-4.762	260	9943	277	-9760	9.8	513	12	-330	277	0.00	LLAP
2393	300	100	74.25	-4.762	260	10413	262	-9759	9.8	513	12	141	263	0.00	LLAP
2394	300	100	74.25	4.762	260	10304	275	-9775	9.8	513	12	16	275	0.00	LLAP
2395	300	100	74.25	4.762	260	10565	232	-9775	9.8	513	12	277	233	0.00	LLAP
2396	300	100	74.25	4.762	260	10460	200	-9775	9.8	512	12	173	200	0.00	LLAP
2397	300	100	74.25	-4.762	260	10344	240	-9760	9.8	512	12	72	241	0.00	LLAP
2398	300	100	74.25	-4.762	260	10321	221	-9760	9.8	513	12	48	222	0.00	LLAP
2399	300	100	74.25	-4.762	260	10329	258	-9759	9.8	513	12	57	259	0.00	LLAP
2400	300	100	74.25	-4.762	260	10273	270	-9761	9.8	513	12	0	270	0.00	LLAP
2401	300	100	74.25	-4.762	260	9945	238	-9761	9.8	512	12	-328	239	0.00	LLAP
2402	300	100	74.25	-4.762	260	10638	239	-9760	9.8	513	12	366	240	0.00	LLAP
2403	300	100	74.25	4.762	260	10343	244	-9777	9.8	513	12	54	245	0.00	LLAP
2404	300	100	74.25	4.762	260	10077	155	-9776	9.8	513	12	-212	155	0.00	LLAP
2405	300	100	74.25	4.762	260	10240	206	-9775	9.8	512	12	-47	207	0.00	LLAP
2406	300	100	74.25	-4.762	260	10337	252	-9760	9.8	512	12	64	253	0.00	LLAP
2407	300	100	74.25	-4.762	260	10520	234	-9760	9.8	513	12	247	235	0.00	LLAP
2408	300	100	74.25	-4.762	260	10034	249	-9760	9.8	513	12	-238	250	0.00	LLAP
2409	300	100	74.25	4.762	260	10370	209	-9774	9.8	513	12	83	210	0.00	LLAP
2410	300	100	74.25	4.762	260	9927	222	-9774	9.8	512	12	-359	223	0.00	LLAP
2411	300	100	74.25	4.762	260	10718	199	-9774	9.8	512	12	432	200	0.00	LLAP
2412	300	100	74.25	-4.762	260	10190	250	-9761	9.8	512	12	-84	250	0.00	LLAP
2413	300	100	74.25	-4.762	260	10380	251	-9761	9.8	513	12	107	252	0.00	LLAP
2414	300	100	74.25	-4.762	260	10246	198	-9762	9.8	512	12	-28	199	0.00	LLAP
2415	300	100	74.25	-4.762	260	10226	260	-9761	9.8	512	12	-48	261	0.00	LLAP
2416	300	100	74.25	-4.762	260	10687	247	-9760	9.8	512	12	415	248	0.00	LLAP
2417	300	100	74.25	-4.762	260	10315	193	-9760	9.8	512	12	43	194	0.00	LLAP
2418	300	100	74.25	-4.762	260	10254	202	-9760	9.8	512	12	-19	202	0.00	LLAP

Continued on next page

Table A.2 Continued from previous page

N_{run}	T [ns]	D [ns]	P [W]	B [Gauss]	θ_{pol} [deg.]	ν_{fit} [Hz]	$\Delta\nu_{\mathrm{fit}}$ [Hz]	$\mathrm{DC_B}$ [Hz]	$\Delta\mathrm{DC_B}$ [Hz]	SC [Hz]	ΔSC [Hz]	ν_0 [Hz]	$\Delta\nu_0$ [Hz]	wts. [%]	Data Type
2419	300	100	74.25	-4.762	260	10519	232	-9761	9.8	512	12	246	233	0.00	LLAP
2420	300	100	74.25	-4.762	260	10294	251	-9760	9.8	512	12	22	252	0.00	LLAP
2421	300	100	74.25	4.762	260	10425	207	-9774	9.8	512	12	139	207	0.00	LLAP
2422	300	100	74.25	4.762	260	10458	230	-9773	9.8	512	12	173	230	0.00	LLAP
2423	300	100	74.25	4.762	260	10452	181	-9774	9.8	512	12	165	182	0.00	LLAP
2424	300	100	74.25	-4.762	260	10451	246	-9761	9.8	512	12	178	247	0.00	LLAP
2425	300	100	74.25	-4.762	260	9874	204	-9762	9.8	512	12	-400	205	0.00	LLAP
2426	300	100	74.25	-4.762	260	10688	297	-9762	9.8	512	12	415	298	0.00	LLAP
2427	300	100	74.25	4.762	260	10361	246	-9774	9.8	512	12	76	246	0.00	LLAP
2428	300	100	74.25	4.762	260	9886	211	-9773	9.8	512	12	-399	212	0.00	LLAP
2429	300	100	74.25	4.762	260	10626	202	-9774	9.8	512	12	340	202	0.00	LLAP
2430	300	100	74.25	-4.762	260	10070	292	-9759	9.8	512	12	-201	293	0.00	LLAP
2431	300	100	74.25	4.762	260	10256	57	-9773	9.8	513	12	-31	59	0.00	CWLC
2432	300	100	74.25	4.762	260	10303	63	-9773	9.8	514	12	17	65	0.00	CWLC
2433	300	100	74.25	4.762	260	10337	55	-9773	9.8	514	12	50	57	0.00	CWLC
2434	300	100	74.25	-4.762	260	10168	46	-9762	9.8	514	12	-108	49	0.00	CWLC
2435	300	100	74.25	-4.762	260	10279	56	-9762	9.8	514	12	3	58	0.00	CWLC
2436	300	100	74.25	-4.762	260	10275	58	-9761	9.8	514	12	1	60	0.00	CWLC
2437	300	100	74.25	4.762	260	10355	57	-9773	9.8	514	12	69	59	0.00	CWLC
2438	300	100	74.25	4.762	260	10332	57	-9773	9.8	514	12	45	60	0.00	CWLC
2439	300	100	74.25	4.762	260	10223	59	-9773	9.8	514	12	-64	61	0.00	CWLC
2440	300	100	74.25	-4.762	260	10423	577	-9761	9.8	515	12	146	578	0.00	LLBP
2441	300	100	74.25	-4.762	260	10589	530	-9760	9.8	515	12	313	531	0.00	LLBP
2442	300	100	74.25	-4.762	260	9922	512	-9762	9.8	515	12	-356	512	0.00	LLBP
2443	300	100	74.25	4.762	260	10698	366	-9775	9.8	515	12	408	367	0.00	LLBP
2444	300	100	74.25	4.762	260	11020	474	-9774	9.8	515	12	730	474	0.00	LLBP
2445	300	100	74.25	4.762	260	9878	389	-9774	9.8	515	12	-412	390	0.00	LLBP
2446	300	100	74.25	4.762	260	10555	393	-9775	9.8	516	12	264	394	0.00	LLBP
2447	300	100	74.25	4.762	260	10257	456	-9773	9.8	516	12	-32	456	0.00	LLBP
2448	300	100	74.25	4.762	260	10790	440	-9772	9.8	516	12	502	440	0.00	LLBP
2449	300	100	74.25	4.762	260	10512	430	-9773	9.8	516	12	223	431	0.00	LLBP
2450	300	100	74.25	4.762	260	9096	373	-9774	9.8	516	12	-1194	374	0.00	LLBP
2451	300	100	74.25	4.762	260	10428	475	-9774	9.8	517	12	138	475	0.00	LLBP
2452	300	100	74.25	4.762	260	10426	430	-9773	9.8	515	12	137	430	0.00	LLBP
2453	300	100	74.25	4.762	260	10557	380	-9773	9.8	515	12	269	381	0.00	LLBP
2454	300	100	74.25	4.762	260	9711	372	-9773	9.8	515	12	-578	373	0.00	LLBP
2455	300	100	74.25	-4.762	260	10826	436	-9762	9.8	516	12	549	437	0.00	LLBP
2456	300	100	74.25	-4.762	260	10358	506	-9762	9.8	516	12	80	507	0.00	LLBP
2457	300	100	74.25	-4.762	260	10353	518	-9762	9.8	517	12	75	519	0.00	LLBP
2458	300	100	74.25	4.762	260	9967	391	-9773	9.8	517	12	-323	391	0.00	LLBP
2459	300	100	74.25	4.762	260	9939	426	-9773	9.8	517	12	-351	426	0.00	LLBP
2460	300	100	74.25	4.762	260	10320	484	-9772	9.8	517	12	31	484	0.00	LLBP
2461	300	100	74.25	4.762	260	10241	369	-9772	9.8	517	12	-47	369	0.00	LLBP
2462	300	100	74.25	4.762	260	9761	358	-9773	9.8	516	12	-528	359	0.00	LLBP
2463	300	100	74.25	4.762	260	10767	410	-9772	9.8	516	12	479	411	0.00	LLBP
2464	300	100	74.25	-4.762	260	10301	459	-9763	9.8	516	12	22	459	0.00	LLBP
2465	300	100	74.25	-4.762	260	10034	563	-9762	9.8	516	12	-245	563	0.00	LLBP
2466	300	100	74.25	-4.762	260	10546	458	-9762	9.8	516	12	268	459	0.00	LLBP
2467	300	100	74.25	-4.762	260	9802	416	-9763	9.8	515	12	-476	417	0.00	LLBP
2468	300	100	74.25	-4.762	260	9923	427	-9763	9.8	515	12	-355	427	0.00	LLBP
2469	300	100	74.25	-4.762	260	9814	540	-9762	9.8	515	12	-463	541	0.00	LLBP
2470	300	100	74.25	-4.762	260	9862	535	-9762	9.8	516	12	-416	536	0.00	LLBP
2471	300	100	74.25	-4.762	260	11038	536	-9761	9.8	515	12	762	536	0.00	LLBP
2472	300	100	74.25	-4.762	260	10320	484	-9763	9.8	515	12	42	484	0.00	LLBP
2473	300	100	74.25	4.762	260	10114	391	-9773	9.8	516	12	-174	391	0.00	LLBP
2474	300	100	74.25	4.762	260	10847	372	-9773	9.8	515	12	558	373	0.00	LLBP
2475	300	100	74.25	4.762	260	10396	451	-9773	9.8	515	12	108	452	0.00	LLBP
2476	300	100	74.25	-4.762	260	9754	445	-9762	9.8	516	12	-523	445	0.00	LLBP
2477	300	100	74.25	-4.762	260	9921	463	-9762	9.8	516	12	-357	464	0.00	LLBP
2478	300	100	74.25	-4.762	260	9590	533	-9762	9.8	516	12	-688	533	0.00	LLBP
2479	300	100	74.25	4.762	260	9295	351	-9773	9.8	516	12	-994	351	0.00	LLBP
2480	300	100	74.25	4.762	260	10220	410	-9774	9.8	515	12	-69	410	0.00	LLBP
2481	300	100	74.25	4.762	260	10591	372	-9773	9.8	514	12	305	372	0.00	LLBP
2482	300	100	74.25	4.762	260	10233	382	-9773	9.8	513	12	-53	382	0.00	LLBP
2483	300	100	74.25	4.762	260	10323	330	-9773	9.8	514	12	36	331	0.00	LLBP
2484	300	100	74.25	4.762	260	10314	435	-9774	9.8	514	12	26	435	0.00	LLBP
2485	300	100	74.25	4.762	260	10386	383	-9773	9.8	513	12	100	383	0.00	LLBP
2486	300	100	74.25	4.762	260	10692	388	-9773	9.8	513	12	405	388	0.00	LLBP
2487	300	100	74.25	4.762	260	10493	375	-9772	9.8	513	12	207	375	0.00	LLBP
2488	300	100	74.25	-4.762	260	9867	556	-9761	9.8	513	12	-407	556	0.00	LLBP
2489	300	100	74.25	-4.762	260	9690	408	-9760	9.8	513	12	-584	409	0.00	LLBP
2490	300	100	74.25	-4.762	260	10392	506	-9762	9.8	513	12	118	506	0.00	LLBP
2491	300	100	74.25	-4.762	260	9827	423	-9762	9.8	513	12	-448	423	0.00	LLBP
2492	300	100	74.25	-4.762	260	9413	450	-9762	9.8	514	12	-863	450	0.00	LLBP
2493	300	100	74.25	-4.762	260	10214	611	-9761	9.8	514	12	-61	612	0.00	LLBP
2494	300	100	74.25	-4.762	260	10587	474	-9762	9.8	514	12	311	474	0.00	LLBP
2495	300	100	74.25	-4.762	260	10305	474	-9761	9.8	514	12	29	475	0.00	LLBP
2496	300	100	74.25	-4.762	260	11756	508	-9761	9.8	514	12	1481	508	0.00	LLBP
2497	300	100	74.25	-4.762	260	10158	567	-9761	9.8	514	12	-117	567	0.00	LLBP
2498	300	100	74.25	-4.762	260	11325	552	-9761	9.8	514	12	1050	552	0.00	LLBP
2499	300	100	74.25	-4.762	260	10618	405	-9760	9.8	514	12	344	405	0.00	LLBP
2500	300	100	74.25	-4.762	260	10130	468	-9760	9.8	514	12	-144	468	0.00	LLBP
2501	300	100	74.25	4.762	260	10841	492	-9773	9.8	514	12	554	492	0.00	LLBP
2502	300	100	74.25	4.762	260	10414	402	-9774	9.8	514	12	126	402	0.00	LLBP
2503	300	100	74.25	4.762	260	10398	401	-9773	9.8	514	12	112	401	0.00	LLBP
2504	300	100	74.25	4.762	260	9740	475	-9773	9.8	513	12	-546	476	0.00	LLBP
2505	300	100	74.25	4.762	260	10382	410	-9774	9.8	513	12	95	410	0.00	LLBP
2506	300	100	74.25	4.762	260	10521	468	-9773	9.8	513	12	236	468	0.00	LLBP
2507	300	100	74.25	4.762	260	10184	424	-9772	9.8	513	12	-101	424	0.00	LLBP
2508	300	100	74.25	4.762	260	10447	400	-9773	9.8	513	12	160	401	0.00	LLBP
2509	300	100	74.25	4.762	260	9917	392	-9773	9.8	513	12	-370	393	0.00	LLBP
2510	300	100	74.25	4.762	260	9874	409	-9773	9.8	513	12	-412	409	0.00	LLBP
2511	300	100	74.25	4.762	260	9949	402	-9773	9.8	513	12	-338	402	0.00	LLBP
2512	300	100	74.25	4.762	260	10515	421	-9773	9.8	513	12	229	421	0.00	LLBP
2513	300	100	74.25	-4.762	260	10020	555	-9762	9.8	512	12	-254	555	0.00	LLBP
2514	300	100	74.25	-4.762	260	10472	426	-9763	9.8	512	12	197	426	0.00	LLBP
2515	300	100	74.25	-4.762	260	10121	423	-9762	9.8	512	12	-153	424	0.00	LLBP
2516	300	100	74.25	4.762	260	10202	400	-9774	9.8	514	12	-87	401	0.00	LLBP

Continued on next page

Table A.2 Continued from previous page

N_{run}	T [ns]	D [ns]	P [W]	B [Gauss]	θ_{pol} [deg.]	ν_{fit} [Hz]	$\Delta\nu_{\mathrm{fit}}$ [Hz]	$\mathrm{DC_B}$ [Hz]	$\Delta\mathrm{DC_B}$ [Hz]	SC [Hz]	ΔSC [Hz]	ν_0 [Hz]	$\Delta\nu_0$ [Hz]	wts. [%]	Data Type
2517	300	100	74.25	4.762	260	10305	400	-9774	9.8	514	12	17	400	0.00	LLBP
2518	300	100	74.25	4.762	260	9987	290	-9773	9.8	514	12	-299	291	0.00	LLBP
2519	300	100	74.25	-4.762	260	9880	408	-9763	9.8	514	12	-397	408	0.00	LLBP
2520	300	100	74.25	-4.762	260	10080	493	-9762	9.8	514	12	-196	493	0.00	LLBP
2521	300	100	74.25	-4.762	260	11275	456	-9761	9.8	514	12	999	457	0.00	LLBP
2522	300	100	74.25	-4.762	260	9793	484	-9761	9.8	512	12	-480	484	0.00	LLBP
2523	300	100	74.25	-4.762	260	10341	562	-9762	9.8	512	12	67	562	0.00	LLBP
2524	300	100	74.25	-4.762	260	10842	459	-9761	9.8	513	12	568	460	0.00	LLBP
2525	300	100	74.25	4.762	260	10172	392	-9773	9.8	513	12	-114	392	0.00	LLBP
2526	300	100	74.25	4.762	260	9994	362	-9772	9.8	513	12	-291	362	0.00	LLBP
2527	300	100	74.25	4.762	260	10236	372	-9773	9.8	513	12	-50	372	0.00	LLBP
2528	300	100	74.25	4.762	260	9720	472	-9774	9.8	514	12	-567	472	0.00	LLBP
2529	300	100	74.25	4.762	260	10008	443	-9774	9.8	513	12	-280	444	0.00	LLBP
2530	300	100	74.25	4.762	260	10381	432	-9773	9.8	513	12	94	433	0.00	LLBP
2531	300	100	74.25	-4.762	260	9704	467	-9761	9.8	513	12	-570	467	0.00	LLBP
2532	300	100	74.25	-4.762	260	10707	525	-9761	9.8	513	12	433	526	0.00	LLBP
2533	300	100	74.25	-4.762	260	10823	557	-9760	9.8	513	12	550	558	0.00	LLBP
2534	300	100	74.25	-4.762	260	10305	602	-9761	9.8	513	12	31	603	0.00	LLBP
2535	300	100	74.25	-4.762	260	10469	485	-9761	9.8	513	12	195	485	0.00	LLBP
2536	300	100	74.25	-4.762	260	9639	483	-9760	9.8	513	12	-635	483	0.00	LLBP
2537	300	100	74.25	-4.762	260	10297	379	-9761	9.8	513	12	23	380	0.00	LLBP
2538	300	100	74.25	-4.762	260	10148	492	-9760	9.8	513	12	-125	492	0.00	LLBP
2539	300	100	74.25	-4.762	260	10550	436	-9759	9.8	513	12	278	436	0.00	LLBP
2540	300	100	74.25	-4.762	260	10362	434	-9760	9.8	513	12	89	434	0.00	LLBP
2541	300	100	74.25	-4.762	260	10391	454	-9761	9.8	513	12	117	454	0.00	LLBP
2542	300	100	74.25	-4.762	260	9785	491	-9761	9.8	513	12	-489	492	0.00	LLBP
2543	300	100	74.25	-4.762	260	10317	589	-9761	9.8	513	12	43	589	0.00	LLBP
2544	300	100	74.25	-4.762	260	10037	431	-9760	9.8	513	12	-236	431	0.00	LLBP
2545	300	100	74.25	-4.762	260	10361	527	-9760	9.8	513	12	88	527	0.00	LLBP
2546	300	100	74.25	-4.762	260	10551	402	-9761	9.8	513	12	277	402	0.00	LLBP
2547	300	100	74.25	-4.762	260	10814	592	-9761	9.8	513	12	540	593	0.00	LLBP
2548	300	100	74.25	-4.762	260	9863	422	-9760	9.8	513	12	-410	422	0.00	LLBP
2549	300	100	74.25	-4.762	260	10496	450	-9759	9.8	512	12	224	450	0.00	LLBP
2550	300	100	74.25	-4.762	260	9978	500	-9761	9.8	512	12	-295	500	0.00	LLBP
2551	300	100	74.25	-4.762	260	10532	517	-9760	9.8	512	12	259	517	0.00	LLBP
2552	300	100	74.25	4.762	260	10021	417	-9774	9.8	513	12	-266	417	0.00	LLBP
2553	300	100	74.25	4.762	260	9894	323	-9775	9.8	512	12	-394	324	0.00	LLBP
2554	300	100	74.25	4.762	260	10618	288	-9774	9.8	512	12	331	288	0.00	LLBP
2555	300	100	74.25	-4.762	260	10243	502	-9761	9.8	512	12	-30	503	0.00	LLBP
2556	300	100	74.25	-4.762	260	10396	426	-9761	9.8	513	12	123	427	0.00	LLBP
2557	300	100	74.25	-4.762	260	10217	507	-9760	9.8	512	12	-56	508	0.00	LLBP
2558	300	100	74.25	4.762	260	10625	446	-9775	9.8	512	12	338	446	0.00	LLBP
2559	300	100	74.25	4.762	260	10620	353	-9774	9.8	512	12	334	353	0.00	LLBP
2560	300	100	74.25	4.762	260	11062	347	-9775	9.8	512	12	775	347	0.00	LLBP
2561	300	100	74.25	4.762	260	10380	388	-9774	9.8	512	12	94	389	0.00	LLBP
2562	300	100	74.25	4.762	260	10314	287	-9775	9.8	512	12	27	287	0.00	LLBP
2563	300	100	74.25	4.762	260	10621	406	-9773	9.8	512	12	336	406	0.00	LLBP
2564	300	100	74.25	4.762	260	10182	477	-9775	9.8	512	12	-105	477	0.00	LLBP
2565	300	100	74.25	4.762	260	10457	482	-9773	9.8	512	12	173	483	0.00	LLBP
2566	300	100	74.25	4.762	260	10180	489	-9774	9.8	512	12	-106	490	0.00	LLBP
2567	300	100	74.25	4.762	260	10578	415	-9773	9.8	512	12	293	415	0.00	LLBP
2568	300	100	74.25	4.762	260	10371	489	-9774	9.8	512	12	85	489	0.00	LLBP
2569	300	100	74.25	4.762	260	10290	453	-9774	9.8	512	12	4	453	0.00	LLBP
2570	300	100	74.25	-4.762	260	9344	524	-9759	9.8	512	12	-928	524	0.00	LLBP
2571	300	100	74.25	-4.762	260	10110	434	-9760	9.8	512	12	-162	434	0.00	LLBP
2572	300	100	74.25	-4.762	260	9891	469	-9761	9.8	512	12	-382	470	0.00	LLBP
2573	300	100	74.25	4.762	260	10278	356	-9774	9.8	511	12	-7	357	0.00	LLBP
2574	300	100	74.25	4.762	260	10172	439	-9772	9.8	511	12	-112	439	0.00	LLBP
2575	300	100	74.25	4.762	260	10381	453	-9774	9.8	512	12	95	453	0.00	LLBP
2576	300	100	74.25	4.762	260	9948	376	-9775	9.8	512	12	-338	377	0.00	LLBP
2577	300	100	74.25	4.762	260	10331	316	-9774	9.8	512	12	46	316	0.00	LLBP
2578	300	100	74.25	4.762	260	10419	371	-9773	9.8	512	12	134	371	0.00	LLBP
2579	300	100	74.25	4.762	260	10843	316	-9773	9.8	512	12	558	316	0.00	LLBP
2580	300	100	74.25	4.762	260	9979	394	-9775	9.8	512	12	-307	394	0.00	LLBP
2581	300	100	74.25	4.762	260	10916	336	-9775	9.8	512	12	629	336	0.00	LLBP
2582	300	100	74.25	-4.762	260	10284	486	-9760	9.8	512	12	12	486	0.00	LLBP
2583	300	100	74.25	-4.762	260	9888	599	-9760	9.8	512	12	-384	599	0.00	LLBP
2584	300	100	74.25	-4.762	260	9926	514	-9760	9.8	512	12	-345	514	0.00	LLBP
2585	300	100	74.25	4.762	260	9567	347	-9775	9.8	512	12	-720	347	0.00	LLBP
2586	300	100	74.25	4.762	260	10662	483	-9775	9.8	512	12	376	484	0.00	LLBP
2587	300	100	74.25	4.762	260	9977	429	-9774	9.8	511	12	-309	429	0.00	LLBP
2588	300	100	74.25	4.762	260	10176	364	-9774	9.8	511	12	-110	364	0.00	LLBP
2589	300	100	74.25	4.762	260	10264	391	-9774	9.8	511	12	-21	391	0.00	LLBP
2590	300	100	74.25	4.762	260	10138	386	-9774	9.8	511	12	-147	386	0.00	LLBP
2591	300	100	74.25	4.762	260	10279	379	-9775	9.8	512	12	-8	380	0.00	LLBP
2592	300	100	74.25	4.762	260	10248	361	-9774	9.8	512	12	-38	362	0.00	LLBP
2593	300	100	74.25	4.762	260	11024	387	-9774	9.8	512	12	738	388	0.00	LLBP
2594	300	100	74.25	4.762	260	11277	78	-9773	9.8	501	12	1003	79	0.00	FDET
2595	300	100	74.25	4.762	260	11280	57	-9771	9.8	501	12	1008	59	0.00	FDET
2596	300	100	74.25	4.762	260	11248	77	-9771	9.8	501	12	976	79	0.00	FDET
2597	300	100	74.25	-4.762	260	11557	169	-9763	9.8	502	12	1292	170	0.00	FDET
2598	300	100	74.25	4.762	260	11198	136	-9772	9.8	501	12	925	137	0.00	FDET
2599	300	100	74.25	4.762	260	11178	62	-9771	9.8	501	12	906	64	0.00	FDET
2600	300	100	74.25	4.762	260	11173	56	-9771	9.8	502	12	900	58	0.00	FDET
2601	300	100	74.25	4.762	260	11164	52	-9773	9.8	502	12	889	55	0.00	FDET
2602	300	100	74.25	4.762	260	11222	96	-9771	9.8	502	12	949	97	0.00	FDET
2603	300	100	74.25	4.762	260	11150	78	-9769	9.8	497	12	885	80	0.00	FDET
2604	300	100	74.25	4.762	260	11093	66	-9771	9.8	499	12	823	67	0.00	FDET
2605	300	100	74.25	4.762	260	11228	58	-9771	9.8	498	12	959	60	0.00	FDET
2606	300	100	74.25	4.762	260	10272	70	-9772	9.8	524	13	-23	72	0.00	FDET
2607	300	100	74.25	4.762	260	10186	59	-9770	9.8	524	13	-107	61	0.00	FDET
2608	300	100	74.25	4.762	260	10330	80	-9773	9.8	525	13	33	82	0.00	FDET
2609	300	100	74.25	4.762	260	10207	69	-9773	9.8	525	13	-90	71	0.00	FDET
2610	300	100	74.25	4.762	260	10361	53	-9772	9.8	524	13	64	55	0.00	FDET
2611	300	100	74.25	4.762	260	10238	65	-9772	9.8	524	13	-58	67	0.00	FDET
2612	300	100	74.25	4.762	260	10326	48	-9772	9.8	524	13	30	50	0.00	FDET
2613	300	100	74.25	4.762	260	10305	69	-9770	9.8	524	13	11	71	0.00	FDET
2614	300	100	74.25	4.762	260	10178	72	-9770	9.8	524	13	-116	73	0.00	FDET

Continued on next page

Table A.2 Continued from previous page

N_{run}	T [ns]	D [ns]	P [W]	B [Gauss]	θ_{pol} [deg.]	ν_{fit} [Hz]	$\Delta\nu_{\mathrm{fit}}$ [Hz]	$\mathrm{DC_B}$ [Hz]	$\Delta\mathrm{DC_B}$ [Hz]	SC [Hz]	ΔSC [Hz]	ν_0 [Hz]	$\Delta\nu_0$ [Hz]	wts. [%]	Data Type
2615	300	100	74.25	4.762	260	10182	62	-9770	9.8	524	13	-111	64	0.00	FDET
2616	300	100	74.25	-4.762	260	10211	57	-9764	9.8	524	13	-76	59	0.00	FDET
2617	300	100	74.25	-4.762	260	10334	60	-9764	9.8	524	13	46	62	0.00	FDET
2618	300	100	74.25	-4.762	260	10184	63	-9764	9.8	524	13	-104	65	0.00	FDET
2619	300	100	74.25	-4.762	260	10165	49	-9763	9.8	524	13	-122	52	0.00	FDET
2620	300	100	74.25	-4.762	260	10268	60	-9765	9.8	524	13	-20	62	0.00	FDET
2621	300	100	74.25	-4.762	260	10198	50	-9765	9.8	524	13	-91	53	0.00	FDET
2622	300	100	74.25	-4.762	260	10261	58	-9763	9.8	523	13	-25	60	0.00	FDET
2623	300	100	74.25	-4.762	260	10247	64	-9762	9.8	522	13	-37	66	0.00	FDET
2624	300	100	74.25	-4.762	260	10274	77	-9764	9.8	520	13	-10	79	0.00	FDET
2625	300	100	74.25	-4.762	260	10263	53	-9764	9.8	520	12	-22	56	0.00	FDET
2626	300	100	74.25	-4.762	260	10331	60	-9764	9.8	522	13	46	62	0.00	FDET
2627	300	100	74.25	-4.762	260	10139	51	-9762	9.8	523	13	-146	54	0.00	FDET
2628	300	100	74.25	-4.762	260	10266	57	-9763	9.8	523	13	-20	59	0.00	FDET
2629	300	100	74.25	-4.762	260	10179	61	-9764	9.8	523	13	-108	63	0.00	FDET
2630	300	100	74.25	-4.762	260	10295	55	-9764	9.8	523	13	8	57	0.00	FDET
2631	300	100	74.25	-4.762	260	10228	47	-9763	9.8	523	13	-59	49	0.00	FDET
2632	300	100	74.25	4.762	260	10253	80	-9769	9.8	523	13	-38	82	0.00	FDET
2633	300	100	74.25	4.762	260	10330	65	-9769	9.8	523	13	38	67	0.00	FDET
2634	300	100	74.25	4.762	260	10313	67	-9771	9.8	523	13	19	68	0.00	FDET
2635	300	100	74.25	4.762	260	10319	58	-9768	9.8	524	13	28	60	0.00	FDET
2636	300	100	74.25	4.762	260	10325	64	-9770	9.8	524	13	32	66	0.00	FDET
2637	300	100	74.25	4.762	260	10299	72	-9770	9.8	524	13	5	74	0.00	FDET
2638	300	100	74.25	4.762	260	10247	73	-9770	9.8	524	13	-47	74	0.00	FDET
2639	300	100	74.25	4.762	260	10392	50	-9769	9.8	524	13	99	52	0.00	FDET
2640	300	100	74.25	4.762	260	10407	67	-9770	9.8	524	13	113	69	0.00	FDET
2641	300	100	74.25	4.762	260	10324	74	-9770	9.8	523	13	31	76	0.00	FDET
2642	300	100	74.25	-4.762	260	10243	62	-9764	9.8	521	13	-42	64	0.00	FDET
2643	300	100	74.25	-4.762	260	10287	78	-9762	9.8	523	13	2	80	0.00	FDET
2644	300	100	74.25	-4.762	260	10115	88	-9764	9.8	525	13	-174	90	0.00	FDET
2645	300	100	74.25	-4.762	260	10228	66	-9765	9.8	524	13	-62	68	0.00	FDET
2646	300	100	74.25	-4.762	260	10320	75	-9764	9.8	523	13	32	77	0.00	FDET
2647	300	100	74.25	-4.762	260	10410	70	-9762	9.8	523	13	125	72	0.00	FDET
2648	300	100	74.25	-4.762	260	10242	82	-9764	9.8	524	13	-46	83	0.00	FDET
2649	300	100	74.25	-4.762	260	10156	103	-9764	9.8	524	13	-132	104	0.00	FDET
2650	300	100	74.25	-4.762	260	10258	75	-9765	9.8	525	13	-31	77	0.00	FDET
2651	300	100	74.25	-4.762	260	10243	124	-9764	9.8	524	13	-46	125	0.00	FDET
2652	300	100	74.25	4.762	260	10210	89	-9771	9.8	524	13	-84	91	0.00	FDET
2653	300	100	74.25	4.762	260	10280	108	-9772	9.8	524	13	-15	110	0.00	FDET
2654	300	100	74.25	4.762	260	10175	71	-9771	9.8	524	13	-120	73	0.00	FDET
2655	300	100	74.25	4.762	260	10313	89	-9771	9.8	524	13	19	91	0.00	FDET
2656	300	100	74.25	4.762	260	10354	68	-9772	9.8	524	13	59	70	0.00	FDET
2657	300	100	74.25	4.762	260	10368	89	-9773	9.8	524	13	71	90	0.00	FDET
2658	300	100	74.25	4.762	260	10376	74	-9772	9.8	525	13	80	76	0.00	FDET
2659	300	100	74.25	4.762	260	10340	84	-9772	9.8	524	13	44	86	0.00	FDET
2660	300	100	74.25	4.762	260	10287	59	-9772	9.8	524	13	-9	61	0.00	FDET
2661	300	100	74.25	4.762	260	10338	91	-9771	9.8	524	13	43	92	0.00	FDET
2662	300	100	74.25	4.762	260	10300	75	-9771	9.8	524	13	5	76	0.00	FDET
2663	300	100	74.25	4.762	260	10290	62	-9771	9.8	524	13	-5	64	0.00	FDET
2664	300	100	74.25	4.762	260	10312	70	-9772	9.8	524	13	16	72	0.00	FDET
2665	300	100	74.25	4.762	260	10365	66	-9772	9.8	524	13	69	68	0.00	FDET
2666	300	100	74.25	4.762	260	10186	62	-9772	9.8	524	13	-109	64	0.00	FDET
2667	300	100	74.25	4.762	260	10304	62	-9771	9.8	524	13	9	64	0.00	FDET
2668	300	100	74.25	4.762	260	10220	69	-9772	9.8	524	13	-76	71	0.00	FDET
2669	300	100	74.25	4.762	260	10340	45	-9772	9.8	523	13	44	47	0.00	FDET
2670	300	100	74.25	4.762	260	10310	70	-9772	9.8	523	13	15	72	0.00	FDET
2671	300	100	74.25	4.762	260	10403	70	-9772	9.8	523	13	108	72	0.00	FDET
2672	300	100	74.25	4.762	260	10333	68	-9772	9.8	523	13	38	70	0.00	FDET
2673	300	100	74.25	4.762	260	10362	68	-9771	9.8	523	13	68	70	0.00	FDET
2674	300	100	74.25	4.762	260	10337	66	-9771	9.8	523	13	43	67	0.00	FDET
2675	300	100	74.25	4.762	260	10175	63	-9772	9.8	523	13	-119	65	0.00	FDET
2676	300	100	74.25	4.762	260	10280	70	-9772	9.8	524	13	-16	71	0.00	FDET
2677	300	100	74.25	4.762	260	10293	72	-9771	9.8	524	13	-2	74	0.00	FDET
2678	300	100	74.25	4.762	260	10297	65	-9771	9.8	524	13	2	67	0.00	FDET
2679	300	100	74.25	4.762	260	10335	62	-9773	9.8	524	13	39	64	0.00	FDET
2680	300	100	74.25	4.762	260	10238	56	-9772	9.8	523	13	-58	58	0.00	FDET
2681	300	100	74.25	4.762	260	10264	67	-9773	9.8	524	13	-33	68	0.00	FDET
2682	300	100	74.25	4.762	260	10305	73	-9772	9.8	524	13	9	75	0.00	FDET
2683	300	100	74.25	4.762	260	10132	62	-9772	9.8	524	13	-164	64	0.00	FDET
2684	300	100	74.25	4.762	260	10370	53	-9771	9.8	524	13	75	55	0.00	FDET
2685	300	100	74.25	4.762	260	10362	54	-9772	9.8	524	13	66	56	0.00	FDET
2686	300	100	74.25	4.762	260	10286	71	-9772	9.8	524	13	-10	73	0.00	FDET
2687	300	100	74.25	4.762	260	10394	61	-9772	9.8	524	13	98	63	0.00	FDET
2688	300	100	74.25	4.762	260	10283	62	-9772	9.8	524	13	-13	64	0.00	FDET
2689	300	100	74.25	4.762	260	10189	69	-9772	9.8	524	13	-107	71	0.00	FDET
2690	300	100	74.25	4.762	260	10454	58	-9772	9.8	524	13	157	60	0.00	FDET
2691	300	100	74.25	4.762	260	10279	53	-9773	9.8	524	13	-19	56	0.00	FDET
2692	300	100	74.25	-4.762	260	10217	73	-9763	9.8	525	13	-71	74	0.00	FDET
2693	300	100	74.25	-4.762	260	10070	81	-9763	9.8	525	13	-217	83	0.00	FDET
2694	300	100	74.25	-4.762	260	10101	106	-9763	9.8	525	13	-187	107	0.00	FDET
2695	300	100	74.25	-4.762	260	10237	99	-9763	9.8	525	13	-51	100	0.00	FDET
2696	300	100	74.25	-4.762	260	10424	91	-9762	9.8	525	13	137	93	0.00	FDET
2697	300	100	74.25	-4.762	260	10209	83	-9763	9.8	525	13	-79	84	0.00	FDET
2698	300	100	74.25	-4.762	260	10183	83	-9762	9.8	525	13	-103	85	0.00	FDET
2699	300	100	74.25	-4.762	260	10195	92	-9762	9.8	525	13	-92	94	0.00	FDET
2700	300	100	74.25	-4.762	260	10286	79	-9762	9.8	525	13	-1	80	0.00	FDET
2701	300	100	74.25	-4.762	260	10126	80	-9761	9.8	524	13	-160	82	0.00	FDET
2702	300	100	74.25	-4.762	260	10209	73	-9762	9.8	524	13	-77	74	0.00	FDET
2703	300	100	74.25	-4.762	260	10298	107	-9762	9.8	524	13	11	108	0.00	FDET
2704	300	100	74.25	-4.762	260	10086	87	-9762	9.8	524	13	-201	88	0.00	FDET
2705	300	100	74.25	-4.762	260	10248	79	-9762	9.8	525	13	-39	81	0.00	FDET
2706	300	100	74.25	-4.762	260	10184	89	-9763	9.8	524	13	-103	91	0.00	FDET
2707	300	100	74.25	-4.762	260	10173	84	-9762	9.8	524	13	-113	85	0.00	FDET
2708	300	100	74.25	-4.762	260	10130	80	-9761	9.8	524	13	-155	82	0.00	FDET
2709	300	100	74.25	-4.762	260	10149	75	-9760	9.8	524	13	-135	77	0.00	FDET
2710	300	100	74.25	-4.762	260	10314	82	-9762	9.8	524	13	28	84	0.00	FDET
2711	300	100	74.25	-4.762	260	10111	72	-9762	9.8	525	13	-175	74	0.00	FDET
2712	300	100	74.25	-4.762	260	10215	97	-9761	9.8	525	13	-70	98	0.00	FDET

Continued on next page

Table A.2 Continued from previous page

$N_{\rm run}$	T [ns]	D [ns]	P [W]	B [Gauss]	$\theta_{\rm pol}$ [deg.]	$\nu_{\rm fit}$ [Hz]	$\Delta\nu_{\rm fit}$ [Hz]	$\rm DC_B$ [Hz]	$\Delta\rm DC_B$ [Hz]	SC [Hz]	ΔSC [Hz]	ν_0 [Hz]	$\Delta\nu_0$ [Hz]	wts. [%]	Data Type
2713	300	100	74.25	-4.762	260	10265	94	-9762	9.8	525	13	-22	95	0.00	FDET
2714	300	100	74.25	-4.762	260	10024	89	-9763	9.8	525	13	-263	90	0.00	FDET
2715	300	100	74.25	-4.762	260	10264	64	-9762	9.8	525	13	-23	66	0.00	FDET
2716	300	100	74.25	-4.762	260	10126	99	-9761	9.8	525	13	-160	100	0.00	FDET
2717	300	100	74.25	-4.762	260	10399	107	-9763	9.8	524	13	111	108	0.00	FDET
2718	300	100	74.25	-4.762	260	10269	71	-9763	9.8	524	13	-18	73	0.00	FDET
2719	300	100	74.25	-4.762	260	10173	76	-9762	9.8	524	13	-113	77	0.00	FDET
2720	300	100	74.25	-4.762	260	10066	60	-9762	9.8	524	13	-220	62	0.00	FDET
2721	300	100	74.25	-4.762	260	10189	88	-9762	9.8	524	13	-97	89	0.00	FDET
2722	300	100	74.25	-4.762	260	10243	106	-9762	9.8	524	13	-43	108	0.00	FDET
2723	300	100	74.25	-4.762	260	10339	84	-9763	9.8	524	13	52	85	0.00	FDET
2724	300	100	74.25	-4.762	260	10290	78	-9763	9.8	524	13	3	79	0.00	FDET
2725	300	100	74.25	-4.762	260	10165	67	-9761	9.8	524	13	-120	69	0.00	FDET
2726	300	100	74.25	-4.762	260	10251	72	-9762	9.8	524	13	-36	74	0.00	FDET
2727	300	100	74.25	-4.762	260	10389	67	-9763	9.8	524	13	102	69	0.00	FDET
2728	300	100	74.25	-4.762	260	10238	96	-9763	9.8	524	13	-49	97	0.00	FDET
2729	300	100	74.25	-4.762	260	10332	73	-9763	9.8	525	13	44	74	0.00	FDET
2730	300	100	74.25	-4.762	260	10205	77	-9762	9.8	525	13	-82	78	0.00	FDET
2731	300	100	74.25	-4.762	260	10280	82	-9764	9.8	525	13	-9	83	0.00	FDET
2732	300	100	74.25	4.762	260	10402	76	-9772	9.8	525	13	105	78	0.00	FDET
2733	300	100	74.25	4.762	260	10378	72	-9771	9.8	525	13	82	74	0.00	FDET
2734	300	100	74.25	4.762	260	10330	76	-9772	9.8	525	13	33	78	0.00	FDET
2735	300	100	74.25	4.762	260	10344	78	-9770	9.8	524	13	49	79	0.00	FDET
2736	300	100	74.25	4.762	260	10361	68	-9772	9.8	524	13	64	70	0.00	FDET
2737	300	100	74.25	4.762	260	10253	72	-9772	9.8	524	13	-43	74	0.00	FDET
2738	300	100	74.25	4.762	260	10298	76	-9772	9.8	524	13	1	78	0.00	FDET
2739	300	100	74.25	4.762	260	10250	55	-9772	9.8	524	13	-46	57	0.00	FDET
2740	300	100	74.25	4.762	260	10388	79	-9772	9.8	524	13	92	81	0.00	FDET
2741	300	100	74.25	4.762	260	10273	56	-9772	9.8	524	13	-23	58	0.00	FDET
2742	300	100	74.25	4.762	260	10440	73	-9773	9.8	524	13	143	75	0.00	FDET
2743	300	100	74.25	4.762	260	10211	93	-9772	9.8	524	13	-85	94	0.00	FDET
2744	300	100	74.25	4.762	260	10198	76	-9772	9.8	524	13	-98	78	0.00	FDET
2745	300	100	74.25	4.762	260	10174	67	-9772	9.8	524	13	-122	69	0.00	FDET
2746	300	100	74.25	4.762	260	10337	74	-9772	9.8	524	13	41	76	0.00	FDET
2747	300	100	74.25	4.762	260	10324	78	-9772	9.8	524	13	28	79	0.00	FDET
2748	300	100	74.25	4.762	260	10159	62	-9772	9.8	524	13	-137	64	0.00	FDET
2749	300	100	74.25	4.762	260	10194	87	-9771	9.8	524	13	-101	88	0.00	FDET
2750	300	100	74.25	4.762	260	10163	71	-9773	9.8	524	13	-133	72	0.00	FDET
2751	300	100	74.25	4.762	260	10380	77	-9772	9.8	524	13	84	79	0.00	FDET
2752	300	100	74.25	-4.762	260	10259	79	-9762	9.8	523	13	-26	80	0.00	FDET
2753	300	100	74.25	-4.762	260	10210	58	-9763	9.8	523	13	-76	60	0.00	FDET
2754	300	100	74.25	-4.762	260	10153	80	-9764	9.8	523	13	-134	81	0.00	FDET
2755	300	100	74.25	-4.762	260	10169	73	-9763	9.8	523	13	-117	75	0.00	FDET
2756	300	100	74.25	-4.762	260	10251	76	-9763	9.8	523	13	-35	77	0.00	FDET
2757	300	100	74.25	-4.762	260	10247	62	-9763	9.8	523	13	-40	64	0.00	FDET
2758	300	100	74.25	-4.762	260	10121	68	-9763	9.8	523	13	-165	70	0.00	FDET
2759	300	100	74.25	-4.762	260	10185	68	-9762	9.8	523	13	-101	70	0.00	FDET
2760	300	100	74.25	-4.762	260	10205	65	-9763	9.8	524	13	-82	67	0.00	FDET
2761	300	100	74.25	-4.762	260	10171	82	-9763	9.8	524	13	-116	84	0.00	FDET
2762	300	100	74.25	-4.762	260	10101	79	-9764	9.8	524	13	-187	81	0.00	FDET
2763	300	100	74.25	-4.762	260	10194	67	-9763	9.8	524	13	-93	69	0.00	FDET
2764	300	100	74.25	-4.762	260	10191	51	-9763	9.8	524	13	-95	54	0.00	FDET
2765	300	100	74.25	-4.762	260	10201	54	-9763	9.8	524	13	-85	56	0.00	FDET
2766	300	100	74.25	-4.762	260	10222	70	-9763	9.8	524	13	-65	72	0.00	FDET
2767	300	100	74.25	-4.762	260	10228	53	-9763	9.8	524	13	-59	55	0.00	FDET
2768	300	100	74.25	-4.762	260	10176	113	-9762	9.8	524	13	-110	114	0.00	FDET
2769	300	100	74.25	-4.762	260	10202	106	-9763	9.8	524	13	-85	108	0.00	FDET
2770	300	100	74.25	-4.762	260	10235	95	-9764	9.8	525	13	-54	96	0.00	FDET
2771	300	100	74.25	-4.762	260	10177	74	-9762	9.8	525	13	-110	76	0.00	FDET
2772	300	100	74.25	4.762	260	10240	69	-9772	9.8	525	13	-56	70	0.00	FDET
2773	300	100	74.25	4.762	260	10249	94	-9771	9.8	525	13	-47	95	0.00	FDET
2774	300	100	74.25	4.762	260	10476	58	-9771	9.8	525	13	180	60	0.00	FDET
2775	300	100	74.25	4.762	260	10295	83	-9771	9.8	525	13	-1	85	0.00	FDET
2776	300	100	74.25	4.762	260	10379	94	-9772	9.8	525	13	82	96	0.00	FDET
2777	300	100	74.25	4.762	260	10326	84	-9771	9.8	525	13	30	86	0.00	FDET
2778	300	100	74.25	4.762	260	10308	73	-9770	9.8	524	13	13	75	0.00	FDET
2779	300	100	74.25	4.762	260	10173	134	-9772	9.8	523	13	-122	135	0.00	FDET
2780	300	100	74.25	4.762	260	10258	89	-9772	9.8	523	13	-37	91	0.00	FDET
2781	300	100	74.25	4.762	260	10404	87	-9771	9.8	523	13	110	89	0.00	FDET
2782	300	100	37.5	-4.762	260	9790	159	-9763	9.8	250	6	-223	160	0.00	FDET
2783	300	100	37.5	-4.762	260	9991	117	-9764	9.8	249	6	-22	118	0.00	FDET
2784	300	100	37.5	-4.762	260	9915	97	-9763	9.8	248	6	-96	97	0.00	FDET
2785	300	100	37.5	-4.762	260	9967	110	-9763	9.8	247	6	-43	111	0.00	FDET
2786	300	100	37.5	-4.762	260	9736	157	-9762	9.8	247	6	-273	157	0.00	FDET
2787	300	100	37.5	-4.762	260	9754	214	-9763	9.8	247	6	-256	214	0.00	FDET
2788	300	100	37.5	-4.762	260	9895	91	-9764	9.8	246	6	-116	92	0.00	FDET
2789	300	100	37.5	-4.762	260	9960	73	-9763	9.8	246	6	-49	74	0.00	FDET
2790	300	100	37.5	-4.762	260	9959	95	-9763	9.8	245	6	-49	96	0.00	FDET
2791	300	100	37.5	-4.762	260	9958	102	-9763	9.8	245	6	-50	102	0.00	FDET
2792	300	100	37.5	4.762	260	9968	98	-9770	9.8	245	6	-47	98	0.00	FDET
2793	300	100	37.5	4.762	260	9830	102	-9771	9.8	245	6	-186	103	0.00	FDET
2794	300	100	37.5	4.762	260	9885	101	-9771	9.8	244	6	-130	101	0.00	FDET
2795	300	100	37.5	4.762	260	9975	94	-9770	9.8	244	6	-38	95	0.00	FDET
2796	300	100	37.5	4.762	260	9820	97	-9772	9.8	244	6	-196	98	0.00	FDET
2797	300	100	37.5	4.762	260	9913	96	-9772	9.8	244	6	-103	96	0.00	FDET
2798	300	100	37.5	4.762	260	10006	107	-9771	9.8	244	6	-9	107	0.00	FDET
2799	300	100	37.5	4.762	260	9801	91	-9772	9.8	244	6	-215	91	0.00	FDET
2800	300	100	37.5	4.762	260	9766	86	-9770	9.8	244	6	-247	86	0.00	FDET
2801	300	100	37.5	4.762	260	9788	87	-9771	9.8	244	6	-226	88	0.00	FDET
2802	300	100	37.5	-4.762	260	9954	94	-9763	9.8	243	6	-52	94	0.00	FDET
2803	300	100	37.5	-4.762	260	9998	90	-9762	9.8	242	6	-6	91	0.00	FDET
2804	300	100	37.5	-4.762	260	10006	103	-9762	9.8	246	6	-1	104	0.00	LLBP
2805	300	100	37.5	-4.762	260	10035	132	-9763	9.8	244	6	28	132	0.00	LLBP
2806	300	100	37.5	-4.762	260	9799	139	-9763	9.8	244	6	-208	140	0.00	LLBP
2807	300	100	37.5	-4.762	260	10077	103	-9763	9.8	244	6	71	103	0.00	LLBP
2808	300	100	37.5	-4.762	260	9977	130	-9763	9.8	243	6	-30	131	0.00	LLBP
2809	300	100	37.5	-4.762	260	9920	161	-9763	9.8	243	6	-86	161	0.00	LLBP
2810	300	100	37.5	-4.762	260	10030	116	-9763	9.8	244	6	23	117	0.00	LLBP

Continued on next page

Table A.2 Continued from previous page

N_{run}	T [ns]	D [ns]	P [W]	B [Gauss]	θ_{pol} [deg.]	ν_{fit} [Hz]	$\Delta\nu_{\mathrm{fit}}$ [Hz]	$\mathrm{DC_B}$ [Hz]	$\Delta\mathrm{DC_B}$ [Hz]	SC [Hz]	ΔSC [Hz]	ν_0 [Hz]	$\Delta\nu_0$ [Hz]	wts. [%]	Data Type
2811	300	100	37.5	-4.762	260	10108	136	-9764	9.8	244	6	100	137	0.00	LLBP
2812	300	100	37.5	-4.762	260	9927	124	-9762	9.8	243	6	-78	124	0.00	LLBP
2813	300	100	37.5	-4.762	260	10058	166	-9764	9.8	243	6	51	167	0.00	LLBP
2814	300	100	37.5	-4.762	260	9928	110	-9763	9.8	243	6	-78	110	0.00	LLBP
2815	300	100	37.5	-4.762	260	10058	110	-9762	9.8	243	6	53	111	0.00	LLBP
2816	300	100	37.5	-4.762	260	9665	116	-9763	9.8	242	6	-340	116	0.00	LLBP
2817	300	100	37.5	-4.762	260	9828	123	-9764	9.8	242	6	-177	124	0.00	LLBP
2818	300	100	37.5	-4.762	260	10163	134	-9761	9.8	243	6	159	135	0.00	LLBP
2819	300	100	37.5	-4.762	260	10007	133	-9763	9.8	243	6	1	134	0.00	LLBP
2820	300	100	37.5	-4.762	260	9725	156	-9763	9.8	243	6	-281	156	0.00	LLBP
2821	300	100	37.5	-4.762	260	9993	197	-9762	9.8	243	6	-13	197	0.00	LLBP
2822	300	100	37.5	-4.762	260	10172	177	-9762	9.8	243	6	167	177	0.00	LLBP
2823	300	100	37.5	-4.762	260	10065	181	-9762	9.8	243	6	61	181	0.00	LLBP
2824	300	100	37.5	4.762	260	9893	170	-9772	9.8	242	6	-122	170	0.00	LLBP
2825	300	100	37.5	4.762	260	9958	115	-9773	9.8	242	6	-57	115	0.00	LLBP
2826	300	100	37.5	4.762	260	9672	125	-9771	9.8	242	6	-341	126	0.00	LLBP
2827	300	100	37.5	4.762	260	9642	121	-9772	9.8	242	6	-371	121	0.00	LLBP
2828	300	100	37.5	4.762	260	9939	106	-9771	9.8	242	6	-75	107	0.00	LLBP
2829	300	100	37.5	4.762	260	9956	140	-9772	9.8	242	6	-58	141	0.00	LLBP
2830	300	100	37.5	4.762	260	9787	120	-9771	9.8	242	6	-226	121	0.00	LLBP
2831	300	100	37.5	4.762	260	9897	125	-9771	9.8	242	6	-116	126	0.00	LLBP
2832	300	100	37.5	4.762	260	9672	115	-9771	9.8	242	6	-340	116	0.00	LLBP
2833	300	100	37.5	4.762	260	9925	117	-9771	9.8	242	6	-88	118	0.00	LLBP
2834	300	100	37.5	4.762	260	9951	143	-9772	9.8	242	6	-63	143	0.00	LLBP
2835	300	100	37.5	4.762	260	9811	115	-9772	9.8	242	6	-203	116	0.00	LLBP
2836	300	100	37.5	4.762	260	9753	116	-9770	9.8	243	6	-260	116	0.00	LLBP
2837	300	100	37.5	4.762	260	9796	127	-9771	9.8	243	6	-218	128	0.00	LLBP
2838	300	100	37.5	4.762	260	9932	86	-9771	9.8	242	6	-81	87	0.00	LLBP
2839	300	100	37.5	4.762	260	9886	100	-9772	9.8	242	6	-128	101	0.00	LLBP
2840	300	100	37.5	4.762	260	9877	145	-9769	9.8	242	6	-135	145	0.00	LLBP
2841	300	100	37.5	4.762	260	9652	117	-9773	9.8	241	6	-362	117	0.00	LLBP
2842	300	100	37.5	4.762	260	9829	118	-9772	9.8	242	6	-185	119	0.00	LLBP
2843	300	100	37.5	4.762	260	9851	132	-9771	9.8	243	6	-163	133	0.00	LLBP
2844	300	100	74.25	-4.762	260	10163	79	-9763	9.8	509	12	-109	81	0.00	LLBP
2845	300	100	74.25	-4.762	260	10400	112	-9763	9.8	512	12	126	113	0.00	LLBP
2846	300	100	74.25	-4.762	260	10146	117	-9762	9.8	513	12	-129	118	0.00	LLBP
2847	300	100	74.25	-4.762	260	10058	93	-9763	9.8	514	12	-220	94	0.00	LLBP
2848	300	100	74.25	-4.762	260	10332	99	-9763	9.8	513	12	56	100	0.00	LLBP
2849	300	100	74.25	-4.762	260	10242	86	-9763	9.8	513	12	-34	87	0.00	LLBP
2850	300	100	74.25	-4.762	260	10337	101	-9764	9.8	513	12	60	103	0.00	LLBP
2851	300	100	74.25	-4.762	260	10242	92	-9762	9.8	514	12	-34	94	0.00	LLBP
2852	300	100	74.25	-4.762	260	10343	103	-9763	9.8	514	12	66	104	0.00	LLBP
2853	300	100	74.25	-4.762	260	10186	86	-9764	9.8	514	12	-92	87	0.00	LLBP
2854	300	100	74.25	4.762	260	10186	74	-9771	9.8	514	12	-99	76	0.00	LLBP
2855	300	100	74.25	4.762	260	10022	103	-9772	9.8	515	12	-265	104	0.00	LLBP
2856	300	100	74.25	4.762	260	10054	93	-9772	9.8	515	12	-233	94	0.00	LLBP
2857	300	100	74.25	4.762	260	10079	73	-9772	9.8	515	12	-208	75	0.00	LLBP
2858	300	100	74.25	4.762	260	10067	90	-9772	9.8	514	12	-219	92	0.00	LLBP
2859	300	100	74.25	4.762	260	10110	79	-9771	9.8	514	12	-176	80	0.00	LLBP
2860	300	100	74.25	4.762	260	10193	74	-9771	9.8	514	12	-92	76	0.00	LLBP
2861	300	100	74.25	4.762	260	10079	91	-9770	9.8	514	12	-205	92	0.00	LLBP
2862	300	100	74.25	4.762	260	10132	107	-9771	9.8	514	12	-153	108	0.00	LLBP
2863	300	100	74.25	4.762	260	10036	89	-9771	9.8	514	12	-248	91	0.00	LLBP
2864	300	100	74.25	4.762	260	10123	82	-9771	9.8	513	12	-162	83	0.00	LLBP
2865	300	100	74.25	4.762	260	10179	87	-9772	9.8	514	12	-106	88	0.00	LLBP
2866	300	100	74.25	4.762	260	10111	87	-9770	9.8	514	12	-173	89	0.00	LLBP
2867	300	100	74.25	4.762	260	10202	78	-9771	9.8	514	12	-82	79	0.00	LLBP
2868	300	100	74.25	4.762	260	10072	104	-9771	9.8	514	12	-212	105	0.00	LLBP
2869	300	100	74.25	4.762	260	10134	103	-9772	9.8	513	12	-151	105	0.00	LLBP
2870	300	100	74.25	4.762	260	10191	76	-9771	9.8	513	12	-94	77	0.00	LLBP
2871	300	100	74.25	4.762	260	10160	99	-9771	9.8	514	12	-125	100	0.00	LLBP
2872	300	100	74.25	4.762	260	10018	89	-9772	9.8	514	12	-268	90	0.00	LLBP
2873	300	100	74.25	4.762	260	10041	82	-9771	9.8	514	12	-244	83	0.00	LLBP
2874	300	100	74.25	-4.762	260	10149	120	-9764	9.8	514	12	-128	121	0.00	LLBP
2875	300	100	74.25	-4.762	260	10285	111	-9763	9.8	514	12	8	112	0.00	LLBP
2876	300	100	74.25	-4.762	260	10299	96	-9764	9.8	514	12	21	97	0.00	LLBP
2877	300	100	74.25	-4.762	260	10295	88	-9763	9.8	513	12	18	89	0.00	LLBP
2878	300	100	74.25	-4.762	260	10134	70	-9763	9.8	513	12	-143	71	0.00	LLBP
2879	300	100	74.25	-4.762	260	10242	110	-9764	9.8	514	12	-36	111	0.00	LLBP
2880	300	100	74.25	-4.762	260	10258	93	-9763	9.8	514	12	-19	94	0.00	LLBP
2881	300	100	74.25	-4.762	260	10174	117	-9763	9.8	515	12	-104	118	0.00	LLBP
2882	300	100	74.25	-4.762	260	10405	114	-9763	9.8	516	12	126	115	0.00	LLBP
2883	300	100	74.25	-4.762	260	10385	125	-9763	9.8	516	12	105	126	0.00	LLBP
2884	300	100	74.25	4.762	260	9920	97	-9771	9.8	516	12	-367	98	0.00	LLBP
2885	300	100	74.25	4.762	260	10179	103	-9771	9.8	515	12	-108	104	0.00	LLBP
2886	300	100	74.25	4.762	260	10054	97	-9770	9.8	515	12	-231	99	0.00	LLBP
2887	300	100	74.25	4.762	260	10053	73	-9771	9.8	515	12	-233	75	0.00	LLBP
2888	300	100	74.25	4.762	260	10128	77	-9771	9.8	515	12	-159	78	0.00	LLBP
2889	300	100	74.25	4.762	260	10005	72	-9773	9.8	515	12	-283	74	0.00	LLBP
2890	300	100	74.25	4.762	260	10049	65	-9770	9.8	515	12	-237	67	0.00	LLBP
2891	300	100	74.25	4.762	260	10006	86	-9771	9.8	515	12	-281	88	0.00	LLBP
2892	300	100	74.25	4.762	260	10077	90	-9772	9.8	515	12	-210	92	0.00	LLBP
2893	300	100	74.25	4.762	260	10127	96	-9772	9.8	515	12	-160	98	0.00	LLBP
2894	300	100	37.5	4.762	260	9733	118	-9770	9.8	246	6	-283	118	0.00	LLBP
2895	300	100	37.5	4.762	260	9863	107	-9771	9.8	245	6	-153	107	0.00	LLBP
2896	300	100	37.5	4.762	260	9560	155	-9771	9.8	244	6	-455	155	0.00	LLBP
2897	300	100	37.5	4.762	260	9548	115	-9769	9.8	244	6	-466	115	0.00	LLBP
2898	300	100	37.5	4.762	260	9911	132	-9771	9.8	244	6	-105	132	0.00	LLBP
2899	300	100	37.5	4.762	260	9753	122	-9771	9.8	244	6	-263	122	0.00	LLBP
2900	300	100	37.5	4.762	260	9792	97	-9770	9.8	245	6	-223	98	0.00	LLBP
2901	300	100	37.5	4.762	260	9600	125	-9771	9.8	246	6	-417	125	0.00	LLBP
2902	300	100	37.5	4.762	260	10005	125	-9771	9.8	244	6	-10	126	0.00	LLBP
2903	300	100	37.5	4.762	260	9848	100	-9770	9.8	244	6	-166	100	0.00	LLBP
2904	300	100	37.5	-4.762	260	10136	118	-9764	9.8	244	6	128	119	0.00	LLBP
2905	300	100	37.5	-4.762	260	9575	121	-9764	9.8	245	6	-434	122	0.00	LLBP
2906	300	100	37.5	-4.762	260	9996	137	-9764	9.8	245	6	-13	138	0.00	LLBP
2907	300	100	37.5	-4.762	260	10076	107	-9763	9.8	245	6	67	107	0.00	LLBP
2908	300	100	37.5	-4.762	260	9913	138	-9764	9.8	245	6	-96	139	0.00	LLBP

Continued on next page

Table A.2 Continued from previous page

N_{run}	T [ns]	D [ns]	P [W]	B [Gauss]	θ_{pol} [deg.]	ν_{fit} [Hz]	$\Delta\nu_{\text{fit}}$ [Hz]	DC_{B} [Hz]	$\Delta\text{DC}_{\text{B}}$ [Hz]	SC [Hz]	ΔSC [Hz]	ν_0 [Hz]	$\Delta\nu_0$ [Hz]	wts. [%]	Data Type
2909	300	100	37.5	-4.762	260	9673	136	-9765	9.8	245	6	-337	136	0.00	LLBP
2910	300	100	37.5	-4.762	260	9967	117	-9763	9.8	246	6	-43	117	0.00	LLBP
2911	300	100	37.5	-4.762	260	9834	168	-9764	9.8	246	6	-176	168	0.00	LLBP
2912	300	100	37.5	-4.762	260	9485	120	-9764	9.8	247	6	-526	120	0.00	LLBP
2913	300	100	37.5	-4.762	260	9814	164	-9762	9.8	246	6	-194	164	0.00	LLBP
2914	300	100	74.25	-4.762	260	10177	94	-9764	9.8	514	12	-100	95	0.00	LLBP
2915	300	100	74.25	-4.762	260	10119	95	-9763	9.8	517	12	-160	97	0.00	LLBP
2916	300	100	74.25	-4.762	260	10104	77	-9764	9.8	516	12	-176	78	0.00	LLBP
2917	300	100	74.25	-4.762	260	10206	80	-9762	9.8	516	12	-72	82	0.00	LLBP
2918	300	100	74.25	-4.762	260	10155	78	-9763	9.8	517	12	-125	79	0.00	LLBP
2919	300	100	74.25	-4.762	260	10112	63	-9764	9.8	517	12	-168	65	0.00	LLBP
2920	300	100	74.25	-4.762	260	10196	95	-9763	9.8	517	12	-84	97	0.00	LLBP
2921	300	100	74.25	-4.762	260	10220	113	-9762	9.8	517	12	-60	115	0.00	LLBP
2922	300	100	74.25	-4.762	260	10288	91	-9763	9.8	518	12	7	92	0.00	LLBP
2923	300	100	74.25	-4.762	260	10166	97	-9763	9.8	518	12	-115	99	0.00	LLBP
2924	300	100	37.5	-4.762	260	9868	99	-9764	9.8	249	6	-145	100	0.00	LLBP
2925	300	100	37.5	-4.762	260	9945	120	-9763	9.8	248	6	-66	120	0.00	LLBP
2926	300	100	37.5	-4.762	260	10005	132	-9764	9.8	248	6	-7	133	0.00	LLBP
2927	300	100	37.5	-4.762	260	9856	99	-9764	9.8	248	6	-156	100	0.00	LLBP
2928	300	100	37.5	-4.762	260	9820	115	-9763	9.8	248	6	-191	115	0.00	LLBP
2929	300	100	37.5	-4.762	260	9712	150	-9762	9.8	248	6	-299	150	0.00	LLBP
2930	300	100	37.5	-4.762	260	9966	99	-9764	9.8	248	6	-47	99	0.00	LLBP
2931	300	100	37.5	-4.762	260	9872	109	-9763	9.8	249	6	-140	109	0.00	LLBP
2932	300	100	37.5	-4.762	260	9839	154	-9763	9.8	249	6	-173	154	0.00	LLBP
2933	300	100	37.5	-4.762	260	10150	126	-9762	9.8	250	6	139	126	0.00	LLBP
2934	300	100	74.25	4.762	260	10154	92	-9772	9.8	517	12	-135	93	0.00	LLBP
2935	300	100	74.25	4.762	260	9890	86	-9770	9.8	520	12	-401	88	0.00	LLBP
2936	300	100	74.25	4.762	260	10058	79	-9771	9.8	521	13	-235	80	0.00	LLBP
2937	300	100	74.25	4.762	260	9945	75	-9774	9.8	522	13	-352	77	0.00	LLBP
2938	300	100	74.25	4.762	260	10017	86	-9772	9.8	523	13	-278	87	0.00	LLBP
2939	300	100	74.25	4.762	260	10061	65	-9773	9.8	523	13	-235	67	0.00	LLBP
2940	300	100	74.25	4.762	260	10233	67	-9773	9.8	523	13	-63	68	0.00	LLBP
2941	300	100	74.25	4.762	260	10114	58	-9772	9.8	523	13	-182	60	0.00	LLBP
2942	300	100	74.25	4.762	260	10027	90	-9771	9.8	524	13	-268	92	0.00	LLBP
2943	300	100	74.25	4.762	260	10017	67	-9770	9.8	524	13	-277	68	0.00	LLBP
2944	300	100	74.25	-4.762	260	10156	97	-9763	9.8	524	13	-131	99	0.00	LLBP
2945	300	100	74.25	-4.762	260	10258	74	-9762	9.8	523	13	-27	75	0.00	LLBP
2946	300	100	74.25	-4.762	260	10283	108	-9764	9.8	523	13	-5	109	0.00	LLBP
2947	300	100	74.25	-4.762	260	10314	75	-9764	9.8	525	13	25	77	0.00	LLBP
2948	300	100	74.25	-4.762	260	10265	71	-9763	9.8	525	13	-23	73	0.00	LLBP
2949	300	100	74.25	-4.762	260	10052	88	-9764	9.8	525	13	-237	90	0.00	LLBP
2950	300	100	74.25	-4.762	260	10114	87	-9763	9.8	526	13	-174	88	0.00	LLBP
2951	300	100	74.25	-4.762	260	10138	90	-9764	9.8	526	13	-152	91	0.00	LLBP
2952	300	100	74.25	-4.762	260	10089	92	-9764	9.8	525	13	-200	94	0.00	LLBP
2953	300	100	74.25	-4.762	260	10114	103	-9762	9.8	526	13	-174	105	0.00	LLBP
2954	300	100	37.5	4.762	260	9791	111	-9772	9.8	256	6	-237	111	0.00	LLBP
2955	300	100	37.5	4.762	260	9841	120	-9771	9.8	255	6	-185	120	0.00	LLBP
2956	300	100	37.5	4.762	260	9686	84	-9772	9.8	255	6	-342	85	0.00	LLBP
2957	300	100	37.5	4.762	260	9823	126	-9770	9.8	255	6	-201	127	0.00	LLBP
2958	300	100	37.5	4.762	260	9984	134	-9771	9.8	255	6	-41	134	0.00	LLBP
2959	300	100	37.5	4.762	260	9742	90	-9770	9.8	254	6	-282	91	0.00	LLBP
2960	300	100	37.5	4.762	260	10024	114	-9771	9.8	253	6	0	114	0.00	LLBP
2961	300	100	37.5	4.762	260	10005	119	-9770	9.8	253	6	-19	120	0.00	LLBP
2962	300	100	37.5	4.762	260	9888	80	-9772	9.8	254	6	-137	81	0.00	LLBP
2963	300	100	37.5	4.762	260	9682	139	-9771	9.8	254	6	-342	139	0.00	LLBP
2964	300	100	74.25	4.762	260	10079	89	-9771	9.8	522	13	-214	90	0.00	LLBP
2965	300	100	74.25	4.762	260	10171	73	-9771	9.8	524	13	-123	75	0.00	LLBP
2966	300	100	74.25	4.762	260	10160	107	-9771	9.8	523	13	-134	108	0.00	LLBP
2967	300	100	74.25	4.762	260	10310	119	-9771	9.8	524	13	15	120	0.00	LLBP
2968	300	100	74.25	4.762	260	10091	54	-9771	9.8	524	13	-204	57	0.00	LLBP
2969	300	100	74.25	4.762	260	10018	73	-9771	9.8	524	13	-278	75	0.00	LLBP
2970	300	100	74.25	4.762	260	10227	59	-9772	9.8	525	13	-69	61	0.00	LLBP
2971	300	100	74.25	4.762	260	10149	79	-9771	9.8	525	13	-147	80	0.00	LLBP
2972	300	100	74.25	4.762	260	10230	88	-9772	9.8	525	13	-68	90	0.00	LLBP
2973	300	100	74.25	4.762	260	10258	90	-9772	9.8	525	13	-38	91	0.00	LLBP
2974	300	100	37.5	-4.762	260	10043	119	-9764	9.8	258	6	22	119	0.00	LLBP
2975	300	100	37.5	-4.762	260	9859	118	-9763	9.8	256	6	-160	118	0.00	LLBP
2976	300	100	37.5	-4.762	260	9948	146	-9763	9.8	256	6	-71	146	0.00	LLBP
2977	300	100	37.5	-4.762	260	10194	123	-9763	9.8	255	6	175	124	0.00	LLBP
2978	300	100	37.5	-4.762	260	9903	151	-9763	9.8	255	6	-115	151	0.00	LLBP
2979	300	100	37.5	-4.762	260	9981	139	-9764	9.8	255	6	-37	139	0.00	LLBP
2980	300	100	37.5	-4.762	260	10026	128	-9764	9.8	255	6	8	128	0.00	LLBP
2981	300	100	37.5	-4.762	260	10033	113	-9764	9.8	255	6	15	114	0.00	LLBP
2982	300	100	37.5	-4.762	260	9940	115	-9762	9.8	255	6	-77	116	0.00	LLBP
2983	300	100	37.5	-4.762	260	9924	102	-9763	9.8	254	6	-93	102	0.00	LLBP
2984	300	100	37.5	4.762	260	9887	84	-9772	9.8	254	6	-140	85	0.00	LLBP
2985	300	100	37.5	4.762	260	9719	108	-9772	9.8	254	6	-308	109	0.00	LLBP
2986	300	100	37.5	4.762	260	9887	105	-9772	9.8	254	6	-139	105	0.00	LLBP
2987	300	100	37.5	4.762	260	9847	122	-9771	9.8	254	6	-179	123	0.00	LLBP
2988	300	100	37.5	4.762	260	9952	103	-9772	9.8	254	6	-74	104	0.00	LLBP
2989	300	100	37.5	4.762	260	9830	112	-9771	9.8	254	6	-195	113	0.00	LLBP
2990	300	100	37.5	4.762	260	9913	96	-9772	9.8	253	6	-112	97	0.00	LLBP
2991	300	100	37.5	4.762	260	9857	118	-9771	9.8	253	6	-166	119	0.00	LLBP
2992	300	100	37.5	4.762	260	10169	123	-9772	9.8	253	6	145	124	0.00	LLBP
2993	300	100	37.5	4.762	260	9638	120	-9772	9.8	253	6	-387	120	0.00	LLBP
2994	300	100	74.25	4.762	260	10057	77	-9772	9.8	519	12	-234	79	0.00	LLBP
2995	300	100	74.25	4.762	260	10139	84	-9772	9.8	522	13	-155	86	0.00	LLBP
2996	300	100	74.25	4.762	260	10151	84	-9772	9.8	522	13	-144	86	0.00	LLBP
2997	300	100	74.25	4.762	260	10015	72	-9772	9.8	522	13	-279	74	0.00	LLBP
2998	300	100	74.25	4.762	260	10044	79	-9771	9.8	523	13	-250	81	0.00	LLBP
2999	300	100	74.25	4.762	260	10208	83	-9772	9.8	523	13	-87	84	0.00	LLBP
3000	300	100	74.25	4.762	260	10173	95	-9771	9.8	523	13	-121	97	0.00	LLBP
3001	300	100	74.25	4.762	260	10268	73	-9772	9.8	523	13	-27	74	0.00	LLBP
3002	300	100	74.25	4.762	260	10053	92	-9772	9.8	523	13	-242	93	0.00	LLBP
3003	300	100	74.25	4.762	260	10035	87	-9771	9.8	523	13	-258	89	0.00	LLBP
3004	300	100	37.5	4.762	260	10006	108	-9771	9.8	256	6	-21	109	0.00	LLBP
3005	300	100	37.5	4.762	260	9692	109	-9771	9.8	254	6	-334	110	0.00	LLBP
3006	300	100	37.5	4.762	260	9898	105	-9771	9.8	254	6	-126	105	0.00	LLBP

Continued on next page

Table A.2 Continued from previous page

N_{run}	T [ns]	D [ns]	P [W]	B [Gauss]	θ_{pol} [deg.]	ν_{fit} [Hz]	$\Delta\nu_{\mathrm{fit}}$ [Hz]	$\mathrm{DC_B}$ [Hz]	$\Delta\mathrm{DC_B}$ [Hz]	SC [Hz]	ΔSC [Hz]	ν_0 [Hz]	$\Delta\nu_0$ [Hz]	wts. [%]	Data Type
3007	300	100	37.5	4.762	260	9923	108	-9773	9.8	254	6	-104	108	0.00	LLBP
3008	300	100	37.5	4.762	260	9684	117	-9771	9.8	253	6	-340	117	0.00	LLBP
3009	300	100	37.5	4.762	260	9921	127	-9773	9.8	253	6	-105	127	0.00	LLBP
3010	300	100	37.5	4.762	260	9845	108	-9772	9.8	253	6	-179	109	0.00	LLBP
3011	300	100	37.5	4.762	260	9799	105	-9772	9.8	252	6	-224	105	0.00	LLBP
3012	300	100	37.5	4.762	260	10086	89	-9772	9.8	251	6	62	90	0.00	LLBP
3013	300	100	37.5	4.762	260	10139	116	-9772	9.8	251	6	116	117	0.00	LLBP
3014	300	100	37.5	-4.762	260	10133	135	-9762	9.8	250	6	120	136	0.00	LLBP
3015	300	100	37.5	-4.762	260	9863	125	-9763	9.8	250	6	-150	125	0.00	LLBP
3016	300	100	37.5	-4.762	260	9925	131	-9763	9.8	250	6	-87	132	0.00	LLBP
3017	300	100	37.5	-4.762	260	10110	106	-9763	9.8	249	6	98	107	0.00	LLBP
3018	300	100	37.5	-4.762	260	9843	127	-9763	9.8	248	6	-168	127	0.00	LLBP
3019	300	100	37.5	-4.762	260	10057	120	-9764	9.8	248	6	45	121	0.00	LLBP
3020	300	100	37.5	-4.762	260	9984	102	-9763	9.8	248	6	-27	103	0.00	LLBP
3021	300	100	37.5	-4.762	260	9846	119	-9763	9.8	247	6	-164	119	0.00	LLBP
3022	300	100	37.5	-4.762	260	9764	133	-9763	9.8	247	6	-246	134	0.00	LLBP
3023	300	100	37.5	-4.762	260	9992	99	-9763	9.8	247	6	-18	99	0.00	LLBP
3024	300	100	74.25	4.762	260	10081	80	-9771	9.8	512	12	-202	82	0.00	LLBP
3025	300	100	74.25	4.762	260	10007	90	-9771	9.8	515	12	-279	92	0.00	LLBP
3026	300	100	74.25	4.762	260	10064	88	-9772	9.8	515	12	-223	89	0.00	LLBP
3027	300	100	74.25	4.762	260	10038	80	-9771	9.8	515	12	-248	82	0.00	LLBP
3028	300	100	74.25	4.762	260	10154	83	-9771	9.8	515	12	-132	84	0.00	LLBP
3029	300	100	74.25	4.762	260	10150	89	-9772	9.8	515	12	-137	90	0.00	LLBP
3030	300	100	74.25	4.762	260	10117	74	-9770	9.8	515	12	-168	76	0.00	LLBP
3031	300	100	74.25	4.762	260	10220	94	-9771	9.8	515	12	-66	95	0.00	LLBP
3032	300	100	74.25	4.762	260	10082	94	-9771	9.8	516	12	-205	95	0.00	LLBP
3033	300	100	74.25	4.762	260	10104	80	-9771	9.8	515	12	-183	81	0.00	LLBP
3034	300	100	74.25	-4.762	260	10168	97	-9763	9.8	515	12	-110	98	0.00	LLBP
3035	300	100	74.25	-4.762	260	10154	79	-9764	9.8	515	12	-125	80	0.00	LLBP
3036	300	100	74.25	-4.762	260	10241	85	-9764	9.8	516	12	-38	87	0.00	LLBP
3037	300	100	74.25	-4.762	260	10175	104	-9763	9.8	516	12	-104	105	0.00	LLBP
3038	300	100	74.25	-4.762	260	10208	96	-9763	9.8	515	12	-70	97	0.00	LLBP
3039	300	100	74.25	-4.762	260	10215	94	-9764	9.8	515	12	-64	95	0.00	LLBP
3040	300	100	74.25	-4.762	260	10347	81	-9763	9.8	515	12	69	83	0.00	LLBP
3041	300	100	74.25	-4.762	260	10203	98	-9763	9.8	515	12	-75	99	0.00	LLBP
3042	300	100	74.25	-4.762	260	10199	73	-9763	9.8	514	12	-78	74	0.00	LLBP
3043	300	100	74.25	-4.762	260	10181	97	-9763	9.8	514	12	-96	99	0.00	LLBP
3044	300	100	37.5	4.762	260	9656	124	-9771	9.8	245	6	-360	124	0.00	LLBP
3045	300	100	37.5	4.762	260	9827	89	-9771	9.8	244	6	-188	90	0.00	LLBP
3046	300	100	37.5	4.762	260	9727	101	-9771	9.8	243	6	-287	102	0.00	LLBP
3047	300	100	37.5	4.762	260	9827	104	-9771	9.8	243	6	-187	104	0.00	LLBP
3048	300	100	37.5	4.762	260	10013	107	-9771	9.8	243	6	0	108	0.00	LLBP
3049	300	100	37.5	4.762	260	9625	118	-9771	9.8	243	6	-389	119	0.00	LLBP
3050	300	100	37.5	4.762	260	9823	119	-9771	9.8	243	6	-190	120	0.00	LLBP
3051	300	100	37.5	4.762	260	9738	109	-9771	9.8	243	6	-276	110	0.00	LLBP
3052	300	100	37.5	4.762	260	10102	130	-9772	9.8	242	6	88	130	0.00	LLBP
3053	300	100	37.5	4.762	260	9814	105	-9771	9.8	243	6	-199	105	0.00	LLBP
3054	300	100	37.5	-4.762	260	9967	129	-9764	9.8	243	6	-39	129	0.00	LLBP
3055	300	100	37.5	-4.762	260	9709	136	-9764	9.8	243	6	-297	136	0.00	LLBP
3056	300	100	37.5	-4.762	260	9822	116	-9763	9.8	242	6	-183	117	0.00	LLBP
3057	300	100	37.5	-4.762	260	9689	132	-9761	9.8	242	6	-314	132	0.00	LLBP
3058	300	100	37.5	-4.762	260	9924	147	-9763	9.8	243	6	-82	148	0.00	LLBP
3059	300	100	37.5	-4.762	260	9900	121	-9763	9.8	242	6	-105	122	0.00	LLBP
3060	300	100	37.5	-4.762	260	9899	109	-9763	9.8	242	6	-106	109	0.00	LLBP
3061	300	100	37.5	-4.762	260	10000	148	-9763	9.8	242	6	-5	149	0.00	LLBP
3062	300	100	37.5	-4.762	260	10010	156	-9764	9.8	242	6	3	157	0.00	LLBP
3063	300	100	37.5	-4.762	260	9894	110	-9763	9.8	242	6	-111	111	0.00	LLBP
3064	300	100	74.25	-4.762	260	10105	113	-9764	9.8	510	12	-168	114	0.00	LLBP
3065	300	100	74.25	-4.762	260	10277	99	-9763	9.8	511	12	3	100	0.00	LLBP
3066	300	100	74.25	-4.762	260	10164	88	-9764	9.8	511	12	-111	90	0.00	LLBP
3067	300	100	74.25	-4.762	260	10009	108	-9764	9.8	512	12	-267	110	0.00	LLBP
3068	300	100	74.25	-4.762	260	10132	83	-9764	9.8	512	12	-144	84	0.00	LLBP
3069	300	100	74.25	-4.762	260	10387	113	-9763	9.8	512	12	112	114	0.00	LLBP
3070	300	100	74.25	-4.762	260	10158	84	-9763	9.8	512	12	-118	85	0.00	LLBP
3071	300	100	74.25	-4.762	260	10351	85	-9763	9.8	513	12	74	87	0.00	LLBP
3072	300	100	74.25	-4.762	260	10248	97	-9764	9.8	514	12	-29	98	0.00	LLBP
3073	300	100	74.25	-4.762	260	10172	82	-9764	9.8	514	12	-106	83	0.00	LLBP
3074	300	100	74.25	-4.762	260	10282	107	-9763	9.8	514	12	5	108	0.00	LLBP
3075	300	100	74.25	-4.762	260	10234	107	-9763	9.8	514	12	-43	108	0.00	LLBP
3076	300	100	74.25	-4.762	260	10218	120	-9763	9.8	514	12	-59	121	0.00	LLBP
3077	300	100	74.25	-4.762	260	10260	90	-9763	9.8	514	12	-17	91	0.00	LLBP
3078	300	100	74.25	-4.762	260	10029	79	-9763	9.8	514	12	-248	81	0.00	LLBP
3079	300	100	74.25	-4.762	260	10176	102	-9762	9.8	515	12	-101	103	0.00	LLBP
3080	300	100	74.25	-4.762	260	10147	76	-9762	9.8	515	12	-130	77	0.00	LLBP
3081	300	100	74.25	-4.762	260	10118	100	-9764	9.8	516	12	-161	102	0.00	LLBP
3082	300	100	74.25	-4.762	260	10222	98	-9764	9.8	516	12	-57	99	0.00	LLBP
3083	300	100	74.25	-4.762	260	10275	96	-9763	9.8	516	12	-4	97	0.00	LLBP
3084	300	100	74.25	-4.762	260	10102	107	-9763	9.8	518	12	-180	108	0.00	LLBP
3085	300	100	74.25	-4.762	260	10145	87	-9764	9.8	518	12	-136	89	0.00	LLBP
3086	300	100	74.25	-4.762	260	10242	109	-9763	9.8	517	12	-39	110	0.00	LLBP
3087	300	100	74.25	-4.762	260	10249	83	-9763	9.8	516	12	-31	85	0.00	LLBP
3088	300	100	74.25	-4.762	260	10409	97	-9763	9.8	515	12	131	98	0.00	LLBP
3089	300	100	74.25	-4.762	260	10292	90	-9764	9.8	515	12	13	91	0.00	LLBP
3090	300	100	74.25	-4.762	260	10205	114	-9763	9.8	516	12	-73	115	0.00	LLBP
3091	300	100	74.25	-4.762	260	10233	103	-9764	9.8	516	12	-47	104	0.00	LLBP
3092	300	100	74.25	-4.762	260	10384	81	-9764	9.8	516	12	104	82	0.00	LLBP
3093	300	100	74.25	-4.762	260	10403	104	-9764	9.8	516	12	124	105	0.00	LLBP
3094	300	100	37.5	4.762	260	10000	144	-9768	9.8	246	6	-15	144	0.00	LLBP
3095	300	100	37.5	4.762	260	9768	134	-9771	9.8	245	6	-248	135	0.00	LLBP
3096	300	100	37.5	4.762	260	10085	133	-9771	9.8	244	6	69	133	0.00	LLBP
3097	300	100	37.5	4.762	260	9771	130	-9769	9.8	244	6	-243	130	0.00	LLBP
3098	300	100	37.5	4.762	260	9792	137	-9769	9.8	244	6	-220	138	0.00	LLBP
3099	300	100	37.5	4.762	260	9782	139	-9768	9.8	244	6	-229	139	0.00	LLBP
3100	300	100	37.5	4.762	260	9728	123	-9770	9.8	244	6	-286	123	0.00	LLBP
3101	300	100	37.5	4.762	260	9835	137	-9770	9.8	244	6	-178	137	0.00	LLBP
3102	300	100	37.5	4.762	260	10026	133	-9770	9.8	244	6	12	133	0.00	LLBP
3103	300	100	37.5	4.762	260	9756	133	-9770	9.8	244	6	-258	133	0.00	LLBP
3104	300	100	37.5	-4.762	260	9942	125	-9764	9.8	244	6	-66	126	0.00	LLBP

Continued on next page

Table A.2 Continued from previous page

N_{run}	T [ns]	D [ns]	P [W]	B [Gauss]	θ_{pol} [deg.]	ν_{fit} [Hz]	$\Delta\nu_{\mathrm{fit}}$ [Hz]	$\mathrm{DC_B}$ [Hz]	$\Delta\mathrm{DC_B}$ [Hz]	SC [Hz]	ΔSC [Hz]	ν_0 [Hz]	$\Delta\nu_0$ [Hz]	wts. [%]	Data Type
3105	300	100	37.5	-4.762	260	9943	113	-9764	9.8	244	6	-65	113	0.00	LLBP
3106	300	100	37.5	-4.762	260	9794	141	-9765	9.8	245	6	-215	141	0.00	LLBP
3107	300	100	37.5	-4.762	260	10022	123	-9765	9.8	245	6	12	124	0.00	LLBP
3108	300	100	37.5	-4.762	260	10013	151	-9764	9.8	246	6	2	152	0.00	LLBP
3109	300	100	37.5	-4.762	260	10271	131	-9764	9.8	246	6	261	132	0.00	LLBP
3110	300	100	37.5	-4.762	260	9828	101	-9764	9.8	247	6	-182	101	0.00	LLBP
3111	300	100	37.5	-4.762	260	9872	114	-9764	9.8	247	6	-140	115	0.00	LLBP
3112	300	100	37.5	-4.762	260	10081	113	-9764	9.8	248	6	69	114	0.00	LLBP
3113	300	100	37.5	-4.762	260	10052	166	-9764	9.8	249	6	40	166	0.00	LLBP
3114	300	100	74.25	4.762	260	9765	127	-9771	9.8	517	12	-522	128	0.00	LLBP
3115	300	100	74.25	4.762	260	10112	71	-9771	9.8	520	12	-179	73	0.00	LLBP
3116	300	100	74.25	4.762	260	10037	102	-9772	9.8	521	13	-255	103	0.00	LLBP
3117	300	100	74.25	4.762	260	10011	85	-9772	9.8	522	13	-282	87	0.00	LLBP
3118	300	100	74.25	4.762	260	10014	85	-9772	9.8	521	13	-279	87	0.00	LLBP
3119	300	100	74.25	4.762	260	10122	84	-9771	9.8	521	13	-170	86	0.00	LLBP
3120	300	100	74.25	4.762	260	10058	108	-9771	9.8	521	13	-234	109	0.00	LLBP
3121	300	100	74.25	4.762	260	10010	61	-9772	9.8	521	13	-283	63	0.00	LLBP
3122	300	100	74.25	4.762	260	10144	100	-9771	9.8	522	13	-149	101	0.00	LLBP
3123	300	100	74.25	4.762	260	10099	91	-9770	9.8	522	13	-194	92	0.00	LLBP
3124	300	100	37.5	-4.762	260	9924	136	-9764	9.8	253	6	-94	136	0.00	LLBP
3125	300	100	37.5	-4.762	260	9874	145	-9763	9.8	252	6	-142	145	0.00	LLBP
3126	300	100	37.5	-4.762	260	10160	160	-9763	9.8	251	6	146	161	0.00	LLBP
3127	300	100	37.5	-4.762	260	10089	143	-9764	9.8	251	6	74	143	0.00	LLBP
3128	300	100	37.5	-4.762	260	9897	155	-9764	9.8	252	6	-119	155	0.00	LLBP
3129	300	100	37.5	-4.762	260	9767	151	-9763	9.8	252	6	-248	152	0.00	LLBP
3130	300	100	37.5	-4.762	260	9639	174	-9762	9.8	252	6	-375	174	0.00	LLBP
3131	300	100	37.5	-4.762	260	9888	125	-9763	9.8	253	6	-128	125	0.00	LLBP
3132	300	100	37.5	-4.762	260	9751	131	-9762	9.8	253	6	-264	132	0.00	LLBP
3133	300	100	37.5	-4.762	260	10004	138	-9764	9.8	253	6	-12	139	0.00	LLBP
3134	300	100	37.5	-4.762	260	10102	132	-9764	9.8	253	6	85	133	0.00	LLBP
3135	300	100	37.5	-4.762	260	9847	109	-9764	9.8	253	6	-170	110	0.00	LLBP
3136	300	100	37.5	-4.762	260	9825	134	-9763	9.8	253	6	-191	135	0.00	LLBP
3137	300	100	37.5	-4.762	260	9951	135	-9763	9.8	253	6	-65	136	0.00	LLBP
3138	300	100	37.5	-4.762	260	10127	134	-9764	9.8	253	6	110	134	0.00	LLBP
3139	300	100	37.5	-4.762	260	9973	157	-9764	9.8	253	6	-43	158	0.00	LLBP
3140	300	100	37.5	-4.762	260	9903	145	-9764	9.8	253	6	-113	146	0.00	LLBP
3141	300	100	37.5	-4.762	260	9936	94	-9763	9.8	253	6	-80	94	0.00	LLBP
3142	300	100	37.5	-4.762	260	10179	130	-9763	9.8	253	6	164	131	0.00	LLBP
3143	300	100	37.5	-4.762	260	9628	141	-9763	9.8	253	6	-389	142	0.00	LLBP
3144	300	100	74.25	4.762	260	10079	82	-9771	9.8	520	12	-211	83	0.00	LLBP
3145	300	100	74.25	4.762	260	10056	115	-9771	9.8	521	13	-237	116	0.00	LLBP
3146	300	100	74.25	4.762	260	10209	88	-9771	9.8	522	13	-85	89	0.00	LLBP
3147	300	100	74.25	4.762	260	10186	105	-9771	9.8	523	13	-108	106	0.00	LLBP
3148	300	100	74.25	4.762	260	10117	95	-9770	9.8	523	13	-177	96	0.00	LLBP
3149	300	100	74.25	4.762	260	10092	107	-9770	9.8	524	13	-203	108	0.00	LLBP
3150	300	100	74.25	4.762	260	9985	97	-9772	9.8	524	13	-311	98	0.00	LLBP
3151	300	100	74.25	4.762	260	10076	76	-9771	9.8	525	13	-220	78	0.00	LLBP
3152	300	100	74.25	4.762	260	9975	80	-9771	9.8	525	13	-320	82	0.00	LLBP
3153	300	100	74.25	4.762	260	10041	86	-9773	9.8	525	13	-257	88	0.00	LLBP
3154	300	100	74.25	4.762	260	9994	67	-9772	9.8	524	13	-302	69	0.00	LLBP
3155	300	100	74.25	4.762	260	10200	94	-9772	9.8	524	13	-96	95	0.00	LLBP
3156	300	100	74.25	4.762	260	10126	76	-9772	9.8	524	13	-170	78	0.00	LLBP
3157	300	100	74.25	4.762	260	10057	104	-9772	9.8	525	13	-240	106	0.00	LLBP
3158	300	100	74.25	4.762	260	10226	75	-9771	9.8	525	13	-70	77	0.00	LLBP
3159	300	100	74.25	4.762	260	10067	105	-9770	9.8	524	13	-228	106	0.00	LLBP
3160	300	100	74.25	4.762	260	10051	96	-9772	9.8	525	13	-245	97	0.00	LLBP
3161	300	100	74.25	4.762	260	10086	98	-9771	9.8	525	13	-210	100	0.00	LLBP
3162	300	100	74.25	4.762	260	10472	125	-9772	9.8	525	13	176	127	0.00	LLBP
3163	300	100	74.25	4.762	260	10065	85	-9772	9.8	525	13	-232	86	0.00	LLBP
3164	300	100	74.25	4.762	260	10110	104	-9771	9.8	525	13	-187	105	0.00	LLBP
3165	300	100	74.25	4.762	260	10182	102	-9771	9.8	525	13	-114	103	0.00	LLBP
3166	300	100	74.25	4.762	260	10163	109	-9771	9.8	525	13	-133	110	0.00	LLBP
3167	300	100	74.25	4.762	260	10106	92	-9772	9.8	525	13	-191	93	0.00	LLBP
3168	300	100	74.25	4.762	260	10199	78	-9772	9.8	524	13	-97	80	0.00	LLBP
3169	300	100	74.25	4.762	260	10000	93	-9770	9.8	524	13	-295	95	0.00	LLBP
3170	300	100	74.25	4.762	260	10184	76	-9772	9.8	524	13	-112	77	0.00	LLBP
3171	300	100	74.25	4.762	260	10121	88	-9771	9.8	525	13	-174	89	0.00	LLBP
3172	300	100	74.25	4.762	260	10103	111	-9770	9.8	524	13	-192	112	0.00	LLBP
3173	300	100	74.25	4.762	260	10246	63	-9772	9.8	524	13	-50	65	0.00	LLBP
3174	300	100	37.5	-4.762	260	9625	102	-9763	9.8	256	6	-395	103	0.00	LLBP
3175	300	100	37.5	-4.762	260	9800	145	-9763	9.8	255	6	-218	145	0.00	LLBP
3176	300	100	37.5	-4.762	260	9863	161	-9762	9.8	254	6	-154	162	0.00	LLBP
3177	300	100	37.5	-4.762	260	10079	117	-9763	9.8	254	6	61	117	0.00	LLBP
3178	300	100	37.5	-4.762	260	9721	150	-9763	9.8	254	6	-296	150	0.00	LLBP
3179	300	100	37.5	-4.762	260	9957	150	-9763	9.8	254	6	-60	151	0.00	LLBP
3180	300	100	37.5	-4.762	260	10036	135	-9762	9.8	254	6	20	136	0.00	LLBP
3181	300	100	37.5	-4.762	260	9950	140	-9762	9.8	254	6	-65	140	0.00	LLBP
3182	300	100	37.5	-4.762	260	10024	141	-9763	9.8	254	6	8	142	0.00	LLBP
3183	300	100	37.5	-4.762	260	9931	129	-9763	9.8	253	6	-85	130	0.00	LLBP
3184	300	100	37.5	4.762	260	9827	105	-9771	9.8	254	6	-198	106	0.00	LLBP
3185	300	100	37.5	4.762	260	9950	112	-9771	9.8	254	6	-75	113	0.00	LLBP
3186	300	100	37.5	4.762	260	9731	89	-9772	9.8	253	6	-294	90	0.00	LLBP
3187	300	100	37.5	4.762	260	9954	106	-9771	9.8	253	6	-70	107	0.00	LLBP
3188	300	100	37.5	4.762	260	9899	101	-9771	9.8	253	6	-125	101	0.00	LLBP
3189	300	100	37.5	4.762	260	9932	128	-9772	9.8	253	6	-92	128	0.00	LLBP
3190	300	100	37.5	4.762	260	9743	144	-9771	9.8	252	6	-280	144	0.00	LLBP
3191	300	100	37.5	4.762	260	9767	121	-9772	9.8	253	6	-258	121	0.00	LLBP
3192	300	100	37.5	4.762	260	9650	122	-9772	9.8	253	6	-376	123	0.00	LLBP
3193	300	100	37.5	4.762	260	10134	119	-9772	9.8	253	6	109	119	0.00	LLBP
3194	300	100	37.5	-4.762	260	9770	139	-9763	9.8	252	6	-245	140	0.00	LLBP
3195	300	100	37.5	-4.762	260	9993	127	-9761	9.8	253	6	-21	127	0.00	LLBP
3196	300	100	37.5	-4.762	260	10139	136	-9763	9.8	253	6	124	136	0.00	LLBP
3197	300	100	37.5	-4.762	260	9916	133	-9763	9.8	253	6	-100	133	0.00	LLBP
3198	300	100	37.5	-4.762	260	10043	118	-9765	9.8	253	6	26	119	0.00	LLBP
3199	300	100	37.5	-4.762	260	9975	114	-9763	9.8	253	6	-41	114	0.00	LLBP
3200	300	100	37.5	-4.762	260	10010	148	-9763	9.8	252	6	-5	148	0.00	LLBP
3201	300	100	37.5	-4.762	260	9732	136	-9763	9.8	252	6	-283	137	0.00	LLBP
3202	300	100	37.5	-4.762	260	10034	142	-9762	9.8	252	6	19	143	0.00	LLBP

Continued on next page

Table A.2 Continued from previous page

N_{run}	T [ns]	D [ns]	P [W]	B [Gauss]	θ_{pol} [deg.]	ν_{fit} [Hz]	$\Delta\nu_{\mathrm{fit}}$ [Hz]	$\mathrm{DC_B}$ [Hz]	$\Delta\mathrm{DC_B}$ [Hz]	SC [Hz]	ΔSC [Hz]	ν_0 [Hz]	$\Delta\nu_0$ [Hz]	wts. [%]	Data Type
3203	300	100	37.5	-4.762	260	9871	151	-9763	9.8	253	6	-145	151	0.00	LLBP
3204	300	100	74.25	-4.762	260	10281	103	-9763	9.8	518	12	-1	105	0.00	LLBP
3205	300	100	74.25	-4.762	260	10306	90	-9763	9.8	520	12	23	91	0.00	LLBP
3206	300	100	74.25	-4.762	260	10220	94	-9763	9.8	520	12	-64	95	0.00	LLBP
3207	300	100	74.25	-4.762	260	10111	99	-9763	9.8	521	13	-173	100	0.00	LLBP
3208	300	100	74.25	-4.762	260	10354	117	-9763	9.8	522	13	69	118	0.00	LLBP
3209	300	100	74.25	-4.762	260	10233	104	-9763	9.8	522	13	-52	106	0.00	LLBP
3210	300	100	74.25	-4.762	260	10173	99	-9762	9.8	523	13	-111	100	0.00	LLBP
3211	300	100	74.25	-4.762	260	10164	109	-9763	9.8	523	13	-121	110	0.00	LLBP
3212	300	100	74.25	-4.762	260	10122	107	-9763	9.8	523	13	-164	109	0.00	LLBP
3213	300	100	74.25	-4.762	260	10250	134	-9763	9.8	523	13	-36	135	0.00	LLBP
3214	300	100	74.25	-4.762	260	10202	100	-9762	9.8	523	13	-83	101	0.00	LLBP
3215	300	100	74.25	-4.762	260	10436	89	-9763	9.8	523	13	150	91	0.00	LLBP
3216	300	100	74.25	-4.762	260	10100	140	-9763	9.8	523	13	-186	141	0.00	LLBP
3217	300	100	74.25	-4.762	260	10247	98	-9763	9.8	524	13	-39	99	0.00	LLBP
3218	300	100	74.25	-4.762	260	10291	119	-9762	9.8	524	13	5	120	0.00	LLBP
3219	300	100	74.25	-4.762	260	10150	112	-9763	9.8	524	13	-137	113	0.00	LLBP
3220	300	100	74.25	-4.762	260	10372	84	-9763	9.8	523	13	86	86	0.00	LLBP
3221	300	100	74.25	-4.762	260	10270	107	-9763	9.8	524	13	-17	108	0.00	LLBP
3222	300	100	74.25	-4.762	260	10240	96	-9762	9.8	523	13	-45	97	0.00	LLBP
3223	300	100	74.25	-4.762	260	10136	96	-9764	9.8	523	13	-151	97	0.00	LLBP
3224	300	100	37.5	4.762	260	9857	108	-9771	9.8	255	6	-168	109	0.00	LLBP
3225	300	100	37.5	4.762	260	9810	97	-9771	9.8	253	6	-215	98	0.00	LLBP
3226	300	100	37.5	4.762	260	9804	110	-9771	9.8	253	6	-220	111	0.00	LLBP
3227	300	100	37.5	4.762	260	9708	112	-9771	9.8	253	6	-316	113	0.00	LLBP
3228	300	100	37.5	4.762	260	9868	118	-9771	9.8	253	6	-155	119	0.00	LLBP
3229	300	100	37.5	4.762	260	9711	103	-9770	9.8	252	6	-311	103	0.00	LLBP
3230	300	100	37.5	4.762	260	9903	132	-9770	9.8	252	6	-120	132	0.00	LLBP
3231	300	100	37.5	4.762	260	9916	101	-9772	9.8	251	6	-107	102	0.00	LLBP
3232	300	100	37.5	4.762	260	9735	114	-9771	9.8	252	6	-288	115	0.00	LLBP
3233	300	100	37.5	4.762	260	9667	115	-9772	9.8	252	6	-357	116	0.00	LLBP
3234	300	100	37.5	4.762	260	9761	93	-9771	9.8	252	6	-263	94	0.00	LLBP
3235	300	100	37.5	4.762	260	9851	91	-9772	9.8	252	6	-172	92	0.00	LLBP
3236	300	100	37.5	4.762	260	9636	108	-9772	9.8	252	6	-387	109	0.00	LLBP
3237	300	100	37.5	4.762	260	9968	119	-9772	9.8	251	6	-54	120	0.00	LLBP
3238	300	100	37.5	4.762	260	9885	156	-9770	9.8	251	6	-136	156	0.00	LLBP
3239	300	100	37.5	4.762	260	9770	120	-9771	9.8	251	6	-252	120	0.00	LLBP
3240	300	100	37.5	4.762	260	9885	121	-9772	9.8	252	6	-138	122	0.00	LLBP
3241	300	100	37.5	4.762	260	9947	118	-9771	9.8	252	6	-76	118	0.00	LLBP
3242	300	100	37.5	4.762	260	9881	121	-9771	9.8	252	6	-142	121	0.00	LLBP
3243	300	100	37.5	4.762	260	9895	121	-9771	9.8	252	6	-128	122	0.00	LLBP

Final measured result of the $2^3\mathrm{P}_1$-to-$2^3\mathrm{P}_2$ transition $\nu_{12} = 2\,291\,176\,590(25)\mathrm{Hz}$

End of Table